UNIVERSIDAD MIGUEL HERNÁNDEZ DE ELCHE.
INSTITUTO DE BIOINGENIERÍA

TESIS DOCTORAL

Synthesis of Silicon Phthalocyanines as Linkers for the Construction of SURMOFs

MEMORIA PARA OPTAR AL GRADO DE DOCTOR PRESENTADA POR:

Víctor José Sobrino Bastán

Bajo la dirección de:

Prof. Dra. Ángela Sastre Santos

Y la codirección de:

Prof. Dr. Luis Martín Gomis.

Programa de Doctorado en Bioingeniería

Elche, 2025

Indicios de calidad.

La tesis doctoral titulada "***Synthesis of Silicon Phthalocyanines as Linkers for the Construction of SURMOFs***" realizada por Víctor José Sobrino Bastán, con DNI: 74388870Q, bajo la dirección de la Prof. Dra. Ángela Sastre Santos y la codirección del Prof. Dr. Luis Martín Gomis se presenta bajo la modalidad de Tesis Convencional con los siguientes índices de calidad según el campo de evaluación de la ANEP de Química y como indicio de calidad se presenta con trabajos previamente publicados o aceptados para publicación y que se enumeran a continuación**:**

V. Sobrino-Bastán, L. Martín-Gomis and Á. Sastre-Santos, **Synthesis of 4-methylthiophenyl silicon phthalocyanines axially substituted with carboxylic acids for MOF materials**, *J. Porphyrins Phthalocyanines*, 2023, *27*, 331–339. DOI: 10.1142/S1088424622500961. Factor de impacto: 2.141. Área de conocimiento: Química general. Puesto que ocupa/ total de revistas en el área:252/408 (Q3)

H. Chen, L. Martín-Gomis, Z. Xu, J. C. Fischer, I. A. Howard, D. Herrero, V. Sobrino-Bastán, Á. Sastre-Santos, R. Haldar and C. Wöll, **Tunable J-type aggregation of silicon phthalocyanines in a surface-anchored metal–organic framework thin film**, *Phys. Chem. Chem. Phys.*, 2023, *25*, 20598–20607. DOI: 10.1039/D3CP90117C. Factor de impacto: 5.487. Área de conocimiento: Química y Física Teórica. Puesto que ocupa / total de revistas en el área: 69/189 (Q2).

La Dra. Dña. Piedad Nieves de Aza Moya, Coordinadora de la Comisión Académica del Programa de Doctorado en Bioingeniería de la Universidad Miguel Hernández de Elche por Resolución Rectoral 3120/19, de 09 de diciembre de 2019.

INFORMA

Que la tesis doctoral titulada "**Synthesis of Silicon Phthalocyanines as Linkers for the Construction of SURMOFs**", ha sido realizada por D. Víctor José Sobrino Bastán bajo la dirección la Prof. Dra. Ángela Sastre Santos y la codirección del Prof. Dr. Luis Martín Gomis, da su conformidad para que sea presentada a la Comisión de Doctorado de la Universidad Miguel Hernández.

Y para que así conste, y a los efectos oportunos, firma el presente documento en Elche, a___ de de 2025.

Fdo.: Prof. Dra. Piedad Nieves de Aza Moya

Coordinadora del Programa de Doctorado en Bioingeniería

La Dra. Dña. Ángela Sastre Santos, directora, y el Dr. D. Luis Martín Gomis, codirector,

CERTIFICAN Que el presente trabajo titulado "**Synthesis of Silicon Phthalocyanines as Linkers for the Construction of SURMOFs**", el cual constituye la memoria que presenta el graduado VÍCTOR JOSÉ SOBRINO BASTÁN para optar al Grado de Doctor por la Universidad Miguel Hernández de Elche, ha sido realizado bajo su dirección en el Instituto de Bioingeniería, cumpliendo todos los requisitos necesarios y dan su conformidad a la lectura de la tesis doctoral, conforme a los términos y condiciones definidos en su Plan de Investigación y de acuerdo al Código de Buenas Prácticas de la Universidad Miguel Hernández de Elche.

Y para que conste, expiden y firman el presente certificado en Elche, a __de __de 2025.

Fdo.: Prof. Dra. Ángela Sastre Santos

Fdo. Prof. Dr. Luis Martín Gomis.

El trabajo realizado a lo largo de la tesis doctoral ha sido posible gracias a la siguiente financiación:

- "AYUDA PARA LA FORMACIÓN PREDOCTORAL EN COLABORACIÓN CON EMPRESAS" Proyecto de investigación "Improving energy efficiency in buildings with printed perovskite solar cells on the ceramic tiles using phthalocyanines as components" con código de resolución rectoral 04588/2021 por delegación, RR 00278/2021 de 12 febrero, DOGV núm. 9024 de 19/02/2021). Financiado por la Conselleria de Innovación, Universidades, Ciencia y Sociedad Digital, Generalitat Valenciana. Responsable: Prof. Dra. Ángela Sastre Santos

- "AYUDAS DE MOVILIDAD PARA LA OBTENCIÓN DE LA MENCIÓN DE DOCTORADO INTERNACIONAL EN EL TÍTULO DE DOCTORA O DOCTOR POR LA UNIVERSIDAD MIGUEL HERNÁNDEZ DE ELCHE" Proyecto de investigación: "Preparación de redes metal-orgánicas (MOFs) con Ftalocianinas de Silicio". Código línea de subvención: 04-422-4- 2024-0157-S; Vista la Resolución Rectoral n.º 01466/2024 de fecha 10/06/2024 publicada en el DOGV el 14 de junio de 2024.

Agradecimientos

Esta ha sido una experiencia profundamente enriquecedora que me ha permitido adentrarme en el mundo de la investigación y dedicarme a lo que verdaderamente me apasiona. Esta oportunidad se la debo, principalmente, a mi directora de tesis, la **Dra. Ángela Sastre Santos**. Cuando me encontraba trabajando en un laboratorio de biología molecular en Liverpool, me llamó para ofrecerme la posibilidad de realizar una tesis doctoral bajo su dirección. Aquella llamada me llenó de alegría y marcó un antes y un después en mi vida.

Durante estos años, Ángela ha sido un referente para mí, por su integridad, su compromiso, y, sobre todo, por su amor y dedicación a la ciencia. Ha sido una guía constante y un ejemplo por seguir.

También quiero agradecer a mi cotutor, el **Dr. Luis Martín Gomis**, por brindarme la oportunidad de desarrollar habilidades clave tanto a nivel profesional como personal. Gracias a él he podido fortalecer mi iniciativa, capacidad de resolución de problemas, autonomía y, especialmente, la resiliencia ante circunstancias adversas. Gracias por tu apoyo, que no olvidaré.

Otras personas fundamentales durante este camino han sido mis compañeros y compañeras del grupo de investigación, tanto actuales como quienes ya siguieron otros rumbos:

Fernando, ejemplo de dedicación y esfuerzo, con una curiosidad contagiosa y siempre dispuesto a aportar una idea, un dato curioso o una reflexión que enriquece cualquier conversación. **Belén**, una gran compañera, siempre dispuesta a ayudar, escuchar y disfrutar de los pequeños momentos. Pieza clave en el funcionamiento del laboratorio, gracias también por tu dedicación con el equipo de masas.

Javi, excelente investigador y, aún más, gran docente. Fue fundamental para entender varios de mis resultados y para orientarme en distintas reacciones sintéticas.

Ana, con quien siempre ha sido un placer compartir espacio y experiencias. Tu trayectoria y energía han sido clave para cohesionar el grupo, especialmente entre los más jóvenes. **Desi, Nathalie y Jorge**, ejemplos de conciliación profesional y pasión por la docencia. Siempre accesibles y dispuestos a explicar y colaborar, han sido fuente de inspiración en lo profesional y lo académico. **Conchi, Julio y Enrique**, profesores generosos y cercanos.

También deseo agradecer al Prof. **Christof Wöll** y a los doctores **Hartmut, Bruno y Cucu** por su apoyo durante mi estancia en el KIT. Gracias por brindarme la posibilidad de conocer nuevas tecnologías, otro entorno científico y una institución puntera en investigación.

A los jóvenes del laboratorio, **José, Irene y Lydia**, gracias por los buenos momentos compartidos, las cervezas tras el trabajo, las fiestas y aquella inolvidable cena de Navidad. Habéis sido parte esencial de esta experiencia, tanto en lo humano como en lo académico.

A **Alberto y Ariadna**, nuevas incorporaciones al grupo, ha sido un placer coincidir con vosotros, aunque el tiempo fue breve. Estoy seguro de que lograréis grandes cosas.

Una mención especial a **Adrián**, compañero, amigo "circustancial" y propietario reciente de un nuevo hogar. Aunque podrías encajar entre los jóvenes del laboratorio, todos sabemos que no es así, mereces un apartado propio. Gracias por tantas tardes compartidas, por las experiencias vividas y por soportar mis momentos más excéntricos. Aunque fuéramos solo dos, no podemos olvidar al siempre presente "Bejo".

A mis amigos de siempre, **Manus, Luiso, Karmo, Chemon, Andrés, Jose, Richard, Patri, Laura y Camilo**, gracias por vuestro apoyo incondicional durante estos años. Por soportar mis desvaríos sobre la tesis y por ofrecerme una vía de escape de las responsabilidades académicas. En especial a **Jose**, gracias por nuestras conversaciones camino al trabajo.

A mi familia, especialmente a mis padres, verdaderos ejemplos de superación y resiliencia. Gracias por brindarme las herramientas, la confianza y el esfuerzo necesarios para llegar hasta aquí, mucho más lejos de lo que cualquiera de nosotros imaginaba cuando comencé mis estudios, incapaz siquiera de escribir dos frases seguidas correctamente.

A mi madre, por su amor incondicional y su apoyo constante. Has sido la mejor madre posible, incluso cuando yo no siempre supe demostrar apego. A mi padre, por ser la persona que, desde pequeño, siempre supo responder mis preguntas con sabiduría, y por enseñarme, con su ejemplo, lo que significan el compromiso y la perseverancia.

Y finalmente, a **Tefi**, mi compañera de vida y mi fuente inagotable de inspiración. Qué decir que no te haya dicho ya: te amo. No que te quiero, sino que te amo. Gracias por estar a mi lado cuando sentía que no podía más, por tu apoyo incondicional, por tus abrazos, por bailar conmigo en mis días grises, por comer helado, por descubrir conmigo el mundo, por mostrarme tu país y su maravillosa cultura, por enseñarme a disfrutar del té, por nuestras tardes de pizza, por ayudar a conectar y conocer mejor mi espiritualidad, por nuestros "Elvis, Yuyito" y por todos los que vendrán. Gracias por acompañarme en este camino, por hacerme salir de mi zona de confort, por enseñarme a descubrir el mundo desde otra perspectiva y por sostener nuestra relación incluso en la distancia. Gracias por ser mi colibrí. Estoy seguro de que lo que nos depara la vida a partir de ahora va a ser más chilero.

Abstract.

This doctoral work stems from a previous collaboration between the research group of Prof. Ángela Sastre Santos and Prof. Christof Wöll, where axially substituted silicon phthalocyanines (SiPcs) were employed for the generation of SURMOFs. The project is structured in two main parts: first, the design, synthesis, and characterization of sixteen axially functionalized SiPcs aimed at tuning electronic and steric properties; and second, the incorporation of selected derivatives as ditopic linkers in Zn-based SURMOF thin films and their evaluation as photoresponsive devices. This synergy between molecular synthesis and supramolecular assembly seeks to establish design principles that connect ligand chemistry with the performance of next-generation photoactive materials.

Chapter 1: Synthesis of Silicon Phthalocyanines with Donor and Acceptor Substituents in the Peripheral Positions for the Generation of SURMOFs.

Ten novel SiPc derivatives bearing ditopic axial substituents and peripheral electron-donating or electron-withdrawing groups were successfully synthesized. The compounds were obtained via cyclotetramerization of phthalonitriles followed by axial ligand exchange from dichlorinated intermediates. Comprehensive characterization by ^{1}H-NMR, HR MALDI-TOF MS, UV-Vis spectroscopy, and cyclic voltammetry confirmed their molecular structures, optical properties, and redox behaviour. These SiPc derivatives were subsequently investigated as potential ditopic linkers for the construction of Zn-based SURMOF films. The resulting thin films were characterized by *out-of-plane* X-ray diffraction (XRD), FT-IRRAS, and UV-Vis spectroscopy

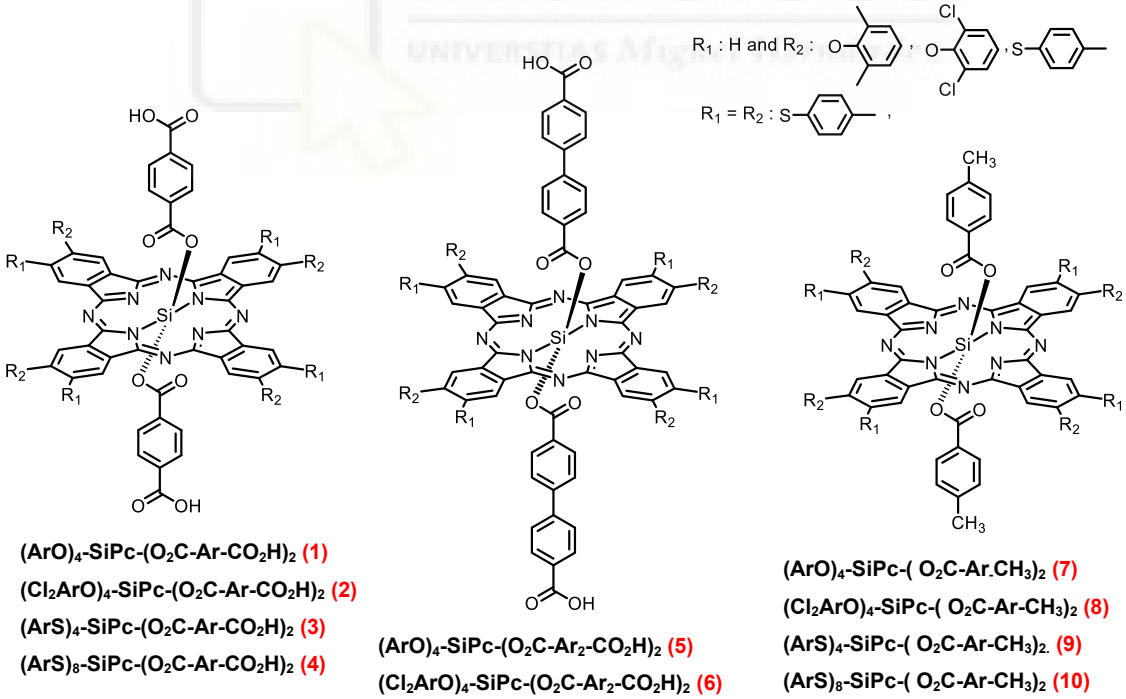

***Figure 1**. Structure of the target molecules studied in chapter 1.*

Chapter 2: Synthesis of Silicon Phthalocyanines with Azo and Pyridine Substituents in the Axial Positions for the Generation of SURMOFs.

Three novel SiPcs were designed and synthesized to explore their potential as functional linkers for the construction of Zn-based SURMOFs. The first group comprises two SiPcs axially functionalized with (*E*)-4-[(4-hydroxyphenyl)diazinyl]benzoic acid units, incorporating azo moieties capable of photoisomerization to confer light-responsive behavior. One of these derivatives additionally features *tert*-butyl substituents at the periphery to enhance solubility during the SURMOF fabrication process.

Finally, a derivative was functionalized with axial pyridine groups, aiming to assess their coordination capacity and influence on the structural assembly of the resulting SURMOFs. A comprehensive characterization by ^{1}H-NMR, HR MALDI-TOF MS, UV-Vis spectroscopy, and cyclic voltammetry confirmed their molecular structures, optical properties, and redox behaviour. These SiPc derivatives were subsequently investigated as potential ditopic linkers for the construction of Zn-based SURMOF films. The resulting thin films were characterized by *out-of-plane* X-ray diffraction (XRD), FT-IRRAS, and UV-Vis spectroscopy.

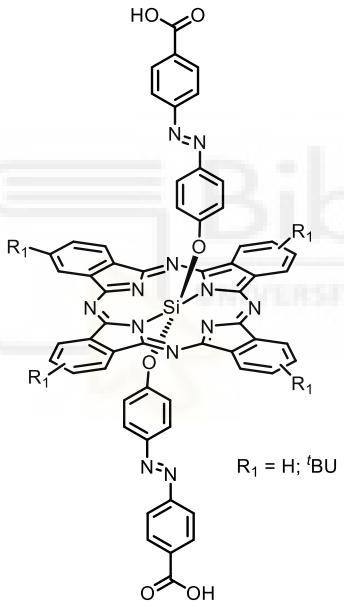

SiPc-(O-Ar-Azo-Ar-CO_2H)$_2$. (11)

(^{t}Bu)$_4$SiPc-(O-Ar-Azo-Ar-CO_2H)$_2$. (12)

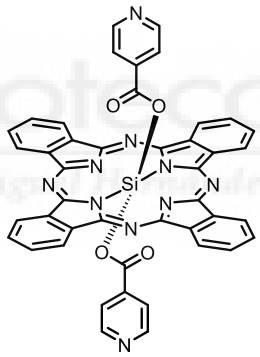

SiPc-(O_2CPy)$_2$. (13)

Figure 2. *Structure of the target molecules studied in chapter 2.*

Chapter 3: Synthesis of Water Soluble Silicon Phthalocyanines for the Generation of SURMOFs

Two SiPc mesylate salts bearing phenyl and biphenyl axial groups, designed to improve water solubility and biocompatibility through the methylation of peripheral pyridine groups, while preserving carboxylic acid functionalities essential for SURMOF integration were synthetized. A reference SiPc axially substituted with 4-methylbenzoyl groups was also synthesized for comparative purposes

Finally, a characterization by ^{1}H-NMR, HR MALDI-TOF MS, and UV-Vis spectroscopy, confirmed their molecular structures and optical properties. These SiPc derivatives were subsequently investigated as potential ditopic linkers for the construction of Zn-based SURMOF films. The resulting thin films were tested by XRD.

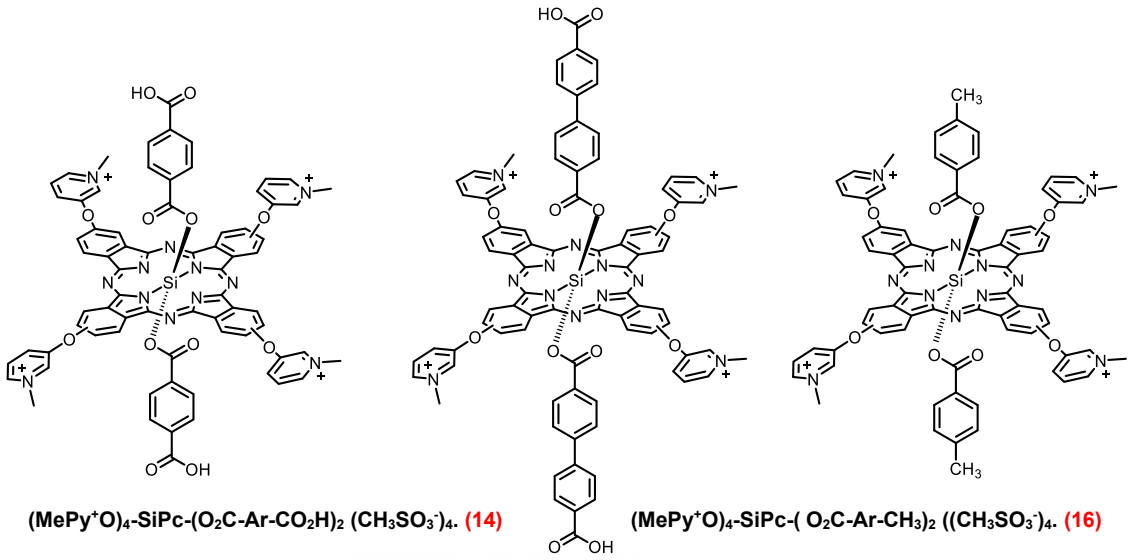

$(MePy^{+}O)_4$-SiPc-$(O_2C$-Ar-$CO_2H)_2$ $(CH_3SO_3^{-})_4$. (14)

$(MePy^{+}O)_4$-SiPc-$(O_2C$-Ar_2-$CO_2H)_2$ $(CH_3SO_3^{-})_4$. (15)

$(MePy^{+}O)_4$-SiPc-$(O_2C$-Ar-$CH_3)_2$ $((CH_3SO_3^{-})_4$. (16)

***Figure 3**. Structure of the silicon phthalocyanines studied in chapter 3.*

Resumen.

Este trabajo doctoral surge de una colaboración previa entre el grupo de investigación de la Prof.ª Ángela Sastre Santos y el Prof. Christof Wöll, en la que se emplearon ftalocianinas de silicio (SiPcs) sustituidas axialmente para la generación de materiales tipo SURMOF. El proyecto consta de dos partes principales: en primer lugar, el diseño, síntesis y caracterización de dieciséis SiPcs funcionalizadas axialmente con el objetivo de modular las propiedades electrónicas y estéricas; y en segundo lugar, la incorporación de diversas moléculas como enlazadores ditópicos en películas delgadas de SURMOFs basadas en zinc, así como la evaluación de estos sistemas como dispositivos fotoactivos. Esta sinergia entre la síntesis molecular y el autoensamblaje supramolecular busca establecer principios de diseño que conecten la química de los ligandos con el rendimiento de materiales fotoactivos de nueva generación.

Capítulo 1: Síntesis de ftalocianinas de silicio con sustituyentes donadores y aceptores en las posiciones periféricas para la generación de SURMOFs

Se sintetizaron con éxito diez nuevas SiPc con sustituyentes axiales ditópicos y grupos periféricos de carácter dador o aceptor de electrones. Los compuestos se obtuvieron mediante ciclotetramerización de ftalonitrilos, seguida de un intercambio de ligandos axiales a partir de intermedios diclorados. Se caracterizaron exhaustiva mediante ^{1}H-NMR, HR MALDI-TOF MS, espectroscopía UV-Vis y voltametría cíclica. Confirmando sus estructuras moleculares, propiedades ópticas y comportamiento redox. Posteriormente, estos derivados de SiPc fueron evaluados como posibles enlazadores ditópicos para la construcción de películas delgadas de SURMOF basadas en zinc. Las películas obtenidas se caracterizaron mediante difracción de rayos X fuera del plano (XRD), FT-IRRAS y espectroscopía UV-Vis.

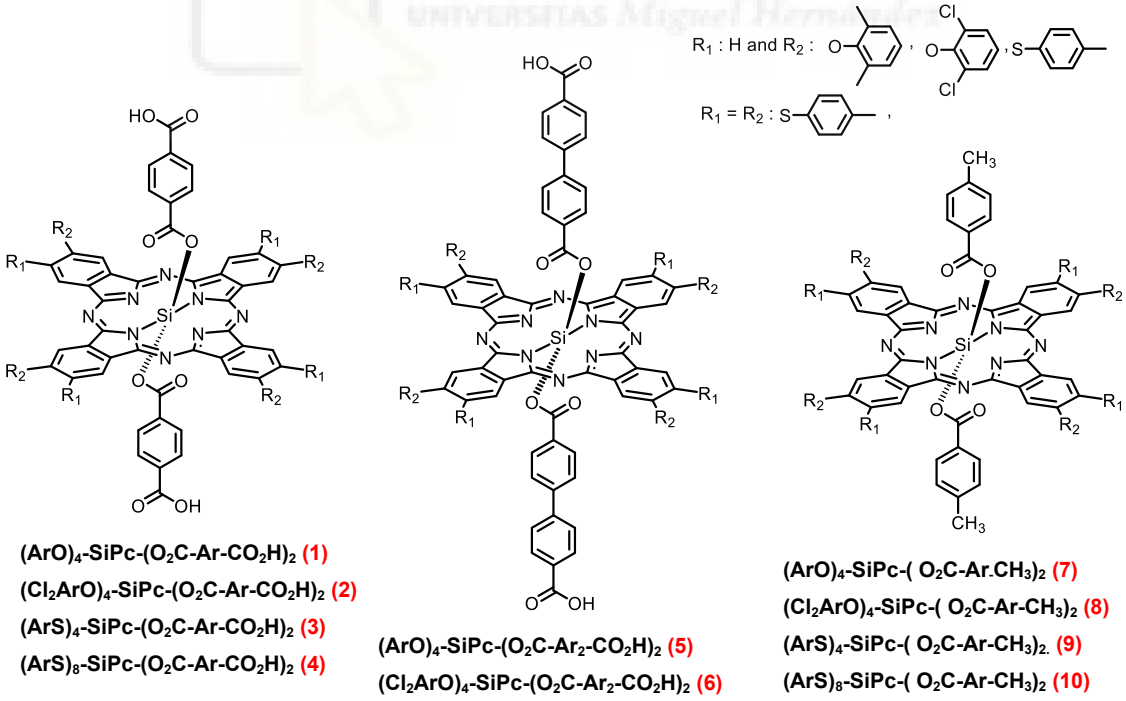

***Figura 1**. Estructura de las moléculas a estudio en el capítulo 1.*

Capítulo 2: Síntesis de ftalocianinas de silicio con sustituyentes azo y piridina en las posiciones axiales para la generación de SURMOFs.

Se diseñaron y sintetizaron tres nuevas SiPc con el objetivo de estudiar su potencial como enlazadores funcionales en la construcción de SURMOFs basados en zinc El primer grupo incluye dos SiPcs funcionalizadas axialmente con ácido (E)-4-[(4-hidroxifenil)diazinil]benzoico, que incorporan grupos azo capaces de fotoisomerizarse confiriendo así un comportamiento fotoactivo. Uno de estos derivados presenta además sustituyentes terc-butilo en la periferia, con el fin de mejorar la solubilidad durante el proceso de fabricación del SURMOF.

Además, se sintetizó un derivado funcionalizado con grupos piridina en posición axial, con el propósito de evaluar su capacidad de coordinación y su influencia en el ensamblaje estructural de los SURMOFs resultantes.

Los compuestos resultantes se caracterización mediante ^{1}H-NMR, HR MALDI-TOF MS, espectroscopía UV-Vis y voltametría cíclica confirmando sus estructuras moleculares, propiedades ópticas y comportamiento redox. Posteriormente, estos derivados de SiPc se evaluaron como posibles enlazadores ditópicos para la construcción de películas delgadas de SURMOFs basados en Zn. Las películas obtenidas se caracterizaron mediante difracción de rayos X fuera del plano (XRD), FT-IRRAS y espectroscopía UV-Vis.

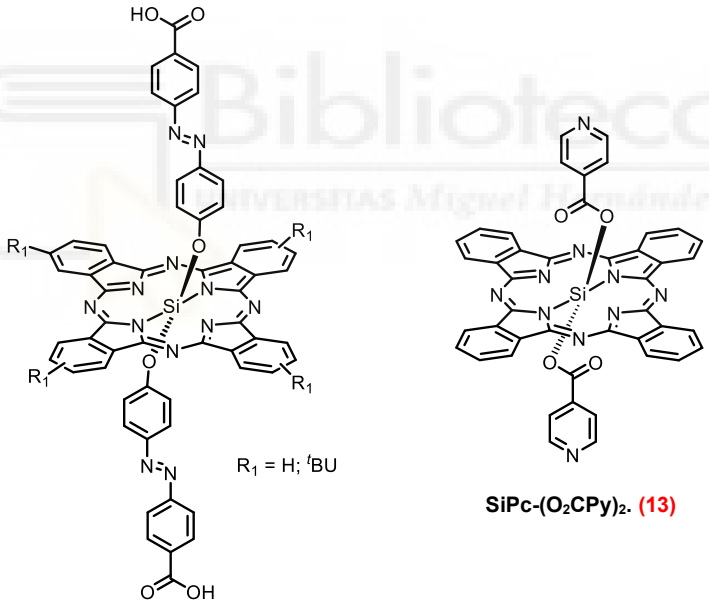

SiPc-(O-Ar-Azo-Ar-CO_2H)$_2$. (11)
(^{t}Bu)$_4$SiPc-(O-Ar-Azo-Ar-CO_2H)$_2$. (12)

SiPc-(O_2CPy)$_2$. (13)

Figura 2. *Estructura de las moléculas objetivo estudiadas en el capítulo 2.*

Capítulo 3: Síntesis de ftalocianinas de silicio solubles en agua para la generación de SURMOFs.

Se sintetizaron dos sales SiPc mesiladas con grupos axiales de tipo fenil y bifenil, diseñadas para mejorar la solubilidad en agua y la biocompatibilidad mediante la metilación de los grupos piridina periféricos, manteniendo a la vez las funcionalidades de ácido carboxílico

esenciales para su integración en los SURMOFs. Del mismo modo, se sintetizó una SiPc de referencia, funcionalizada axialmente con grupos 4-metilbenzoíco, con fines comparativos.

La caracterización mediante ^{1}H-NMR, HR MALDI-TOF MS y espectroscopía UV-Vis confirmó sus estructuras moleculares y propiedades ópticas. Posteriormente, estos derivados de SiPc fueron evaluados como posibles enlazadores ditópicos para la construcción de películas delgadas de SURMOFs basadas en zinc. Las películas obtenidas fueron analizadas mediante difracción de rayos X (XRD).

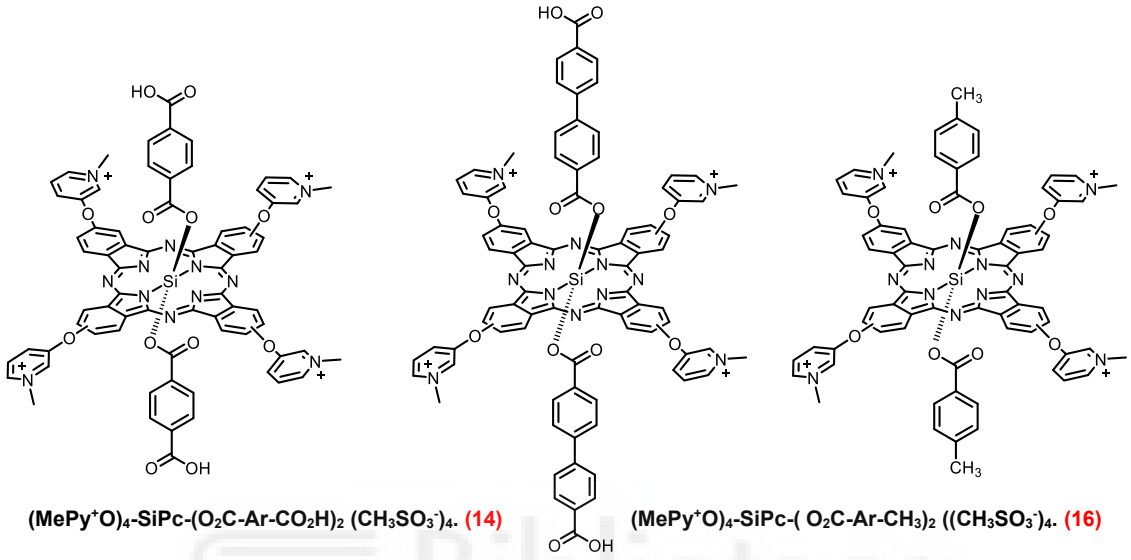

$(MePy^{+}O)_4$-SiPc-$(O_2C$-Ar-$CO_2H)_2$ $(CH_3SO_3^{-})_4$. (14)

$(MePy^{+}O)_4$-SiPc-$(O_2C$-Ar_2-$CO_2H)_2$ $(CH_3SO_3^{-})_4$. (15)

$(MePy^{+}O)_4$-SiPc-$(O_2C$-Ar-$CH_3)_2$ $((CH_3SO_3^{-})_4$. (16)

***Figura 3**. Estructuras de las ftalocianinas de silicio estudiadas en el capítulo 3.*

Contents

List of Abbreviations

^{1}H-NMR	Hydrogen Nuclear Magnetic Resonance
^{13}C-NMR	Carbon Nuclear Magnetic Resonance
$Ag/AgNO_3$	Silver/Silver Nitrate Reference Electrode
Ar	Aryl Group
ArO	Aryloxy Group
ArS	Arylthio Group
Azo	Azo Group (–N=N–)
Bn	Benzyl
BTC	Benzene-1,3,5-tricarboxylic Acid
$CDCl_3$	Deuterated Chloroform
$CHCl_3$	Chloroform
Cl_2Ar	2,6-Dichlorophenyl
COOEt	Ethyl Carboxylate
DBN	1,5-Diazabicyclo[4.3.0]non-5-ene
DBU	1,8-Diazabiciclo[5.4.0]undec-7-ene
DCM	Dichloromethane
DMAE	Dimethylaminoethanol
DMF	*N,N'*-Dimethylformamide
DMSO-d_6	Deuterated Dimethyl Sulfoxide
DPV	Differential Pulse Voltammetry
EtOH	Ethanol
eV	Electronvolts
Fc/Fc^+	Ferrocene/Ferrocenium Redox Couple
FT-IRRAS	Fourier-Transform Infrared Reflection Absorption Spectroscopy
FTIR	Fourier Transform Infrared Spectroscopy
FTO	Fluorine-Doped Tin Oxide
GC	Glassy Carbon Electrode

HR MALDI-TOF MS	High-Resolution Matrix-Assisted Laser Desorption/Ionization Time-of-Flight Mass Spectrometry
HOMO	Highest Occupied Molecular Orbital
Hz	Hertz
IDE	Interdigitated Electrode
IL	Ionic Liquid
J-aggregation	J-type Molecular Aggregation
JSC	Short-Circuit Current Density
LbL	Layer-by-Layer
LPE	Liquid-Phase Epitaxy
LUMO	Lowest Unocuppied Molecular Orbital
Me	Methyl
MeOH	Methanol
μM	Micromolar
mmol	Millimol
MOF	Metal-Organic Framework
MPcs	Metallophthalocyanines
MW	Microwave
nm	Nanometer
NMP	N-Methyl-2-pyrrolidone
OLED	Organic Light-Emitting Diode
P3HT	Poly(3-hexylthiophene)
PCBM	[6,6]-Phenyl-C_{61}-Butyric Acid Methyl Ester
Pc	Phthalocyanine
PDI	Perylenediimide
PDT	Photodynamic Therapy
PIT	Photoimmunotherapy
ppm	Parts per Million

PTT	Photothermal Therapy
Py	Pyridine
QCM	Quartz Crystal Microbalance
QED	Quantum Electrodynamical
ROS	Reactive Oxygen Species
rpm	Revolutions per Minute
sccm	Standard Cubic Centimeters per Minute
SEC	Size Exclusion Chromatography
SiPc	Silicon Phthalocyanine
SURMOF	Surface-Mounted Metal-Organic Framework
$TBAPF_6$	Tetrabutylammonium Hexafluorophosphate
^{t}Bu	*tert*-Butyl
TCTPM	Tetrahedral Ligand 4,4',4",4'"-Tetracyanotetraphenylmethane
THF	Tetrahydrofurane
TLC	Thin Layer Chromatography
TMS	Tetramethylsilane
UV-Vis	Ultraviolet-Visible Spectroscopy
UV-Ozone	Ultraviolet-Ozone Surface Cleaning
XRD	X-ray Diffraction

Introduction

Chemistry of Phthalocyanines, MOFs, and SURMOFs

1.Phthalocyanines

The discovery of phthalocyanines dates to 1907, when Braun and Tcherniac observed a pale blue coloration during the synthesis of *o*-cyanobenzamide, suggesting the presence of an unknown compound (**Scheme 1.i**).[1]

However, it was not until 1927 that Diesbach and von der Weid accidentally synthesized the first copper-phthalocyanine through the cyanation of 1,2-dibromobenzene. This discovery led to increasing scientific interest in these novel compounds (**Scheme 1.ii**).[2]

A year later, in 1928, phthalocyanine was again accidentally synthesized at the Scottish Dyes's Grangemouth plant, during the preparation of phthalimide from phthalic anhydride and ammonia. A crack in the glass reactor allowed contact between the reaction mixture and the steel lining, resulting in the formation of a blue impurity, later identified as a phthalocyanine (**Scheme 1.iii**).

The structural elucidation of these molecules was made possible through the pioneering work of Reginald Linstead and his collaborators,[3,4] complemented by Robertson's X-ray diffraction studies.[5] Their contributions provided a deeper understanding of the structural and electronic properties of phthalocyanines, establishing the foundation for the development of a wide range of applications from pigments and dyes to electronic devices and sensors.

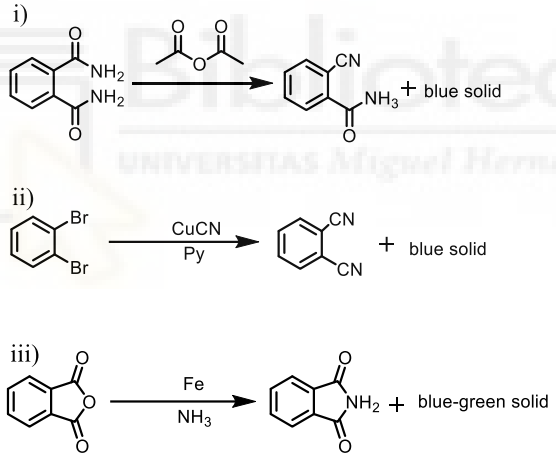

***Scheme 1**. Synthesis of i) 2-cyanobenzamine, ii) phthalonitrile, and iii) phthalimide.*

1.1. Structure and Properties

Phthalocyanines are synthetic macrocyclic compounds that are structurally analogous to natural porphyrins (**Figure 1.i**). Their structure consists of four isoindole subunits (**Figure 1.ii**), linked at positions 1 and 3 by nitrogen atoms, which confer a high degree of rigidity to the molecule. This arrangement results in a planar aromatic system characterized by 42 π-electrons,

[1] A. Braun, J. Tchemiac*, Ber. Dtsch. Chem. Ges*., **1907**, *40*, 2709-2714.

[2] H. de Diesbach, E. von der Weid, *Helv. Chim. Acta.*, **1927**, *10*, 886-88.

[3] R.P. Linstead, *J. Chem. Soc.,* **1934,** *1016-1017*.

[4] a) G. T. Byme, R. P. Linstead, A. R. Lowe, *J. Chem. Soc.*, **1934**, *1017–1022*. b) R. P. Linstead, A. R. Lowe, *J. Chem. Soc.*, **1934**, *1022–1027*. c) C. E. Dent, R. E. Linstead, A. R. Lowe, *J. Chem. Soc.*, **1934**, *1033–1039*. d) J. A. Elvidge, R. P. Linstead, *J. Chem. Soc.*, **1955**, *3536–3544*. e) C. E. Dent, R. E. Linstead, *J. Chem. Soc.*, **1934**, *1027–1031*.

[5] a) J. M. Robertson, *J. Chem. Soc.,* **1935**, *615–621*. b) J. M. Robertson, *J. Chem. Soc.,* **1936,** *1195–1209.* c) J. M. Robertson, I. Woodward, *J. Chem. Soc.,* **1937**, *219–230*.

where the principal electronic delocalization occurs within the 18 π-electrons of the core macrocycle (**Figure 1.iii**). These structural features play a crucial role in defining their chemical, thermal, and photophysical properties.

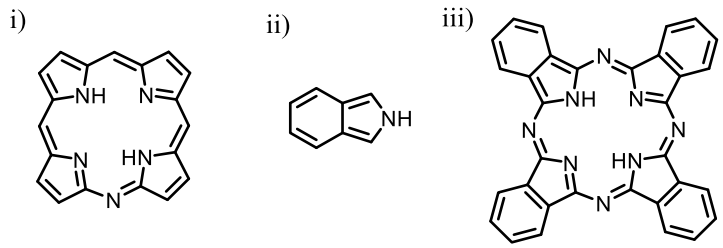

***Figure 1**. Structures of i) porphyrin, ii) isoindole, and iii) free-base phthalocyanine.*

The central cavity of phthalocyanines can accommodate a wide range of metal ions, including transition metals, lanthanides, actinides, and metalloids. This diversity leads to the formation of metallophthalocyanines (MPcs), whose electronic properties differ from those of free-base phthalocyanines.

The UV-Vis absorption spectra of phthalocyanines feature two prominent bands: the Soret band, a broad absorption band centered around 350 nm, and the Q band, which appears as a single band in metallophthalocyanines or as two bands in free-base phthalocyanines around 680 nm. These absorption bands originate from π-π* HOMO-LUMO transitions, with the Q band exhibiting high molar extinction coefficients in the order of 10^5 M^{-1} cm^{-1} (**Figure 2**).

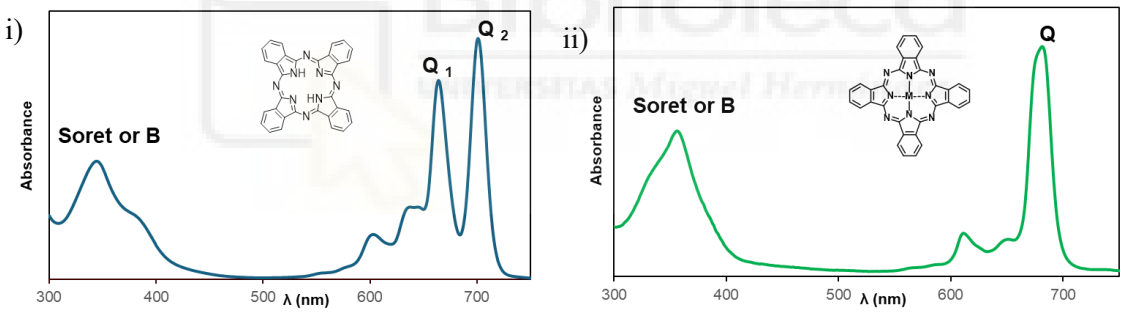

***Figure 2**. UV-Vis spectrum of i) a H_2Pc and ii) an MPc.*

Despite their extensive conjugation phthalocyanines are generally insoluble in most organic solvents, but they dissolve in strong acids and high-boiling-point solvents such as DMSO or DMF. Their solubility and optical properties can be adjusted through peripheral (β) and non-peripheral (α) substituents (**Figure 3**), while the incorporation of certain metal atoms, such as silicon, allows the functionalization of the axial positions.[6]

[6] M. Hanack, M. Lang, *Adv. Mater.*, **1994**, *6*, 819–833.

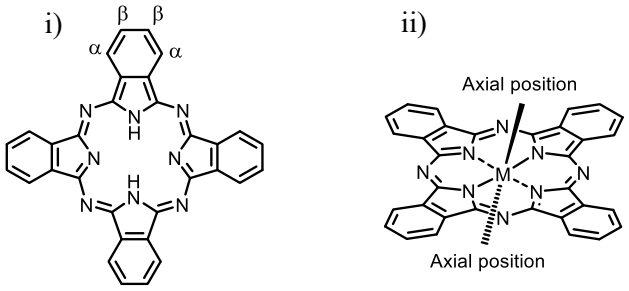

Figure 3. Structures of free-base and metallophthalocyanines with their potential functionalization positions.

Beyond their optical properties, phthalocyanines exhibit valuable electrochemical behaviour, making them a subject of numerous studies. Their stability, adjustable HOMO-LUMO band gap, and redox capacity can be modulated by both, the metal ion at the core and the nature of the peripheral substituents.[7,8]

The central metal in a phthalocyanine, can influence the electronic properties of the delocalized π-electron system, either by donating, withdrawing, or stabilizing charge depending on its nature.[9] For instance transition metals such as iron and cobalt, exhibit multiple oxidation states, making them highly reactive compared to free-base phthalocyanines.[10] Whereas metals like copper and zinc confer a higher electrochemical stability. This is because Cu^{2+} and Zn^{2+} tend to remain in a fixed oxidation state without frequent changes compared to free-base phthalocyanines, which are more susceptible to oxidation due to their higher electron density in the conjugated system.[11,12]

Additionally, peripheral substituents play a key role in modulating the donor-acceptor character of phthalocyanines. Electron-donating groups such as $-NH_2$, -OH or -SH, increase electron density in the phthalocyanine ring, whereas electron-withdrawing groups like $-NO_2$, -CN, and $-CF_3$ reduce it. Moreover, bulky substituents introduce steric effects, modifying the planarity of the molecule. These electrochemical modifications are evident in the UV-Vis spectra, where electron-donating groups produce a red shift in the Q-band, while electron-withdrawing groups result in a blue shift (**Figure 4**).[13]

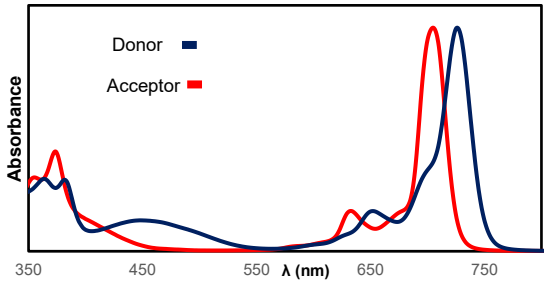

Figure 4. *UV-Vis spectrum of donor (blue) and acceptor (red) phthalocyanines.*

Another distinctive feature of phthalocyanines is their strong tendency to self-aggregate due to π-π stacking interactions, which can significantly influence their solid-state properties. The

[7] E. Demir, H. Silah, B. Uslu, *Crit. Rev. Anal. Chem.*, **2020**, *52,* 425–461.

[8] A. B. Sorokin, *Chem. Rev*, **2013**, *9*, 8152–8191.

[9] H. Matsuura, M. Ogata, K. Miyake, H. Fukuyama, *J. Phys. Soc. Jpn.*, **2012**, *81*, 104705.

[10] K. P. C. Hundi, J. Hur, *Micromachines*, **2024**, *15*, 1061.

[11] F. Wang, Z. Liu, C. Yang, H. Zhong, G. Nam, P. Zhang, R. Dong, Y. Wu, J. Cho, J. Zhang, X. Feng, *Adv. Mater*, **2019**, *31*, 1905361.

[12] A. Giraudeau, A. Louati, M. Gross, J. J. Andre, J. Simon, C. H. Su, K. M. Kadish, *Inorg. Chem*, **1983**, *22*, 1601–1607.

[13] N. Kobayashi, H. Ogata, N. Nonaka, EA Luk'yanets, *Chem. euros. J.* ,**2003**, 9,5123-34.

aggregation behaviour of these molecules depends on multiple factors, such as the nature of the central metal, the peripheral groups, and the presence of axial substituents.[14]

Phthalocyanines exhibit different aggregation behaviours, which can be categorized into three main types:

Stacking: This arrangement results from π-π interactions between aromatic rings, leading to highly ordered structure stabilized by van der Waals forces, which play a crucial role in the stability of these aggregates (**Figure 5.i**).[15]

Sheets: Certain phthalocyanines bearing functional groups such as -NH_2, -OH, and -COOH can assemble into two-dimensional sheets,[16] where hydrogen bonding and metal coordination facilitates layer formation and enhances structural integrity (**Figure 5.ii**).[17]

3-D structures: In more complex scenarios, the combination of π-π interactions, metal coordination, and hydrogen bonding can result in the formation of three-dimensional architectures. The characteristics of these structures are modulated by the nature of the phthalocyanine and its substituents. Certain metallophthalocyanines promote axial substitution, facilitating the formation of structures with larger pore sizes or expanded unit cell dimensions (**Figure 5.iii**). Similarly, the size and bulkiness of peripheral substituents affect steric hindrance, which in turn modulates intermolecular interactions and packing efficiency. These mechanisms allow the construction of highly organized frameworks, such as MOFs and SURMOFs.[18,19]

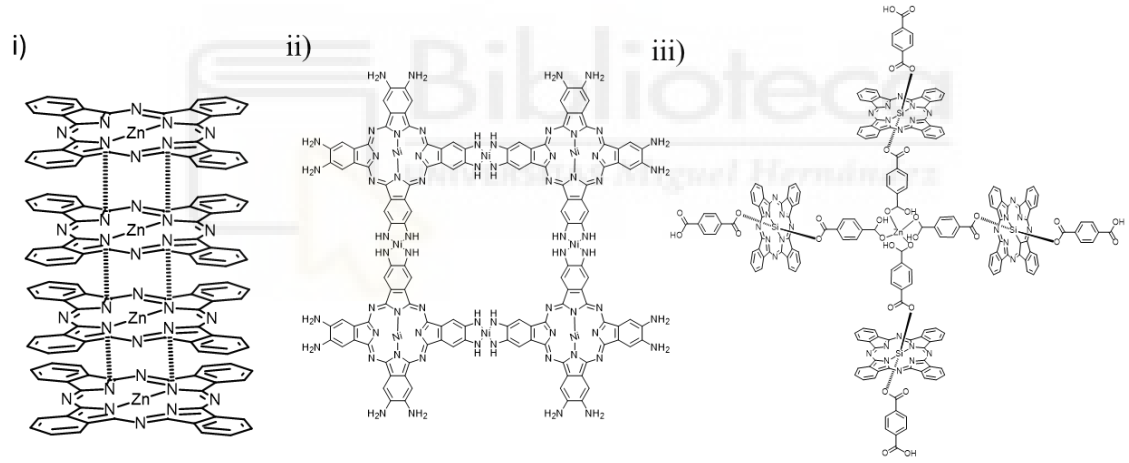

Figure 5*. The figure shows different types of aggregation i) stacking, ii) sheets, iii) 3-D structure.*

These aggregation patterns impact both molecular organization, optical and electronic properties. The formation of highly ordered structures can enhance charge mobility, improving electrical conductivity,[20] while π-π interactions between aromatic rings can modulate

[14] A. Snow, *The Porphyrin Handbook*, **2003**, 129–176.

[15] K. Hatsusaka, K. Ohta, I. Yamamoto, H. Shirai, *J. Mater. Chem.*,**2001**, *11*, 423-433.

[16] E. Biemmi, C. Scherb, T. Bein, *J. Am. Chem. Soc.*, **2007**, *129*, 8054 -8055.

[17] H. Jia, Y. Yao, J. Zhao, Y. Gao, Z. Luo, P. Du, *J. Mater. Chem. A* **2018**, *6*, 1188–1195.

[18] R. Haldar, Z. Fu, R. Joseph, D. Herrero, L. Martín-Gomis, B. S. Richards, I. A. Howard, Á. Sastre-Santos, C. Wöll, *Chem. Sci.* **2020**, *11,* 7972–7978.

[19] H. Chen, L. Martín-Gomis, Z. Xu, J.C, Fischer, I.A. Howard, A. D. Herrero, V. Sobrino-Bastán, Á. Sastre-Santos, R. Haldar, C. Wöll. *Phys. Chem. Chem. Phys.* **2023**, *25*, 19626.

[20] M. Dumm, P. Lunkenheimer, A. Loidl, B. Assmann, H. Homborg, P. Fulde, *J. Chem. Phys.,* **1996**, *104*, 5048–5053.

optoelectronic properties by altering electronic delocalization and energy transfer processes, leading to bathochromic shifts in UV-Vis spectra.[21,22]

1.2. Synthesis of Phthalocyanines

The synthesis of phthalocyanines can be achieved through different methods, with the most common method involving the cyclotetramerization of precursors at high temperatures.

The most common precursors are phthalonitrile, diiminoisoindoline, phthalimide, 2-cyanobenzamide, phthalic anhydride, and phthalic acid. Except for phthalonitrile and diiminoisoindoline, an external nitrogen source is necessary for the cyclotetramerization process with urea commonly used for this purpose.

The synthesis of metallophthalocyanines can be achieved through direct coordination of a metal ion during the cyclotetramerization process or by the introduction of the metal ion in a free-base phthalocyanine (M = H_2). Alternatively, they can be obtained by transmetalation, using labile complexes with alkali metals such as lithium, magnesium, or sodium (**Scheme 2**).[23]

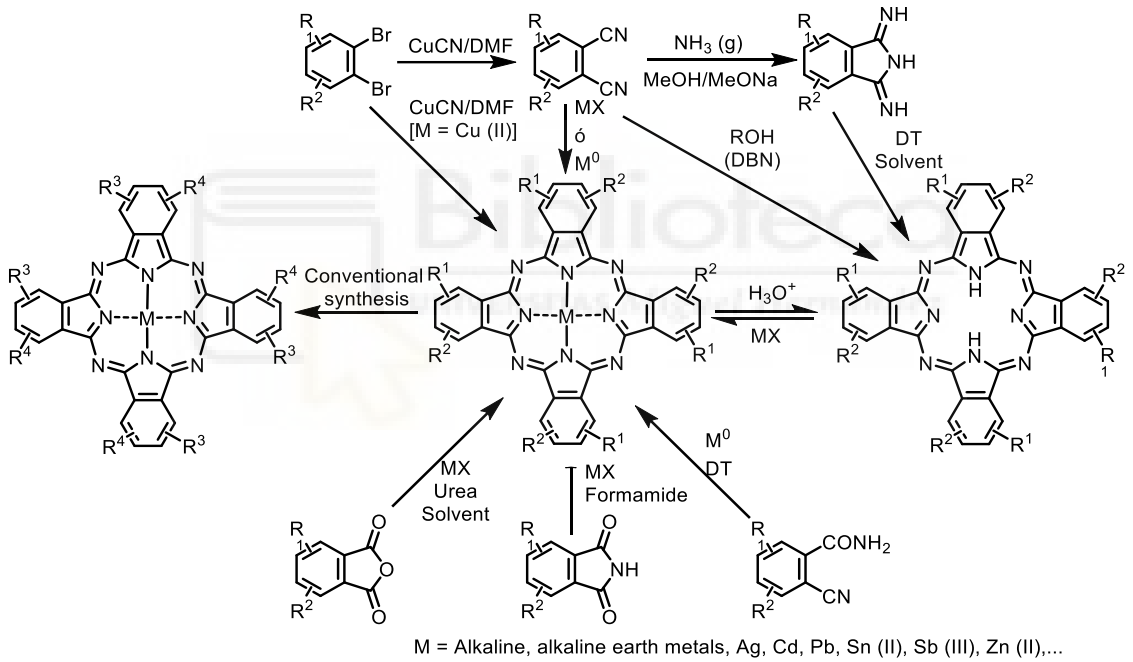

***Scheme 2**. Methods for the synthesis of symmetric phthalocyanines.*

1.2.1. Synthesis of Symmetrical Phthalocyanines

The synthesis of symmetrical phthalocyanines relies on the condensation of four identical subunits in a cyclotetramerization process. This reaction requires strict conditions, as high temperatures and polar high-boiling point solvents, such as DMAE, pentanol, DMF, hydroquinone or quinoline. The presence of a non-nucleophilic base, like DBU or DBN acts as a catalyst in the reaction. Moreover, the addition of a metallic salt facilitates the formation of the

[21] K. Kasuga, K. Yashiki, T. Sugimori, M. Handa, *J. Porphyrins Phthalocyanines*, **2005**, **9**, 646–650.

[22] A. A. Zanfolim, D. Volpati, C. A. Olivati, A. E. Job, C. J. L. Constantino, *J. Phys. Chem. C*, **2010**, *114*, 12422–12429.

[23] P. A. Barrett, D. A. Frye, R. P. Linstead, *J. Chem. Soc.,* **1938**, *1157–1165.*

metallophthalocyanine ring by acting as a template, by stabilizing the macrocycle during synthesis.[24]

Phthalocyanines offer 16 potential positions for functionalization, distributed across two α and two β positions on each isoindoline subunit. This structural versatility allows for the introduction of different substituents, leading to a broad range of substituted phthalocyanines.[25]

Many of these modifications have been achieved using pre-substituted precursors, such as phthalonitrile or diiminoisoindoline. The synthesis of tetrasubstituted phthalocyanines results in a mixture of regioisomers with C_{4h}, C_{2v}, C_s, and D_{2h} symmetries (**Figure 6**). Separating these isomers is challenging and often requires advanced chromatographic techniques, such as HPLC,[26] or prolonged recrystallization processes.[27] Nevertheless, this isomeric heterogeneity can enhance certain phthalocyanine properties, such as increased solubility in organic solvents, without significantly altering their spectroscopic and electrochemical characteristics.

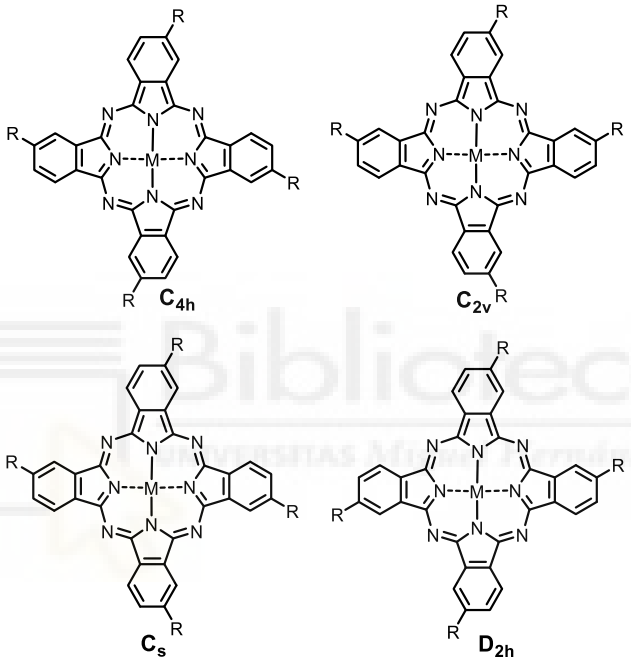

Figure 6. *Regioisomers of a tetrasubstituted phthalocyanine*.

1.2.2. Asymmetric Phthalocyanines

Asymmetric phthalocyanines are those in which at least one isoindole subunit is substituted with a functional group that differs from the others. Three substitution patterns can be distinguished: (I) one unit is different from the others (A_3B pattern); (II) adjacent units that have the same substituents (AABB pattern), and (III) opposite units that have the same substituents (ABAB pattern) (**Figure 7**).

[24] V. N. Nemykin, E. A. Lukyanets, *Arkivoc* **2010**, *24*, 136-208.

[25] M. Hanack, H. Heckmann, R. Polley, in *Houben-Weyl., Methods in Organic Chemistry*, **1997**, *9*, 717–832.

[26] M. Hanack, D.Y. Meng, A. Beck, M. Sommerauer, L.R. Subramanian, *J. Chem. Soc., Chem. Commun.*, **1993**, 58–60.

[27] M. Brewis, G.J. Clarkson, P. Humberstone, S. Makhseed, N.B. McKeown, *Chem. Eur. J.*, **1998**, 4, 1633–1640.

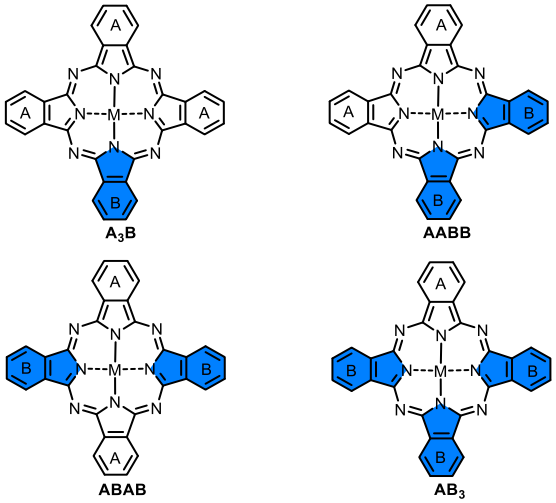

Figure 7. *Structure of asymmetric phthalocyanines.*

Several methods can be used to synthesize asymmetric phthalocyanines, with statistical cyclotetramerization being the most common. This method involves the cyclotetramerization of two different phthalonitriles or diiminoisoindolines, resulting in a statistical distribution of the six possible phthalocyanines (A_4, A_3B, AABB, ABAB, AB_3, B_4).[28] Despite its lack of selectivity, it is the most widely used method (**Figure 8.i**).

The ring expansion method represents the first selective approach for synthesizing A_3B phthalocyanines. This method requires the previous synthesis of a subphthalocyanine which undergoes ring expansion to form the final asymmetric phthalocyanine (**Figure 8.ii**).[29]

Leznoff and Hall developed a method to selectively synthesize asymmetric phthalocyanines using a polymeric support.[30] By immobilizing the reactants, this method minimizes the formation of side products. However, the synthetic process requires two additional steps, increasing its complexity (**Figure 8.iii**).

Cross-condensation of the substrate can occur if one of the reactants, like 1,3,3-trichloroisoindolenine, is unable to self-condense.[31] Lowering the temperature at which phthalocyanine formation occurs promotes cross-condensation over self-condensation, thus promoting the formation of ABAB and A_3B phthalocyanines (**Figure 8.iv**).[32] Additionally, the selective formation of AABB and A_3B phthalocyanines can be achieved by employing trimeric or dimeric precursor units with a different co-reactant. In this approach, the dimer is pre-synthesized using lithium alkoxide in methanol before being incorporated into the phthalocyanine framework (**Figure 8.iv**).[32]

[28] N. B. McKeown, I. Chambrier, M. J. Cook, *J. Chem. Soc., Perkin Trans. 1* **1990**, *1169*–1177.

[29] C. G. Claessens, D. González Rodríguez, T. Torres, *Chem. Rev.* **2002**, *102*, 835.

[30] C. C. Leznoff, T. W. Hall, *Tetrahedron Lett.* **1928**, *23*, 3023.

[31] C. C. Leznoff, S. Greenberg, B. Khouw, A. B. P. Lever, *Can. J. Chem.* **1987**, *65*, 1705–1713.

[32] a) E. Güzel, D. P. Medina, M. Medel, M. Kandaz, T. Torres, M. S. Rodríguez-Morgade, *J. Mater. Chem. C* **2021**, *9*, 10802–10810. b) J. Y. M. Chan, D. K. P. Ng, *J. Org. Chem.* **2022**, *87*, 7213–7218.

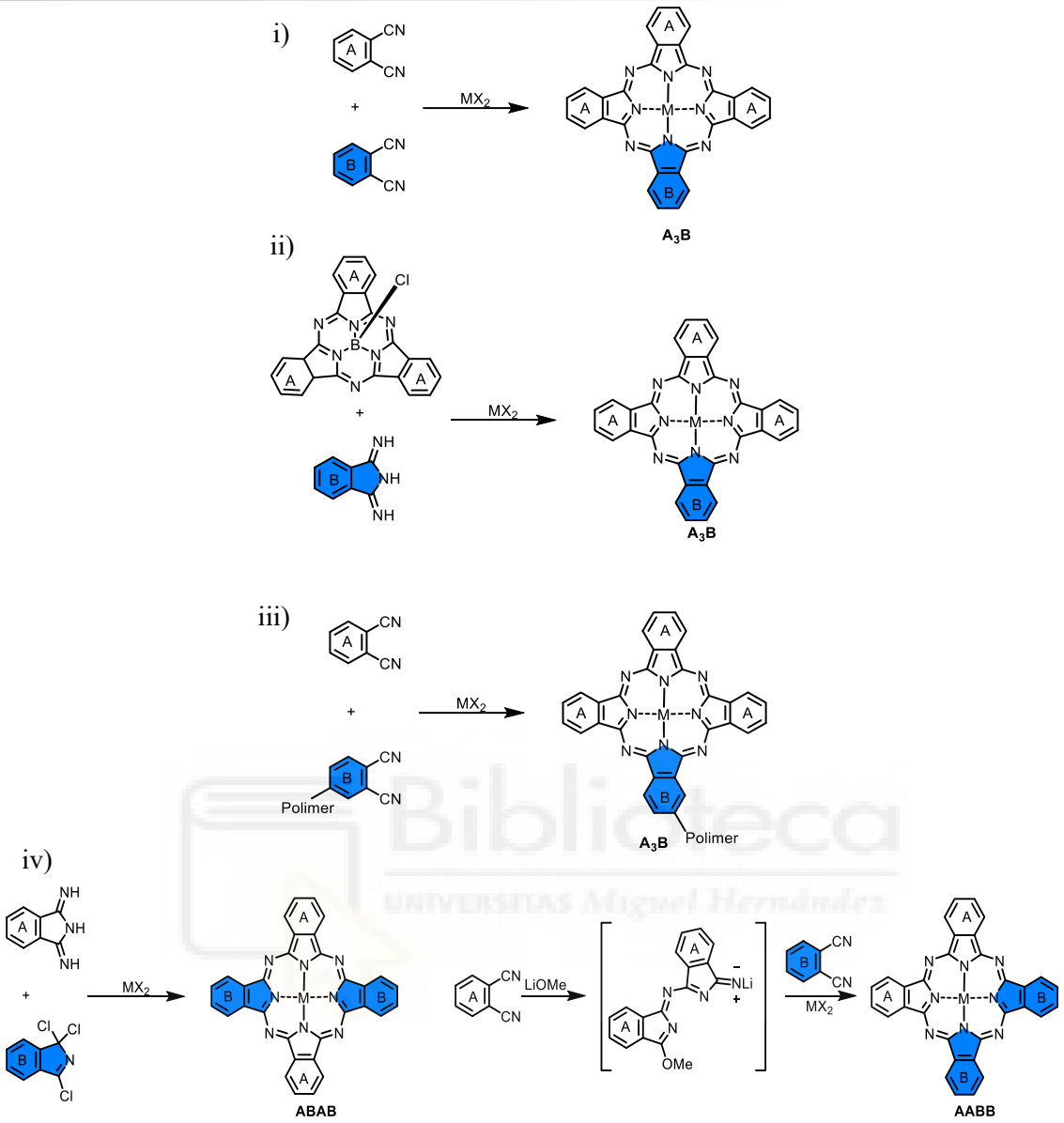

Figure 8. *Synthesis of asymmetric phthalocyanines.*

1.3. Phthalocyanines with Axial Substitution

As previously mentioned, certain metallophthalocyanines have the capacity to form axial bonds. This coordination property can modulate their electronic and optical properties.[33]

To facilitate the formation of axial bonds, the structure of the metal ion plays a fundamental role. These ions should possess an incomplete *d* orbital configuration, a small ionic radius, and a high affinity for coordinated covalent bonding, allowing an interaction with axial

[33] J. Andzelm, A. M. Rawlett, J. A. Orlicki, J. F. Snyder, K. K. Baldridge, *J. Chem. Theory Comput.*, **2007**, *3*, 870–877.

ligands.[34] Transition metals such as Ti,[35] V,[36] Mn,[37] Fe,[38] Co[39] and Ni[40] exhibit this capacity. Other metals that share these characteristics include Al,[41] Ga[42] and Si,[43] which can also engage in axial coordination.

Axial coordination substituents can have an influence beyond electronic effects, it can also affect the solubility and chemical reactivity of phthalocyanines, allowing further functionalization. This modification depends on both the metal introduced and the nature of the axial ligand.[44,45] As mentioned in **section 1.1**, metallophthalocyanines modify optical properties, exhibiting a single Q band compared to the two bands observed in free-base phthalocyanines.

Silicon phthalocyanines have traditionally been the preferred choice for axial substitution. This is due to several factors, such as:

- SiPcs exhibit highly covalent Si–N bonds, in contrast to the metal-nitrogen bonds found in other phthalocyanines.[46]
- Silicon metal allows for two axial coordination sites, enabling the synthesis of both symmetric and asymmetric axially substituted phthalocyanines.[45]
- The Q band in SiPcs, like in other phthalocyanines, can be modulated by the nature of the peripheral and non-peripheral substituents. Acceptor substituents induce a bathochromic shift due to their electron-withdrawing effect.[47] In contrast, non-bulky substituents, can promote aggregation, leading to an increase in Q-band width and a decrease in its intensity.[48]
- Like other phthalocyanines, SiPcs exhibit fluorescence due to their extended π-conjugation.[49] However, their fluorescence can be lower than that of free-base phtalocyanines due to their tendency to aggregate.[48]
- As mentioned in **section 1.1**, SiPcs can form different types of aggregates. In the case of axially substituted SiPcs, there can be a formation of J-type π-π aggregates of considerable length due to these axial bonds.[50]

[34] T. J. Martins, L. B. Negri, L. Pernomian, K. D. C. F. Faial, C. Xue, R. N. Akhimie, M. R. Hamblin, C. Turro, R. S. da Silva, *Front. Mol. Biosci.*, **2021**, *7*, 595830.

[35] Y. Arslanoğlu, E. Hayran, E. Hamuryudan, *Dyes Pigm.*, **2013**, *97*, 340–346.

[36] G. Mbambisa, T. Nyokong, *Polyhedron*, **2008,** 27, 2799–2804.

[37] N. Montenegro-Pohlhammer, R. Sánchez-de-Armas, G. Cárdenas-Jirón, C. J. Calzado, *J. Phys. Chem. C* **2019,** *123,* 46.

[38] M. P. Oyarzún, N. Silva, D. Cortés-Arriagada, J. F. Silva, I. O. Ponce, M. Flores, K. Tammeveski, D. Bélanger, A. Zitolo, F. Jaouen, J. H. Zagal, *Electrochim. Acta* **2021,** *398,* 139263.

[39] J. Riquelme, K. Neira, J. F. Marco, P. Hermosilla-Ibáñez, W. Orellana, J. H. Zagal, F. Tasca, *Electrochim. Acta* **2018,** *265,* 547–555.

[40] J. Hong, T. J. Fauvell, W. Helweh, X. Zhang, L. X. Chen, *J. Photochem. Photobiol. A Chem.* **2019,** *372,* 270–278.

[41] N. Brasseur, R. Ouellet, C. La Madeleine, J. E. van Lier, *Br. J. Cancer*, **1999**, 80, 1533–1541.

[42] D. Lorenzoni, C. A. Z. Souto, M. B. Araujo, C. de Souza Berger, L. C. D. da Silva, M. O. Baratti, J. N. Ribeiro, D. C. Endringer, M. C. C. Guimarães, A. R. da Silva**,** *J. Photochem. Photobiol. B: Biol.* **2019,** *198,* 111582.

[43] Y. Zhang, Y.-K. Cheung, D. K. P. Ng, W.-P. Fong, *Angew. Chem. Int. Ed.* **2021**, *70*, 485–495.

[44] J.-W. Hofman, F. van Zeeland, S. Turker, H. Talsma, S. A. G. Lambrechts, D. V. Sakharov, W. E. Hennink, C. F. van Nostrum, *J. Med. Chem.*, **2007**, *50*, 1823–1830.

[45] D. M. Răsădean, T. M. Gianga, A. H. Swan, G. Kociok-Köhn, G. D. Pantoș, *Org. Lett.*, **2018**, *20*, 9, 2503–2506.

[46] M. H. Qiao, Y. Cao, J. F. Deng, G. Q. Xu, *Chem. Phys. Lett.*, **2000**, *325*, 508–512

[47] Y. Ogura, M. Nakano, H. Maeda, M. Segi, T. Furuyama, *Molecules*, **2022**, *27*, 2766.

[48] A.K. Pal, S. Varghese, D.B. Cordes, A.M.Z. Slawin, I.D.W. Samuel, E. Zysman-Colman, *Sci. Rep.*, **2017**, *7*, 12282.

[49] A. Ogunsipe, T. Nyokong, *J. Porphyrins Phthalocyanines,* **2005**, *9,* 2, 118–126.

[50] T. Doane, A. Chomas, S. Srinivasan, C. Burda, *Chem. Eur. J*. **2014**, *20*, 8030–8039.

1.3.1. Synthesis of Axially Substituted SiPcs

The synthesis of these compounds needs the previous formation of an intermediate, into which the desired substituent is introduced.[51] Dichlorophthalocyanines, derived from the cyclotetramerizations of diiminoisoindoline with a $SiCl_4$, are the most common intermediate. During this process, hydroxylated phthalocyanines can be produced by a base-catalysed hydrolysis of the chlorinated precursors.[52] Both phthalocyanines exhibit the ability to form axial bonds with different functional groups. Dichlorophthalocyanines can form bonds with groups such as alcohols, phenols, and carboxylic acids.[53] Hydroxyphthalocyanines, on the other hand, can form bonds with silane groups.[54] To achieve this reaction, it must be produced on nonpolar solvents in the presence of mild base **(Scheme 3)**.[55]

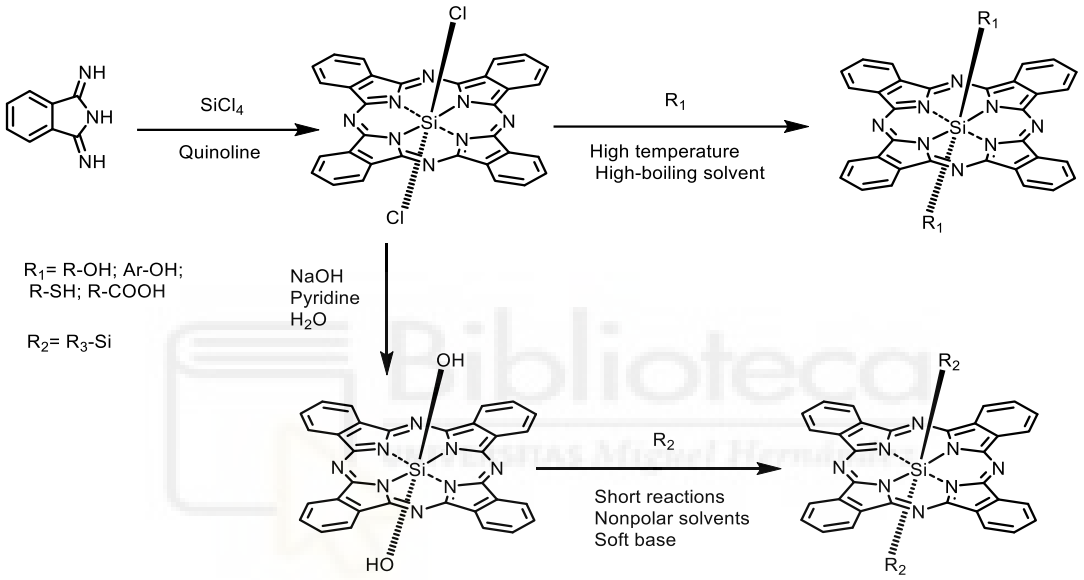

***Scheme 3**. Synthesis of symmetrical axially substituted SiPcs.*

In comparison to their symmetric analogues, a limited number of SiPc derivates with asymmetric axial linkers have been synthesized.

To synthesize these kinds of phthalocyanines, different synthetic routes have been employed. One of these routes, starts from symmetric phthalocyanines with axial bulky groups, because they have a steric hindrance and a higher lability in the silicon bonds. The method involves the selective hydrolysis of Si-O-Si phthalocyanines as precursors and it was carried out by adding trichloroacetic acid in DCM at room temperature, obtaining a hydroxylated intermediate, which was subsequently subjected to a nucleophilic substitution reaction where the –OH group was replaced by the desired substituent (**Scheme 4.i**).[56] Another alternative route, also

[51] K. Mitra, M.C.T Hartman, *Org. Biomol. Chem*., **2021**, *19*, 1168-1190.

[52] J.-W. Hofman, F. van Zeeland, S. Turker, H. Talsma, S. A. G. Lambrechts, D. V. Sakharov, W. E. Hennink C. F. van Nostrum*, J. Med. Chem.*, **2007**, *50*, 1485–1494

[53] R. Rafaeloff, F. J. Kohl, P. C. Krueger, M. E. Kenney, *J. Inorg. Nucl. Chem.* **1966**, *28*, 899–902.

[54] E. van de Winckel, B. David, M. M. Simoni, J. A. González-Delgado, A. de la Escosura, Â. Cunha, T. Torres, *Dyes Pigm.* **2017,** *145,* 239–245.

[55] H. M. Anula, J. C. Berlin, H. Wu, Y.-S. Li, X. Peng, M. E. Kenney, M. A. J. Rodgers, *J. Phys. Chem. A* **2006**, *110*, 5215–5223.

[56] Lowery, M. K.; Starshak, A. J.; Esposito, J. N.; Krueger, P. C.; Kenney, M. E. *Inorg. Chem.* **1965**, *4*, 128.

starting from these symmetric Si-O-Si phthalocyanines, yields asymmetric SiPcs during the purification process by crystallization. In this case, the choice of solvent is crucial for obtaining the desired compound, as it promotes the selective precipitation of the target molecule (**Scheme 4.ii**).[57]

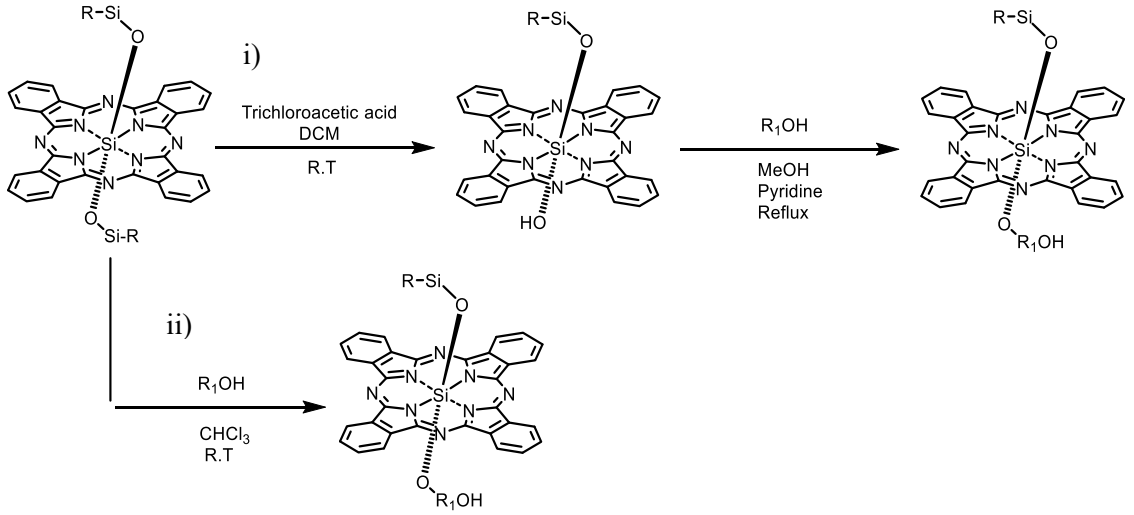

***Scheme 4**. Synthesis of asymmetrical SiPcs with axial Si–OR bonds.*

Other synthetic method involves the preparation of monochlorophthalocyanines. This is achieved by the reaction of diiminoisoindolines dissolved in quinoline under reflux conditions with alkyltrichlorosilanes instead of $SiCl_4$.[58] Subsequently, starting from this asymmetric SiPc, the desired phthalocyanine can be obtained through a Grignard reaction (**Scheme 5.i**).[59]

The last method of synthesis starts from dichlorophthalocyanines and involves a nucleophilic substitution of the chlorine atoms by the desired substituents. In this case, the reactivity of the substituents must be considered, adjusting the number of moles added to improve the formation of the desired compound. However, an inconvenient of this method is the formation of symmetric phthalocyanines, which can decrease the yield of the reaction (**Scheme 5.ii**).[60]

[57] P.-C. Lo, J.-D. Huang, D. Y. Y. Cheng, E. Y. M. Chan, W.-P. Fong, W.-H. Ko, D. K. P. Ng, *Chem. – Eur. J.* **2004**, *10*, 4831–4838.

[58] J. N. Esposito, J. E. Lloyd, M. E. Kenney, *Inorg. Chem.* **1966**, *5*, 1979–1984.

[59] K. Tamao, M. Akita, H. Kato, M. Kumada, *J. Organomet. Chem.* **1988**, *341*, 165–179.

[60] L. Martín-Gomis, K. Ohkubo, F. Fernández-Lázaro, S. Fukuzumi, Á. Sastre-Santos, *Org. Lett.* **2007**, *9*, 3441–3444.

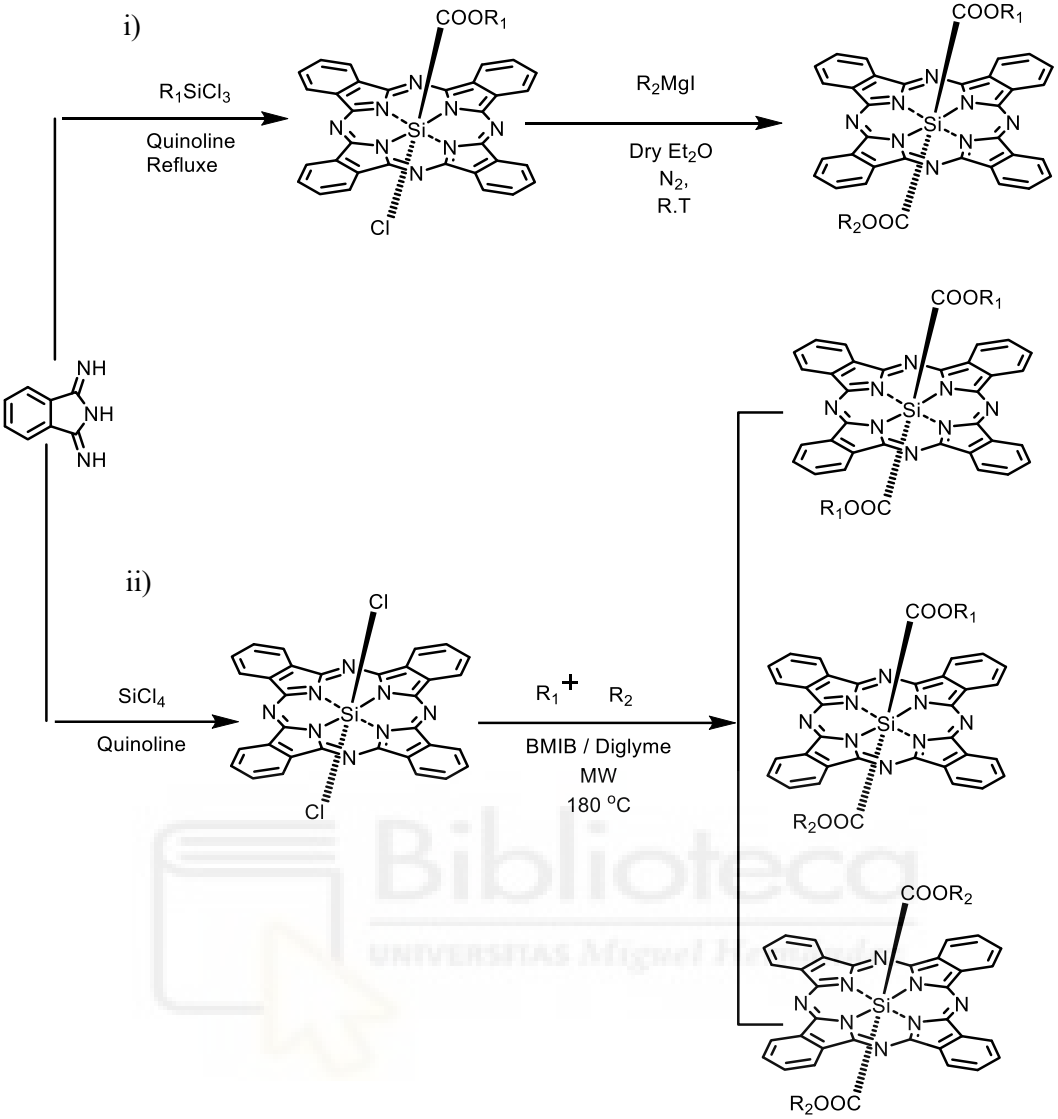

***Scheme 5**. Synthesis of asymmetrical SiPcs with axial Si-C bonds.*

1.4. Applications of Silicon Phthalocyanines.

Due to their intense colour and high stability, phthalocyanines have been exploited commercially as dyes and pigments since their discovery. Moreover, different types of phthalocyanines have been used for multiple applications in numerous research fields.[61,62] In this work, we will focus on the applications of SiPcs.

SiPc derivates have unique optical, redox and electronic properties, as described previously. Their structural diversity, achieved by versatile functionalization at peripheral, non-peripheral and axial positions, allow their use in fields such as biomedicine, photovoltaics, optoelectronic and photocatalysis.

[61] a) C.C. Leznoff, A.B.P. Lever, *Phthalocyanines*, **1989**, Vols. 1–4. b) N.B. McKeown, *Phthalocyanine Mater*, **1998**.

[62] a) J. Zhao, H. Lyu, Z. Wang, C. Ma, S. Jia, W. Kong, B. Shen, *Separation and Purification Technology*, **2023**, *312*, 123404-123431. b) J. Rak, M. Kabesova, J. Benes, P. Pouckova, D. Vetvicka, *Life,* **2023**, *13*, 305-324. c) Z. Jiang, Y. Ding, J.F. Lovell, Y. Zhang, *Photoacoustics*, **2022**, *28*, 100426-100440. d) H.-g. Wang, Q. Wu, L. Cheng, L. Chen, M. Li, G. Zhu, *Energy Storage Materials*, **2022**, *52*, 495-513.

The biomedical applications of SiPcs primarily stem from their light-responsive properties, making them effective therapeutic agents against cancer,[63] antibacterial[64] and antifungal agents.[65] SiPcs have demonstrated high potential for *in vitro* and *in vivo* bioimaging due to their strong near-infrared emission.[66,67] Additionally, their intense Q-band absorption in the near-infrared region has facilitated their use in photodynamic therapy (PDT),[68] photoimmunotherapy (PIT)[69] and photothermal therapy (PTT).[70]

You's research group developed SiPcs as multifunctional drug carriers, integrating fluorescence imaging, far-red light-mediated drug release, and the combined effects of singlet oxygen-induced PDT and local chemotherapy.[71,72] To achieve this, they utilized a singlet oxygen-labile aminoacrylate bond to attach combretastatin and paclitaxel at the axial positions of SiPcs (**Figure 9**).[73,74] The drug-conjugated SiPcs exhibited lower cytotoxicity than the free drugs, with drug release triggered by light irradiation, which generated singlet oxygen to cleave the aminoacrylate linker.

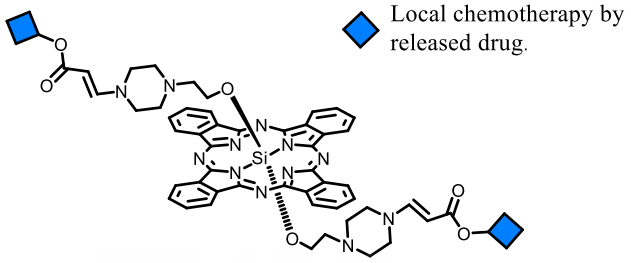

Figure 9. *Structure of SiPc carrier of drug and singlet oxygen-mediated drug release.*

SiPcs are also employed in solar cell applications, serving as additives,[75] acceptors,[76]donors,[77] and cross-linking components.[78] Their chemical and thermal stability, along with their strong absorption in the red and near-infrared regions, make them valuable materials for expanding the light-harvesting window and enhancing power conversion efficiency.

Ameri and co-workers group successfully synthesized SiPcs derivates with bulky *tert*-butyl groups at the periphery and pyrene carboxylic acid groups at the axial positions. These

[63] P.-C. Lo, M. S. Rodríguez-Morgade, R. K. Pandey, D. K. P. Ng, T. Torres, F. Dumoulin, *Chem. Soc. Rev.* **2020**, *49*, 1041–1056.

[64] M. Lam, M. L. Dimaano, P. Oyetakin-White, M. A. Retuerto, J. Chandra, P. K. Mukherjee, M. A. Ghannoum, K. D. Cooper, E. D. Baron, *Antimicrob. Agents Chemother.* **2014**, *58*, 3029–3034.

[65] A. Galstyan, R. Schiller, U. Dobrindt, *Angew. Chem. Int. Ed.* **2017**, *56*, 10362–10366.

[66] J. Mao, Y. Zhang, J. Zhu, C. Zhang, Z. Guo, *Chem. Commun.* **2009**, 908–910.

[67] W. Li, W. Dong, Q. Liu, G. Lv, M. Xie, X. Sun, L. Qiu, J. Lin, *J. Photochem. Photobiol., B* **2019**, *190*, 1–7.

[68] M. A. Hutnick, S. Ahsanuddin, L. Guan, M. Lam, E. D. Baron, J. K. Pokorski, *Biomacromolecules*, **2017**, *18*, 379–385

[69] K. Ito, M. Mitsunaga, T. Nishimura, M. Saruta, T. Iwamoto, H. Kobayashi, H. Tajiri, *Bioconjugate Chem.*, **2017**, *28*, 1458–1469

[70] X. Li, J. F. Lovell, J. Yoon and X. Chen, *Nat. Rev. Clin. Oncol.*, *2020*, *17*, 657–674

[71] A. M. L. Hossion, M. Bio, G. Nkepang, S. G. Awuah, Y. You, *ACS Med. Chem. Lett.* **2013**, *4*, 124–127.

[72] G. Nkepang, M. Bio, P. Rajaputra, S. G. Awuah, Y. You, *Bioconjugate Chem.* **2014**, *25*, 2175–2188.

[73] M. Bio, P. Rajaputra, G. Nkepang, Y. You, *J. Med. Chem.*, **2014**, *57*, 3401–3409.

[74] P. Thapa, M. Li, M. Bio, P. Rajaputra, G. Nkepang, Y. Sun, S. Woo and Y. You, *J. Med. Chem.*, **2016**, *59*, 3204–3214.

[75] S. Honda, H. Ohkita, H. Benten, S. Ito, *Chem. Commun*. **2010**, *46*, 6596–6598.

[76] M.-T. Dang, T. M. Grant, H. Yan, D. S. Seferos, B. H. Lessard, T. P. Bender, *J. Mater. Chem. A* **2017**, *5*, 12168–12182.

[77] B. H. Lessard, R. T. White, M. AL-Amar, T. Plint, J. S. Castrucci, D. S. Josey, Z.-H. Lu, T. P. Bender, *ACS Appl. Mater. Interfaces* **2015**, *7*, 5076–5088.

[78] T. M. Grant, D. S. Josey, K. L. Sampson, T. Mudigonda, T. P. Bender, B. H. Lessard, *Chem. Rec.* **2019**, 19, 1093–1112.

compounds were specifically designed for the fabrication of ternary electron acceptors in bulk heterojunction solar cells based on P3HT/PCBM.[79] The resulting devices showed a 20% increase in short-circuit current density (JSC) and a 50% improvement in power conversion efficiency compared to the reference device. This performance boost was attributed to an improved fill factor and enhanced charge carrier mobility (**Figure 10**).

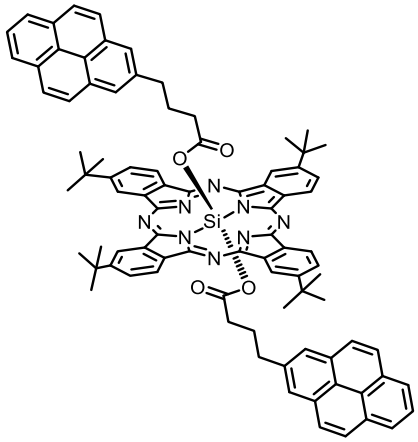

Figure 10. *Structure of bis-ester SiPc.*

Samuel and co-workers investigated the optoelectronic and electroluminescent properties of SiPcs as emitters in organic light-emitting diodes (OLEDs), leveraging their near-infrared luminescence.[80] To achieve this, they employed SiPc-i and SiPc-ii (**Figure 11**). Both SiPcs exhibited a maximum emission around 698-709 nm with a narrow full width at half maximum of 21-27 nm.

Doping the emissive layer of the device with 10% of SiPc-i resulted in a higher quality device, characterized by reduced porosity and surface roughness compared to SiPc-ii (**Figure 11**). These results indicated the crucial role of the axial ligand in the device's optoelectronic properties.

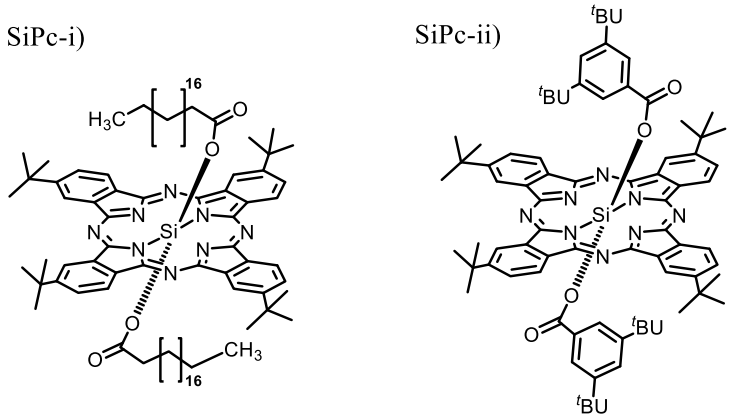

Figure 11. *Structure of bis-ester SiPc for OLED.*

[79] L. Ke, J. Min, M. Adam, N. Gasparini, Y. Hou, J. D. Perea, W. Chen, H. Zhang, S. Fladischer, A.-C. Sale, E. Spiecker, R. R. Tykwinski, C. J. Brabec, T. Ameri, *Adv. Energy Mater.* **2016**, *6*, 1502355.

[80] E. Zysman-Colman, S. S. Ghosh, G. Xie, S. Varghese, M. Chowdhury, N. Sharma, D. B. Cordes, A. M. Z. Slawin, I. D. W. Samuel, *ACS Appl. Mater. Interfaces* **2016**, 8, 9247–9253.

SiPcs also function as efficient photocatalysts due to their robust photostability, intense solar spectrum absorption tunable at the molecular level and their ability to initiate photoinduced electron transfer reactions.[81]

Previously, covalently functionalized SiPc-graphene-based organic hybrid compounds have been synthesized as enhanced solar catalysts.[82] The nitrogen-doped SiPc-graphene hybrid (N-usRGO/SiPc) demostrated strong visible light absorption.[82]The 90% quenching of SiPc fluorescence and enhanced photocurrent responses observed for N-usRGO/SiPc demonstrated an efficient photoinduced electron transfer process from SiPc to N-usRGO via covalent bonds (**Figure 12)**.

These properties were attributed to the enhanced visible light driven catalytic activity of usRGO/SiPc compared to SiPc-free N-usRGO.

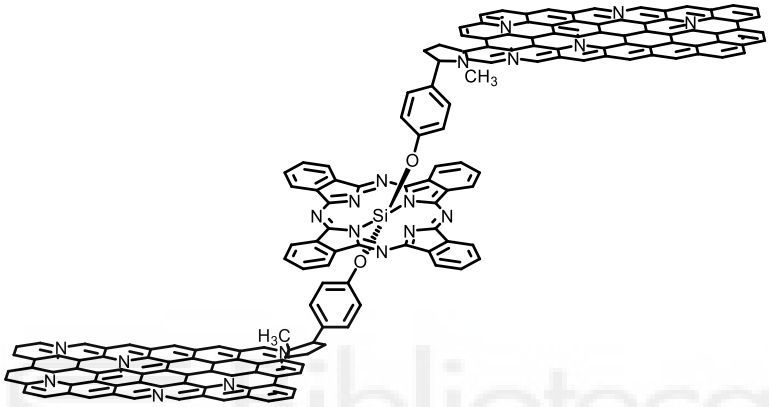

Figure 12. *Structure of N-usRGO/SiPc nanocomposites.*

[81] S. Zhu, D. Wang, *Adv. Energy Mater.* **2017**, *7*, 1700841.

[82] J. Huang, Y. Wu, D. Wang, Y. Ma, Z. Yue, Y. Lu, M. Zhang, Z. Zhang, P. Yang, *ACS Appl. Mater. Interfaces* **2015**, *7*, 3732–3741.

2. Metal-Organic Frameworks (MOFs)

Metal-Organic Frameworks (MOFs) represent a novel category of coordination materials characterized by a high crystallinity and porosity, with surface areas that can reach up to 10.000 m^2/g.[83,84] These structures are composed of organic ligands as a linker, coordinated to metal nodes through strong coordination interactions (**Figure 13**).

To form stable three-dimensional networks, linkers must feature two or more functional groups, allowing them to coordinate effectively with metal ions or metal clusters.[85] This structural design provides MOFs with the unique ability to accommodate guest molecules within their internal cavities in a temporary and reversible manner. The versatility in the selection of ligands and metals enables precise modulation of pore size,[86] making MOFs a versatile platform for diverse applications such as gas store,[87] catalysis,[88] and molecular separation. [89]

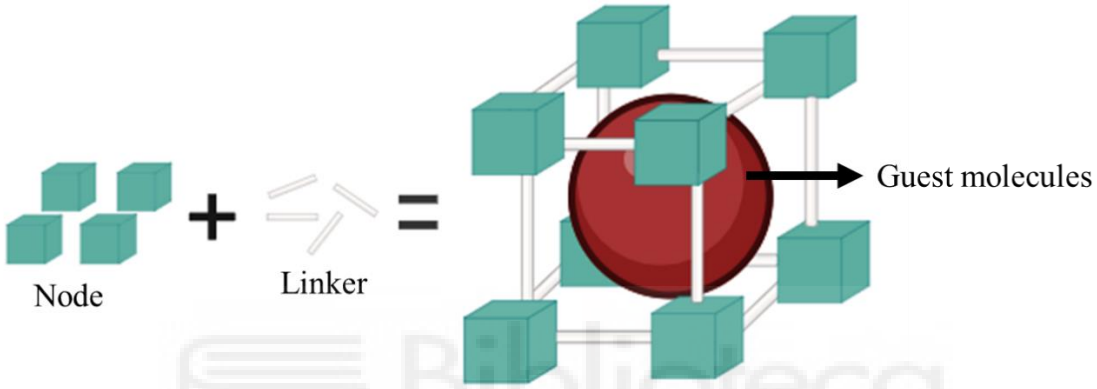

***Figure 13**. Representation of a metal-organic network or MOF.*

The term MOFs emerged in the 1990s within the field of coordination chemistry, which explores the combination of inorganic and organic components to create materials with well-defined crystalline and porous structures.

The concept of three-dimensional frameworks was introduced in 1990 by Hoskins and Robson,[90] who employed tetrahedral Cu(I) centres linked by the tetrahedral ligand 4,4',4",4'" teracyanotetraphenylmethane (TCTPM). The resulting framework adopts a diamonded network with tetragonal cavities (**Figure 14**). These three-dimensional molecular rod frameworks laid the foundation for what would later be recognized as MOFs.

[83] O. M. Yaghi, G. Li, H. Li, *Nature* **1995,** *378,* 703.

[84] X. Zhang, Z. Chen, X. Liu, S. L. Hanna, X. Wang, R. Taheri-Ledari, A. Maleki, P. Li, O. K. Farha, *Chem. Soc. Rev.* **2020**, *49,* 7406.

[85] O. M. Yaghi, *J. Am. Chem. Soc.* **2016,** *138,* 15507–15509.

[86] H. K. Chae, D. Y. Siberio-Perez, J. Kim, Y. Go, M. Eddaoudi, A. J. Matzger, M. O'Keeffe, O. M. Yaghi, *Nature* **2004,** *427,* 523

[87] R. Babarao, J. Jiang, *Langmuir* **2008,** *24,* 6270–6278.

[88] N. Huang, K. Wang, H. Drake, P. Cai, J. Pang, J. Li, S. Che, L. Huang, Q. Wang, H.-C. Zhou, *J. Am. Chem. Soc.* **2018,** *140,* 6383–6390.

[89] T. Jia, Y. Gu, F. Li, *J. Environ. Chem. Eng.* **2022,** *10,* 108300.

[90] B.F. Hoskins, R. Robson, *J. Am. Chem. Soc.* **1989**, *111*, 5962–5964.

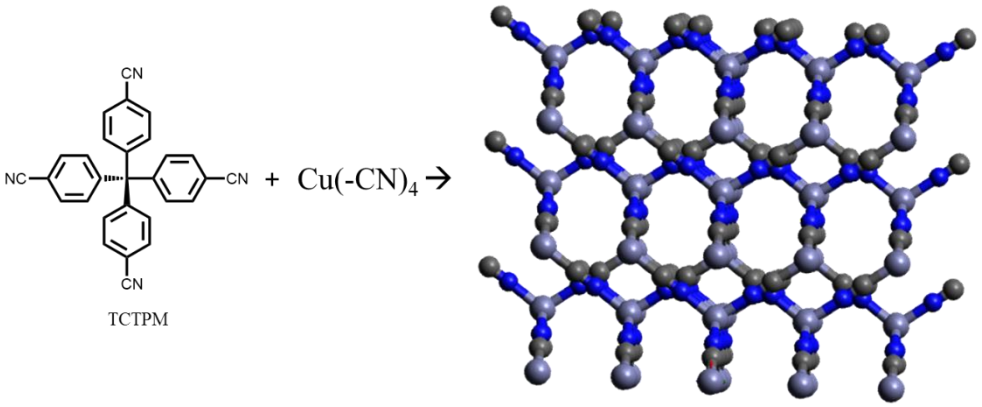

***Figure 14**. Diamonded framework of tetrahedrally coordinated Cu(I) ions linked by TCTPM as organic linker.*

However, it was not until 1995 that the term MOFs was formally introduced by Omar Yaghi and his research group.[91] They successfully synthesized a diamond network using triangular planar Cu(I) as the metal center and the 4,4'-bipyridine (4,4'-bpy) as the organic ligand (**Figure 15**). Yaghi and his group demonstrated that a rational selection of organic linkers and transition metals enables the construction of highly porous, stable, and structurally well-defined three-dimensional architectures.

These advancements marked the emergence of a new generation of highly functional materials, now known as Metal-Organic Frameworks, highlighting the critical role of coordination chemistry and molecular design in the development of these innovative materials

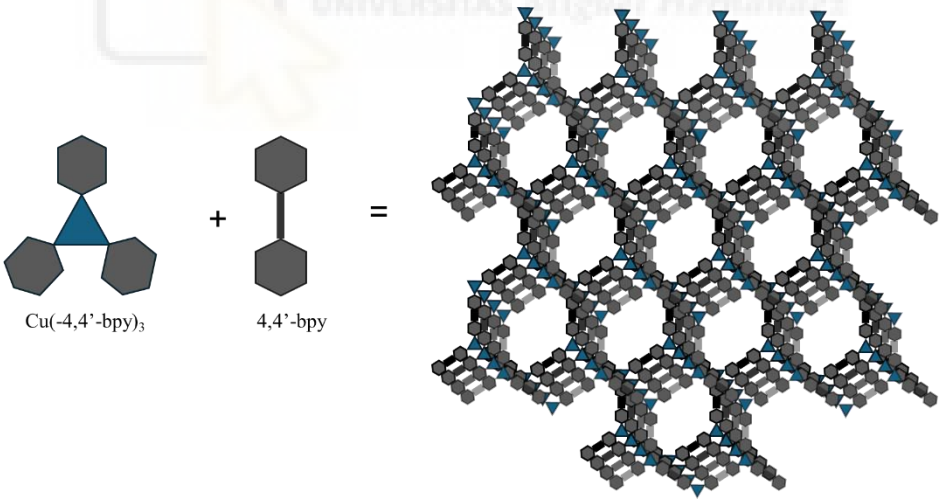

***Figure 15**. Diamonded framework of trigonal planar coordinated Cu(I) ions linked by 4,4'-bpy as organic linker.*

[91] O.M. Yaghi, H. Li, *J. Am. Chem. Soc.* **1995**, *117,* 10401.

2.1. Structural Components in MOF and their Interactions

MOFs are a highly crystalline and porous materials whose structures are defined by the interaction between metal nodes and organic linkers. The combination of these components determines the structural, chemical, and functional properties of the resulting MOF, allowing for a wide range of applications. To date, over 100,000 different MOF structures have been reported, with new variations emerging each year (**Figure 16**).[84]

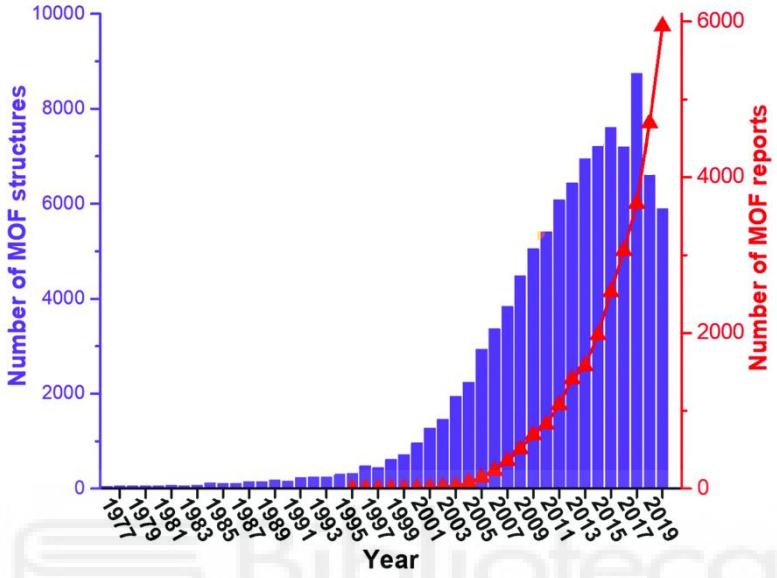

Figure 16. *Evolution of the number of MOF structures registered in the Cambridge Structural Database (CSD) and related publications found in Web of Science from 1976 to 2019. Image adapted by reference.*[2]

The election of metal significantly influences the structure, stability, and functional characteristics of the resulting material.[92] Metals act as coordination centers, linking with organic ligands to form highly ordered porous networks.[93,94] This role depends on several intrinsic characteristics, including oxidation state, ionic radius, and electronic configuration.

Transition metals, alkali metals, alkaline earth metals, and rare earth elements are commonly employed due to their ability to exhibit multiple oxidation states, which expands the possible structural geometries. For example, metals such as iron (Fe^{2+}/Fe^{3+}) or cobalt (Co^{2+}) tend to form octahedral geometries when coordinated to six ligands,[95,96] whereas zinc (Zn^{2+}) and cupper (Cu^{+}) commonly adopt tetrahedral arrangements.[97,98] Additionally, divalent cupper (Cu^{2+}), may favour square planar coordination,[99] further influencing the MOF's electronic and mechanical properties (**Figure 17**).

[92] M. Eddaoudi, D. B. Moler, H. Li, B. Chen, T. M. Reineke, M. O'Keeffe, O. M. Yaghi, *Acc. Chem. Res.* **2001,** *34,* 319–330.

[93] O. M. Yaghi, M. O'Keeffe, N. W. Ockwig, H. K. Chae, M. Eddaoudi, J. Kim, *Nature* **2003,** *423,* 705–714

[94] J. Kim, B. Chen, T. M. Reineke, H. Li, M. Eddaoudi, D. B. Moler, M. O'Keeffe, O. M. Yaghi, *J. Am. Chem. Soc.* **2001,** *123,* 8239–8247.

[95] a) T. R. Whitfield, X. Wang, L. Liu, A. J. Jacobson, *Solid State Sci.*, **2005**, *7*, 1096–1103. b) H. Wang, L. Shi, H. Cao, Z. Xiong, S. Ma, J. Pan, Z. Chen, *CrystEngComm*, **2024**, *26*, 13.

[96] S. S. Pedro, P. Brandão, F.-N. Shi, J. C. G. Tedesco, M. S. Reis, *Polyhedron*, **2014,** *81*, 210–215.

[97] M. J. Manos, E. E. Moushi, G. S. Papaefstathiou, A. J. Tasiopoulos, *Cryst. Growth Des.*, **2012**, *12*, 5471–5480.

[98] W. Zhang, B. E. G. Lucier, V. V. Terskikh, S. Chen, Y. Huang, *Chem. Sci.*, **2024**, *15*, 18.

[99] H. Zeng, X.-J. Xie, Y. Wang, D. Luo, R.-J. Wei, W. Lu, D. Li, *Chem. Sci.*, **2022**, *13*, 12876–12882.

As well, the ionic radius of the metal is another key factor in MOF design. Metals with large radii, such as rare earth elements, tend to produce MOFs with large pores, making them ideal for gas storage and molecular separation.[100,101] In contrast, small metal ions like aluminium (Al^{3+}) induce compact structures, enhancing thermal and chemical stability.[102,103]

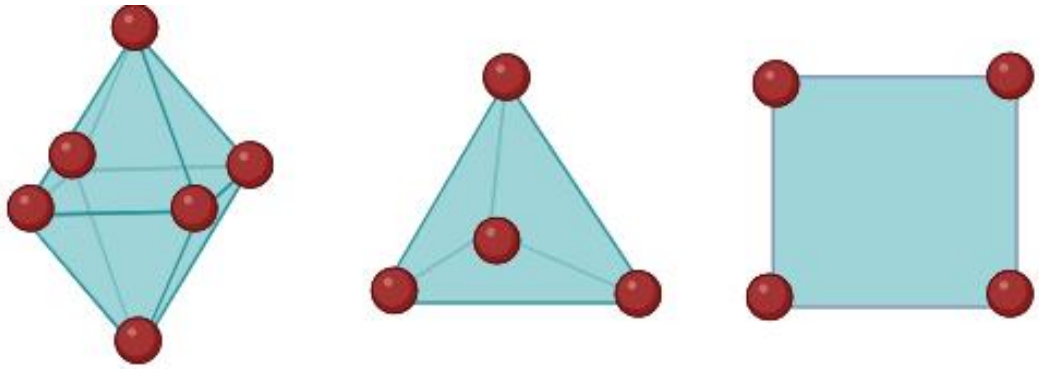

***Figure 17**. Scheme of diverse geometries structures of MOFs.*

Other determinant element in MOFs synthesis, are organic linkers (**Figure 18**) as the connecting elements between metal nodes playing a fundamental role in determining pore size, structural rigidity, and functional properties.

The length of the linker directly affects pore size. Long ligands such as 4,4'-biphenyldicarboxylic acid or phthalocyanines generate MOFs with large pores,[104,105] whereas short linkers like terephthalic acid result in MOFs with small pores and more compact structures.[106]

In a similar matter, the rigidity of the linker plays a crucial role in determining the properties of MOFs. Rigid linkers, such as planar aromatic compounds as terephthalic acid and triphenylene, often result in highly ordered and stable MOF structures.[107,108] In contrast flexible linkers, as aliphatic dicarboxylic acids, can introduce flexibility and adaptability into the MOF structures, due to rotation around C-C bonds.[108]

Likewise, the geometry of the ligand affects the spatial arrangement of the MOFs' structure. Linear ligands, present an extended and unbranched geometry, promote the formation of 1D or 2D dimensional structures. This is exemplified by MOFs constructed from linear dicarboxylic acids or polypyridines.[109,110] In contrast, branched ligands with multiple coordination

[100] B. Li, H.-M. Wen, W. Zhou, B. Chen, *J. Phys. Chem. Lett.*, **2014**, *5*, 3468–3479.

[101] E. Loukopoulos, PN Trikalitis, Eur. *J. Inorg. Chem*. **2025**, *28,* 202400606.

[102] N. Stock, *Metal-Organic Frameworks: Aluminium-Based Frameworks*, in *Encyclopedia of Inorganic and Bioinorganic Chemistry*, R. A. Scott (Ed.), Wiley, **2014**, 1–16.

[103] H. Li, X. Feng, D. Ma, M. Zhang, Y. Zhang, Y. Liu, J. Zhang, B. Wang,*ACS Appl. Mater. Interfaces.* **2018** *10*, 3160-3163.

[104] W. Zhang, H. Yin, Z. Yu, X. Jia, J. Liang, G. Li, Y. Li, K. Wang, *Nanomaterials*, **2022**, *12*, 2062.

[105] M. Wang, H. Shi, P. Zhang, Z. Liao, M. Wang, H. Zhong, F. Schwotzer, A. Shaygan Nia, E. Zschech, S. Zhou, S. Kaskel, R. Dong, X. Feng, *Adv. Funct. Mater.* **2020,** *30*, 2002664.

[106] S. Yuan, L. Huang, Z. Huang, D. Sun, J.-S. Qin, L. Feng, J. Li, X. Zou, T. Cagin, H.-C. Zhou, *J.Am. Química. Soc*., **2020**, *142*, 4732–4738.

[107] X.-L. Lv, S. Yuan, L.-H. Xie, HF Darke, Y. Chen, T. He, C. Dong, B. Wang, Y.-Z. Zhang, J.-R. Li, H.-C. Zhou, *J. Am. Chem. Soc.,* **2019**, *141*, 10283–10293.

[108] a) B. Gibbons, M. Cai, AJ Morris, *J. Am. Chem. Soc*., **2022,** *144*, 17723–17736. b) M. Jeon, J.-S. Lee, M. Kim, J.-W. Seo, H. Kim, HR Moon, S.-J. Choi, J. Kim, *ACS Appl. Mater. Interfaces*, **2024**, *16*, 62382–62391.

[109] A. López-Periago, O. Vallcorba, C. Frontera, C. Domingo, J.A Ayllón, *Dalton Trans*., **2015**, *44*, 7548-7553.

[110] F. Nie, R. Yu, L. Wang, L. Jiang, Q. Wu, W. Xu, X. Fu, *ACS Omega*, **2023**, *8*, 43463–43473.

sites allow the construction of complex three-dimensional structures, as seen in MOFs based on tri-carboxylic acids like benzene-1,3,5-tricarboxylic acid (BTC) or porphyrin.[111,112]

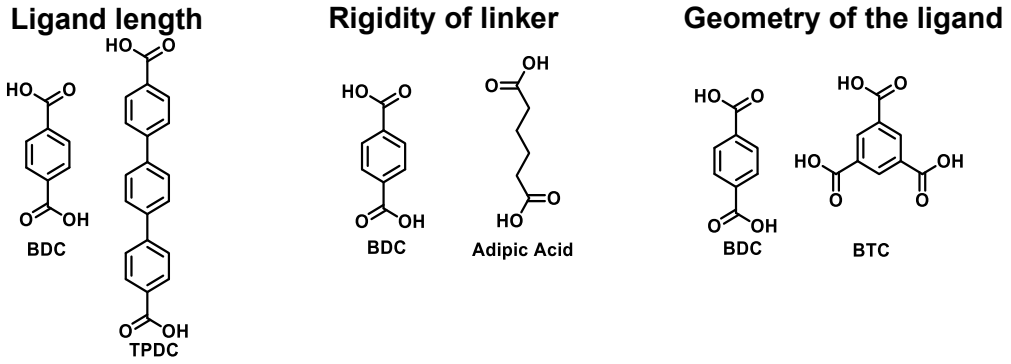

***Figure 18**. The diversity of geometry of the different ligands for MOFs.*

The chemical nature of linkers is another determining factor in the properties of MOFs. The incorporation of specific functional groups into the linkers, such as azo, amino, carboxyl, and heterocyclic groups, allows for the tuning of MOF properties (**Figure 19**). For example, linkers containing azo groups, which can coordinate with metal ions like Co^{2+} and Cu^{2+},can confer photo responsiveness, allowing control over pore opening and closing.[113] Amino groups, commonly interacting with Zr^{4+} or Al^{3+}, impart basic properties, generating MOFs appropriate for acid-base reactions.[114] Heterocyclic linkers such as imidazole and pyridine can coordinate with Cu^{2+}, Zn^{2+}, and Co^{2+}, acting as Lewis bases.[115]

Furthermore, the incorporation of linkers with semiconducting and optical properties such as phthalocyanines[116] or naphthalenediimides,[117] lets the creation of MOFs for electro-optical devices.

Once the different metal nodes and organic linkers, as well as their influence on the structural properties of MOFs, have been identified, it is essential to analyse the interactions that occur between them. In this context, functional groups play a fundamental role, as they mediate these interactions and significantly influence the final architecture of the MOF.

The most relevant interactions between linkers and nodes in MOF formation are coordinate covalent bonds. Usually, these bonds are established when functional groups in the linker donate electron pairs to the vacant orbitals of the metal node, thereby forming a stable coordination network.[118]

---

111 L. Xu, E.-Y. Choi, Y.-U. Kwon, *Inorg. Chem. Commun.*, **2008**, *11*, 1190–1193.

112 C.-M. Zeng, S.-Y. Luo, X. Wang, F.-L. Cao, Z.-S. Zhang, W.-H. Zhang, C.-L. Dai, D. J. Young, *Chem. Asian J.*, **2024**, *19*, 202400237.

113 A. B. Kanj, K. Müller, L. Heinke, *Macromol. Rapid. Commun.*, **2018,** *39*, 1700239.

114 S. Wang, M. Wahiduzzaman, L. Davis, A. Tissot, W. Shepard, J. Marrot, C. Martineau-Corcos, D. Hamdane, G. Maurin, S. Devautour-Vinot, C. Serre, *Nat. Commun.*, **2018**, *9,* 4937.

115 F.-M. Zhang, L.-Z. Dong, J.-S. Qin, W. Guan, J. Liu, S.-L. Li, M. Lu, Y.-Q. Lan, Z.-M. Su, H.-C. Zhou, J. *Am. Chem. Soc.*, **2017**, *139*, 6183–6189.

116 R. Haldar, Z. Fu, R. Joseph, D. Herrero, L. Martín-Gomis, B. S. Richards, I. A. Howard, Á. Sastre-Santos, C. Wöll, *Chem. Sci.* **2020**, *11,* 7972–7978.

117 R. Haldar, A. Mazel, R. Joseph, M. Adams, I. A. Howard, B. S. Richards, M. Tsotsalas, E. Redel, S. Diring, F. Odobel, C. Wöll, *Chem. Eur. J.*, **2017**, *23*, 14316–14322.

118 D. E. P. Vanpoucke, *J. Phys. Chem. C*, **2017**, *121*, 8014–8022.

Carboxylic acids groups are the most employed linkers for MOF synthesis due to their capacity to form stable coordinate covalent bonds. In these interactions, the oxygen atom of the carbonyl group acts as an electron donor, coordinating with metals as Zn^{2+}, Al^{3+}, and Fe^{3+}.[119]

Similarly, amine groups are frequently utilized in MOF design, functioning as Lewis bases by donating electron pairs from the nitrogen atom to metal ions such as Zr^{4+}, leading to the formation of robust coordination bonds.[120] Hydroxyl groups also serve as coordination sites, particularly with metals like Ti^{4+} and Al^{3+} while simultaneously contributing to MOF stability through the establishment of additional hydrogen bonds within the framework.[121]

In addition to these commonly used functional groups, nitrogen-containing heterocycles, such as pyridine, imidazole, and triazole, play a crucial role in MOF formation. These moieties coordinate with transition metals such as Cu^{2+}, Zn^{2+}, Fe^{2+} and Co^{2+}, acting as Lewis bases and influencing the electronic properties of the resulting materials.[122] Likewise, sulfonic acid groups introduce strong Brønsted acidity, facilitating the bond coordination with metals such as Cr^{3+} and Zr^{4+} and promoting acid-catalyzed MOF formation.[123] Similarly, phosphonate exhibit strong binding affinities toward metal centers like Al^{3+} and Zr^{4+}, yielding highly stable coordination networks.[124]

Finally, nitroxide and radical-containing groups have been explored for their ability to coordinate with metal ions such as Cu^{2+} and Mn^{2+}, leading to the formation of MOFs with intrinsic magnetic properties, expanding their potential applications in advanced functional materials.[125]

[119] a) N. L. Rosi, J. Eckert, M. Eddaoudi, D. T. Vodak, J. Kim, M. O'Keeffe, O. M. Yaghi, *Science*, **2003**, *300*, 1127–1129. b) T. R. Whitfield, X. Wang, L. Liu, A. J. Jacobson, *Solid State Sci.*, **2005**, *7*, 1096–1103. **c**) T. Loiseau, C. Serre, C. Huguenard, G. Fink, F. Taulelle, M. Henry, T. Bataille, G. Férey, *Chem. Eur. J.*, **2004**, *10*, 1373–1382.

[120] S. Wang, M. Wahiduzzaman, L. Davis, A. Tissot, W. Shepard, J. Marrot, C. Martineau-Corcos, D. Hamdane, G. Maurin, S. Devautour-Vinot, C. Serre, *Nat. Commun.*, **2018**, *9*, 4937.

[121] D. Yang, B. C. Gates, *Adv. Mater.*, **2024**, *36*, 2305611.

[122] a) Y. Cheng, A. Kondo, H. Noguchi, H. Kajiro, K. Urita, T. Ohba, K. Kaneko, H. Kanoh, *Langmuir*, **2009**, *25*, 4510–4513. b) K. S. Park, Z. Ni, A. P. Côté, J. Y. Choi, R. Huang, F. J. Uribe-Romo, H. K. Chae, M. O'Keeffe, O. M. Yaghi, *Proc. Natl. Acad. Sci. U.S.A.*, **2006**, *103*, 10186–10191. **c**) W. Wang, Z. Xiao, H. Lin, R. Wang, L. Zhang, D. Sun, *RSC Adv.*, **2016**, *6*, 16575–16580.

[123] a) S.-S. Liu, Z. Han, J.-S. Yang, S.-Z. Huang, X.-Y. Dong, S.-Q. Zang, *Inorg. Chem.,* **2020**, *59*, 396–402. b) L. Ma, L. Xu, H. Jiang, X. Yuan, *RSC Adv.*, **2019**, *9*, 5692–5700.

[124] G. K. H. Shimizu, R. Vaidhyanathan, J. M. Taylor, *Chem. Soc. Rev.*, **2009**, *38*, 1430–1449.

[125] M. G. F. Vaz, M. Knobel, N. L. Speziali, A. M. Moreira, A. F. C. Alcântara, H. O. Stumpf, J. Braz. *Chem. Soc.*, **2002**, *13*, 183–189.

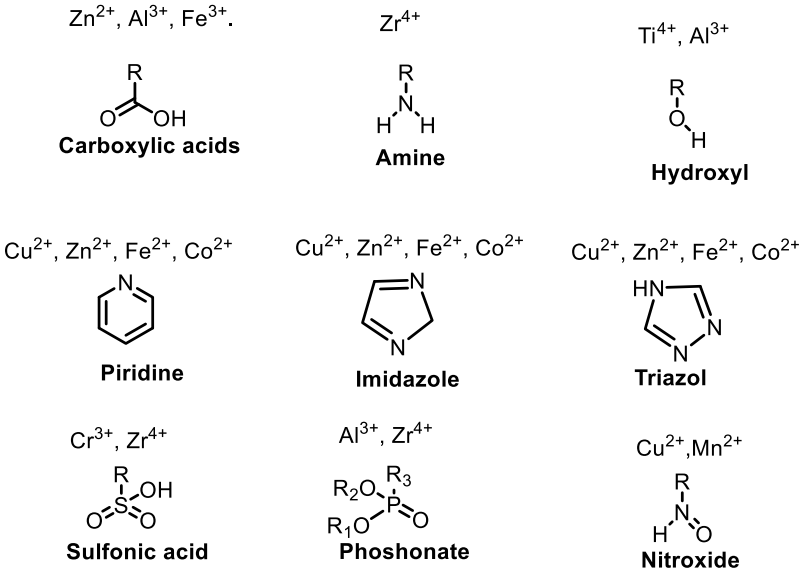

***Figure 19**. Main functional groups which interact with metals to generate MOFs.*

2.2. Methods for MOF Synthesis

The synthetic routes available for MOFs are numerous and diverse, representing an additional factor to be considered when designing and tuning their physicochemical properties. The most commonly employed approaches are outlined below.

Solvothermal synthesis: This technique offers a versatile approach of MOFs synthesis, providing control over crystal morphology. In this method, the metal salt and organic linkers are dissolved in organic solvents under elevated temperature and pressure conditions, this method allows control the pore size and the formation of highly crystalline structures. However, the high costs and specialized equipment limit its scalability for industrial.[126]

Hydrothermal synthesis: This technique for the preparation of MOFs, uses an aqueous medium in under elevated temperature and pressure conditions. This method offers versatility in MOF synthesis and benefits from the low cost and non-toxicity of solvent, it also suffers from limitations in the solubility of organic compounds and slow crystallization kinetics, which can prolong reaction times.[127]

Microwave-assisted synthesis: This method employs microwave radiation to heat solvent with metal precursors and organic linkers, producing a rapid increase in temperature and homogeneous reaction conditions. This method reduces reaction times and energy consumption compared to solvothermal and hydrotermal methods. However, the difficult to scaling up reactions and the formation of undesired products limit the use of this technique for MOF synthesis.[128]

Electrochemical deposition: This case involves immersing a conductive substrate in a solution containing the metal node and organic linker. The application of an appropriate electrical potential provokes the reduction of metal ions on the substrate surface and then react with the

[126] Y. R. Lee, J. Kim, W. S. Ahn, *Korean J. Chem. Eng.*, **2013**, *30*, 1667–1680.
[127] Y. Liang, W.-G. Yuan, S.-F. Zhang, Z. He, J. Xue, X. Zhang, L.-H. Jing, D.-B. Qin, *Dalton Trans.*, **2016**, *45*, 1382–1390.
[128] I. Thomas-Hillman, A. Laybourn, C. Dodds, S.W. Kingman, *J. Mater. Chem. A*, **2018**, *6*, 11564–11581.

ligands to form the MOF film. This method allows the control of the crystal orientation by the control of deposition conditions.[129]

Chemical Vapor Deposition (CVD): This technique involves the deposition of a solid film onto a substrate from the reaction of vapor-phase chemical precursors. In this method, the substrate is placed in a reaction chamber, and then metal and organic linkers are introduced in vapor form. These precursors react on the substrate surface, forming the MOF film. This method offers advantages such as precise control over film thickness, high purity, and large-area deposition. However, the technique also requires specialized equipment and the reaction conditions, as temperature and pressure are difficult to optimize.[130]

Heteroepitaxy: This method is a crystal growth process in which a layer of MOF is deposited onto a substrate of different crystalline composition. This way, it allows the fabrication of MOF films with specific crystalline orientations, which can influence the properties of the material and enables the functionalization of substrate surfaces with MOF properties. However, the selection of substrate can be difficult due to the requirement of a good match between MOF structures and the limited availability of suitable substrates.[131]

These synthetic strategies offer control over bulk MOF properties, but the development of thin-film MOF architectures, such as SURMOFs, has emerged as a crucial step for integrating these materials into advanced technologies.

2.3. Surface-Mounted MOF (SURMOF)

In conventional MOF synthesis, appropriate reaction conditions typically yield crystalline powders characterized by excellent structural and functional properties.[132] However, to enable the integration of these materials into more advanced technological applications, it becomes imperative to develop homogeneous and well-oriented thin-film coatings.[133] Powdered MOFs present inherent limitations, notably due to their lack of long-range crystal orientation and poor adhesion to substrates. Furthermore, the inherent surface roughness of deposited MOF powders compromises their optical clarity, which restricts their application in devices where transparency is essential, such as in optoelectronics devices.[134]

In response to these challenges, significant attention has been directed toward the development of methods for the controlled deposition of MOF films, giving rise to the concept of "*Surface-mounted Metal-Organic-Frameworks*" (**SURMOFs**) **(Figure 20.i)**.[135,136] These materials are specifically engineered to overcome the drawbacks associated with powder-based coatings, offering the possibility to fabricate homogeneous, crystalline thin films with tunable optical and electronic properties.

[129] a) D. B. Bailmare, B. V. Malozyomov, A. D. Deshmukh, *Commun. Chem*., **2024,** *7*, 178. b) N. Campagnol, T. R. C. Van Assche, M. Li, L. Stappers, M. Dincă, J. F. M. Denayer, K. Binnemans, D. E. De Vos, J. Fransaer, *J. Mater. Chem. A*, **2016**, *4*, 3914.

[130] S. Han, C. B. Mullins, *ChemSusChem*, **2020**, *13*, 5433–5442.

[131] S. Wannapaiboon, M. Tu y R. A. Fischer, *Adv. Funct. Mater*., **2014**, *24*, 2696–2705.

[132] T. Zhao, F. Jeremias, I. Boldog, B. Nguyen, S. K. Henninger, C. Janiak, *Dalton Trans.* **2015**, *44*, 16791–16801.

[133] D.-H. Chen, H. Gliemann, C. Wöll, *Chem. Phys. Rev*. **2023**, *4*, 011305.

[134] Y. Koseki, K. Okada, S. Hashimoto, S. Hirouchi, A. Fukatsu, M. Takahashi, *Nanoscale* **2024**, *16*, 15010–15017.

[135] D. Zacher, O. Shekhah, C. Wöll, R. A. Fischer, *Chem. Soc. Rev*. **2009**, *38*, 1418–1429.

[136] D. Bradshaw, A. Garai, J. Huo, *Chem. Soc. Rev*. **2012**, *41*, 2344–2381.

Two primary strategies have been established for the synthesis of SURMOFs: the top-down and bottom-up approaches (**Figure 20.ii)**.[137] Top-down methodologies involves the immobilization of pre-formed MOF crystals onto solid substrates[138] via techniques such as dip coating, spray coating, drop casting, or the Langmuir-Blodgett method.[108,139] While these techniques are relatively straightforward to implement, the resulting films often exhibit suboptimal characteristics. This is primarily due to the weak physisorption interactions between the MOF particles and the substrate,[140] which leads to poor adhesion, low surface coverage, and significant roughness, factors that severely limit their technological applicability.

In contrast, bottom-up approaches enable the direct formation of MOFs on the substrate from molecular precursors, facilitating improved control over film quality and structure.[141] This strategy allows for superior substrate adhesion, enhanced control of crystal orientation, and reduced surface roughness, thereby producing films better suited for advanced applications. Common bottom-up techniques include direct solvothermal growth,[106] electrochemical deposition,[142] and liquid-phase epitaxy layer-by-layer (LPE-LbL).[143]

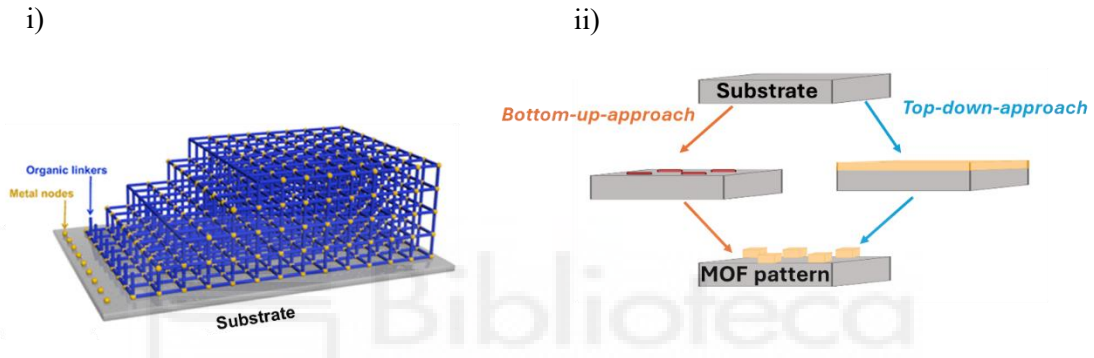

***Figure 20**. i) Scheme of SURMOF. ii) Scheme of the bottom-up and top-down patterning approaches.*

Following the discussion on synthetic strategies for the fabrication of SURMOFs, it is essential to consider two fundamental parameters that govern the successful growth of these structures: the deposition technique employed and the careful selection and preparation of the substrate.[144,104] Among these, substrate functionalization plays a critical role, as it not only ensures strong interactions between the substrate surface and the structural building units of the MOF,[145] but also promotes the oriented and uniform growth of crystalline layers an essential feature for enabling their integration into advanced functional devices.[104]

SURMOFs can be grown on a wide variety of substrates, ranging from rigid to flexible materials.[146] Planar substrates such TiO_2, fluorine-doped tin oxide (FTO), quartz, SiO_2, and Au have been widely used due to their stability and compatibility with various deposition

[137] . Falcaro, R. Ricco, C. M. Doherty, K. Liang, A. J. Hill, M. J. Styles, *Chem. Soc. Rev.* **2014**, *43*, 5513–5560.
[138] D. Zacher, R. Schmid, C. Wöll, R. A. Fischer, *Angew. Chem., Int. Ed.* **2011**, *50*, 176–199.
[139] E. V. Ermakova, A. A. Ezhov, A. E. Baranchikov, Y. G. Gorbunova, M. A. Kalinina, V. V. Arslanov, *J. Colloid Interface Sci.* **2018**, *530*, 521–531.
[140] A. L. Semrau, Z. Zhou, S. Mukherjee, M. Tu, W. Li, R. A. Fischer, *Langmuir* **2021**, *37*, 23, 7094–7106.
[141] J. Aizenberg, A. J. Black, G. M. Whitesides, *Nature* **1999**, *398*, 495–498.
[142] X. Zhang, K. Wan, P. Subramanian, M. Xu, J. Luo, J. Fransaer, *J. Mater. Chem. A* **2020**, *8*, 7569–7587.
[143] Z. Wang, C. Wöll, *Adv. Mater. Technol.* **2019**, *4*, 1800413.
[144] L. Wågberg, J. Erlandsson, *Adv. Mater.* **2021**, *33*, 2001474.
[145] O. Shekhah, H. Wang, T. Strunskus, P. Cyganik, D. Zacher, R. Fischer, C. Wöll, *Langmuir* **2007**, *23*, 7440–7442.
[146] S. M. George, *Chem. Rev.* **2010**, *110*, 111–131.

techniques.[147,148] Additionally, flexible substrates, including aluminium foil, plastic fibres, polymer films, and metal oxides, have been employed to explore the mechanical versatility of MOF films.[145,146]

Among the various strategies available for achieving uniform and oriented SURMOF growth, the layer-by-layer liquid-phase epitaxy (LPE) method has emerged as a particularly effective approach.[149,150] This technique enables the fabrication of highly crystalline films with precise control over thickness and orientation.

2.4. Layer-by-Layer Deposition Techniques for SURMOFs

Another critical step in the fabrication of SURMOFs involves the choice of an appropriate coating technique. Several liquid-phase epitaxy (LPE) based methods have been developed to produce high-quality, defect-free SURMOFs with controlled thickness, crystal orientation, and surface morphology. These approaches enable the fabrication of monolithic films with minimal porosity and cracking, key attributes for their integration into high performance devices. Among the most widely explored LPE methods are spray coating,[151] robotic dipping,[120] automated pump systems,[152] quartz crystal microbalance (QCM) method,[153] and spin coating.[154]

The spin coating method is a versatile and rapid method for depositing oriented or polycrystalline MOF thin films (**Figure 21)**.[133] It offers numerous advantages, including high throughput, short reaction times for thin film preparation, low solvent and reagent consumption relative to other LPE variants.[103] The thickness of SURMOFs can be controlled by adjusting the number of deposition cycles. This method can be automated, for example, using a spin coating system equipped with four micro-syringes. Two of these syringes contain solutions of metal precursors and linkers, while the other two contain pure solvent to remove uncoordinated metal precursors and byproducts. During the process, metal precursor and linker solutions are deposited onto the substrate at controlled time intervals, followed by spin coating at specific speeds. Deposition steps are separated by rinsing with pure solvent to ensure coating uniformity.[155] The centrifugal forces generated during rotation allow the droplets to spread homogeneously across the substrate, resulting in high-quality thin films.

147 M. C. Wasson, C. T. Buru, K. O. Kirlikovali, O. K. Farha, *Matter* **2020**, *2*, 286–287.

148 Y.-H. Xiao, Y.-B. Tian, Z.-G. Gu, J. Zhang, *EnergyChem,* **2021**, *3*, 100065.

149 S. Rana, R. Rajendra, B. Dhara, P. K. Jha, N. Ballav, *Adv. Mater. Interfaces* **2016**, *3*, 1500738.

150 M. Yao, X. Lv, Z. Fu, W. Li, W. Deng, G. Wu, G. Xu, *Angew. Chem. Int. Ed.* **2017**, *56*, 16510.

151 H. K. Arslan, O. Shekhah, J. Wohlgemuth, M. Franzreb, R. A. Fischer, C. Wöll, *Adv. Funct. Mater.* **2011**, *21*, 4228–4231.

152 H. K. Arslan, O. Shekhah, D. C. F. Wieland, M. Paulus, C. Sternemann, M. A. Schroer, S. Tiemeyer, M. Tolan, R. A. Fischer, C. Wöll, *J. Am. Chem. Soc.* **2011**, *133*, 8158–8161.

153 V. Stavila, J. Volponi, A. M. Katzenmeyer, M. C. Dixon, M. D. Allendorf, *Chem. Sci.* **2012**, *3*, 1531–1540.

154 V. Chernikova, O. Shekhah, M. Eddaoudi, *ACS Appl. Mater. Interfaces* **2016**, *8*, 20459–20464.

155 Z.-G. Gu, J. Zhang, *Coordination Chemistry Reviews* **2019**, *378*, 513–532.

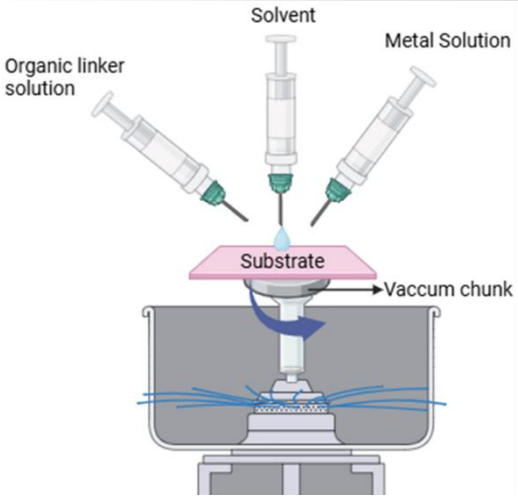

***Figure 21**. Schematic representation of spin coating.*

The spin coating technique was employed for the synthesis of HKUST-1, zeolitic imidazolate frameworks (ZIF-8), Cu_2-$(bdc)_2XH_2O$ (bdc=benzene-1,4-dicarboxylic acid) where parameters, such as solvent volume, number of cycles, and spin coating speed, could be optimized to control the final film thickness.[133]

2.5. Characterization methods

Surface characterization techniques play a fundamental role in elucidating the structural features of MOFs and SURMOFs. In this thesis, X-ray diffraction (XRD), fourier-transform infrared reflection absorption spectroscopy (FT-IRRAS), and ultraviolet-visible spectroscopy (UV-Vis) were employed.

XRD has been employed for the analysis of crystalline materials since 1912. This technique is widely used to characterize materials by providing detailed insights into the atomic arrangement of crystalline substances, including salts, metals, minerals, semiconductors, and a wide array of inorganic, organic, and biological molecules.[156] Furthermore, XRD is particularly suitable for the investigation of crystalline thin films by analysing the relative angles and intensities of the diffracted X-ray peaks.

In addition to structural identification, XRD can be employed to evaluate host guest interactions within MOF structures by comparing diffraction patterns before and after guest molecule incorporation. Variations in diffraction peaks can reveal structural changes, thereby allowing a qualitative estimation of guest molecule localization within the framework.

XRD operates on the principle that atoms in a crystalline material diffract incident X-rays in specific directions. When X-rays of a given wavelength (λ) strike a crystal at an angle (θ), diffraction occurs according to "*Bragg's Law*", which relates the interplanar spacing (d) of the crystal lattice to the diffraction angle:

$$2d.Sin\theta = \lambda$$

***Equation 1**. **λ**= wavelength; **θ** = crystal incidence angle, **d** =interplanar spacing.*

[156] Y. Waseda, E. Matsubara, K. Shinoda, *X-Ray Diffraction Crystallography: Introduction, Examples and Solved Problems*, Springer, **2011**, 67–167.

The resulting diffraction pattern is recorded as a series of peaks whose positions and intensities depend on the crystal structure. In powder XRD, the random orientation of the crystallites within the sample allows for the collection of complete diffraction data (**Figure 22).**

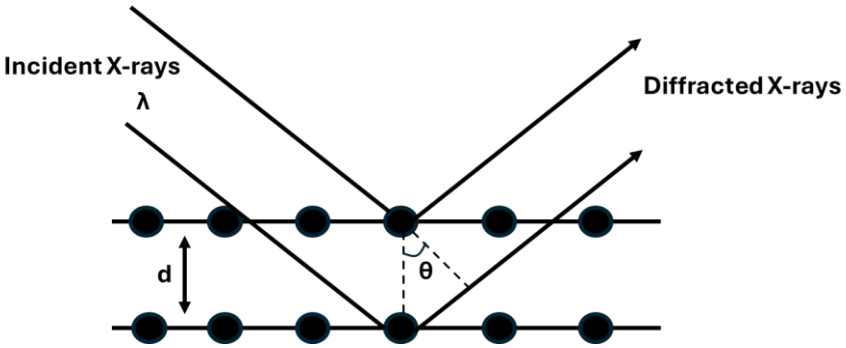

Figure 22. *Depicting X-ray diffraction in a crystal based on "Bragg's law".*

The IRRAS is another surface sensitive technique used to probe the molecular structure and bonding environment of materials by exciting vibrational modes through the absorption of infrared (IR) photons. This technique is particularly useful for identifying the presence of specific functional groups based on their characteristic absorption bands. For instance, in the context of this work, symmetric and asymmetric stretching vibrations of carboxylate groups commonly found in MOF linkers typically produce well-defined absorption peaks around 1400 and 1600 cm^{-1}.[157,158]

The most widely adopted approach for recording IR spectra today is *Fourier Transform Infrared Spectroscopy* (FTIR), which offers several advantages over traditional dispersive methods.[159,160] These include enhanced spectral resolution, improved signal to noise ratio, and significantly faster acquisition times. The core component of an FTIR system is the Michelson interferometer (**Figure 23**), which splits a broad IR beam into two optical paths and recombines them to generate constructive and destructive interference. This interference pattern, known as an interferogram, passes through the sample, where specific wavelengths are absorbed by the material. The resulting signal is then transformed via a Fourier transform to produce the final IR spectrum, which reveals the absorption characteristics of the sample.

[157] K. Saito, T. Xu, H. Ishikita, *J. Phys. Chem. B* **2022**, *126*, 4999–5006.

[158] I. Fleming, D. Williams, *Spectroscopic Methods in Organic Chemistry,* **2019**.

[159] T. Hasegawa, *Quantitative Infrared Spectroscopy for Understanding of a Condensed Matter*, **2017.**

[160] W. W. Parson, *Modern Optical Spectroscopy*, **2009**.

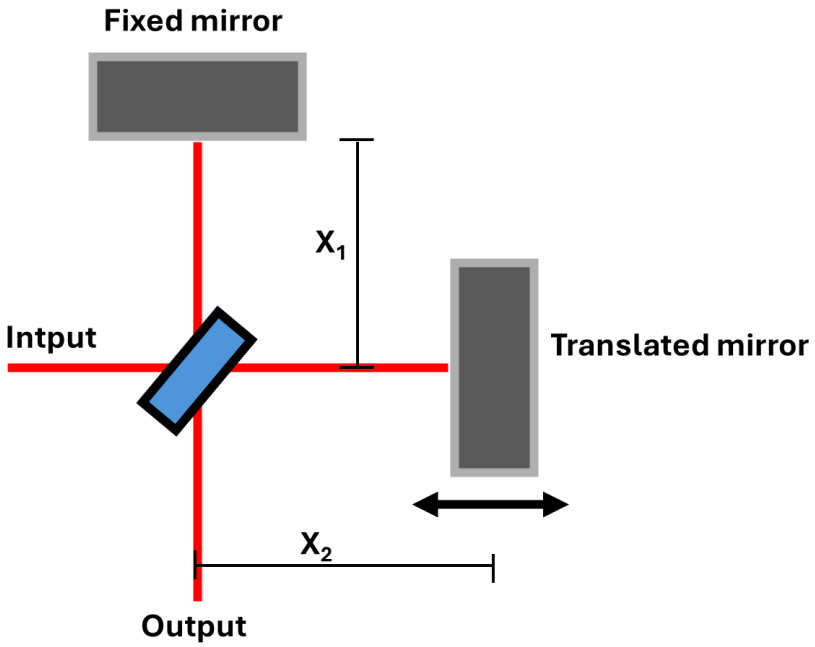

Figure 23. *Representation of a Michelson interferometer, where an incoming IR beam is split into two paths: one with a fixed optical length(x_1) and another with a variable path controlled by a movable mirror (x_2). The recombined beams interfere constructively or destructively depending on the phase shift introduced by the mirror displacement.*

In IRRAS, the IR beam is directed at the sample surface at a grazing incidence angle. This configuration maximizes the interaction between the incoming radiation and the thin film, thereby enhancing the sensitivity of the measurement to surface-bound species and molecular vibrations within the uppermost layers.

The final technique employed in this study for the characterization of SURMOFs is UV-Vis, one of the most widely used analytical methods for obtaining absorbance or reflectance spectra of materials within the UV-Vis spectral range. While this technique is commonly applied to liquid samples, it is also suitable for analysing gases and even solid materials.

UV-Vis spectroscopy is based on the electronic transitions that occur when molecules absorb radiant energy. This energy promotes electrons from the ground state to an excited state, typically involving transitions from the orbital HOMO to the orbital LUMO. The excited species formed as a result is commonly referred to as an antibonding or excited state.

A standard UV-Vis spectrophotometer setup is illustrated in **Figure 24**. In a typical double beam configuration, the incoming light is split into two separate beams before reaching the sample. One of the beams serves as a reference, representing 100% transmission (or 0% absorbance), while the other passes through the sample. The detector compares the intensity of both beams, allowing for the calculation of absorbance and the generation of a UV-Vis spectrum.

This method offers a rapid and non-destructive means of probing the optical properties of materials and, when combined with the other surface characterization techniques, provides essential insight into the structural features of SURMOFs.

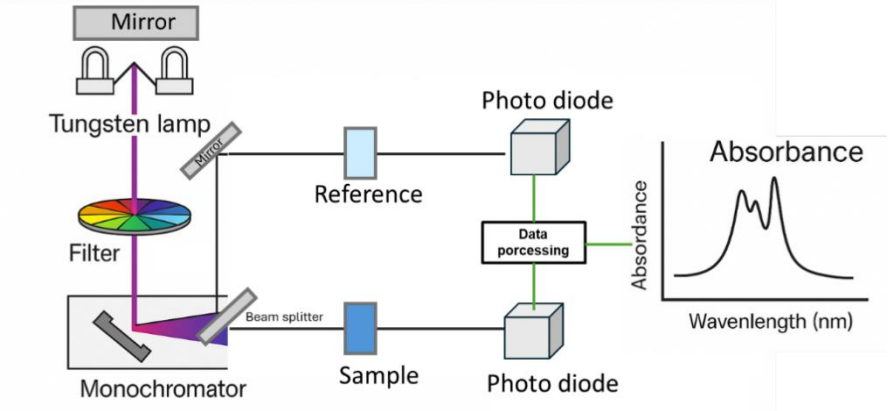

Figure 24. *Representation of UV-Vis spectrophotometer, showing the main components of the system: tungsten lamps, monochromator, sample and reference cells, detector, and signal processor.*

BACKGROUND

1. Silicon Phthalocyanines

Silicon phthalocyanines, as previously mentioned, have demonstrated remarkable versatility across various applications. A study conducted by our research group focused on a silicon phthalocyanine axially functionalized with 4-hydroxy-4-nitroazobenzene groups (**Figure 25**).[161] This compound represented the first reported silicon-azobenzene conjugate and was significant due to its ability to be modulated by light, stemming from the interaction between the azo group and the phthalocyanine core.

In this system, fluorescence emission is governed by the isomerization state of the azo group. Upon irradiation in the π-π* (300-420 nm) or n-π* (450-500 nm) regions, a decrease in the B band was observed, accompanied by an increase in the 400-500 nm region, while the Q band remained unchanged. These spectral changes indicate an *E* to *Z* isomerization, directly influencing the compound's optical properties. Moreover, in the *Z* isomerized state, fluorescence was reduced but could be restored upon reversing the isomerization. This reversible and photomodulable behaviour remained stable over multiple cycles, highlighting the robustness of the photoinduced process.

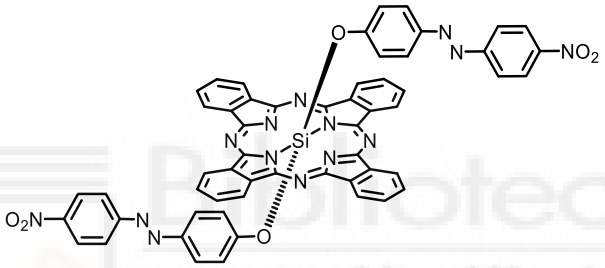

Figure 25. Structure of SiPc-(OArAzoNO$_2$)$_2$

Another relevant example of axial substitution in SiPcs from the research group of Dr. Ángela Sastre-Santos involves the investigation of the influence of donor-acceptor distance in multicomponent systems based on silicon phthalocyanines axially functionalized with C_{60} fullerene units.[162]

In this study, two novel dyads, C_{60}-SiPc-C_{60} **1** and **2**, were synthesized and fully characterized. These dyads differ in the length of the spacer connecting the SiPc core to the fullerenes: dyad **1** incorporates a phenylene spacer, whereas dyad **2** features a long biphenylene linker, increasing the donor-acceptor distance by approximately 4.3 Å (**Figure 26**).

Photophysical studies revealed a clear dependence between the structural distance and the efficiency of the photoinduced electron transfer process. Dyad **1** exhibited a charge separation rate constant (k_{cs}) of 2.7×10^9 s^{-1} significantly higher than that of dyad **2**, which was determined to be 9.1×10^8 s^{-1}. This difference confirms that increasing the donor-acceptor distance slows down the charge separation process.

These findings highlight the critical role of molecular design in donor-acceptor systems, demonstrating that even small structural modifications can have a pronounced impact on the rate and efficiency of electron transfer.

---

[161] J. L. Rodríguez-Redondo, Á. Sastre-Santos, F. Fernández-Lázaro, D. Soares, G. C. Azzellini, B. Elliott, L. Echegoyen, *Chem. Commun*. **2006**, 1265.

[162] L. Martín-Gomis, S. Seetharaman, D. Herrero, P. A. Karr, F. Fernández-Lázaro, F. D'Souza, Á. Sastre-Santos, *ChemPhysChem* **2020**, *21*, 2254–2262.

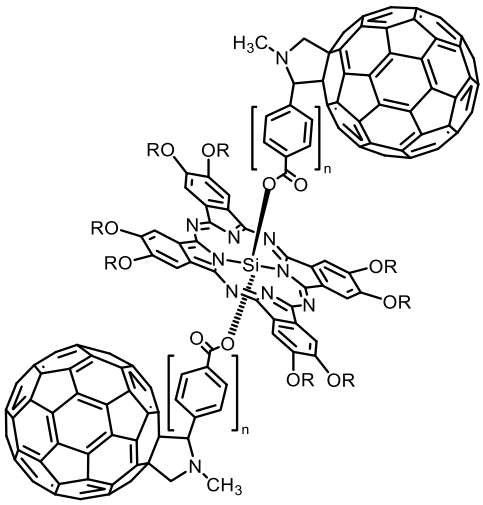

***Figure 26**. Structure of C_{60}-SiPc-C_{60}.*

Another significant contribution from the research group of Dr. Ángela Sastre-Santos in the field of axially functionalized SiPcs is the synthesis and characterization of three bisperylenediimide-SiPc triads [$(PDI)_2$-SiPc **1**, **2**, and **3**], in which perylenediimide (PDI) fragments are connected to the SiPc core via rigid or flexible linkers.[163] (**Figure 27**).

Notably, triad **3** was prepared using a novel synthetic strategy based on click chemistry, affording the target compound in a remarkable yield of 80 %. In triad **1**, the PDI and SiPc units are connected orthogonally through a rigid spacer, whereas triads **2** and **3** feature aliphatic flexible linkers, leading to inclined (**2**) or nearly parallel (**3**) arrangements between donor and acceptor units.

Photophysical analysis revealed the occurrence of intramolecular photoinduced electron transfer processes, which were investigated and compared with reference compounds by means of time resolved emission and transient absorption spectroscopy. Charge separated (CS) states were observed in all three triads, with lifetimes of 0.9, 1.3, and 2.0 ns for triads **1**, **2**, and **3**, respectively, as determined by femtosecond laser flash photolysis.

A particularly relevant finding was the effect of $Mg(ClO_4)_2$, which significantly increased the lifetime of the CS states to 59 μs (**1**), 110 μs (**2**), and 200 μs (**3**). This enhancement is attributed to a reduction in the CS state energy ($SiPc^{+}$-PDI^{-}/Mg^{2+}), which falls below the energy of the individual triplet excited states (^{3}SiPc*-PDI and SiPc^{3}PDI*), thus decoupling the charge recombination process and prolonging charge separation.

These results highlight the crucial role of spacer rigidity and donor-acceptor orientation in modulating the efficiency of photoinduced electron transfer events.

[163] F. J.Céspedes-Guirao, L. Martín-Gomis, K. Ohkubo, S. Fukuzumi, F. Fernández-Lázaro, Á. Sastre-Santos, *Chem. Eur. J*. **2011**, *17*, 9153–9163.

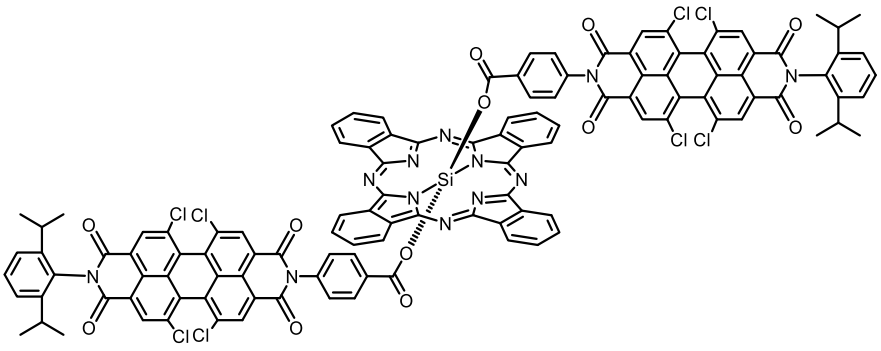

***Figure 27**. Structure of triad PDI-SiPc- PDI 1.*

Beyond axial functionalization, another pivotal strategy in SiPc synthesis has been the incorporation of distinct groups as pyridine at the periphery. This structural modification followed by their methylation, has significantly improved water solubility and enhanced antimicrobial activity, thereby broadening the scope of SiPc applications in biomedicine and antimicrobial surface treatments (**Figure 28**).[164] In this research, toxicity studies conducted in the absence of light demonstrated that this SiPc exhibited no cytotoxic effects up to a 75% cell concentration, supporting its potential biocompatibility for therapeutic applications. Although *in vitro* limited cellular absorption, experimental data nonetheless showed that this SiPc effectively induced complete inactivation of *Candida albicans* when applied at low concentrations under low-intensity light irradiation.

These findings suggest that, despite its limited cellular absorption, the high-water solubility of this SiPc ensures efficient circulation in aqueous media, facilitating its interaction with microbial cells and significantly enhancing its antimicrobial efficacy.

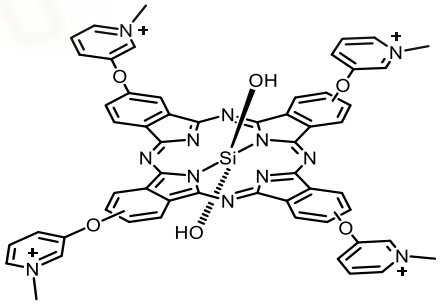

***Figure 28**. Structure of $(Py^{+}O)_4$-SiPc-$(OH)_2$.*

In line with these advances, Torres and co-workers synthesized a series of silicon phthalocyanines bearing pyridinium groups at the periphery and bulky axial substituents, specifically designed to overcome the limitations of water solubility and aggregation.[165] These derivatives, functionalized with eight *N*-methylpyridyloxy substituents and stabilized by sterically demanding axial ligands, exhibited excellent solubility in aqueous media, high singlet oxygen quantum yields, and negligible dark cytotoxicity. Importantly, they proved highly effective in the photodynamic inactivation of Gram-positive bacteria such as *Staphylococcus aureus* and methicillin-resistant *Staphylococcus aureus*, while showing more limited activity against

[164] V. Mantareva, I. Angelov, V. Kussovski, R. Dimitrov, L. Lapok, D. Wöhrle, *Eur. J. Med. Chem.* 2011, **46**, 4430.

[165] E. van de Winckel, B. David, M. M. Simoni, J. A. González-Delgado, A. de la Escosura, A. Cunha, T. Torres, *Dyes Pigm.* 2017, **145**, 239.

Escherichia coli. These findings underscore the potential of cationic SiPcs as photosensitizers for antimicrobial photodynamic therapy. The structure of hydroxy phthalocyanines is shown in **Figure 29**.

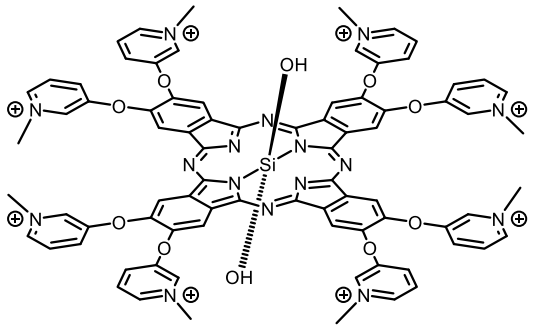

***Figure 29**. Structure of $(Py^{+}O)_8$-SiPc-$(OH)_2$.*

2. Phthalocyanines in MOFs

Beyond their diverse applications, phthalocyanines can be further functionalized and incorporated into advanced materials such as Metal-Organic Frameworks (MOFs), expanding their potential in optoelectronic and catalytic applications. MOFs represent a class of highly crystalline and porous coordination materials characterized by their exceptionally large surface areas.[166,167]

Within this framework, phthalocyanines have emerged as promising candidates for integration into MOF architectures, not only due to their conjugated structure but also because of their ability to form aggregated or crystalline arrangements. Their incorporation as organic linkers allow for precise modulation of π-interactions (HOMO-LUMO), which modulate their optical properties such as absorption, emission, and J-type aggregation.[168]

These features make the phthalocyanines an important element in the development of advanced MOF-based materials with tunable electronic and optical properties,[169] opening new avenues for the design of functional materials for applications in organic photovoltaics, photosensors, and other optoelectronic devices.

Despite their potential, the incorporation of phthalocyanines into MOFs remains relatively underexplored, with only a few examples reported in the literature. In 2018, Pingwu Du's research group successfully utilized phthalocyanines as linkers in the synthesis of a two-dimensional MOF.[170] In this study, nickel phthalocyanines, functionalized at the periphery with amino groups, were employed as bridging units, coordinating with nickel atoms that served as structural nodes within the MOF. The phthalocyanine core not only acted as a structural component but also functioned as a catalytic center for the oxygen evolution reaction due to its capacity to generate reactive oxygen species (ROS). The results of this work demonstrated that phthalocyanines can form crystalline MOF structures (**Figure 30**).

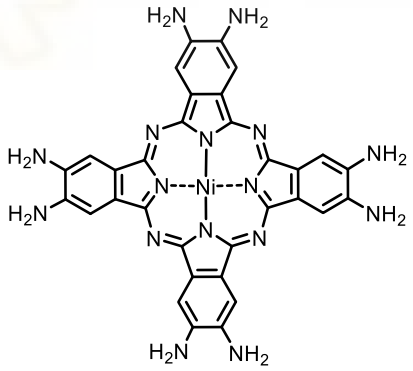

Figure 30. Structure of NiPc

Further expanding on this concept, Nobuo Kimizuka's research group developed another two-dimensional MOF (Cu-CuPc), incorporating copper phthalocyanines functionalized with hydroxyl groups at their periphery (**Figure 31**). This MOF was subsequently employed as a cathode material in lithium-ion batteries, where it exhibited both efficient ion transport and

166 O. M. Yaghi, G. Li, H. Li, *Nature* **1995,** *378,* 703.

167 X. Zhang, Z. Chen, X. Liu, S. L. Hanna, X. Wang, R. Taheri-Ledari, A. Maleki, P. Li, O. K. Farha, *Chem. Soc. Rev*. **2020**, *49,* 7406.

168 M.L. Alfieri, L. Panzella, O. Crescenzi, A. Napolitano, M. d'Ischia, Eur. J. *Org. Chem*. **2021**, *18*, 2519–2532.

169 S. Shimizu, N. Kobayashi. *Chem. Sci. Electron. Syst.* **2015**, 273–291.

170 H. Jia, Y. Yao, J. Zhao, Y. Gao, Z. Luo, P. Du, *J. Mater. Chem. A* **2018**, *6*, 1188–1195.

enhanced durability.[171] The combination of redox activity and intrinsic conductivity highlights its potential for energy storage applications, further illustrating the versatility of phthalocyanine-based MOFs in advanced energy devices.

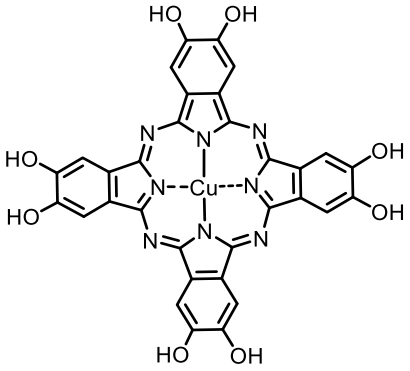

Figure 31. *Structure of CuPc.*

One of the most recent studies in this field is the work conducted by the research groups of Professors Christof Wöll and Stefan Bräse. This study reports, for the first time, an ABAB linker based on zinc phthalocyanine (Zn-Pc), specifically designed to avoid statistical condensation and to enable the controlled formation of ditopic linkers in MOFs. These linkers were used for the layer-by-layer growth of SURMOFs, generating highly ordered structures through zinc paddle-wheel nodes[172] **(Figure 32**).

The structure of the resulting Zn-ZnPc SURMOF revealed a rare triclinic arrangement, in contrast to the typical orthorhombic symmetry observed in MOFs constructed from ditopic carboxylate linkers.[173] This deviation is attributed to the steric influence of bis(trifluoromethyl)phenyl substituents, which induce a significant distortion in the phthalocyanine core, resulting in a saddle-shaped conformation. The minimum spacing between adjacent isoindole units was approximately 7.5 Å, and short F-F intermolecular contacts (~2.7 Å) were observed, promoting a uniform tilt of the chromophores.

UV-Vis spectroscopic analysis revealed a pronounced bathochromic shift of up to 110 nm in the first absorption band, comparing the free Zn-Pc molecule in solution (747 nm) with its distorted conformation within the SURMOF (861 nm).

Finally, the structure was validated by X-ray diffraction, showing close agreement between experimental and theoretical data. For the (100) plane, the experimental 2θ value was 2.67° (d-spacing = 33.05 Å), compared to a calculated value of 2.69° (d-spacing 32.72 Å).

This work highlights the potential of ABAB type phthalocyanine based SURMOFs for applications in optoelectronics and sensing.

[171] H. Nagatomi, N. Yanai, T. Yamada, K. Shiraishi, N. Kimizuka, *Chem. Eur. J.* **2018**, *24*, 1806–1810.

[172] L. S. Langer, M. Stahlberger, X. Liu, Y. Luo, N. E. Häußermann, P. Singhvi, Y. Liu, O. Fuhr, M. Nieger, L. Heinke, T. Heine, C. Wöll, S. Bräse, *Adv. Funct. Mater.* **2025**, *34*, 2401693

[173] R. Haldar, Z. Fu, R. Joseph, D. Herrero, L. Martín-Gomis, B. S. Richards, I. A. Howard, A. Sastre-Santos, C. Wöll, *Chem. Sci.* **2020**, *11,* 7972–7978.

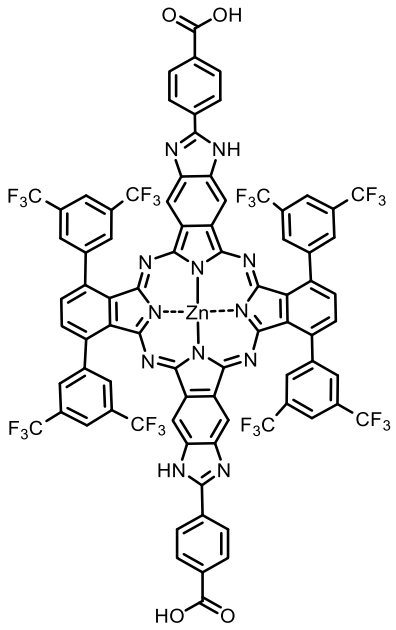

Figure 32. *Structure of ZnPc.*

A particularly relevant precedent to this study is the synthesis of an axially functionalized silicon phthalocyanine bearing two carboxylic acid groups, which served as a linker in the fabrication of SURMOFs using Zn as the coordinating metal node **(Figure 33)**. This research, conducted by Professor Ángela Sastre-Santos' group in collaboration with Professor Wöll's group, demonstrated the viability of integrating silicon phthalocyanines into MOF architectures.[116]

This phthalocyanine **(SiPc-(CO_2H)$_2$)** was embedded within an optical microcavity, giving rise to a novel porous electro-optical material capable of generating quantum electrodynamical (QED) effects, a feature with significant implications for advanced materials science. These QED effects arise when a light beam of a specific wavelength enters the microcavity, inducing coupling between the electronic states of the SiPc molecules and the intrinsic resonance modes of the cavity. This interaction leads to a splitting of the material's polarization levels (cavity + SURMOF). Furthermore, the porous nature of the system enables selective absorption of guest molecules based on pore size, leading to measurable variations in the splitting intensity. This phenomenon can be harnessed for the fabrication of ultrasensitive, nano-structured optical sensors, with potential applications in high-precision detection technologies.

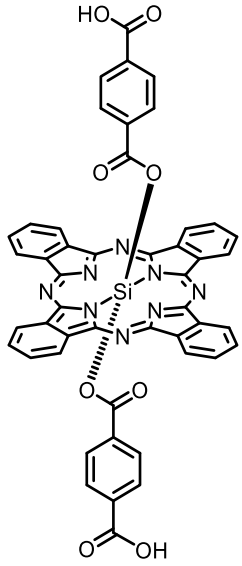

Figure 33. *Structure of axial substituted* ***SiPc-(CO$_2$H)$_2$.***

OBJECTIVES

Chapter 1: Synthesis of Silicon Phthalocyanines with Donor and Acceptor Substituents in the Peripheral Positions for the Generation of SURMOFs.

As mentioned in the introduction, the donor-acceptor properties of phthalocyanines can be modulated by their peripheral substituents. Building on the background described earlier, our research group, in collaboration with Prof. Christof Wöll, successfully synthesised an axially substituted silicon phthalocyanine for the development of a SURMOF.

Expanding on this successful collaboration, this study aims to design and synthesize six new silicon phthalocyanines functionalized in the peripheral positions with electron-donating groups, such as 2,6-dimethylphenoxy and *p*-methylthiophenoxy, as well as electron-accepting groups, like 2,6-dichlorophenoxy, aiming to fine-tune their electronic properties.

Among these six phthalocyanines, two will incorporate biphenyl axial groups, allowing for the design of SURMOFs with large structural units. Additionally, four reference phthalocyanines functionalized with 4-methylbenzoyl groups in the axial position will be synthesized for comparative characterization. By strategically designing these phthalocyanines, this work aims to explore their potential in developing SURMOFs with tailored architectures and tunable properties, such as charge and energy transfer. The target structures of these newly designed phthalocyanines are depicted in **Figure 34**.

Following the synthesis and full characterization of these compounds, the next objective will focus on integrating the most promising SiPcs into well-ordered SURMOF architectures. This will enable a systematic evaluation of how their molecular design influences thin-film formation.

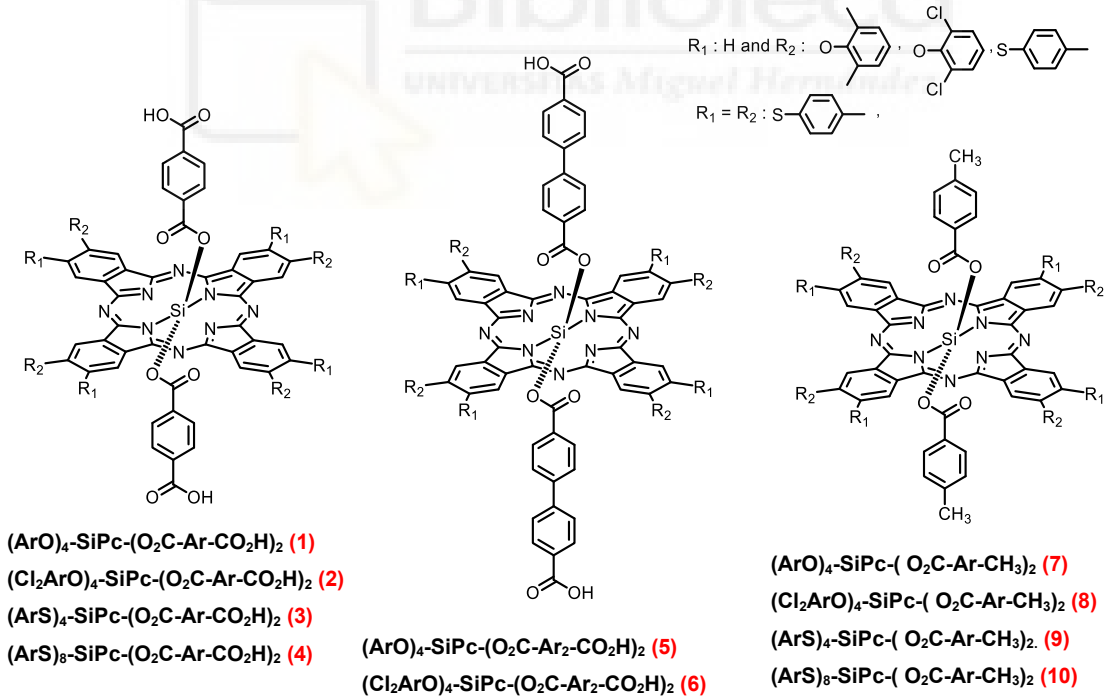

Figure 34. *Target SiPcs with peripheral electron-donating and electron-acceptor groups.*

Once the target molecules are synthesized, the fabrication and characterization of SURMOFs based on the previously obtained SiPcs will be explored, taking advantage of their structural versatility and photophysical properties. A primary objective will be the synthesis of oriented thin films using the spin-coating technique method discussed in the introduction and selected for its high deposition rate, film uniformity, and scalability (**Figure 35).** Deposition

parameters such as spin speed, solution volume, and number of cycles will be systematically optimized for each SiPc to ensure the controlled growth of homogeneous films with tunable thickness.

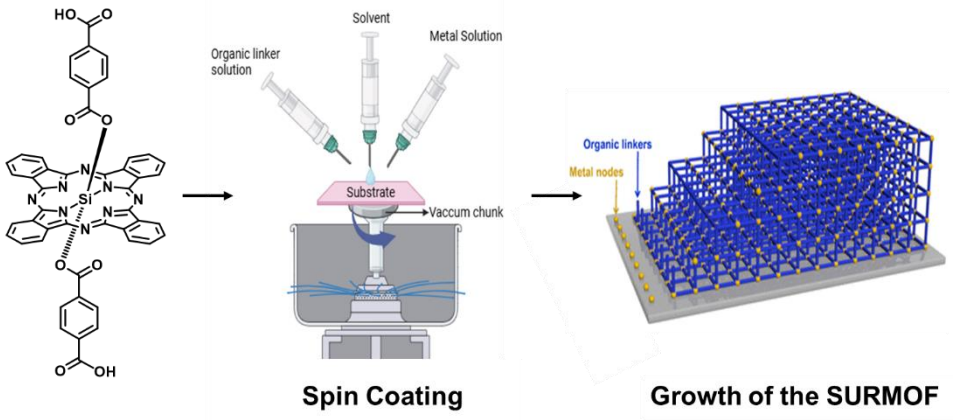

Figure 35. *Schematic representation of SURMOF growth by spin coating.*

Subsequently, the structural characterization of the resulting SURMOFs will be performed. Building on the knowledge previously established by the research group of Prof. Christof Wöll, as described in the **background section**, the crystallinity and molecular organization of the films will be assessed by XRD, confirming *out-of-plane* orientations.

To complement the structural analysis, comprehensive spectroscopic characterization will be conducted. FT-IRRAS spectroscopy will confirm the coordination and assembly of the metal-organic framework, while UV-Vis spectroscopy will reveal potential bathochromic shifts in the Q band, indicative of J-type aggregation due to the ordered arrangement of SiPc chromophores within the SURMOF matrix.

The insights gained from these donor-acceptor systems provided the basis for investigating alternative linker designs, enabling the expansion of structural diversity in the subsequent studies

Chapter 2: Synthesis of Silicon Phthalocyanines with Azo and Pyridine Substituents in the Axial Positions for the Generation of SURMOFs.

In parallel with the development of the first series of SURMOFs described in **Chapter 1**, this part of the work focuses on designing silicon phthalocyanines with new functional groups to explore alternative linker combinations and expand the range of structures and properties achievable in SURMOFs.

Continuing from the background studies described, the synthesis of two silicon phthalocyanines axially functionalized with (*E*)-4-[(4-hydroxyphenyl)diazinyl]benzoic acid groups is proposed to introduce new functionalities and applications in SURMOF-based devices. The inclusion of azo groups will enable the exploitation of their photoisomerization properties, allowing the resulting materials to exhibit light-responsive behaviour. In addition, one of these phthalocyanines will incorporate *tert*-butyl groups at the periphery, to enhance solubility during

the SURMOF synthesis process. This design aims to develop smart, responsive systems. The structures of these newly designed phthalocyanines are illustrated in **Figure 36**.

The next target phthalocyanine will incorporate a pyridine group at the axial positions. This modification is based on the previously described **SiPc-$(CO_2H)_2$**,[116] and the aim is to investigate whether SURMOF formation is possible with this functional group. Additionally, the study will assess whether this modification induces structural changes or variations in its properties.

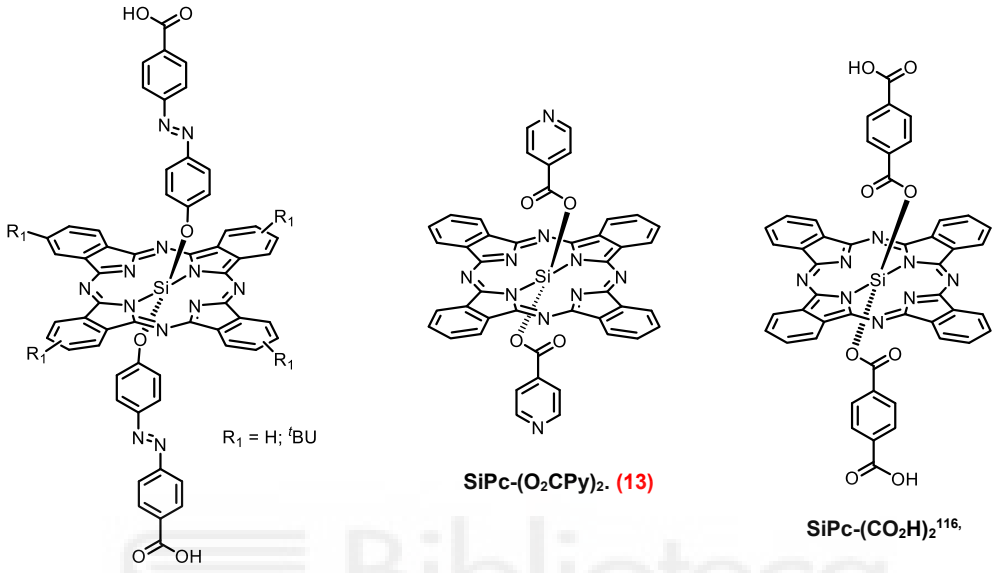

SiPc-$(O_2CPy)_2$. (13)

SiPc-$(CO_2H)_2$[116]

SiPc-(O-Ar-Azo-Ar-$CO_2H)_2$. (11)

(^{t}Bu)$_4$SiPc-(O-Ar-Azo-Ar-$CO_2H)_2$. (12)

Figure 36. *Target SiPcs with complex axial groups.*

Following the synthesis of the target molecules, the subsequent objective, consistent with the approach established in **Chapter 1**, will be the fabrication of SURMOF thin films. The structural order and crystallinity of the resulting materials will be assessed by XRD, while their spectroscopic properties will be evaluated by FT-IRRAS and UV-Vis spectroscopy.

The results obtained from the azo- and pyridine-functionalized systems opened the possibility of combining photochemical responsiveness and structural versatility with additional functionalities.

Chapter 3: Synthesis of Water Soluble Silicon Phthalocyanines for the Generation of SURMOFs.

In parallel with the studies described in **Chapters 1** and **2**, this final objective explores an alternative linker design aimed at combining water solubility, broadening the range of applications for SURMOFs developed in this work.

The final objective will focus on the synthesis and characterization of two silicon phthalocyanine mesylate salts, functionalized with biphenyl axial groups. As previously noted in the background, peripheral modifications of pyridines with methylation of these groups increases water solubility. Furthermore, the incorporation of axial substituents with carboxylic acid groups will make them ideal candidates for the synthesis of SURMOFs that integrate these functionalities. Additionally, one reference phthalocyanine functionalized with 4-methylbenzoyl groups in the axial position will be synthesized for comparative characterization. The structures of these phthalocyanines are depicted in **Figure 37**.

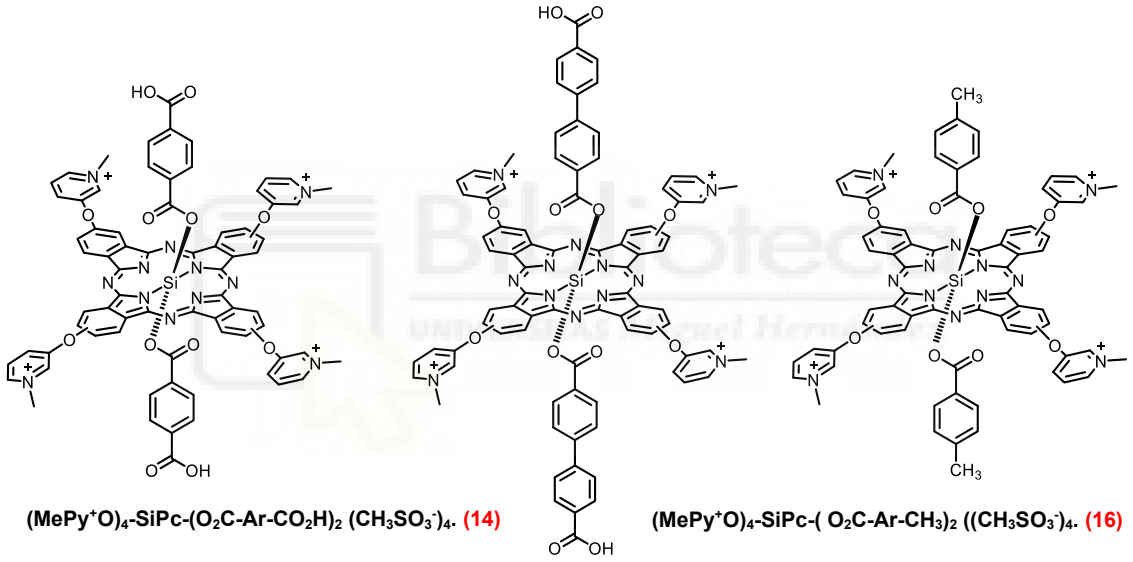

$(MePy^+O)_4$-SiPc-$(O_2C$-Ar-$CO_2H)_2$ $(CH_3SO_3^-)_4$. (14)

$(MePy^+O)_4$-SiPc-$(O_2C$-Ar_2-$CO_2H)_2$ $(CH_3SO_3^-)_4$. (15)

$(MePy^+O)_4$-SiPc-$(O_2C$-Ar-$CH_3)_2$ $((CH_3SO_3^-)_4$. (16)

Figure 37. *Target water soluble SiPcs.*

Following the synthesis of the target molecules, the subsequent objective, consistent with the approach established in **Chapter 1**, will be the fabrication of SURMOF thin films. The structural order and crystallinity of the resulting materials will be assessed by XRD, while their spectroscopic properties will be evaluated by FT-IRRAS and UV-Vis spectroscopy.

Chapter 1:

Synthesis of Silicon Phthalocyanines with Donor and Acceptor Substituents in the Peripheral Positions for the Generation of SURMOFs.

1.Results and Discussions

1.1.Silicon Phthalocyanines with Donor and Acceptor Substituents for SURMOFs.

A general synthetic procedure of the preparation of the different substituted SiPcs is described in **Scheme 1.**

The first step involves the synthesis of the precursor molecules, the first of these being phthalonitrile. Depending on the desired structure, 4-nitrophthalonitrile (R_1=H; R_2=NO_2) or 5,6-dichlorophthalonitrile (R_2=R_1=Cl) is used, which determines the number (4 or 8) of peripheral substituent groups. In the case of molecules with 8 peripheral substituents, lower yields are observed probably due to increased steric hindrance. The reaction is carried out in the presence of different substituted phenol or thiophenol reagents in an alkaline medium, where the deprotonated nucleophilic groups substitute the chlorine or nitro groups through a nucleophilic aromatic substitution, generating the desired functionalized phthalonitrile.

The next step is the ammoniation of the phthalonitriles to obtain diiminoisoindolines. This is achieved by dissolving the precursor compound in methanol, adding sodium methoxide, and exposing the mixture to a stream of gaseous ammonia. In this step, it was observed that the electronegativity of the substituents and steric hindrance play a crucial role, with shorter reaction times and higher yields for peripheral substituents that donate electrons. This is probably due to the increased electronic density in the aromatic ring, which facilitates nitrile activation for nucleophilic addition and subsequent cyclization. Additionally, substituents with lower steric hindrance favour the reaction by allowing greater accessibility.

The synthesis of phthalocyanines begins with the formation of dichlorophthalocyanine precursors through the cyclotetramerization of the corresponding diiminoisoindoline in the presence of $SiCl_4$ as a central agent. The reaction is carried out in quinoline under reflux. This process must be protected from light to prevent the degradation of precursors.

Axial functionalization is achieved through nucleophilic substitution of the axial chlorine atoms in dichlorophthalocyanine, using mostly as reagents formyl aryl carboxylic acids. This step is carried out in a microwave reactor. Subsequently, the aldehyde groups are oxidized to carboxylic acid with the objective to obtain ditopic phthalocyanines, suitable as ligands in the formation of SURMOFs.

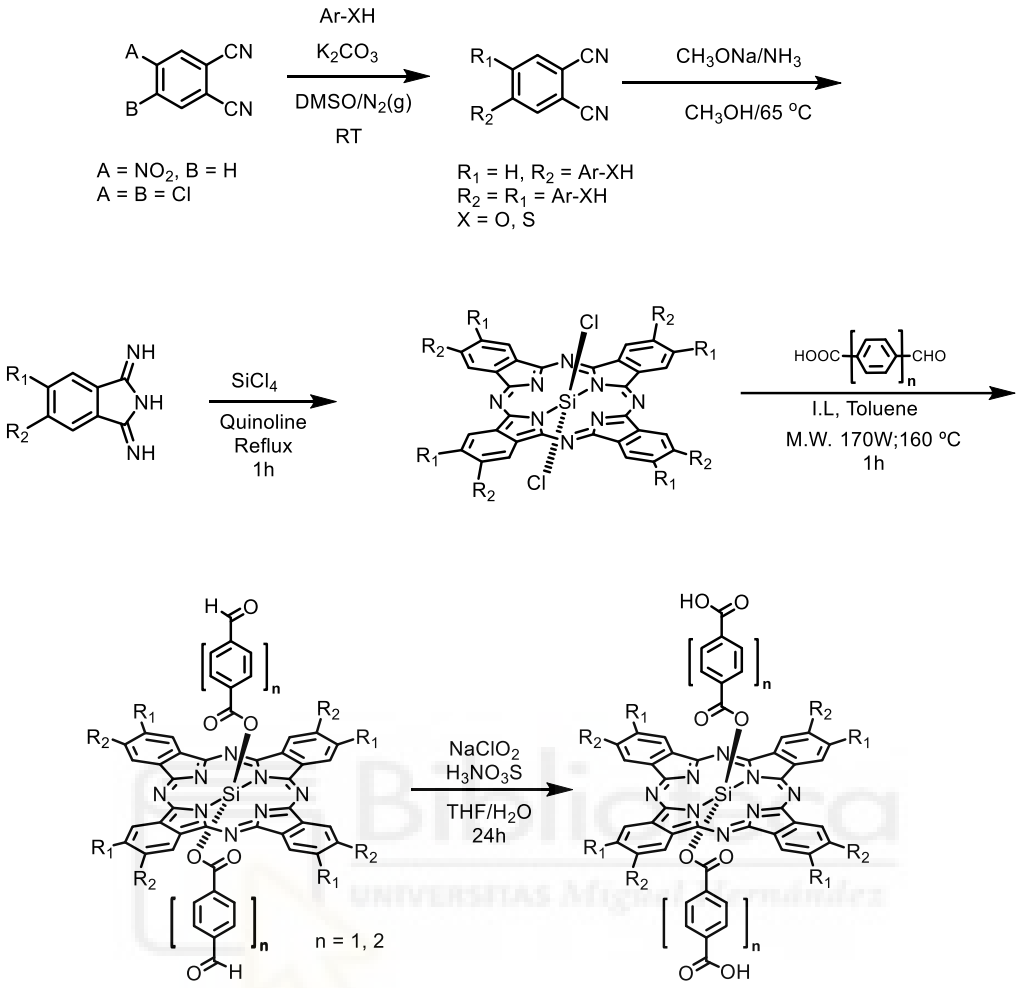

Scheme 1. *Synthetic route of SiPcs experimentally obtained.*

1.1.1. Synthesis and Characterization of tetra 1,6-dimethylphenoxy SiPcs 1, 5 and 7.

For the synthesis of the target molecules, it was first necessary to obtain the phthalocyanine precursor molecules **(Scheme 2)**. The synthesis of 4-(2,6-dimethylphenoxy)phthalonitrile **(17)** was based on methodologies previously reported[174] and was obtained with a yield of 73%. On the other hand, the synthesis of 5-(2,6-dimethylphenoxy)-1,3-diiminoisoindoline **(18)** was carried out by ammoniation following analogous reactions described for structurally similar compounds in **Scheme 1 in section 1.1**. with a yield of 56%. The characterization of these newly synthesized compounds by ^{1}H-NMR is presented in **Annex 1**.

[174] T. Kudo, M. Kimura,K. Hanabusa, H. Shiral T.Sakaguchi, *J. Porphyr. Phthalocyanines*,**1999**,3, 65–69.

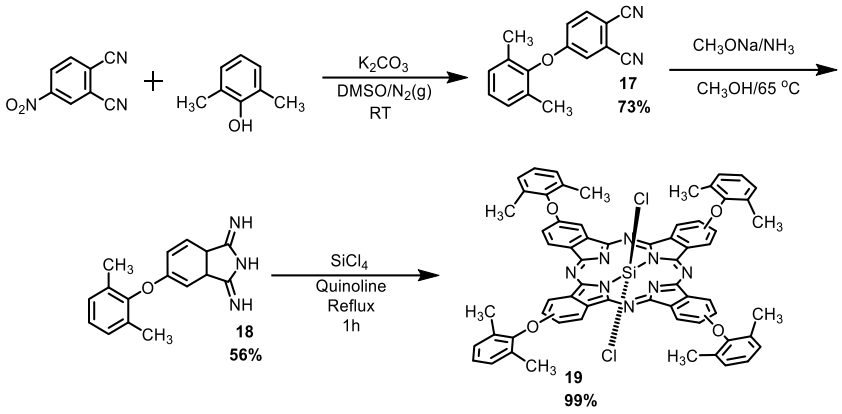

Scheme 2. *Synthesis of 4-(2,6-dimethylphenoxy)phthalonitrile* ***(17),***[174] *5-(2,6-dimethylphenoxy)-1,3-diiminoisoindoline* ***(18)*** *and* $(ArO)_4$*-*$SiPcCl_2$ ***(19)***.

Once the diiminoisoindoline was synthesized, the preparation of $(ArO)_4$-$SiPcCl_2$ **(19)** was carried out by cyclotetramerization using the method generally described previously in **section 1.1**. and with a yield of 99%. The characterization of this phthalocyanine was performed by UV-Vis spectroscopy presented in **Annex 1**.

Starting from the synthesized dichlorophthalocyanine **19**, axial substitution was carried out to obtain the different target compounds, following the strategy described in **Scheme 3**. This procedure involved the reaction of $(ArO)_4$-$SiPcCl_2$ **(19)** with the selected nucleophiles, optimizing the reaction conditions to maximize yields and process selectivity.

The synthesis of $(ArO)_4$-SiPc-$(O_2C$-Ar-$CHO)_2$ **(21)**, $(ArO)_4$-SiPc-$(O_2C$-Ar_2-$CHO)_2$ **(22)**, and $(ArO)_4$-SiPc-$(O_2C$-Ar-$CH_3)_2$ **(7)** was performed by nucleophilic substitution of the chlorine atoms located at the axial positions of $(ArO)_4$-$SiPcCl_2$ **(19)**. For the synthesis of phthalocyanine **21**, 4-formylbenzoic acid was employed as the nucleophile, for the phthalocyanine **22**, 4'-formyl-[1,1'-biphenyl]-4-carboxylic acid **(20)**[166] was used, while the preparation of phthalocyanine **7** required 4-methylbenzoic acid.

Microwave irradiation was employed as an alternative to conventional heating methods for the synthesis. This choice was motivated by several factors, as it allows the reactions to be carried out in a closed system, preventing light-induced degradation of the starting dichlorophthalocyanine. Additionally, microwave reactions offer shorter reaction times, reduced solvent usage, and acceptable yields.

Various reaction conditions were explored for the synthesis of the compounds. Initially, phthalocyanine **21** was synthesized using 6 mL of toluene, 200 W, and 200 °C. However, it was observed that toluene had difficulty to reach the target temperature, resulting in a 66% yield. To address this, the solvent volume was reduced to 3 mL for the synthesis of phthalocyanine **7**, without any further modification. This modification facilitated reaching the target temperature and led to an improved yield of 73%. Finally, phthalocyanine **22** was synthesized using a previously synthesized ionic liquid (I.L) (1,1'-methylenebis(3-methylimidazolium iodide))[175]. In this case, the temperature and power had to be reduced to 160 °C and 170 W, respectively, to prevent decomposition of the compound, 76% yield was obtained. All compounds were

[175] C. M. Jin, B. Twamley, J.M Shreeve, *Organometallics*, **2005**, *24*, 3020–3023.

characterized by ^{1}H-NMR, MALDI-TOF mass spectrometry and UV-Vis spectroscopy **(Annex 1)**.

The synthesis of $(ArO)_4$-SiPc-$(O_2C$-Ar-$CO_2H)_2$ **(1)**, and $(ArO)_4$-SiPc-$(O_2C$-Ar_2-$CO_2H)_2$ **(5)** started with the precursor phthalocyanines **(21)** and **(22)**. An oxidation of the aldehyde groups was carried out using H_3NSO_3 and $NaClO_2$ in a H_2O: THF solution. The reaction was maintained for 24 hours and protected from light to prevent degradation. Resulting product was a blue-green solid with yields of 70% and 75%, respectively.

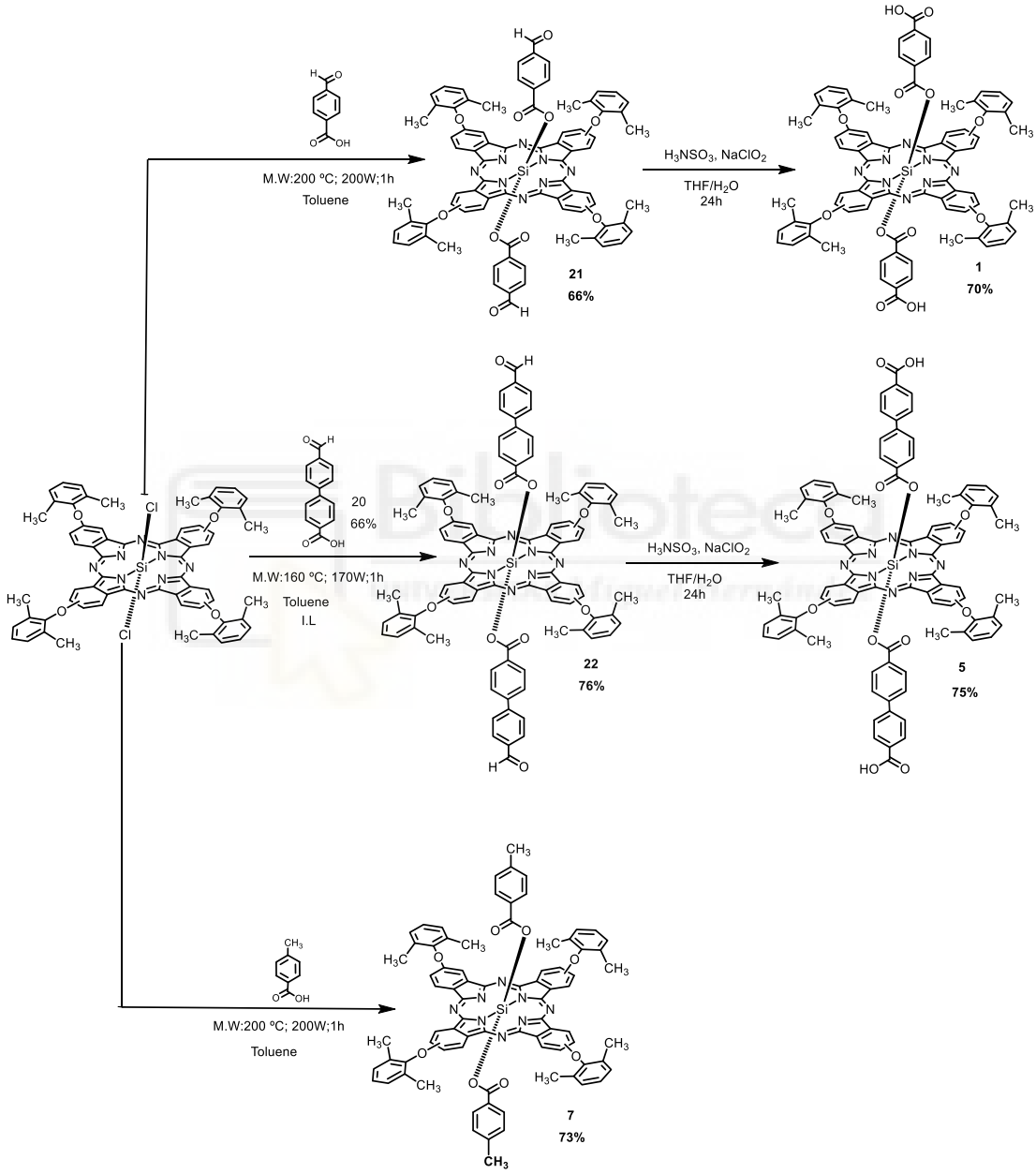

Scheme 3. *Synthesis of $(ArO)_4$-SiPc-$(O_2C$-Ar-$CHO)_2$ **(21)**, $(ArO)_4$-SiPc-$(O_2C$-Ar_2-$CHO)_2$ **(22)**, $(ArO)_4$-SiPc-$(O_2C$-Ar-$CO_2H)_2$ **(1)**, $(ArO)_4$-SiPc-$(O_2C$-Ar_2-$CO_2H)_2$ **(5)** and $(ArO)_4$-SiPc-$(O_2C$-Ar-$CH_3)_2$ **(7)**.*

The ^{1}H-NMR spectra were compared with the reference molecule **7 (Figure 1)**. The ^{1}H-NMR spectrum of reference compound **7**, including signal integration, is also provided in **Annex 1**. Furthermore, the identity of the molecule was confirmed by, MALDI-TOF mass spectrometry, and UV-Vis spectroscopy **(Annex 1)**.

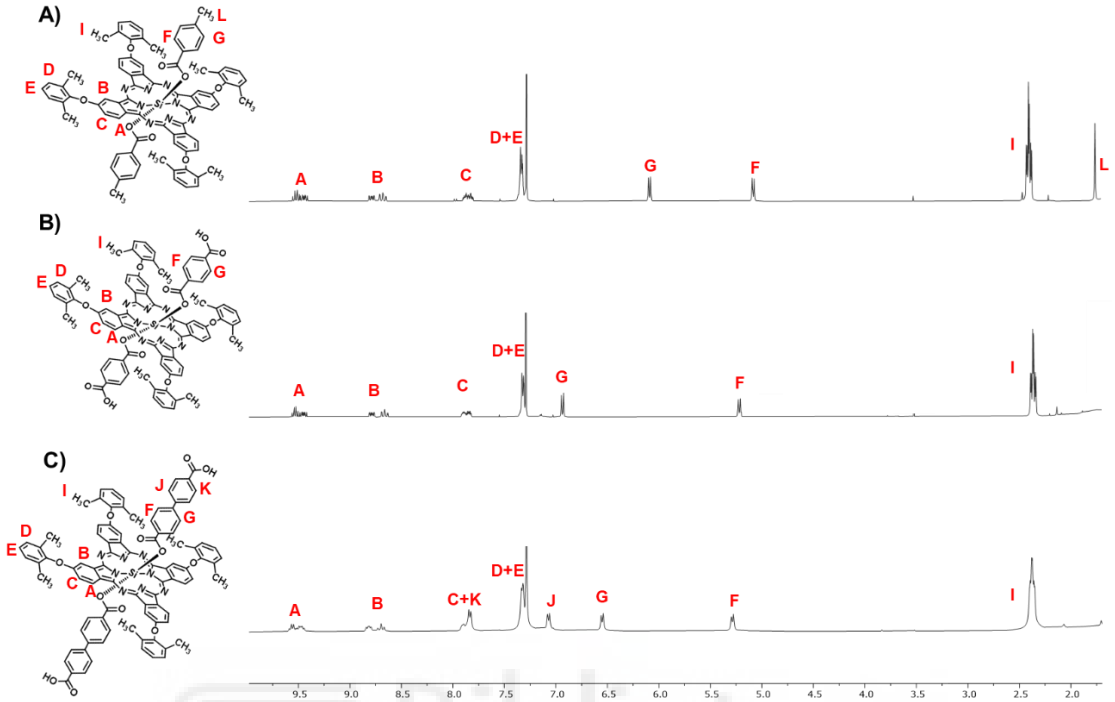

Figure 1. *^{1}H-NMR Spectra of **A)** $(ArO)_4$-SiPc-$(O_2C$-Ar-$CH_3)_2$ **(7)**, **B)** $(ArO)_4$-SiPc-$(O_2C$-Ar-$CO_2H)_2$ **(1)** and **C)** $(ArO)_4$-SiPc-$(O_2C$-Ar_2-$CO_2H)_2$ **(5)** in $CDCl_3$.*

The ^{1}H-NMR spectrum of the reference molecule **A)** $(ArO)_4$-SiPc-$(O_2C$-Ar-$CH_3)_2$ **(7)** in $CDCl_3$, as it serves as a basis for comparison in the characterization of the other compounds.

In phthalocyanine **7**, the **A**, **B**, and **C** signals, corresponding to the hydrogens of the phthalocyanine core, appear as three multiplets, **A** at 9.56-9.37 (4H) ppm, **B** at 8.82-8.61 ppm (4H) and **C** at 7.91-7.68 ppm (4H). The aromatic protons **D** and **E** are detected as a multiplet between 7.37-7.29 ppm (12H). The axial substituents **G** and **F** appear as two doublets at 6.06 ppm (4H) and 5.05 ppm (4H), respectively. The signal corresponding to the axial methyl groups **L** is observed as a singlet at 1.72 ppm (6H); and finally, the signal for protons **I** appears as a multiplet between 2.45-2.31 ppm (24H).

These same signals can be observed for the target compounds **B)** $(ArO)_4$-SiPc-$(O_2C$-Ar-$CO_2H)_2$ **(1)**, and **C)** $(ArO)_4$-SiPc-$(O_2C$-Ar_2-$CO_2H)_2$ **(5)**. Due to the different axial groups present in these molecules, slight variations are observed in their spectra. In the case of $(ArO)_4$-SiPc-$(O_2C$-Ar-$CO_2H)_2$ **(1) (Figure 1.B)**, a shift in the axial signals is observed due to the presence of the carboxylic acid group, where **G** and **F** appear shifted to lower fields compared to the reference molecule, appearing at 6.61 ppm (4H) and 5.19 (4H) ppm.

Similarly, in the case of $(ArO)_4$-SiPc-$(O_2C$-Ar_2-$CO_2H)_2$ **(5) (Figure 1.C)**, the presence of a double aromatic ring results in the appearance of four doublets instead of two, as seen in the previous compounds. In this case, the newly observed signals, **J** and **K**, appear at lower fields compared to the other axial substituents. This phenomenon is attributed to two factors: the increased distance from the phthalocyanine core, which reduces the shielding effect of the π-electron system, causing a downfield shift, and the presence of the carboxylic acid group, which, as in previous cases, influences to the deshielding effect. Consequently, the **K** signal appears at

7.87 ppm (4H), while the **J** signal is observed at 7.04 ppm (4H). For the axial substituents, signals **G** and **F** appear at 6.52 ppm (4H) and 5.35 ppm (4H), respectively.

As expected, the **L** signal is absent in these compounds due to the replacement of the axial methyl group with a carboxylic acid group.

1.1.2. Synthesis and Characterization of tetra 2,6-diclorophenoxy SiPcs 2, 6 and 8.

For the synthesis of the target molecules, it was first necessary to obtain the phthalocyanine precursors **(Scheme 4)**. Although no specific references are available for these compounds, their structural similarity to other known precursors allows us to follow the procedure outlined in **Scheme 1 of section 1.1**.

The synthesis of 4-(2,6-dichlorophenoxy)phthalonitrile **(23)** was carried out via a nucleophilic aromatic substitution reaction, yielding in 70%. While 5-(2,6-dimethylphenoxy)-1,3-diiminoisoindoline **(24)** was obtained through an ammoniation reaction with an isolated yield of 83%. When compared to its analogue, this showed a higher yield, which may be attributed to the presence of chlorine atoms, which act as electron-withdrawing groups, enhancing the nucleophilicity of the molecule and facilitating the ammoniation process. Both compounds were characterized by ^{1}H NMR spectroscopy, as detailed in **Annex 1**.

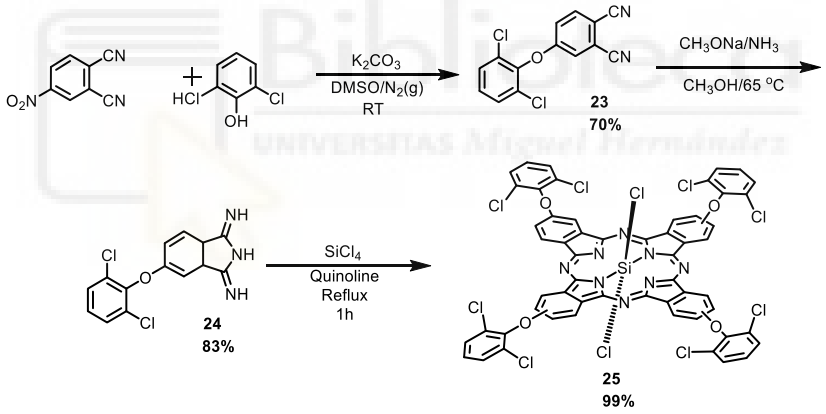

Scheme 4. *Synthesis of 4-(2,6-dichlorophenoxy)phthalonitrile **(23)**, 5-(2,6-dichlorophenoxy)-diiminoisoindoline **(24)** and $(Cl_2ArO)_4$-$SiPcCl_2$ **(25)**.*

Once the diiminoisoindoline was obtained, the synthesis of $(Cl_2ArO)_4$-$SiPcCl_2$ **(25)** was carried out by cyclotetramerization using the previously described method in **Scheme 1 of section 1.1** and yielding 99%. The characterization of this phthalocyanine was performed using UV-Vis spectroscopy, showed in **Annex 1**.

For the synthesis of $(Cl_2ArO)_4$-SiPc-$(O_2C$-Ar-$CO_2H)_2$ **(2)**, $(Cl_2ArO)_4$-SiPc-$(O_2C$-Ar_2-$CO_2H)_2$ **(6)**, and $(Cl_2ArO)_4$-SiPc-$(O_2C$-Ar-$CH_3)_2$ **(8) (Scheme 5)** was carried out following the methodology described in **section 1.1,** to using the same axial substituents as their analogues in this section.

Based on the results previously obtained in MW synthesis, the reaction conditions that yielded the highest efficiency were selected **(as described in section 1.1.1)**. Consequently, all reactions were performed at 160 °C and 170 W for one hour. Toluene was used as the solvent,

and an ionic liquid (1,1'-methylenebis-(3-methylimidazolium) iodide)[175] was added to facilitate an increase in the solvent temperature.

Since the oxidation step used to obtain the final molecules showed very similar yields, we focused our comparison on the axial substitution reactions, where greater variability was observed. A possible explanation for the lower yields may lie in the incorporation of chlorine substituents, which introduce an electron-withdrawing character and could reduce the efficiency of axial coordination, as observed when compared to their analogues in **section 1.1.1.** The reference phthalocyanine **8** exhibited the highest yield, of 64%, in the case of phthalocyanine **26**, a yield of 46% was obtained, which was higher than that of phthalocyanine **27** which had a yield of 23%. This difference is probably attributed to the greater steric hindrance of the introduced axial substituent, significantly reducing the reaction yield.

All compounds were characterized by ^{1}-H-NMR, MALDI-TOF mass spectrometry, and UV-Vis spectroscopy **(Annex 1)**. The ^{1}H-NMR spectrum of reference compound **8**, including signal integration, is also provided in **Annex 1.**

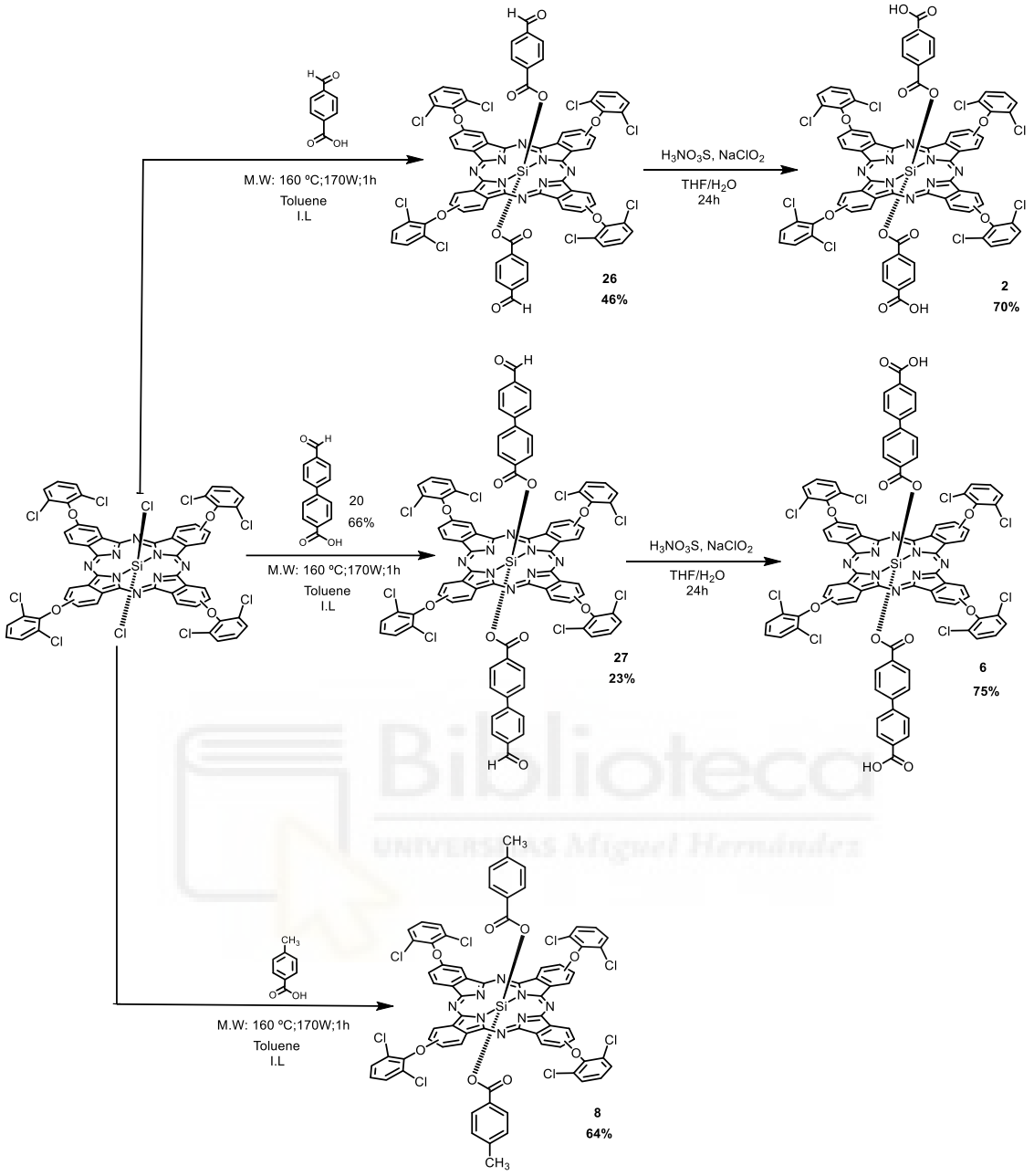

Scheme 5. *Synthesis of $(Cl_2ArO)_4$-SiPc-$(O_2C$-Ar-CHO$)_2$* ***(26)****, $(Cl_2ArO)_4$-SiPc-$(O_2C$-Ar_2-CHO$)_2$* ***(27)****, $(Cl_2ArO)_4$-SiPc-$(O_2C$-Ar-$CO_2H)_2$* ***(2)****, $(Cl_2ArO)_4$-SiPc-$(O_2C$-Ar_2-$CO_2H)_2$* ***(6)*** *and $(Cl_2ArO)_4$-SiPc-$(O_2C$-Ar_2-$CH_3)_2$* ***(8)****.*

Due to the structural similarity with the molecules in **section 1.1.1** and the difficulty of characterization, comparisons will be made with these and with the reference molecule $(Cl_2ArO)_4$-SiPc-$(O_2C$-Ar-$CH_3)_2$ **(8) (Figure 2)**.

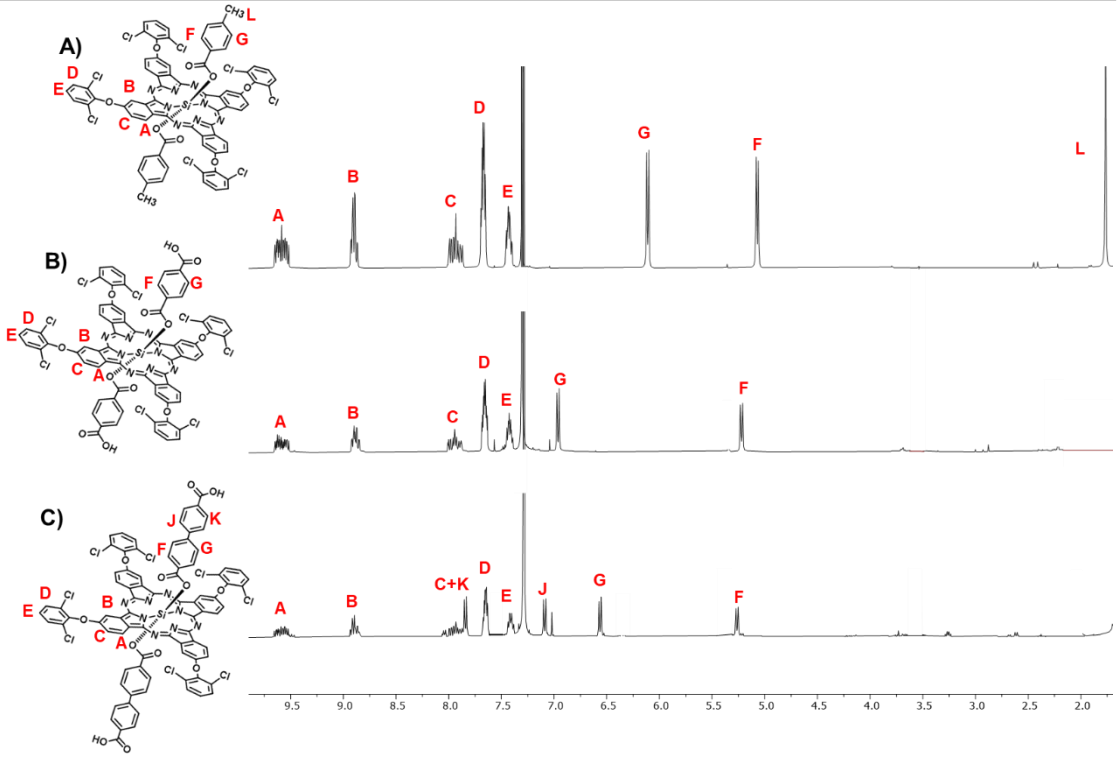

***Figure 2**. ^{1}H-NMR Spectra of **A)** $(Cl_2ArO)_4$-SiPc-$(O_2C$-Ar-$CH_3)_2$ **(8)**, **B)** $(Cl_2ArO)_4$-SiPc-$(O_2C$-Ar-$CO_2H)_2$ **(2)** and **C)** $(Cl_2ArO)_4$-SiPc-$(O_2C$-Ar_2-$CO_2H)_2$ **(6)** in $CDCl_3$.*

The reference molecule $(Cl_2ArO)_4$-SiPc-$(O_2C$-Ar-$CH_3)_2$ **(8) (Figure 2.A)** bearing chlorine atoms in the aryl substituents attached to the peripheral positions of the phthalocyanine ring, exhibits proton signals for the phthalocyanine macrocycle and its substituents that are noticeably shifted compared to those described in **section 1.1.1**. In this case, for phthalocyanine **8**, signals **A**, **B**, and **C**, corresponding to the protons of the phthalocyanine ring, appear as three shifted multiplets: **A** between 9.63-9.45 ppm (4H), **B** between 8.91-8.79 ppm (4H), and **C** between 7.97-7.80 ppm (4H). The aromatic protons **D** and **E** appear as two doublets, with signal **D** between 7.67-7.58 ppm (8H), and signal **E** between 7.43-7.31 ppm (4H). Signals **G** and **F**, corresponding to the axial substituents, appear as two doublets at 6.06 ppm (4H) and 5.02 ppm (4H), respectively. Finally, signal **L**, corresponding to the methyl groups at the axial position, appears as a singlet at 1.72 ppm (6H). As shown in **Figure 2**, these same signals can be observed for the target molecules $(Cl_2ArO)_4$-SiPc-$(O_2C$-Ar-$CO_2H)_2$ **(2) (Figure 2.B)**, and $(Cl_2ArO)_4$-SiPc-$(O_2C$-Ar_2-$CO_2H)_2$ **(6) (Figure 2.C)**. As in **section 1.1.1**, the different axial groups present in these molecules result in slight variations in their spectra. In the case of SiPc **2**, a shift in the axial signals is observed due to the presence of the carboxylic acid group, where **G** and **F** appear shifted downfield compared to the reference molecule, at 6.91 ppm (4H) and 5.17 ppm (4H), respectively.

Similarly, in the case of SiPc **6**, the presence of a double aromatic ring results in the appearance of four doublets instead of two. In this case, the **J** and **K** signals appear at lower fields compared to the other axial substituents. This phenomenon is explained in **section 1.1.1**, where the **K** signal appears at 7.80 ppm (4H), while the **J** signal is observed at 7.05 ppm (4H). For the axial substituents, signals **G** and **F** appear at 6.53 ppm (4H), and 5.23 ppm (4H), respectively.

1.1.3. Synthesis and Characterization of tetra *p*-methylthiophenoxy SiPcs 3 and 9.

The synthesis of the target molecules and the phthalocyanine precursors **(Scheme 6)** followed the synthetic route outlined in **Scheme 1 of section 1.1**. These molecules led to the publication of a scientific paper,[176] where this synthesis is explained in greater detail **(Annex 2)**. The precursor molecules obtained were 4-(*p*-tolylthio)phthalonitrile **(28)** yielding 79% and 5-(*p*-tolylthio)isoindoline-1,3-diimine **(29)**, yielding 96%. Both compounds were characterized by ^{1}H-NMR, as shown in **Annex 1.**

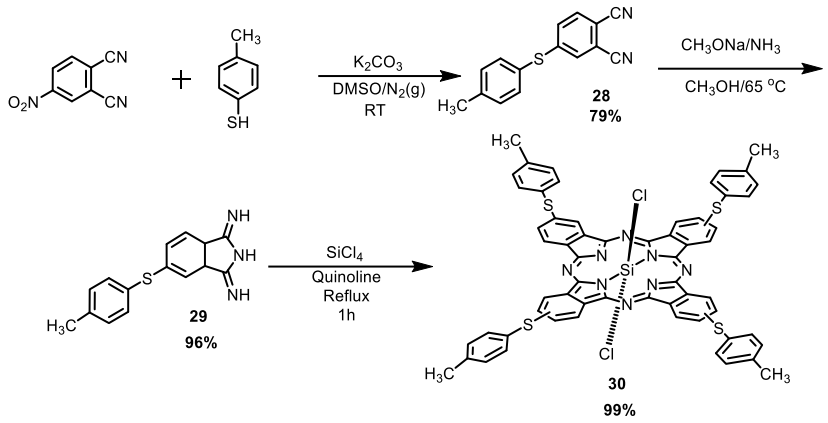

Scheme 6. *Synthesis of 4-(p-tolylthio)phthalonitrile **(28)** and 5-(p-tolylthio)isoindoline-1,3-diimine **(29)** and $(ArS)_4$-$SiPcCl_2$ **(30)**.*

Once the diiminoisoindoline was obtained, the synthesis of $(ArS)_4$-$SiPcCl_2$ **(30)** was carried out following the previously described methodology in **Scheme 1 of section 1.1**. The characterization of this phthalocyanine was performed using UV-Vis spectroscopy, as shown in **Annex 1**.

For the synthesis of the target compound, several modifications were made to optimize the reaction and obtain the desired product **(Scheme 7)**. Instead of performing a nucleophilic substitution of the axial -Cl groups with an aldehyde precursor followed by oxidation, a direct nucleophilic substitution with terephthalic acid was chosen. This decision was made because, following the general synthetic method outlined in the **Scheme 1**, the peripheral *p*-methylthiophenoxy groups underwent uncontrolled oxidation, leading to undesired modifications and preventing the successful synthesis of $(ArS)_4$-SiPc-$(O_2C$-Ar-$CO_2H)_2$ **(3)**.

Due to this modification, the purification process was also adjusted. Instead of using a normal phase chromatography column, size exclusion chromatography was employed. This change was necessary because the carboxylic acid groups tended to be retained by the silica, degrading the target phthalocyanine and resulting in a mixture of compounds with 0, 1, or 2 axial substituents, which were difficult to purify. In contrast, separation based on molecular weight allowed for the successful isolation of the desired compounds.

Finally, as a result of these modifications, the target compound $(ArS)_4$-SiPc-$(O_2C$-Ar-$CO_2H)_2$ **(3)** was obtained with a yield of 26%, while the reference molecule $(ArS)_4$-SiPc-$(O_2C$-Ar-$CH_3)_2$ **(9)** achieved a yield of 50%.

[176] V. Sobrino-Bastán, L. Martín-Gomis, Á. Sastre-Santos, *J. Porphyrins Phthalocyanines,* **2023**, 27, 331–339.

All compounds were characterized by ^{1}-H-NMR, MALDI-TOF mass spectrometry, and UV-Vis spectroscopy **(Annex 1)**.

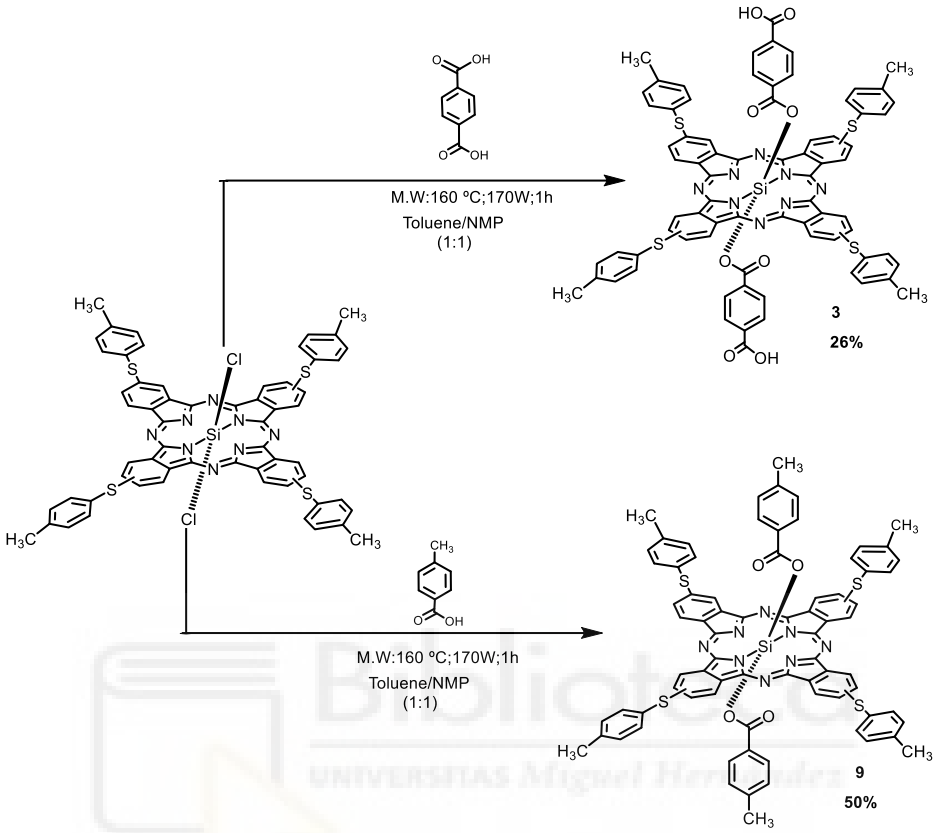

Scheme 7. *Synthesis of $(ArS)_4$-SiPc-$(O_2C$-Ar-$CO_2H)_2$* ***(3)*** *and $(ArS)_4$-SiPc-$(O_2C$-Ar-$CH_3)_2$* ***(9)***.

In this case, **Figure 3** compares the ^{1}H-NMR spectrum of $(ArS)_4$-SiPc-$(O_2C$-Ar-$CO_2H)_2$ **(3)** and the reference phthalocyanine $(ArS)_4$-SiPc-$(O_2C$-Ar-$CH_3)_2$ **(9)** in $CDCl_3$.

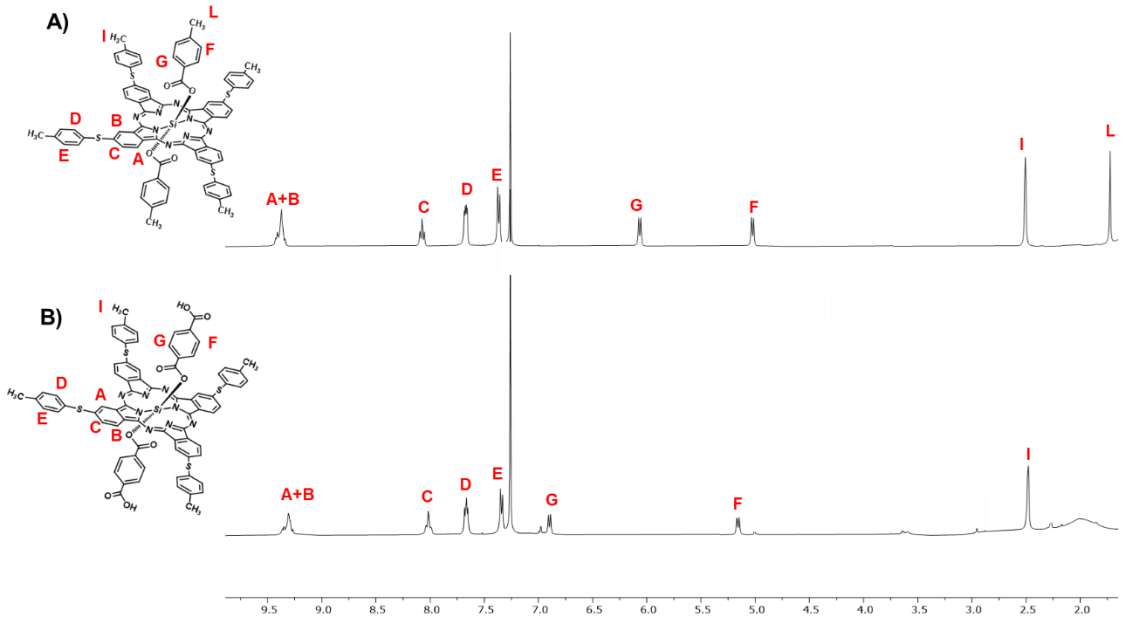

***Figure 3**. ^{1}H-NMR Spectra of **A)** $(ArS)_4$-SiPc-$(O_2C$-Ar-$CH_3)_2$ **(9)** and **B)** $(ArS)_4$-SiPc-$(O_2C$-Ar-$CO_2H)_2$ **(3)** in $CDCl_3$.*

Despite their structural similarity to the molecules discussed in the previous sections, the presence of the *p*-methylthiophenoxy group, which has a stronger electron-donating character, results in a slight upfield shift of the signals corresponding to the phthalocyanine ring and peripheral substituents.

For this, in the reference phthalocyanine **9**, the **A**, **B** and **C** signals appear as three multiplets. The **A** and **B** signals appear together in the range of 9.48-9.35 ppm (8H) and the **C** signal between 8.15-8.06 ppm (4H). The signals corresponding to the peripheral substituent protons **D** appear as a multiplet between 7.71-7.63 (8H) ppm, while the **E** signal is observed as a doublet at 7.39 ppm (8H). The **I** signal, associated with the methyl group, appears as a singlet at 2.53 ppm (12H). The **G** and **F** signals, corresponding to the axial substituents, are detected at 6.09 ppm (4H) and 5.05 ppm (4H), respectively. Additionally, the **L** signal, corresponding to the axial methyl group appears as a singlet at 1.75 ppm (6H).

Similarly, in phthalocyanine **3**, the signals are observed in the same range. as the reference SiPc **9**. However, in phthalocyanine **3**, the axial substituent signals are downfield shifted due to the presence of the carboxylic acid group, with **G** appearing at 6.93 ppm (4H) and **F** at 5.19 ppm (4H).

1.1.4. Synthesis and Characterization of octa *p*-methylthiophenoxy SiPcs 4 and 10.

The synthesis of the target molecules and their precursors **(Scheme 8)** followed the synthetic route described in **Scheme 1 of section 1.1**. These molecules, along with those discussed in **section 1.1.3**, contributed to a scientific article[176] that provides a more detailed account of this synthesis **(Annex 2)**.

The precursor molecules obtained were 4,5-bis(*p*-tolylthio)phthalonitrile **(31)** yielding 69% and 5,6-bis(*p*-tolylthio)-1,3-diiminoisoindoline **(32)**, yielding 75%. Despite the stronger electron-donating character of the substituents, the slightly lower yields compared to their

analogues may be attributed to increased steric hindrance arising from the higher number of substituents. Both of which were characterized by ^{1}H-NMR, as presented in **Annex 1**.

Following the successful synthesis of diiminoisoindoline, the preparation of $(ArS)_8$-$SiPcCl_2$ **(33)** was carried out according to the methodology previously described in **Scheme 1 of section 1.1**. The characterization of this phthalocyanine was performed using UV-Vis spectroscopy, as detailed in **Annex 1**.

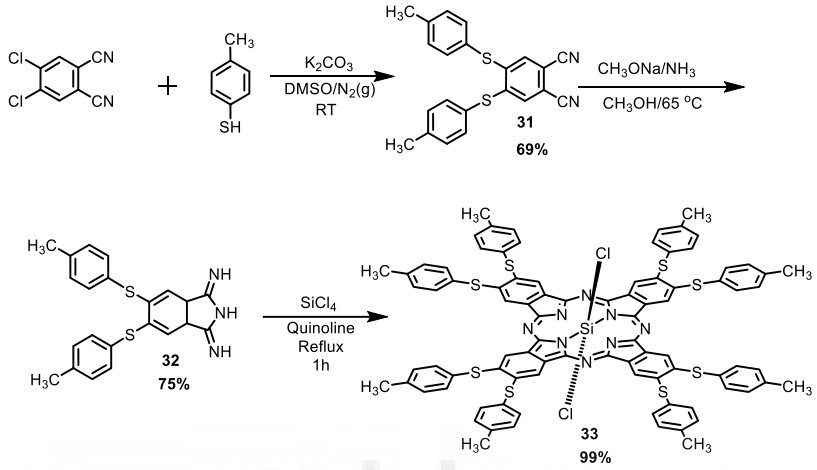

Scheme 8. *Synthesis of 4,5-bis(p-tolylthio)phthalonitrile* ***(31)****; 5,6-bis(p-tolylthio)-1,3-diiminoisoindoline* ***(32)*** *and* $(ArS)_8$-$SiPcCl_2$ ***(33)***.

Several modifications were made to the synthetic route described in **Scheme 1 of section 1.1** for the synthesis of the target compound **(Scheme 9)**. These modifications, along with their justification, are detailed in **section 1.1.3**. Given that the difference between both compounds lies in the number of peripheral substituents, a partial comparison of their synthesis can be made

The yield of $(Cl_2ArO)_4$-SiPc-$(O_2C$-Ar-$CO_2H)_2$ **(4)** was 37%, significantly higher than that of its analogue in **section 1.1.3**. This can be attributed to the higher number of electron-donating peripheral substituents, which favour nucleophilic substitution, leading to increased yields.

Conversely, the yield of $(ArS)_8$-SiPc-(O_2C-Ar-$CH_3)_2$ (**10)** was 54%, slightly lower than its analogue. Although a higher yield might be expected due to the electron-donating character of the phthalocyanine, it is possible that the steric hindrance caused by the increased number of peripheral groups has a more significant impact on the reaction efficiency.

All obtained compounds were characterized by ^{1}H-NMR, MALDI-TOF mass spectrometry, and UV-Vis spectroscopy **(Annex 1)**.

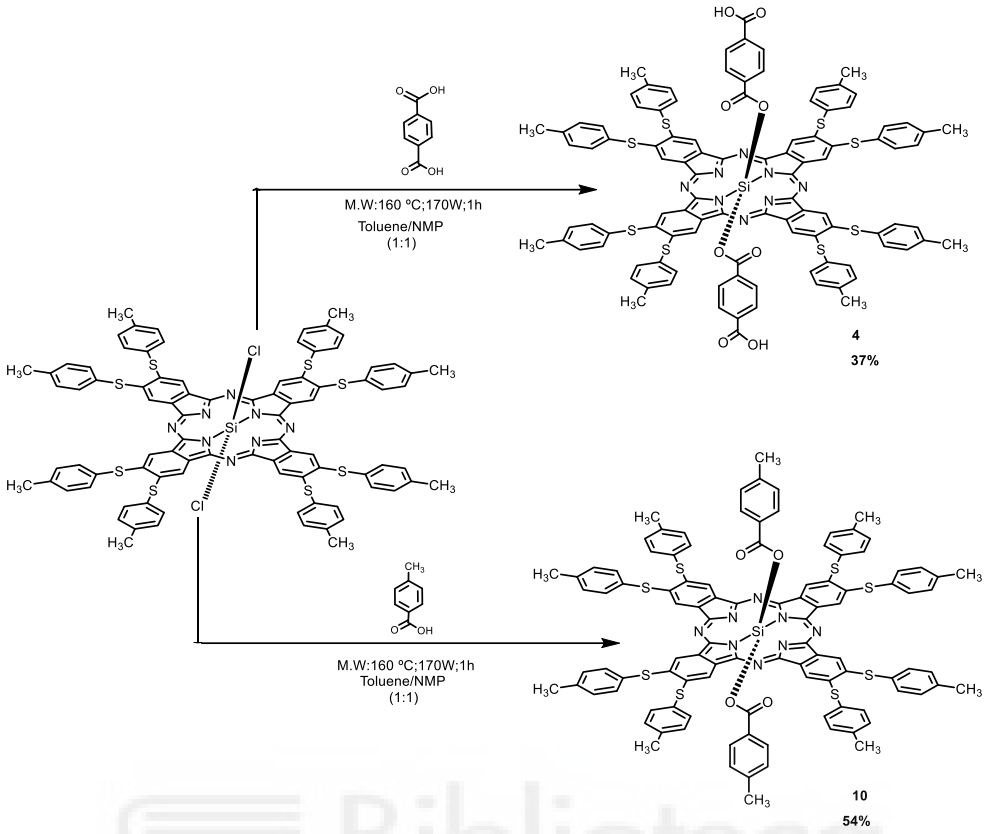

Scheme 9. *Synthesis of $(Cl_2ArO)_4$-SiPc-$(O_2C$-Ar-$CO_2H)_2$* ***(4)*** *and $(ArS)_8$-SiPc-$(O_2C$-Ar-$CH_3)_2$* ***(10)****.*

In this case, **Figure 4** compares the ^{1}H-NMR spectrum of $(ArS)_8$-SiPc-$(O_2C$-Ar-$CO_2H)_2$ **(4)** and the reference phthalocyanine $(ArS)_4$-SiPc-$(O_2C$-Ar-$CH_3)_2$ **(9)** in $CDCl_3$.

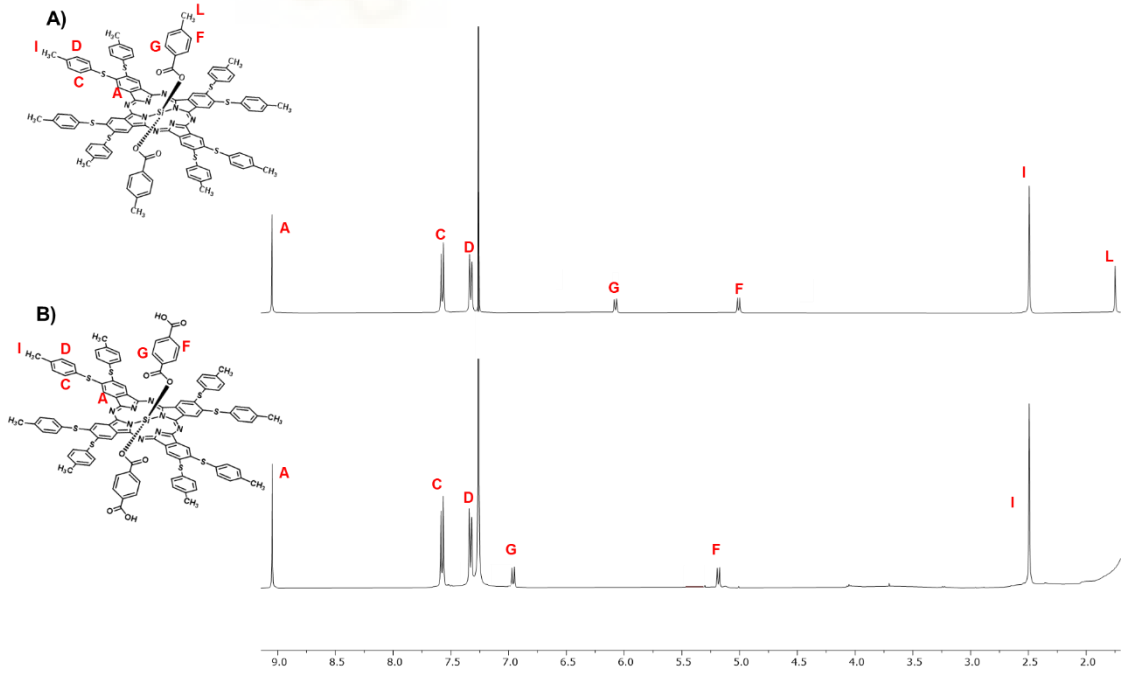

Figure 4*. ^{1}H-NMR Spectra of* ***A)*** *$(ArS)_8$-SiPc-$(O_2C$-Ar-$CH_3)_2$* ***(10)*** *and* ***B)*** *$(Cl_2ArO)_4$-SiPc-$(O_2C$-Ar-$CO_2H)_2$* ***(4)*** *in $CDCl_3$.*

When comparing these spectra with those of the molecules discussed in **section 1.1.3**, several differences can be observed. These differences raise from the increased number of peripheral substituents, which increase the electron-donating character of the molecule, causing a slight upfield shift in the signals corresponding to the phthalocyanine ring. Additionally, the presence of eight peripheral substituents instead of four introduces greater molecular symmetry, leading to the appearance of the ring signals as a singlet rather than two multiplets as seen in their analogues with four peripheral substituents.

Accordingly, in **Figure 4.A** phthalocyanine **10**, the **A** signal, corresponding to the phthalocyanine ring, appears as a singlet at 9.05 ppm (8H). The **C** and **D** signals, associated with the peripheral substituents, are observed as two doublets, one at 7.57 ppm (16H) and the other at 7.33 ppm (16H), respectively. The **I** signal, corresponding to the methyl group, appears as a singlet at 2.49 ppm (24H). The signals of the axial substituent **G** and **F** appear as two doublets, one at 6.08 ppm (4H) and the other at 5.01 ppm (4H), respectively. Finally, the **L** signal, corresponding to the axial methyl group, is detected as a singlet at 1.75 ppm (6H).

In the case of phthalocyanine **4**, the axial substituent signals **G** and **F** also appear as two doublets. However, these axial signals are shifted downfield due to the presence of the carboxylic acid group, as previously mentioned, with **G** appearing at 6.99 ppm (4H) and **F** at 5.21 ppm (4H).

1.2.1. Optical Properties of the Reference Compounds, SiPcs 7, 8, 9 and 10.

To analyse the optical properties of the target molecules, a comparison of their UV-Vis spectra with those of the reference SiPcs **7-10** will be conducted **(Figure 5)**. This approach is justified by the fact that the axial substituents have minimal influence on the optical properties, while the peripheral substituents play a more significant role. By modifying the electron-donating or electron-accepting character of the phthalocyanines, these substituents induce a shift in the Q band, thereby affecting the optical behaviour of the molecules.

Figure 5 presents a comparative analysis of the compounds $(ArO)_4$-SiPc-(O_2C-Ar-$CH_3)_2$ **(7)**, $(Cl_2ArO)_4$-SiPc-(O_2C-Ar-$CH_3)_2$ **(8)**, $(ArS)_4$-SiPc-(O_2C-Ar-$CH_3)_2$ **(9)** and $(ArS)_8$-SiPc-(O_2C-Ar-$CH_3)_2$ **(10)** in $CHCl_3$.

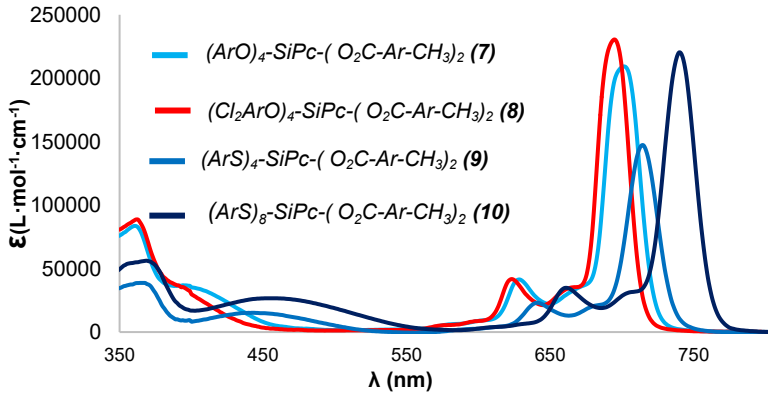

***Figure 5**. UV-Vis spectra of $(ArO)_4$-SiPc-(O_2C-Ar-$CH_3)_2$ **(7)**, $(Cl_2ArO)_4$-SiPc-(O_2C-Ar-$CH_3)_2$ **(8)**, $(ArS)_4$-SiPc-(O_2C-Ar-$CH_3)_2$. **(9)** and $(ArS)_8$-SiPc-(O_2C-Ar-$CH_3)_2$ **(10)** in $CHCl_3$.*

The UV-Vis spectrum of $(ArO)_4$-SiPc-(O_2C-Ar-$CH_3)_2$ **(7)**, exhibits a Q band maximum at 702 nm. In contrast, the introduction of electron-withdrawing chlorine groups in the peripheral

positions of $(Cl_2ArO)_4$-SiPc-(O_2C-Ar-$CH_3)_2$ **(8)** results in a blue shift of the absorption maximum by 7 nm, with the Q band maximum at 695 nm. This shift, attributed to the difference in donor-acceptor character, is a recurring trend in all UV-Vis spectra of donor-acceptor phthalocyanine pairs.

Similarly, the UV-Vis spectrum of $(ArS)_4$-SiPc-(O_2C-Ar-$CH_3)_2$ **(9)** shows a Q band maximum at 714 nm. In the case of $(ArS)_8$-SiPc-(O_2C-Ar-$CH_3)_2$ **(10)** the increased number of thiotolyl groups induces a red shift of 26 nm, with the Q band maximum appearing at 740 nm. Both phthalocyanines exhibit a charge transfer (CT) band in the 400-550 nm range, which is more intense in $(ArS)_8$-SiPc-(O_2C-Ar-$CH_3)_2$ **(10)** due to the influence of the higher number of thiotolyl substituents. However, the Soret band remains relatively unchanged, appearing at 366 nm for phthalocyanine **9**, while in phthalocyanine **10**, it is shifted by 3 nm to 369 nm.

The donor-acceptor character of these four phthalocyanines modulates the Q band shift, with the stronger electron-donating character leading to a more pronounced red shift. In line with this trend, CT band of $(ArO)_4$-SiPc-(O_2C-Ar-$CH_3)_2$ **(7)** appears slightly blue-shifted, while in its chlorinated analogue, $(Cl_2ArO)_4$-SiPc-(O_2C-Ar-$CH_3)_2$ **(8)**, the CT band is red-shifted, with both signals observed in the 350-450 nm range. In contrast, a much more intense charge transfer band, observed between 400-550 nm, is present in $(ArS)_4$-SiPc-(O_2C-Ar-$CH_3)_2$ **(9)** and $(ArS)_8$-SiPc-(O_2C-Ar-$CH_3)_2$ **(10)**, particularly in the latter due to its higher electron-donating nature

To complement this comparison of reference phthalocyanines, a similar analysis was performed for the target molecules **1-4**, in order to verify whether the donor-acceptor trends observed previously are reproduced in these systems **(Figure 6).**

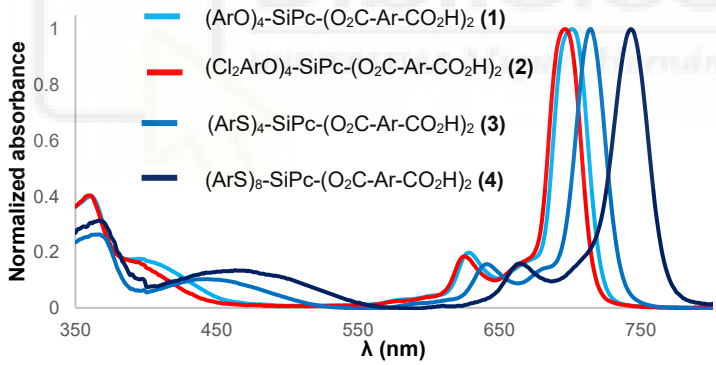

Figure 6. *Normalized UV-Vis spectra of $(ArO)_4$-SiPc-$(O_2C$-Ar-$CO_2H)_2$* ***(1)****, $(Cl_2ArO)_4$-SiPc-$(O_2C$-Ar-$CO_2H)_2$* ***(2)****, $(ArS)_4$-SiPc-$(O_2C$-Ar-$CO_2H)_2$* ***(3)*** *and $(ArS)_8$-SiPc-$(O_2C$-Ar-$CO_2H)_2$* ***(4)*** *in $CHCl_3$.*

The absorption maxima of phthalocyanines display a progressive red shift correlated with the increasing electron-donating character of the substituents. SiPc **2**, which exhibits the most electron-withdrawing profile, shows a Q band at 696 nm. In contrast, SiPc **1**, **3**, and **4** show maxima at 701, 717, and 743 nm, respectively. These results are consistent with the donor-acceptor behavior described previously for the references SiPc and confirm that higher donor character induces a more pronounced bathochromic shift.

1.2.2. Electrochemical Properties of the Reference Compounds, SiPcs 7, 8, 9 and 10.

The study of the electrochemical properties of phthalocyanines was carried out to understand their behaviour for potential optoelectronic applications. The ability of these molecules to transfer charge and participate in redox processes is closely related to the nature of their peripheral substituents as well as the presence of electron-donating or electron-withdrawing groups. In this context, the electrochemical evaluation of the synthesized phthalocyanines will allow for an analysis of the impact of the modifications made, aiming at their future applications in SURMOFs.

Figures 7 and table 1 present the electrochemical measurements obtained by differential pulse voltammetry (DPV) in degassed benzonitrile solutions for the reference compounds of $(ArO)_4$-SiPc-$(O_2C$-Ar-$CH_3)_2$ **(7)**, $(Cl_2ArO)_4$-SiPc-$(O_2C$-Ar-$CH_3)_2$ **(8)**,$(ArS)_4$SiPc-$(O_2C$-Ar-$CH_3)_2$ **(9)** and $(ArS)_8$SiPc-$(O_2C$-Ar-$CH_3)_2$ **(10)**. In all cases, well-defined and reversible waves were observed in both anodic and cathodic regions, confirming the electrochemical stability of the studied systems.

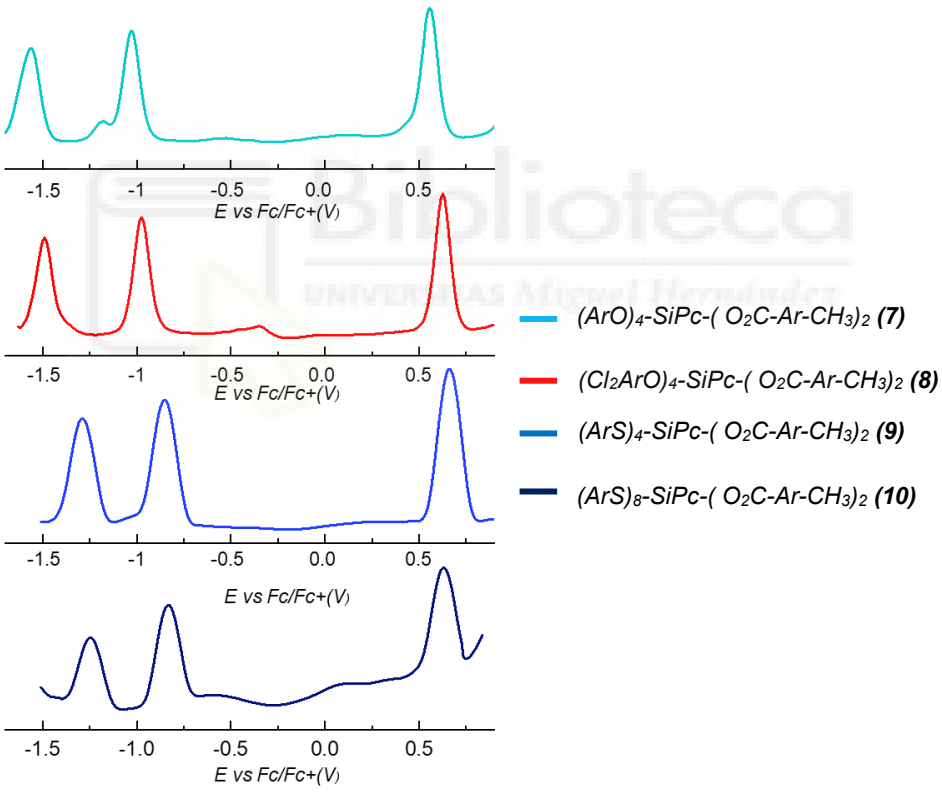

***Figure 7**. Differential pulse voltammogram of $(ArO)_4$-SiPc-$(O_2C$-Ar-$CH_3)_2$ **(7)**, $(Cl_2ArO)_4$-SiPc-$(O_2C$-Ar-$CH_3)_2$ **(8)**, $(ArS)_4$-SiPc-$(O_2C$-Ar-$CH_3)_2$. **(9)** and $(ArS)_8$-SiPc-$(O_2C$-Ar-$CH_3)_2$ **(10)** in benzonitrile, using tetrabutylammonium hexafluorophosphate (Bu_4NPF_6) as the supporting electrolyte, platinum wire, glassy carbon, and non-aqueous $Ag/AgNO_3$ as the counter, working, and reference electrodes, respectively, with ferrocene (Fc/Fc^+) as an internal standard.*

Compound	E_{ox} *(V vs Fc/Fc$^+$)*	$E_{red}I$ *(V vs Fc/Fc$^+$)*	E_{red} II *(V vs Fc/Fc$^+$)*	*E_{Homo} *(eV)*	**E_{Lumo} *(eV)*	***E_g^{EQ} *(eV)*
$(ArO)_4$-SiPc-(O_2C-Ar-$CH_3)_2$ **(7)**	0.57	-1.02	-1.55	4.23	5.82	1.59
$(Cl_2ArO)_4$-SiPc-(O_2C-Ar-$CH_3)_2$ **(8)**	0.67	-0.97	-1.48	4.13	5.77	1.64
$(ArS)_4$-SiPc-(O_2C-Ar-$CH_3)_2$ **(9)**	0.68	-0.84	-1.28	4.12	5.64	1.52
$(ArS)_8$-SiPc-(O_2C-A_2-$CH_3)_2$ **(10)**	0.65	-0.83	-1.24	4.15	5.63	1.48

***Table 1**. $(ArO)_4$-SiPc-(O_2C-Ar-$CH_3)_2$ **(7)**, $(Cl_2ArO)_4$-SiPc-(O_2C-Ar-$CH_3)_2$ **(8)**, $(ArS)_4$-SiPc-(O_2C-Ar-$CH_3)_2$. **(9)**, and $(ArS)_8$-SiPc-(O_2C-Ar-$CH_3)_2$ **(10)** electrochemical properties.*

*E_{HOMO} have been calculated using E_{HOMO} (eV) = -4.8 - E_{ox} (V *vs* Fc/Fc$^+$)
**E_{LUMO} have been calculated using E_{LUMO} (eV) = -4.8 - $E_{red}I$ (V *vs* Fc/Fc$^+$)
***Electrochemical band gap energy ***(E_g^{EQ}) values have been estimated using E_g^{EQ} = (E_{HOMO} -E_{LUMO}) eV

Comparing compounds **7** and **8**, the presence of -Cl groups in the peripheral substituents of phthalocyanine **8** increase its oxidation potential (0.67 V *vs* Fc/Fc$^+$) compared to phthalocyanine **7** (0.57 V *vs* Fc/Fc$^+$). Likewise, the reduction potential is more negative for phthalocyanine **7** (-1.02 and -1.55 V *vs* Fc/Fc$^+$) than for phthalocyanine **8** (-0.97 and -1.48 V *vs* Fc/Fc$^+$). These results indicate that the incorporation of -Cl atoms enhances the electron-accepting nature.

On the other hand, the comparison between phthalocyanine **9** and **10** allows the evaluation of the effect of the number of peripheral 4-methylthiophenyl substituents on the electrochemical properties. It was observed that the oxidation potential of phthalocyanine **9** (0.68 V vs Fc/Fc$^+$) is higher than that of phthalocyanine **10** (0.65 V vs Fc/Fc$^+$), while the reduction potentials of phthalocyanine **10** (-0.83 and -0.84 V vs Fc/Fc$^+$) are more positive compared to phthalocyanine **9**. This confirms that the higher density of donor groups in phthalocyanine **10** enhances its electron-donating capacity.

When analysing all four compounds together, phthalocyanines bearing thiophenyl groups exhibit higher oxidation potentials, indicating greater oxidation stability. Likewise, the reduction potentials are more negative in phthalocyanines **7** and **8**, suggesting lower stability of the reduced species.

Thus, it is confirmed that the most electron-accepting compound is phthalocyanine **8**, due to the presence of -Cl groups, which reduce the electron density of the molecule. In contrast, the most electron-donating compound is phthalocyanine **10**, as the higher number of 4-methylthiophenyl groups increases its electron-donating capacity, confirming the expected trend

1.3.1. Synthesis and Characterization of SURMOFS of SiPc 1,2, 3 and 4.

After the successful synthesis of the target compounds described above, their potential as linkers for the construction of SURMOF structures was evaluated. Due to their ditopic nature, these molecules were considered suitable candidates for coordination with zinc ions (Zn^{2+}) to form frameworks.

The SURMOF films were fabricated via sequential spin-coating on plasma-treated silicon substrates. A 1 mM zinc acetate solution in ethanol and a 20 μM solution of the corresponding SiPc in DMF were alternately deposited for 60 cycles, resulting in uniform and oriented thin films. The spin-coating technique was selected for its rapid processing and reproducibility.

To confirm the formation of the SURMOFs, *out-of-plane* XRD measurements were performed. For the most promising systems, additional characterization was conducted using FT-IRRAS to further corroborate the successful coordination between the linkers and the metal nodes. UV-Visible spectroscopy was subsequently performed to analyze the optical properties of the films, with particular attention given to the observation of bathochromic shifts in the Q-band indicative of *J*-type aggregation.

All experimental work described in this chapter was carried out during a pre-doctoral research stay at the Karlsruhe Institute of Technology (KIT) under the supervision and collaboration of Professor Christof Wöll, Dr. Hartmut Gliemann, and Dr. Anemar Bruno Kanj.

Figure 8.A presents the *out-of-plane* XRD patterns of SURMOF thin films constructed with SiPc derivatives 1-4, compared against simulated reference data. The simulation was generated using CIF data **(Annex 3)** from previous studies.[116] In all cases, the experimental patterns display periodicities in the range of 2.2-2.3 nm (a = b) and 1.1-1.3 nm (c), consistent with a layered SURMOF arrangement.

For Zn-SiPc **1** and Zn-SiPc **2**, the observed periodicities (a = b ≈ 2.2 nm, c ≈ 1.1 nm) show slight shifts compared to the theoretical simulation, likely due to increased steric hindrance introduced by the axial and peripheral substituents. While the general pattern agrees, the signal definition is moderate.

Zn-SiPc **4** exhibits broader and less defined peaks, and deviations in the periodicities (notably c ≈ 1.3 nm) suggest a less ordered framework or possibly incomplete MOF formation.

In contrast, Zn-SiPc **3** displays the most well-defined and intense diffraction peaks, with excellent agreement to the simulated pattern. The periodicities obtained (a = b = 2.4 nm, c = 1.1 nm) indicate a high degree of structural order and successful integration of the linker into the SURMOF architecture. This is further reinforced by the fact that Zn-SiPc **3** is the only system displaying five periodicities in the diffraction peaks, whereas the other samples show only two, highlighting its superior crystallinity.

Due to its superior crystallinity and structural definition, Zn-SiPc **3** was selected for further in-depth characterization. This improved ordering may be attributed to reduced steric hindrance arising from its specific peripheral substituents.

To further confirm the formation of the coordination framework and validate the successful assembly of the SURMOF architecture, the Zn-SiPc **3** sample was analysed by FT-IRRAS spectroscopy. This technique allowed the identification of characteristic vibrational modes associated with the coordination bonds between the phthalocyanine linkers and the Zn^{2+} metal centers, thereby providing complementary structural information to the XRD analysis.

Figure 8.B presents the FT-IRRAS spectrum of the Zn-SiPc **3** SURMOF. The spectrum exhibits characteristic peaks for the carboxylate group (COO^-) interacting with zinc, with an asymmetric stretching vibration around 1600 cm^{-1} and a symmetric stretching vibration at 1400 cm^{-1}. The Si-N stretching vibration of the phthalocyanine is observed at 1300 cm^{-1}, while the C=C and C=N stretching vibrations of the SiPc ring are also located at 1600 cm^{-1}. The *out-of-plane* deformations of the SiPc ring are observed at 700 cm^{-1}. These results confirm the formation of the SURMOF.

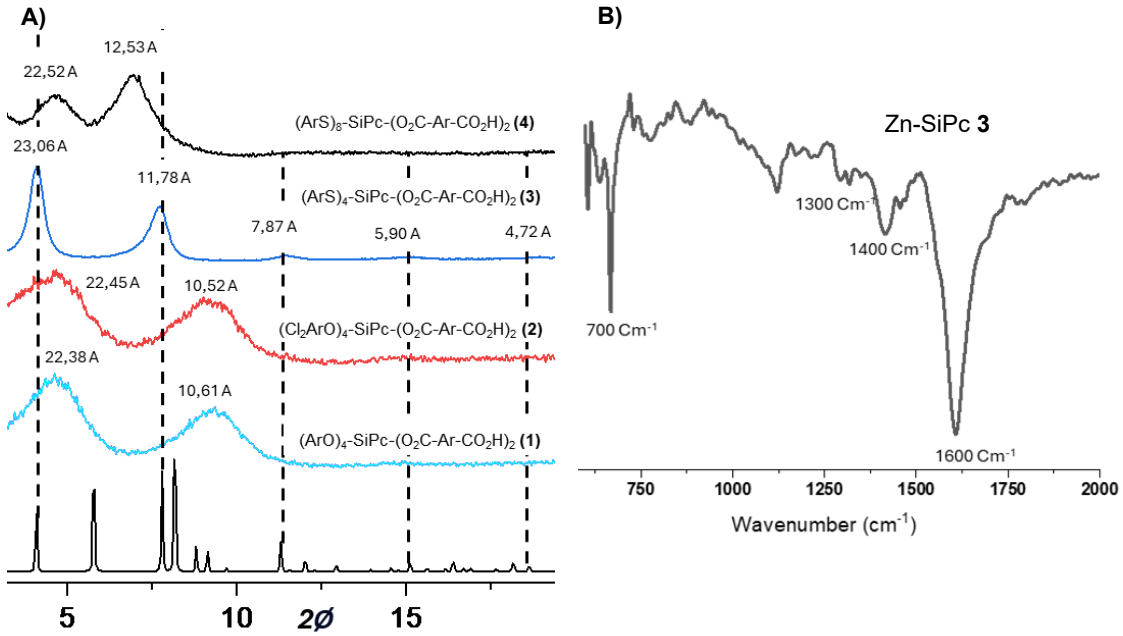

Figure 8. A) *Predicted structure of Zn-**SiPc-(CO₂H)₂** (black)[116] and experimental out-of-plane X-ray diffraction patterns of Zn-SiPc1; Zn-SiPc2; Zn-SiPc3 and Zn-SiPc4 SURMOF structure.* ***B)*** *FT-IRRAS spectra of Zn-SiPc **3**.*

Based on these findings, the Zn-SiPc **3** SURMOF was further characterized by UV-Vis spectroscopy **(Figure 9)**. To assess potential *J*-type aggregation within the framework, the UV-Vis spectrum of the Zn-SiPc **3** SURMOF in solid state, was compared to SiPc **3** $CHCl_3$ solution.

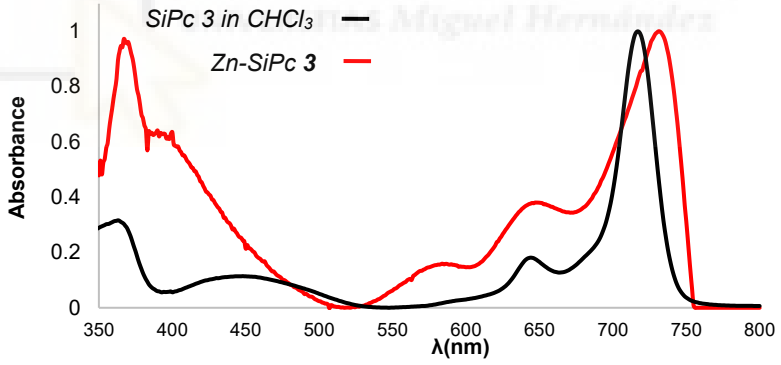

Figure 9*. UV-Vis of SiPc **3** (red) in $CHCl_3$ and Zn-SiPc **3** (black) SURMOF structure.*

The Q band absorption peak is centered at 717 nm in solution and suffers a bathochromic shift to 731 nm in the SURMOF, indicating a 14 nm shift. This bathochromic shift[177] in the Q band is a measurement of the strength of the *J*-type electronic coupling.

[177] A. Ferencz, D. Neher, M. Schulze, G. Wegner, L. Viaene, F. C. De Schryver, *Chem. Phys. Lett.* **1995**, *245*, 23–29.

2. Conclusion.

In this work, the synthesis and complete characterization of ten different silicon phthalocyanines were successfully achieved. These compounds were designed with different axial and peripheral substituents to modulate their electronic, optical, and solubility properties, addressing their suitability for two primary applications: optoelectronic devices and the development of novel SURMOFs.

All molecules were thoroughly characterized by ^{1}H-NMR spectroscopy, UV-Vis spectroscopy, HR-MALDI-TOF mass spectrometry, and, when applicable, electrochemical studies.

Among the SiPcs intended for SURMOFs, $(Cl_2ArO)_4$-SiPc-$(O_2C$-Ar-$CH_2)_2$ **(8)** was identified as the most electron-accepting compound, while $(ArS)_8$-SiPc-$(O_2C$-Ar-$CH_3)_2$ **(10)** exhibited the strongest electron-donating behaviour. These trends were consistently observed across UV-Vis and electrochemical measurements, supporting the donor-acceptor design strategy used.

From the phthalocyanines synthesized and characterized, SiPcs **1-4** were selected for evaluation regarding their ability to form SURMOF-type structures. The compounds $(ArO)_4$-SiPc-$(O_2C$-Ar_2-$CO_2H)_2$ **(5)** and $(Cl_2ArO)_4$-SiPc-$(O_2C$-Ar_2-$CO_2H)_2$ **(6)** was not pursued due to their close structural similarity to phthalocyanines **1** and **2**. Moreover, time constraints during the research stay at the Institute of Functional Interfaces (IFG), Karlsruhe Institute of Technology, also limited the scope of these experiments.

Ultimately, four SiPcs successfully formed crystalline and well-organized SURMOF structures, as evidenced by well-resolved *out-of-plane* XRD patterns. Among them, $(ArS)_4$-SiPc-$(O_2C$-Ar-$CO_2H)_2$ **(3)** yielded SURMOF films that were characterized by UV-Vis and FT-IRRAS spectroscopy, confirming both molecular integrity and successful incorporation of functional groups.

As future work, it would be of interest to assess whether SiPc **1**, **2** and **4** are also capable of forming ordered SURMOFs structures. Preliminary XRD patterns suggest this possibility; however, no further characterization was conducted.

In addition, the donor-acceptor nature of these SiPcs opens the possibility of designing future SURMOFs in which donor and acceptor layers alternate within the framework, a strategy that could be exploited to tailor charge transport and expand their potential applications.

Moreover, their potential performance in photoresponsive applications, such as photodetectors, remains unexplored. Additional studies would be required to confirm the formation of well-defined architectures and to evaluate their suitability for optoelectronic applications.

3. Experimental Section.

3.1. Materials and Methods

Except for specific cases mentioned, the reagents and solvents used in the synthesis processes were obtained from commercial suppliers and used without any additional purification.

-Microwave reactor: Microwave reactions were carried out in a CEM microwave reactor, Discover SP model.

-Chromatographic techniques: Column chromatography was performed on SiO_2 (40-63 mm), and Biorad Biobeads SX-3 (200-400 mesh) was used as the stationary phase for size exclusion chromatography (SEC). TLC plates coated with SiO_2 60F254 were visualized under UV light.

-Nuclear Magnetic Resonance (NMR): NMR spectra were recorded on a Bruker AC 300 or Burker 400MHz spectrometer at 25 ºC, unless otherwise specified using deuterated solvents and referenced to tetramethylsilane (TMS). Coupling constants (*J*) are reported in hertz (Hz). The signals are designated as follows: s = singlet, d = doublet, m = multiplet, and chemical shifts are given in ppm.

-UV-Vis: The measurements for SiPc in solution were recorded on a Perkin Elmer LAMDA 365 UV-WinLab spectrophotometer, using spectrosol-grade solvents. For SURMOF thin films, UV-Vis measurements in the solid state were performed in reflection mode using either a Cary 5000 UV-Vis/NIR spectrometer equipped with a Universal Measurement Accessory (UMA) unit from Agilent Technologies, or a PerkinElmer Lambda 950 UV-Vis/NIR spectrometer equipped with an integrating sphere, allowing accurate determination of the optical response within the multilayer system.

-Mass spectrometry: High-resolution mass spectra were obtained from a Bruker Reflex II matrix-assisted laser desorption/ionization time-of-flight (MALDI-TOF) spectrometer using dithranol as matrix.

-Electrochemistry: The measurements were performed at 298 K in a conventional three-electrode cell using an m-AUTOLAB type III potentiostat/galvanostat (Metrohm, Herisau, Switzerland). Sample solutions (ca. 0.5 mM) were prepared in deaerated PhCN or THF, containing 0.10 M tetrabutylammonium hexafluorophosphate ($TBAPF_6$) as supporting electrolyte; a glassy carbon (GC) as working electrode, an $Ag/AgNO_3$ as reference electrode, a platinum wire as counter electrode were used, and ferrocene/ferrocenium was the internal standard for all measurements.

-X-Ray diffraction (XRD): The XRD measurements for *out-of-plane* (co-planar orientation) were carried out using a Bruker D8-Advance diffractometer equipped with a position sensitive detector Lynxeye in geometry, variable divergence slit, and 2.3° Soller-slit was used on the secondary side.

-FT-IRRAS: The measurements for IRRAS data were recorded using a Biorad Excalibur FTIR spectrometer (FTS 3000) equipped with a grazing incidence reflection unit (Biorad Uniflex) and a narrow band MCT detector.

-Substrate pretreatment: Substrates were cleaned by argon-hydrogen plasma using a Diener Plasma surface treatment system (airflow: 20 sccm, pure hydrogen) for 30 minutes.

3.2.1. Synthesis of 4-(2,6-dimethylphenoxy)phthalonitrile (17).[174]

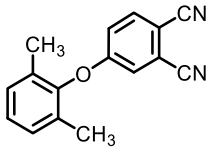

4- nitrophthalonitrile (5 g, 28.88mmol), 2,6-dimethylphenol (5 g, 43.32mmol) and K_2CO_3 (10 g, 43.42 mmol) were mixed in dimethyl sulfoxide (100 mL) under N_2 for 48 h. After that the crude material was precipitated over H_2O/ice and filtered under vacuum. The solid obtained was purified by column chromatography (SiO_2, CH_2Cl_2) yielding 5.26 g (73%) of 4-(2,6-dimethylphenoxy)phthalonitrile **17**[174] as a greenish solid. ^{1}H-NMR (400 MHz, DMSO-d_6, 25 ºC) δ= 8.05 (d, J = 8.8 Hz, 1H), 7.60 (d, J = 2.6 Hz, 1H), 7.27-7.08 (m, 4H), 2.05 (s, 6H).^{13}C-NMR (101 MHz, DMSO-d_6, 25 ºC): δ= 159.9, 148.6, 135.9, 129.7, 128.9, 125.8, 119.9, 118.9, 116.4, 115.3, 114.8,106.9, 15.2.

3.2.2. Synthesis of 5-(2,6-dimethylphenoxy)-1,3-diiminoisoindoline (18).

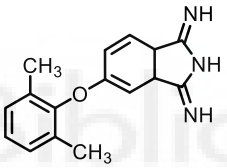

4-(2,6-dimethylphenoxy)phthalonitrile **17**[174] (2.0 g, 8.22 mmol), CH_3ONa (200 mg. 3.68 mmol) were mixed in methanol (150 mL). NH_3 was then bubbled in the solution at the refluxing methanol temperature (65 ºC) for 14 h. Afterwards, the reaction mixture was transferred to a crystallizing dish and the solvent was allowed to evaporate in air. The solid obtained was washed repeatedly with water, dried, and then washed with 50 mL of $CHCl_3$, yielding 1.22 g (56%) 5-(2,6-dimethylphenoxy)-1,3-diiminoisoindoline **18** as a cream-colored solid, which was used in successive reactions without further purification. ^{1}H-NMR (400 MHz, DMSO-d_6, 25 ºC) δ= 7.72-6.62 (m, 6H), 2.09 (s, 6H). ^{13}C-NMR (75 MHz, DMSO-d_6, 25 ºC): 159.4, 150.0, 130.2, 128.9, 125.3, 122.4, 116.2, 106.6,15.6.

3.2.3. Synthesis of $(ArO)_4$-$SiPcCl_2$ (19).

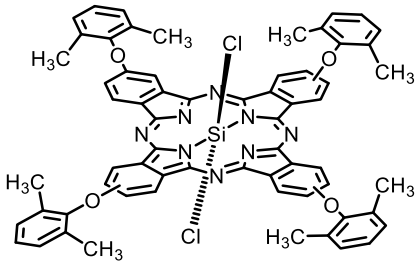

750 mg (2.81 mmol) of 5-(2,6-dimethylphenoxy)-1,3-diiminoisoindoline **18** were dissolved in 7 mL of quinoline. The mixture was purged with N_2 and protected from light. Then

0.7 ml of $SiCl_4$ was added. The reaction was heated to reflux temperature (200 ºC) for 1 hour. After cooling to 60 ºC, 100 mL of acetone was added, forming a suspension which was filtered hot, obtaining a crude solid that was washed with acetone. Yielding 750 mg (99%) of $(ArO)_4$-$SiPcCl_2$ **19** as a blue solid, which was used without further purification in subsequent reactions. UV-Vis ($CHCl_3$) λ_{max}/nm: 356, 374, 638, 712.

3.2.4. Synthesis of 4'-formyl-[1,1'-biphenyl]-4-carboxylic acid (20)[166]

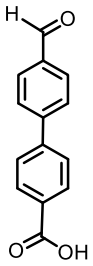

500 mg (2.70 mmol) of 4-bromobenzaldehyde and 540 mg (3.24 mmol) of 4-boronobenzoic acid were dissolved in 15 mL of anhydrous DMF and degassed with argon. The reaction mixture was stirred for 10 minutes at room temperature. Then, 4 mL of 2 M sodium carbonate solution and 140 mg (0.12 mmol) of $Pd(PPh_3)_4$ in 4 mL of DMF were added, and the temperature was increased to 110 °C. The reaction mixture was kept at this temperature overnight. The crude reaction mixture was dissolved in 40 mL of methanol and filtered. The filtrate was concentrated under reduced pressure and redissolved in 60 mL of a methanol/water mixture (5:1). The solution was filtered again to remove impurities. 3 mL of 2 M hydrochloric acid was added to filtered solution, resulting in the formation of a white precipitate which was collected by vacuum filtration. The solid was washed three times with 15 mL of chloroform yielding 400 mg (66%) of 4'-formyl-[1,1'-biphenyl]-4-carboxylic acid **20**[166] as a white solid. ^{1}H-NMR (300 MHz, DMSO-*d*$_6$, 25 ºC): δ= 10.05 (s, 1H), 8.08-7.95 (m, 6H), 7.86 (d, *J* = 9.0 Hz, 2H) ppm. ^{13}C-NMR (125 MHz, DMSO-*d*$_6$, 25 ºC): 192.7, 167.0, 144.6, 142.9, 135.6, 130.6, 130.2, 130.1, 127.7, 127.3 ppm.

3.2.5. Synthesis of $(ArO)_4$-SiPc-$(O_2C$-Ar-$CHO)_2$ (21).

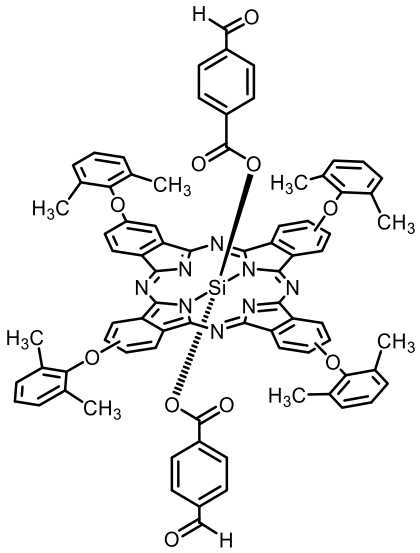

A suspension of 50 mg (0.040 mmol) of $(ArO)_4$-$SiPcCl_2$ **19**, 103 mg (0.680 mmol) of 4-formylbezoic acid and 6 mL of dry toluene. The mixture was heated in microwave reactor while stirring, at constant temperature of 200 ºC for 60 minutes. Then toluene was removed, the resulting solid was washed with 60 mL of methanol. The solid was dissolved in DCM and centrifuged, discarding the precipitate. The solution was concentrated. The resulting solid was purified by column chromatography (SiO_2, CH_2Cl_2). Yielding 40 mg (66%) of $(ArO)_4$-SiPc-$(O_2C$-Ar-$CHO)_2$ **(21)** as a blue-green solid. ^{1}H-NMR (400 MHz, $CDCl_3$, 25 ºC) δ= 9.64-9.49 (m, 4H), 9.47 (s, 2H), 8.89-8.66 (m, 4H), 8.02-7.85 (m, 4H), 7.40-7.32 (m, 12H), 6.83 (d, *J* = 8.5 Hz, 4H), 5.41 (d, *J* = 8.5 Hz, 4H), 2.40-2.32 (m, 24H).UV-Vis ($CHCl_3$) λ_{max}/nm (log ε): 359 (4.99), 631 (4.67), 705 (5.36). MS (MALDI-TOF, dithranol): *m/z* [M^-] calcd for $C_{80}H_{58}N_8O_{10}Si$ 1318.4059, found 1318.5521.

3.2.6 Synthesis of $(ArO)_4$-SiPc-$(O_2C$-Ar_2-$CHO)_2$ (22)

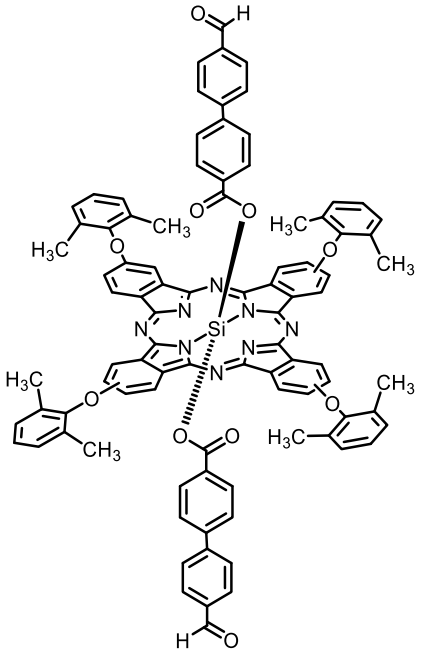

A suspension of 50 mg (0.040 mmol) of $(ArO)_4$-$SiPcCl_2$ **19**, 62 mg (0.28 mmol) of 4'-formyl-[1,1'-biphenyl]-4-carboxylic acid **20**[166], 30 mg (0.07 mmol) of 1,1'-methylenebis(3-methylimidazolium iodide)[175] and 3 mL of dry toluene was heated in a microwave reactor with constant stirring at 160 ºC for 1 hour. Then removed toluene and resulting solid was washed with 60 mL of methanol/ water (3:1). The obtained solid was purified by column chromatography (SiO_2, CH_2Cl_2). Yielding 40 mg (76%) of $(ArO)_4$-SiPc-$(O_2C$-Ar_2-$CHO)_2$ (**22**) as a blue-green solid. ^{1}H-NMR (400 MHz, $CDCl_3$,25 ºC) δ= 9.89 (s, 2H), 9.63-9.43 (m, 4H), 8.87-8.64 (m, 4H), 7.98-7.82 (m, 4H), 7.67 (d, *J* = 8.5 Hz, 4H), 7.40-7.32 (m, 12H), 7.16 (d, *J* = 8.5Hz, 4H), 6.56 (d, *J* = 8.5 Hz, 4H), 5.30 (d, *J* = 8.5 Hz, 4H), 2.40-2.32 (m, 24H). UV-Vis ($CHCl_3$) λ_{max}/nm (log *ε*): 360 (4.45), 630 (4.16), 707 (4.90). MS (MALDI-TOF, dithranol): *m/z* [M^-] calcd for $C_{92}H_{66}N_8O_{10}Si$ 1470.4683 found 1470.4778.

3.2.7 Synthesis of $(ArO)_4$-SiPc-$(O_2C$-Ar-$CO_2H)_2$ (1).

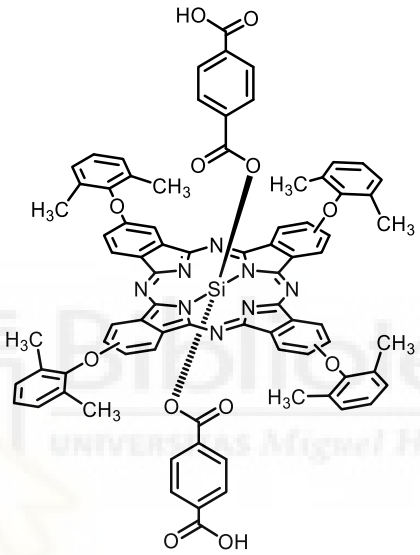

120 mg (0.089 mmol) of $((ArO)_4$-SiPc-$(O_2C$-Ar-$CHO)_2$ **(21)**, was dissolved in 6 mL of THF/H_2O (6:1) mixture. Separately, 65 mg (0.532 mmol) of H_3NSO_3 and 50 mg (0.364 mmol) of $NaClO_2$ were dissolved as well in 6 mL of THF/H_2O (6:1) mixture. This solution was slowly added to the solution of $(ArO)_4$-SiPc-$(O_2C$-Ar-$CHO)_2$ **(21)**. The reaction was protected from light and stirred at room temperature for 24 hours. Then solvents were removed, the obtained solid was washed repeatedly with 3 volumes of MeOH/H_2O (3:1) mixture and one additional volume of MeOH. Yielding 85 mg (70%) of target compound $(ArO)_4$-SiPc-$(O_2C$-Ar-$CO_2H)_2$ **(1)** as a pure blue-green solid. ^{1}H-NMR (400 MHz, $CDCl_3$, 25 ºC) δ= 9.55-9.37 (m, 4H), 8.86-8.51 (m, 4H), 7.91-7.73 (m, 4H), 7.35-7.26 (m, 12H), 6.61 (d, *J*= 8.5 Hz, 4H), 5.19 (d, *J*= 8.5 Hz, 4H), 2.40-2.32 (m, 24H). UV-Vis ($CHCl_3$) λ_{max}/nm (log *ε*): 361 (4.61), 628 (4.61), 701 (5.31). MS (MALDI-TOF, dithranol): m/z [M^+] calcd. $C_{80}H_{58}N_8O_{12}Si$ 1350.3938 found 1350.0153.

3.2.8 Synthesis of $(ArO)_4$-SiPc-$(O_2C$-Ar_2-$CO_2H)_2$ (5).

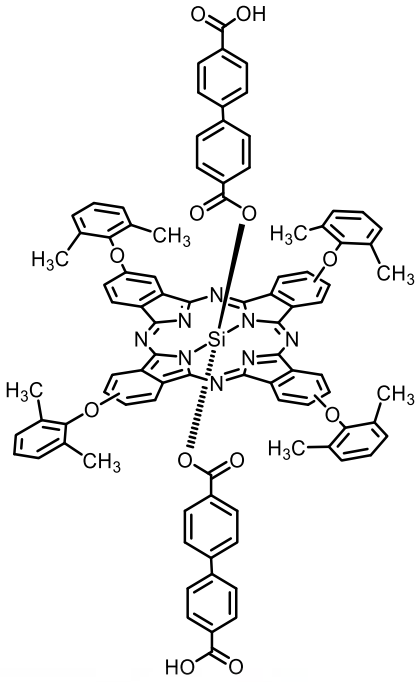

72 mg (0.049 mmol) of $(ArO)_4$-SiPc-$(O_2C$-Ar_2-$CHO)_2$ **(22)**, was dissolved in 6 mL of THF/H_2O mixture. Separately, 30 mg (0.313 mmol) of H_3NSO_3 and 20 mg (0.221 mmol) of $NaClO_2$ were dissolved in 6 mL of THF/H_2O (6:1) as well. This solution was slowly added to the solution of $(ArO)_4$-SiPc-$(O_2C$-Ar_2-$CHO)_2$ **(22)**. The reaction was protected from light and stirred at room temperature for 24 hours. Then the product was precipitated in 30 mL of MeOH and washed repeatedly with 3 volumes of MeOH/H_2O (3:1) mixture and one additional volume of MeOH. Yielding 56 mg (75%) of target compound $(ArO)_4$-SiPc-$(O_2C$-Ar_2-$CO_2H)_2$ **(5)** as a pure blue-green solid. ^{1}H-NMR (400 MHz, $CDCl_3$, 25 ºC) δ= 9.58-9.39 (m, 4H), 8.84-8.61 (m, 4H), 7.91-7.85 (m, 4H), 7.87 (d, *J* = 8.5 Hz, 4H), 7.32-7.26 (m, 12H), 7.04 (d, *J* = 8.5 Hz, 4H), 6.52 (d, *J* = 8.5 Hz, 4H), 5.35 (d, *J* = 8.5 Hz, 4H), 2.40-2.32 (m, 24H).UV-Vis ($CHCl_3$) λ_{max}/nm (log ε): 360 (4.50), 630 (4.21), 702 (4.93). MS (MALDI-TOF, dithranol): *m/z* [M^-] calcd for $C_{92}H_{66}N_8O_{12}Si$ 1502.4573 found 1502.5473.

3.2.9. Synthesis of $(ArO)_4$-SiPc-(O_2C-Ar-$CH_3)_2$ (7).

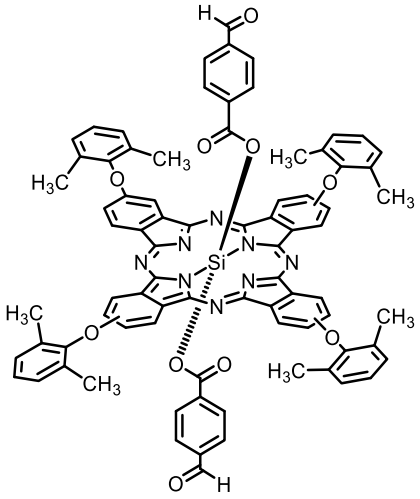

A suspension of 50 mg (0.040 mmol) of $(ArO)_4$-$SiPcCl_2$ **(19)**, 95 mg (0.700 mmol) of 4-methylbezoic acid, and 3 mL of dry toluene was heated in microwave reactor with constant stirring at 200 ºC for 1 hour. Then, toluene was removed, the resulting solid was washed with 60 mL of methanol. The solid was dissolved in DCM and centrifuged, discarding the precipitate. The supernatant was concerted, and the obtained solid was purified by column chromatography (SiO_2, CH_2Cl_2). Yielding 43 mg (73%) of $(ArO)_4$-SiPc-(O_2C-Ar-$CH_3)_2$ **(7)** as a blue-green solid. ^{1}H-NMR (400 MHz, $CDCl_3$, 25 ºC) δ 9.56-9.37 (m, 4H), 8.82-8.61 (m, 4H), 7.91-7.68 (m, 4H), 7.37-7.29 (m,12H), 6.06 (d, *J* = 8.2 Hz, 4H), 5.05 (d, *J* = 8.2 Hz, 4H), 2.45-2.31 (m, 24H) 1.72 (s, 6H). UV-Vis ($CHCl_3$) λ_{max}/nm (log ε): 361 (4.92), 628 (4.62), 702 (5.32). MS (MALDI-TOF, dithranol): *m/z* [M^+] calcd. for $C_{80}H_{62}N_8O_8Si$ 1290.4477, found 1290.6265.

3.2.10. Synthesis of 4-(2,6-dichlorophenoxy)phthalonitrile (23).

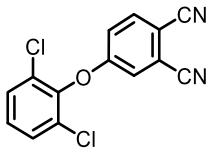

3 g (17.32 mmol) of 4-nitrophtalonitrile, 4.24 g (26 mmol) of 1,3-dichloro-2-hidroxybenzene, 6 g (43.42 mmol) of K_2CO_3 and 80 mL of DMSO were added to a 250 mL round-bottomed flask. A nitrogen atmosphere was established, and the mixture was stirred at room temperature for 24 hours. After this time, the crude product was precipitated over ice/water and filtered under vacuum. The solid obtained was washed with water and then with 50 mL of cold ethanol, yielding 4.2 g (70%) of 4-(2.6-dichlorophenoxy)phthalonitrile **23** as a yellowish solid, which was used in subsequent reactions without further purification. ^{1}H- NMR (400 MHz, $CDCl_3$, 25 ºC) δ= 7.80-7.72 (m, 1H), 7.47 (d, *J* = 8.1 Hz, 2H), 7.33-7.27 (d, *J* = 8.1 Hz 1H), 7.22-7.13 (m, 2H). ^{13}C-NMR (100 MHz, $CDCl_3$, 25 ºC): δ= 158.8, 144.5, 134.8, 128.9, 128.5, 127.3, 119.3, 117.1, 114.4, 114.1, 109.0.

3.2.11. Synthesis of 5-(2,6-dimethylphenoxy)-1,3-diiminoisoindoline (24).

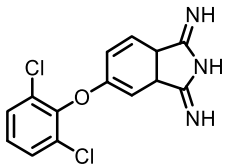

750 mg (2.6 mmol) of 4-(2,6-dichlorophenoxy)phtalonitrile **23**, 75 mg (1.38 mmol) of CH_3ONa and 150 mL of CH_3OH were added to a 250 mL two-necked round bottomed flask. The reaction mixture was at the reflux temperature of methanol (65 ºC) while bubbling NH_3 for 10 hours. After this time, the crude reaction mixture was transferred to a crystallizing dish, the solvent was allowed to evaporate in air, and the resulting solid was washed repeatedly with water. 660 mg (83%) of 5-(2,6-dimethylphenoxy)-1,3-diiminoisoindoline **24**, was obtained as a cream-coloured solid, which was used in subsequent reactions without further purification. ^{1}H-NMR (400 MHz, DMSO-d_6, 25 ºC): δ= 7.81 (d, *J* = 8.2 Hz, 1H), 7.72 (d, *J* = 8.1 Hz, 2H), 7.51-7.39 (m, 2H), 7.16-7.09 (m, 1H) ppm.^{13}C-NMR (101 MHz, DMSO-d_6, 25 ºC): δ= 158.2, 145.4, 129.7, 128.3, 127.8, 122.4, 116.8, 106.7.

3.2.12. Synthesis of $(Cl_2ArO)_4$-$SiPcCl_2$ (25).

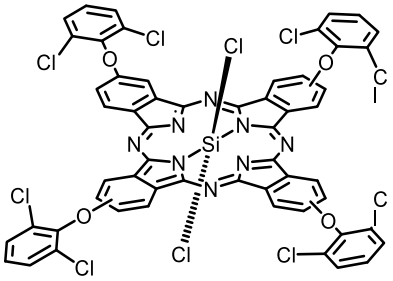

660 mg (1.54 mmol) of 5-(2,6-dichlorophenoxy)-1,3-diiminoisoindoline **24** were dissolved in 7 mL of quinoline. The system was closed purged with N_2 and protected from light. Then 0.7 ml of $SiCl_4$ was added. The reaction was heated to reflux (200 ºC) for 1 hour. After cooling to 60 ºC, 100 mL of acetone was added, forming a suspension which was filtered hot. The solid obtained was washed with acetone. Yielding 650 mg (99%) of $(Cl_2ArO)_4$-$SiPcCl_2$ **25** as a green solid which was used without further purification in subsequent reactions. UV-Vis ($CHCl_3$) λ_{max}/nm: 315, 354, 374, 633, 705 nm.

3.2.13. Synthesis of $(Cl_2ArO)_4$-$SiPc$-$(O_2C$-Ar-$CHO)_2$ (26).

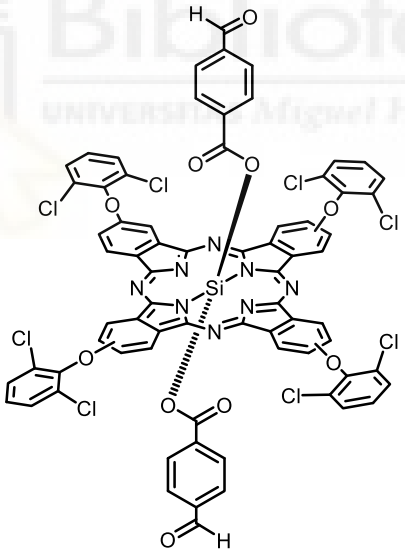

A suspension of 50 mg (0.034 mmol) of $(Cl_2ArO)_4$-$SiPcCl_2$ **25**, 120 mg (0.800 mmol) of 4-formylbenzoic acid, 30 mg (0.07 mmol) of 1,1'-methylenebis(3-methylimidazolium iodide)[175] and 3 mL of dry toluene was heated in a microwave reactor with constant stirring at a target temperature of 160 ºC for 60 min. Then toluene was remover, the obtained solid was washed with 60 ml of MeOH. The solid was dissolved in DCM and centrifuged, discarding the precipitate. The supernatant was concentrated, the obtained solid was purified by column chromatography (SiO_2, CH_2Cl_2). Yielding 27 mg (46%) of $(Cl_2ArO)_4$-$SiPc$-$(O_2C$-Ar-$CHO)_2$ **(26)** as a blue-green solid. ^{1}H-NMR (400 MHz, $CDCl_3$, 25 ºC) δ= 9.65-9.48 (m, 4H), 9.42 (s, 2H), 8.93-8.81 (m, 4H), 8.01-7.84 (m, 4H), 7.68-7.58 (m, 8H), 7.45-7.39 (m, 4H), 6.79 (d, *J* = 8.1 Hz, 4H), 5.29 (d, *J* = 8.1 Hz, 4H). UV-Vis ($CHCl_3$) λ_{max}/nm (log ε): 359 (4.91), 626 (4.60), 689 (5.34). MS (MALDI-TOF, dithranol): m/z [M^-] calcd. $C_{72}H_{34}Cl_8N_8O_{10}Si$ 1482.9703 found 1482.5492.

3.2.14. Synthesis of $(Cl_2ArO)_4$-SiPc-$(O_2C$-Ar_2-$CHO)_2$ (27).

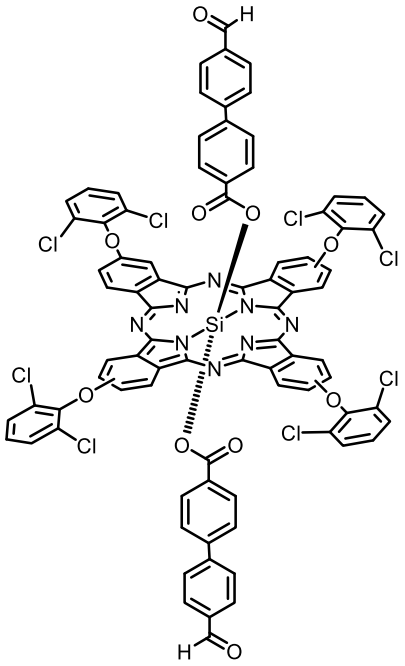

A suspension of 50 mg (0.034 mmol) of $(Cl_2ArO)_4$-$SiPcCl_2$ **25**, 65 mg (0.286 mmol) of of 4'-formyl-[1,1'-biphenyl]-4-carboxylic acid **20,**[166] 30 mg (0.07 mmol) of 1,1'-methylenebis(3-methylimidazolium iodide)[175] and 3 mL of dry toluene, was heated in a microwave reactor with constant stirring at temperature of 160 ºC for 1 hour. Then toluene was removed, and the obtained solid was washed with 60 mL of MeOH. The solid was purified by column chromatography (SiO_2, Hx/AcOEt (1:1)). Yielding 15 mg (23%) of $(Cl_2ArO)_4$-SiPc-$(O_2C$-Ar_2-$CHO)_2$ **(27)** as a pure blue-green solid. ^{1}H NMR (400 MHz, $CDCl_3$, 25 ºC) δ = 9.86 (s, 2H), 9.66-9.48 (m, 4H), 8.94-8.82 (m, 4H), 8.00-7.82 (m, 4H), 7.68-7.58 (m, 8H), 7.63 (d, *J* = 8.1 Hz, 4H), 7.44-7.34 (m, 4H), 7.14 (d, *J* = 8.1 Hz, 4H), 6.54 (d, *J* = 8.2 Hz, 4H), 5.23 (d, *J* = 8.2 Hz, 4H). UV-Vis ($CHCl_3$) λ_{max}/nm (log *ε*): 357 (4.96), 622 (4.49), 691 (5.27). MS (MALDI-TOF, dithranol): *m/z* [M^-] calcd. for $C_{84}H_{43}Cl_8N_8O_{10}Si$ 163.0442, found 1635.4874.

3.2.15. Synthesis of $(Cl_2ArO)_4$-SiPc-$(O_2C$-Ar-$CO_2H)_2$ (2).

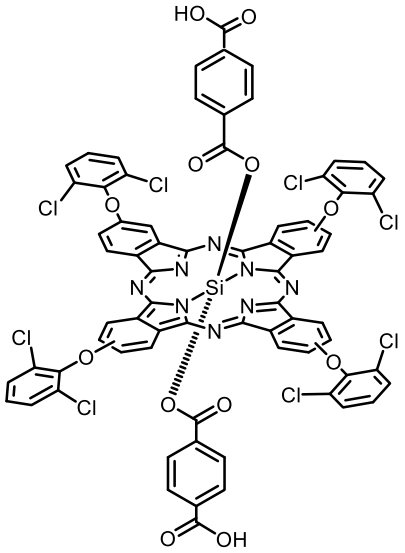

86 mg (0.06 mmol) of $(Cl_2ArO)_4$-SiPc-$(O_2C$-Ar-$CHO)_2$ **(26)**, was dissolved in 3 mL of THF/H_2O (6:1) mixture. Separately, 40 mg (0.36 mmol) of H_3NSO_3 and 32 mg (0.24 mmol) of $NaClO_2$ were dissolved in 3 mL of THF/H_2O (6:1) mixture. This solution was slowly added to the solution of $(Cl_2ArO)_4$-SiPc-$(O_2C$-Ar-$CHO)_2$ **(26)**. The reaction was protected from light and stirred at room temperature for 24 hours. Then, the solvents were removed, and the obtained solid was washed repeatedly with 3 volumes of MeOH/H_2O (3:1) mixture and one additional volume of MeOH. Yielding 62 mg (70%) of the target compound $(Cl_2ArO)_4$-SiPc-$(O_2C$-Ar-$CO_2H)_2$ **(2)** as pure blue-green solid. ^{1}H-NMR (400 MHz, $CDCl_3$, 25 ºC) δ= 9.65-9.42 (m, 4H), 8.93-8.84 (m, 4H), 7.97-7.80 (m, 4H), 7.70-7.63 (m, 8H), 7.56-7.47 (m, 4H), 6.91 (d, *J* = 8.2Hz, 4H), 5.17 (d, *J* = 8.2 Hz, 4H).UV-Vis ($CHCl_3$) λ_{max}/nm (log ε): 360 (4.59), 625 (4.25), 696 (4.98).MS (MALDI-TOF, dithranol): m/z [M^+] calcd. for $C_{72}H_{35}Cl_8N_8O_{12}Si$ 1512.9638 found 1513.1344.

3.2.16. Synthesis of $(Cl_2ArO)_4$-SiPc-$(O_2C$-Ar_2-$CO_2H)_2$ (6).

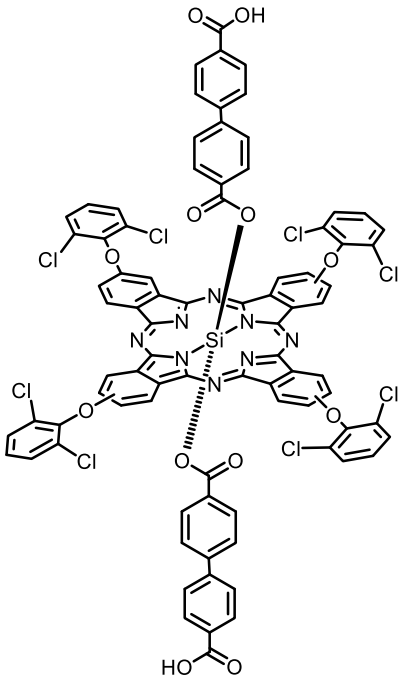

100 mg (0.061 mmol) of $(Cl_2ArO)_4$-SiPc-$(O_2C$-Ar_2-$CHO)_2$ **(27)**, was dissolved in 6 mL of THF/H_2O (6:1) mixture. Separately, 35 mg (0.37 mmol) of H_3NSO_3 and 27 mg (0.25 mmol) of $NaClO_2$ were dissolved in 6 mL of THF/H_2O (6:1) mixture. This solution was slowly added to the solution $(Cl_2ArO)_4$-SiPc-$(O_2C$-Ar_2-$CHO)_2$ **(27)**. The reaction was protected from light and stirred at room temperature for 24 hours. Then, the solvents were removed, and the obtained solid was washed repeatedly with 3 volumes of MeOH/H_2O (3:1) mixture and one additional volume of MeOH. Yielding 76 mg (75%) of the target compound $(Cl_2ArO)_4$-SiPc-$(O_2C$-Ar_2-$CO_2H)_2$ **(6)** as a blue-green solid. ^{1}H-NMR (400 MHz, $CDCl_3$, 25 ºC) δ = 9.65-9.41 (m, 4H), 8.90-8.78 (m, 4H), 7.93-7.82 (m, 4H), 7.80 (d, *J* = 8.1 Hz, 4H), 7.66-7.56 (m, 8H), 7.47-7.32 (m, 4H), 7.05 (d, *J* = 8.1 Hz, 4H), 6.53 (d, *J* = 8.2 Hz, 4H), 5.23 (d, *J* = 8.2 Hz, 4H). UV-Vis ($CHCl_3$) λ_{max}/nm (log *ε*): 358 (4.79), 624 (4.42), 695 (5.16). MS (MALDI-TOF, dithranol): *m/z* [M^+] calcd. for $C_{84}H_{42}C_8N_8O_{12}Si$ 1666.0277 found 1666.1494.

3.2.17. Synthesis of $(Cl_2ArO)_4$-SiPc-(O_2C-Ar-$CH_3)_2$ (8).

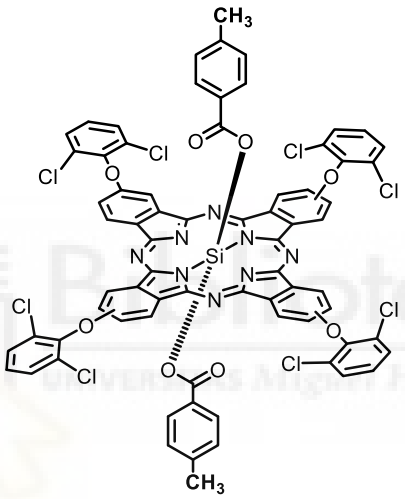

A suspension of 50 mg (0.034 mmol) of $(Cl_2ArO)_4$-SiPcCl_2 **(25)**, 136 mg (0.800 mmol) of 4-methylbezoic acid, 30 mg (0.07 mmol) of 1,1'-methylenebis(3-methylimidazolium) iodide[175] and 4 mL of dry toluene, was heated in a microwave reactor with constant stirring at constant temperature of 160 ºC for 1 hour. Then toluene was removed, and the obtained solid was washed with 60 mL of MeOH. The solid was dissolved in DCM and centrifuged, discarding the precipitate. The supernatant was concentrated, the solid was purified by column chromatography (SiO_2, CH_2Cl_2). Yielding 37 mg (64%) of $(Cl_2ArO)_4$-SiPc-(O_2C-Ar-$CH_3)_2$ **(8)** as a blue-green solid.^{1}H-NMR (400 MHz, $CDCl_3$, 25 ºC) δ = 9.63-9.45 (m, 4H), 8.91-8.79 (m, 4H), 7.97-7.80 (m, 4H), 7.67-7.58 (m, 8H), 7.43-7.31 (m, 4H), 6.06 (d, *J* = 8.1 Hz, 4H), 5.02 (d, *J* = 8.1 Hz, 4H), 1.72 (s, 6H). UV-Vis ($CHCl_3$) λ_{max}/nm (log *ε*): 362 (4.94), 623 (4.62), 695 (5.36).MS (MALDI-TOF, dithranol): m/z [M^-] calcd. for $C_{72}H_{38}Cl_8N_8O_8Si$ 1453.9667, found 1453.3624.

3.2.18. Synthesis of 4-(*p*-tolylthio)phthalonitrile (28).

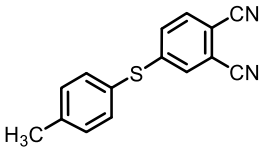

4-Nitrophtalonitrile 2 g (11.55 mmol), 4-methylthiopenol 1,5 g (12.08mmol), and K_2CO_3 2.5 g (18.09 mmol) were mixed in 40 mL of dimethyl sulfoxide. An argon atmosphere was established, and the mixture was stirred for 24 hours. The crude product was precipitate over ice/water and filtered. The solid obtained was washed with water and then with cold ethanol, yielding 2.29 g (79%) of 4-(p-tolythio)phtalonitrile **28** as a pale white solid, which was used in subsequent reactions without further purification. ^{1}H-NMR (400 MHz, $CDCl_3$, 25 ºC) δ 7.57 (d, 1H, *J* = 8.3 Hz), 7.43 (d, 2H, *J* = 8.3 Hz), 7.33-7.23 (m, 4H), 2.44 (s, 3H). ^{13}C-NMR (100 MHz, $CDCl_3$, 25 ºC): δ 149.0, 141.2, 135.3, 133.1, 129.7, 129.5, 124.5, 116.2, 115.5, 115.1, 110.9, 21.3.

3.2.19. Synthesis of 5-(*p*-tolylthio)-diiminoisoindoline (29).

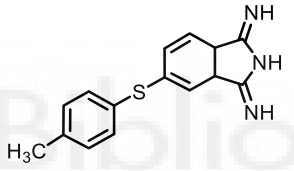

1.8 g (7.20 mmol) of 4-(p-tolythio)phtalonitrile **28** and 0.18 g of MeONa (3.33 mmol) were mixed in 150 mL of methanol. Ammonia was bubbled through the solution at methanol temperature reflux (65 ºC) for 9 hours. The solvent was then evaporated, and the resulting solid was washed repeatedly with water and dried. Yielding 1.85 g (96%) of 5-(p-tolythio)diiminoisoindoline **29** as a pale-white solid, which was used in subsequent reactions without further purification. ^{1}H-NMR (400 MHz, CD_3OD, 25 ºC) δ 7.70 (d, 1H, *J* = 7.9 Hz,), 7.65 (d, 1H, *J* = 1.4 Hz,), 7.41 (d, 2H, *J* = 8. 1 Hz,), 7.34 (dd, 1H, *J* = 7.9Hz *J* = 1,4Hz,), 7.27 (d, 2H, *J* = 8.1Hz,), 2.38 (s, 3H,). ^{13}C-NMR (100 MHz, CD_3OD, 25 ºC) δ 145.4, 140.7, 135.2, 131.8, 131.4, 130.0, 123.0, 121.9, 21.3.

3.2.20. Synthesis and characterisation of $(ArS)_4$-$SiPcCl_2$ (30).

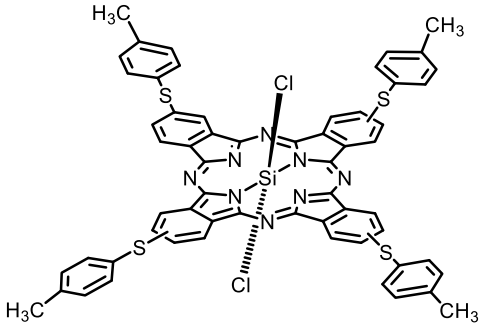

750 mg (2.81 mmol) of 5-(p-tolythio)-diiminoisoindoline **29** was dissolved in 7 mL of quinoline. The system was closed, purged with N_2 and protected from light. Then 0.7 mL of $SiCl_4$ was added, and the mixture was heated to reflux temperature (200 ºC) for 1 hour. The crude product was precipitated in acetone, filtered and washed repeatedly with acetone. Yielding 757

mg (99%) of $(ArS)_4$-$SiPcCl_2$ **30** as a green solid, which was used without further purification in subsequent reactions. UV-Vis ($CHCl_3$) λ_{max}/nm: 377, 455, 652, 726.

3.2.21. Synthesis of $(ArS)_4$-SiPc-$(O_2C$-Ar-$CO_2H)_2$ (3).

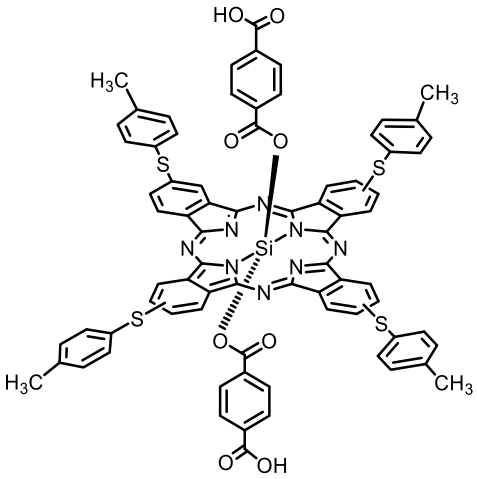

50 mg (0.045 mmol) of $(ArS)_4$-$SiPcCl_2$ **(30)** and 75 mg (0.450 mmol) of terephthalic acid were dissolved in 1 mL Tol/NMP (1:1) mixture. The dissolution was heated in a microwave reactor with constat stirring at constant temperature of 160 ºC for 1 hour. The crude reaction was precipitated in methanol, filtered and purified by size exclusion chromatography (Bio-Beads, THF). Yielding 19 mg (26%) of the target compound $(ArS)_4$-SiPc-$(O_2C$-Ar-$CO_2H)_2$ **(3)** as a pure green solid. ^{1}H-RMN (400 MHz, $CDCl_3$, 25 ºC) δ 9.44-9.23 (m, 8H), 8.15-7.96 (m, 4H), 7.71-7.63 (m, 8H), 7.37 (d, J = 7.8 Hz, 8H), 6.93 (d, J = 8.2 Hz, 4H), 5.19 (d, J = 8.2 Hz, 4H), 2.51 (s, 12H). UV/Vis ($CHCl_3$): λ_{max}/nm (log ε) 363 (4.69), 448 (4.22), 644 (4.44), 717 (5.20). HR-MS (MALDI-TOF, dithranol): *m/z* [M^+] calcd. for $C_{76}H_{50}N_8O_8S_4Si$ 1398.2390, found 1398.2396.

3.2.22. Synthesis of $(ArS)_4$-SiPc-(O_2C-Ar-$CH_3)_2$ (9).

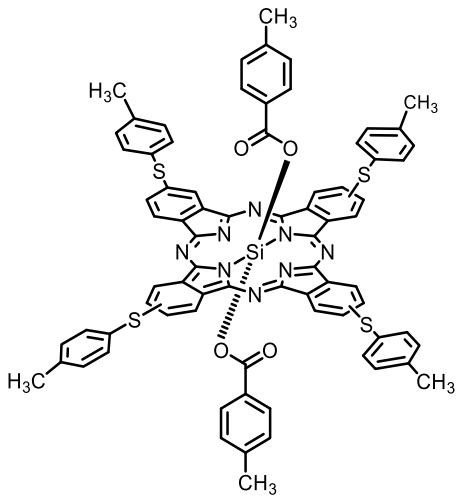

50 mg (0.045 mmol) of $(ArS)_4$-$SiPcCl_2$ **(30)** and 62 mg (0.450 mmol) of 4-methylbenzoic acid were dissolved in 1 mL Tol/NMP (1:1) mixture. The dissolution was heated in a microwave reactor with constat stirring at constant temperature of 160 ºC for 1 hour. The crude product was precipitated in methanol, filtered and purified by column chromatography (SiO_2, $CHCl_3$/Hexane

(3:1)). Yielding 28 mg (48%) of $(ArS)_4$-SiPc-(O_2C-Ar-$CH_3)_2$. **(9)** as a green solid. ^{1}H-NMR (400 MHz, $CDCl_3$, 25 °C) δ = 9.48-9.35 (m, 8H), 8.15-8.06 (m, 4H), 7.39 (d, *J* = 7.9 Hz, 8H), 6.09 (d, *J* = 8.0 Hz, 4H), 5.05 (d, *J* = 8.0 Hz, 4H), 2.53 (s, 12H), 1.75 (s, 6H). UV/Vis ($CHCl_3$) λ_{max}/nm (log *ε*) 366 (4.59), 443 (4.18), 614 (3.63), 714 (5.17). HR-MS (MALDI-TOF, dithranol): *m/z* [M^+] calcd. for $C_{76}H_{54}N_8O_4S_4Si$ 1298.2813, found 1298.2820.

3.2.23. Synthesis and characterisation of 4,5-bis(*p*-tolylthio)phthalonitrile (31).

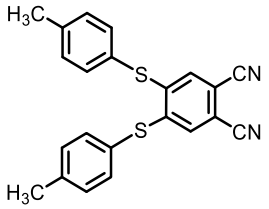

2 g (10.15 mmol) of 5,6-dichlorophthalonitrile, 3.86 g (24.20 mmol) of 4-methylthiophenol, and 21 g (151,94 mmol) of K_2CO_3 were dissolved in 40 mL of dimethyl sulfoxide under an argon atmosphere and stirred for 24 hours. The crude product was precipitated over ice/water and filtered. The solid obtained was washed repeatedly with water and then with cold ethanol. Yielding 2.61 g (69%) of 4,5-bis(*p*-tolythio)phthalonitrile **31** as a pale-white solid, which was used in subsequent reactions without further purification. ^{1}H-NMR (400 MHz, $CDCl_3$, 25 ºC): δ = 7,44 (d, 4H, *J* = 8.0 Hz), 7.33 (d, 4H, *J*= 8.0 Hz,), 6.91 (s, 2H), 2. 46 (s, 6H).^{13}C-NMR (100 MHz, $CDCl_3$, 25 ºC) δ 144.4, 141.3, 135.4, 131.4, 129.3, 124.6, 115.5, 111.2, 21.4.

3.2.24. Synthesis of 5,6-bis(*p*-tolylthio)-diiminoisoindoline (32).

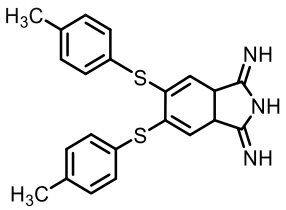

1.5 g (4.03 mmol) of 5,6-bis(p-tolythio)phtalonitrile **31** and 0.15 g on MeONa (2.78 mmol) were dissolved in 150 mL of methanol. NH_3 was bubbled through the solution at the reflux temperature of methanol (65 ºC) for 7 hours. The solvent was then evaporated, and the resulting solid was washed repeatedly with water and dried. Yielding 1.17 g (75%) of 5,6-bis(*p*-tolylthio)diiminoisoindoline **32** as a pale-white solid, which was used in subsequent reactions without further purification. ^{1}H-NMR (400 MHz, CD_3OD, 25 ºC) δ = 7.51 (s, 2H,), 7.37 (d, 4H, *J* = 8.0 Hz), 7.28 (d, 4H, *J* = 8.0 Hz), 2,39 (s, 6H) ppm. ^{13}C-NMR (100 MHz, CD_3OD, 25 ºC) δ 140.5, 134.6, 131.8, 130.2, 123.5, 21.3.

3.2.25. Synthesis of $(ArS)_8$-$SiPcCl_2$ (33).

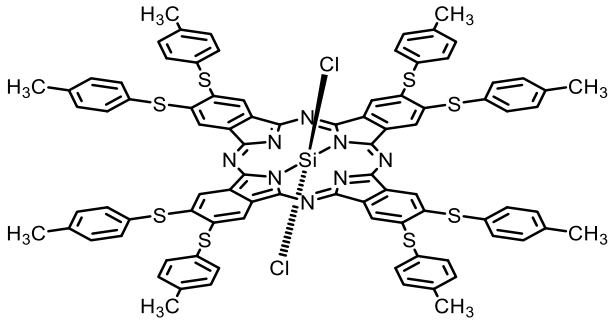

600 mg (1.54 mmol) of 5,6-bis(p-tolythio)-diiminoisoindoline **32** was dissolved in 6 mL of quinoline. The system was closed, purged with N_2 and protected from light. Then 0.6 mL of $SiCl_4$ was added. The mixture was heated to reflux temperature (200 ºC) for 1 hour. The crude product was precipitated in acetone, filtered and washed repeatedly with acetone. Yielding 617 mg (99%) of $(ArS)_8$-$SiPcCl_2$ **(33)** as a green solid, which was used without further purification in subsequent reactions. UV-Vis ($CHCl_3$) λ_{max}/nm: 381, 468, 673, 752 nm.

3.2.26. Synthesis of $(Cl_2ArO)_4$-SiPc-$(O_2C$-Ar-$CO_2H)_2$ (4).

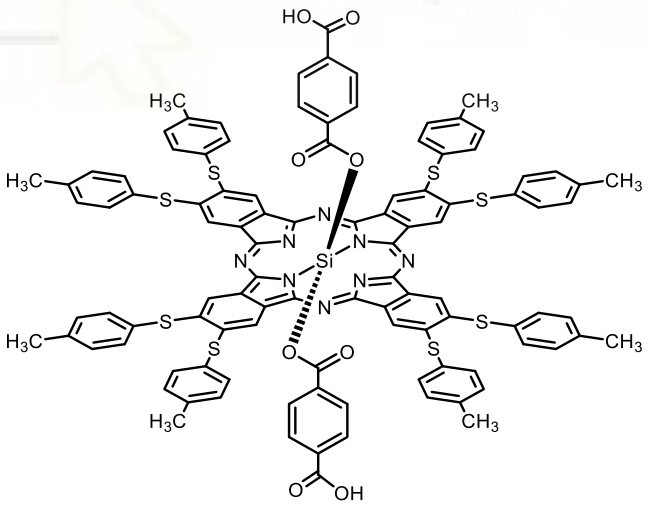

50 mg (0.031 mmol) of $(ArS)_8$-$SiPcCl_2$ **(33)** and 53 mg (0.310 mmol) of terephthalic acid were dissolved in 1 mL Tol/NMP (1:1) mixture. The mixture was heated in a microwave reactor with constant stirring at 160 ºC for 1 hour. The crude reaction was precipitated in methanol, filtered and purified by size exclusion chromatography (Bio-Beads, THF). Yielding 21 mg (37%) of the target compound of $(Cl_2ArO)_4$-SiPc-$(O_2C$-Ar-$CO_2H)_2$ **(4)** as a pure green solid. ^{1}H-RMN (400 MHz, $CDCl_3$, 25 ºC) δ = 9.07 (s, 8H), 7.60 (d, *J* = 7.9 Hz, 16H), 7.35 (d, *J* = 7. 9 Hz, 16H), 6.99 (d, *J* = 8.5 Hz, 4H), 5.21 (d, *J* = 8.5 Hz, 4H), 2.51 (s, 24H). UV/Vis ($CHCl_3$): λ_{max}/nm (log ε) 366 (4.69), 463 (4.33), 665 (4.40), 743 (5.19). MS (MALDI-TOF, dithranol): *m/z* [M^+] calcd. for $C_{104}H_{74}N_8O_8S_8Si$ 1787.3114, found 1787.3124.

3.2.27. Synthesis of $(ArS)_8$-SiPc-(O_2C-Ar-$CH_3)_2$ (10).

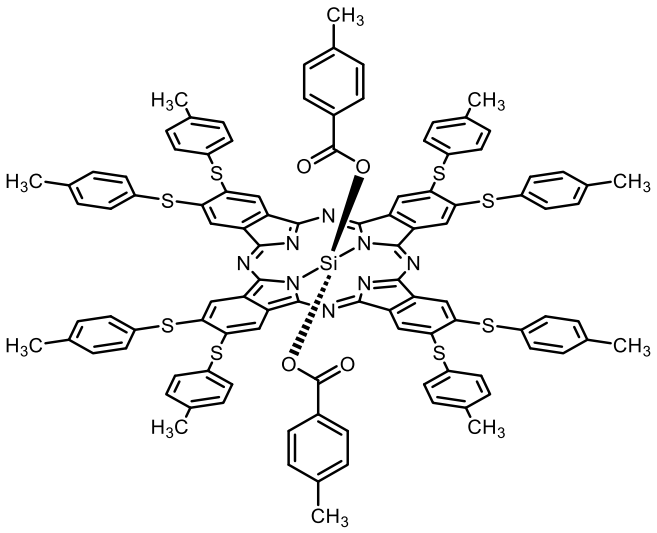

50 mg (0.031 mmol) of $(ArS)_8$-$SiPcCl_2$ **(33)** and 48 mg (0.310 mmol) were dissolved in 1 mL Tol/NMP (1:1) mixture. The mixture was heated in microwave reactor with constant stirring at 160 °C for 1 hour. The crude reaction was precipitated in methanol, filtered, and purified by column chromatography (SiO_2, CH_2Cl_2). Yielding 27 mg (54%) of $(ArS)_8$-SiPc-(O_2C-Ar-$CH_3)_2$ **(10)** as a green solid. ^{1}H-NMR (400 MHz, $CDCl_3$, 25 °C) δ = 9.05 (s, 8H), 7.57 (d, *J* = 8.0 Hz, 16H), 7.33 (d, *J* = 8.0 Hz, 16H), 6.08 (d, *J* = 8.1 Hz, 4H), 5.01 (d, *J* = 8.1 Hz ,4H), 2.49 (s, 24H), 1.75 (s, 6H). UV/Vis ($CHCl_3$) λ_{max}/nm (log ε) 369 (4.75), 453 (4.42), 661 (2.82), 740 (5.34). MS (MALDI-TOF, dithranol): *m/z* [M^+] calcd. for $C_{104}H_{78}N_8O_4S_8Si$ calcd. 1787.3741, found 1787.4230.

3.2.28. Preparation of SURMOFs: Zn-Pc 1, Zn-Pc 2, Zn-Pc 3 and Zn-Pc4.

The Zn-SiPc SURMOF thin films were fabricated using a layer-by-layer spin coating approach. Briefly, a 1 mM ethanolic solution of zinc acetate and a 20 μM solution of SiPc linker (compounds **1**, **2**, **3** and **4**) in DMF were sequentially deposited onto pre-cleaned silicon substrates. Prior to deposition, the substrates were cleaned by Ar-H_2 plasma treatment for 30 minutes. After plasma activation, the substrates were rinsed with absolute ethanol and dried under a nitrogen stream.

The spin coating process was carried out using a spin coater in a layer-by-layer manner. Each metal and linker solution were applied for 10 seconds at a rotation speed of 2000 rpm. After each individual deposition step, the samples were rinsed with ethanol to remove unreacted species and by-products. A total of 60 deposition cycles were performed to build up the SURMOF structure with controlled thickness.

Chapter 2:

Synthesis of Silicon Phthalocyanines with Azo and Pyridine Substituents in the Axial Positions for the Generation of SURMOFs.

1.Results and Discussions

1.1. Silicon Phthalocyanines for the Synthesis of Novel SURMOFs

In this chapter, the synthesis of three novel silicon phthalocyanines, SiPc **11-13**, is presented, designed for subsequent integration into SURMOF architectures, following the approach established in **Chapter 1**. In this case **SiPc 11** an **SiPc 12**, azo-functionalized derivatives are introduced, whose cis-trans photoisomerization can modulate the optical properties of the phthalocyanine and, consequently, those of the resulting SURMOF. Given their close structural and synthetic similarity, compounds **11** and **12** are described sequentially within the same section. While compound **11** incorporates azo-functionalized axial ligands bearing carboxylic acid groups to enable light-responsive behavior and potential pore-size modulation in the resulting SURMOFs, compound **12** introduces *tert*-butyl substituents at the periphery to enhance solubility during film fabrication. This approach allows a direct comparison of how peripheral modifications influence both the synthetic outcome and the subsequent integration into SURMOF architectures.

Additionally, **SiPc 13** incorporates a pyridine group in the axial position, enabling alternative coordination modes beyond the carboxylic acid linkages of SiPcs **11** and **12** employed thus far and allowing its combination to produce a new class of SURMOF. The general synthetic strategy follows the procedure outlined in **Scheme 1 of Chapter 1**, with specific variations indicated where appropriate.

1.1.1. Synthesis and Characterization of SiPc-(O-Ar-Azo-Ar-$CO_2H)_2$ (11) and (^{t}Bu)$_4$SiPc-(O-Ar-Azo-Ar-$CO_2H)_2$(12).

In this case, the precursor phthalocyanine $SiPcCl_2$ **(34)**[179] was synthesized starting from commercially available diiminoisoindoline. The phthalocyanine was obtained through a cyclotetramerization reaction following the protocol described in the **Scheme 1 of section 1.1** and based on established literature procedures.[179] This process is illustrated in **Scheme 1** and the resulting product was characterized by UV-Vis spectroscopy.

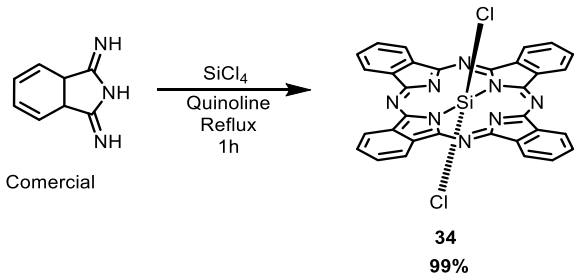

Scheme 15. *Synthesis of $SiPcCl_2$ **(34).***[179]

[179] a) RD.Joyner ,J. Cekada ,RG. Linck , ME. Kenney. Diphe. *Inorg Nucl Chem*. **1960**,*15*,387-8. b) F.H. Moser, A.L. Thomas. Silicon Phthalocyanine. *J. Org. Chem*., **1963**, *28*, 961-963.

The synthesis of SiPc-(O-Ar-Azo-Ar-CHO)$_2$ **(36)** was carried out following the methodology described in **Chapter 1 section 1.1,** using a (*E*)-4-((4-hydroxyphenyl)diazenyl)benzaldehyde[180] as an axial substituent which had been previously synthesized. The selected microwave conditions were those that had yielded the highest efficiency in previous analogous reactions, as detailed **in Chapter 1 section 1.1.1.** Similarly, the oxidation procedure employed to obtain the final silicon phthalocyanine was identical to that described in the same section. This process is illustrated in **Scheme 2**.

As a result, SiPc-(O-Ar-Azo-Ar-CHO)$_2$ **(36)** was obtained in 18% yield, while the final compound SiPc-(O-Ar-Azo-Ar-CO_2H)$_2$ **(11)** was isolated in 53% yield. These moderate yields are consistent with the outcome of the reaction sequence under the given conditions.

All compounds were characterized by ^{1}H-NMR, MALDI-TOF mass spectrometry, and UV-Vis spectroscopy (**Annex 1**).

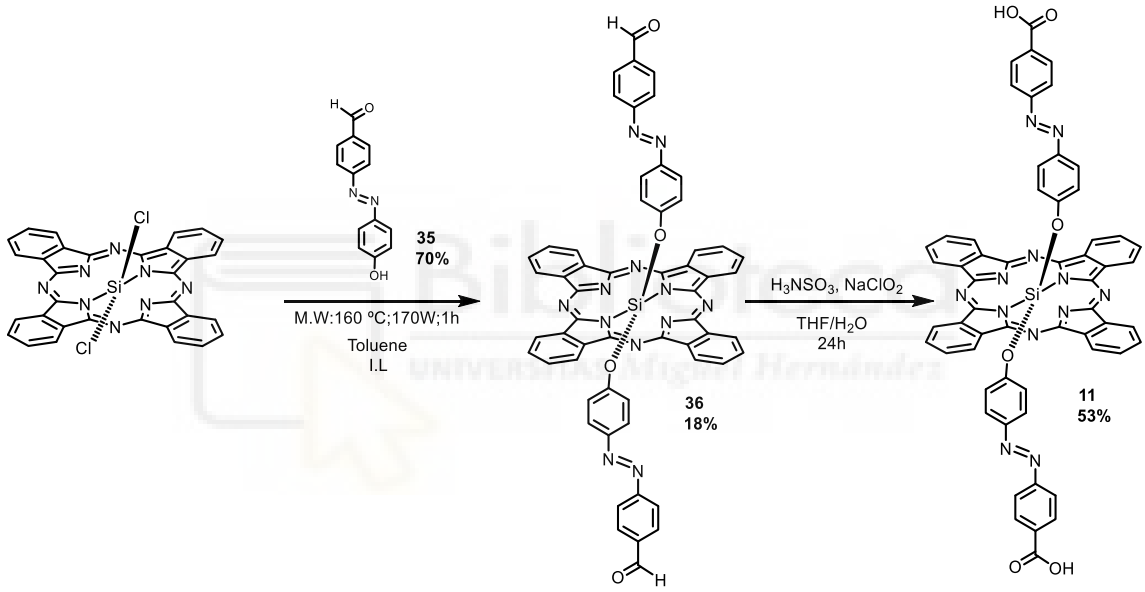

Scheme 2. *Synthesis of SiPc-(O-Ar-Azo-Ar-CHO)$_2$ (**36**) and SiPc-(O-Ar-Azo-Ar-CO_2H)$_2$(**11**).*

Figure 1 shows a comparative analysis of the ^{1}H-NMR spectra of SiPc-(O-Ar-Azo-Ar-CHO)$_2$ **(36)** in $CDCl_3$ and SiPc-(O-Ar-Azo-Ar-CO_2H)$_2$ **(11)** in DMSO-d_6. Although the different solvents used for each spectrum, both spectra clearly exhibit the expected signals associated with the phthalocyanine core and the axial substituents.

[180] Z. Khayat, H. Zali-Boeini, *Dyes Pigment*,**2018,** 159**,** 337-344.

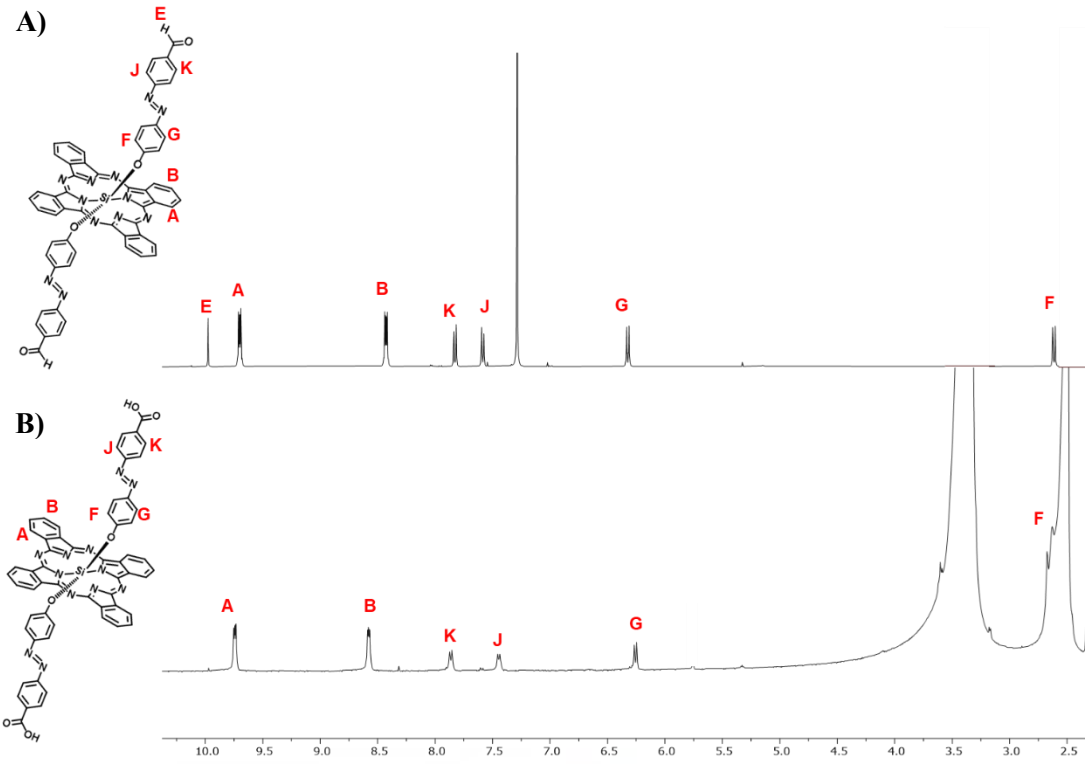

***Figure 1**. [1]H-NMR spectra of **A**) SiPc-(O-Ar-Azo-Ar-CHO)$_2$ **(36)** in $CDCl_3$ and **B**) SiPc-(O-Ar-Azo-Ar-CO_2H)$_2$ **(11)** in DMSO-d_6.*

In the aldehyde derivative **36 (Figure 1.A)**, the **A** and **B** signals corresponding to the phthalocyanine core appear as two distinct multiplets between 9.72-9.63 ppm (8H) and 8.45-8.36 ppm (8H), respectively. In the acid derivative **11**, the same signals are observed as multiplets too.

Regarding the axial substituents, both compounds show four doublets in similar regions: 7.86 ppm (4H) for **K** signal, 7.56 ppm (4H) for **J** signal, 6.29 ppm (4H) for **G** signal, and 2.59 ppm (4H) for **F** signal in compound **36.** Notably, in compound **11**, the **F** signal is partially overlapped with the residual DMSO peak, making it less distinguishable. However, the assignment is supported by the clear observation of this signal at 2.59 ppm in the aldehyde precursor **36**.

Additionally, the aldehyde **E** signal characteristic of compound **36** is observed as a singlet at 9.95 ppm (2H), which is absent in compound **11** due to the oxidation of the aldehyde group into a carboxylic acid. This confirms the successful conversion of the axial substituent through the oxidation process. The use of DMSO-d_6 in compound **11** was necessary due to its poor solubility in $CDCl_3$, attributed to the increased polarity introduced by the carboxylic acid functionalities.

For the synthesis of the target molecules (^{t}Bu)$_4$SiPc-(O-Ar-Azo-Ar-CO_2H)$_2$ **(12)**, it was necessary to first obtain the phthalocyanine precursor **(Scheme 3)**. In this case, the starting material was a commercially available phthalonitrile, and the procedure was carried out following the specific reference reported for this compound.[181]

The synthesis of 5-(*tert*-butyl)-diminoisoindoline **(37)**[181] was obtained through an ammoniation reaction as described in **Scheme 1 of Chapter 1,** with an isolated yield of 56%.

[181] RD.Joyner ,J. Cekada ,RG. Linck , ME. Kenney. Diphe. *Inorg Nucl Chem*. **1960**,*15*,387-8.

The compound was characterized by ^{1}H-NMR spectroscopy, as detailed in **Annex 1**.

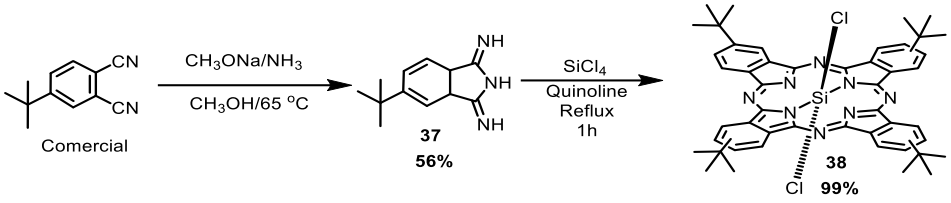

Scheme 3. *Synthesis of 5-(^{t}Bu)-diminoisoindoline **(37)** and .(^{t}Bu)$_4$-SiPcCl$_2$ **(38)**.*[181]

Once the diiminoisoindoline was obtained, the synthesis of (^{t}Bu)$_4$-SiPcCl$_2$ **(38)**[181] was carried out by cyclotetramerization using the previously described method in **Chapter 1 Scheme 1 of section 1.1** and yielding 99%. The characterization of this phthalocyanine was performed using UV-Vis spectroscopy, showed in **Annex 1.**

The synthesis of (^{t}Bu)$_4$SiPc-(O-Ar-Azo-Ar-CHO)$_2$ **(39)** was carried out following the methodology described in **Chapter 1 section 1.1,** using the axial substituent previously synthesized and the same MW conditions as their analogue SiPc **36**. Similarly, the oxidation procedure employed to obtain the final silicon phthalocyanine was identical to that described in the same section (**Scheme 4**). As a result, (^{t}Bu)$_4$SiPc-(O-Ar-Azo-Ar-CHO)$_2$ **(39)** was obtained with a yield of 19% and the final compound (^{t}Bu)$_4$SiPc-(O-Ar-Azo-Ar-CO$_2$H)$_2$ **(12)** was isolated in 86% yield. This increase of yield, when compared to its unsubstituted analogue SiPc **11**, may be attributed to the enhanced solubility conferred by the presence of the bulky *tert*-butyl groups on the periphery of the phthalocyanine.

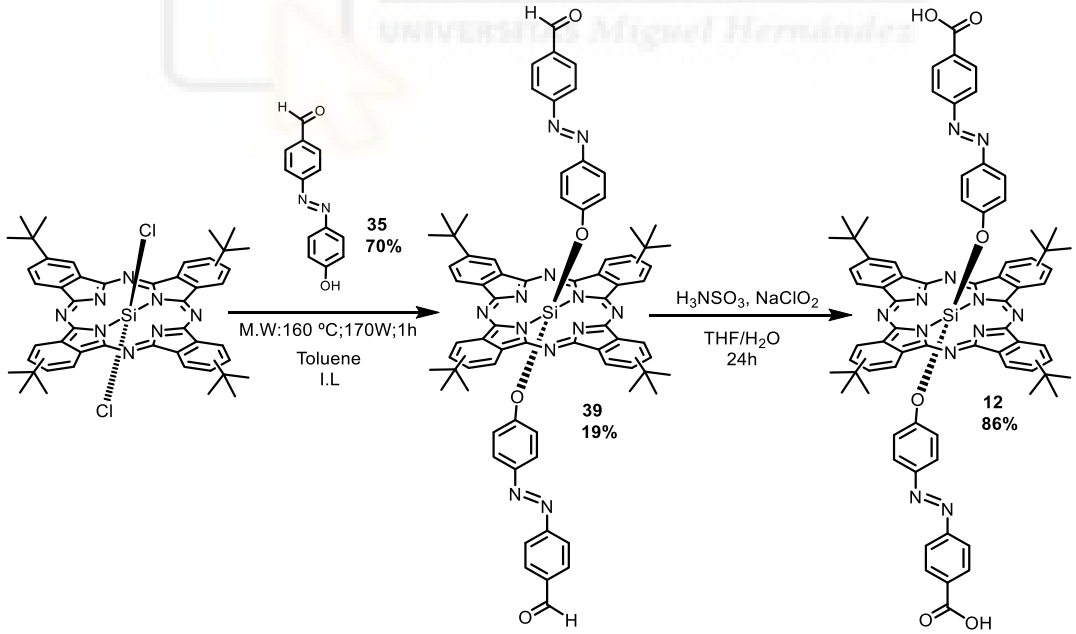

Scheme 4. *Synthesis of (^{t}Bu)$_4$SiPc -(O-Ar-Azo-Ar-CHO)$_2$ **(39)** and (^{t}Bu)$_4$SiPc-(O-Ar-Azo-Ar-CO$_2$H)$_2$ **(12)**.*

All compounds were characterized by ^{1}H-NMR, MALDI-TOF mass spectrometry, and UV-Vis spectroscopy (**Annex 1**).

Figure 2 shows ^{1}H-NMR spectrum of phthalocyanine **12**, which is structurally very similar to its analogue SiPc **11.** A slight shift in the characteristic signals is observed, likely due to the use of a different solvent ($CDCl_3$) for the measurement.

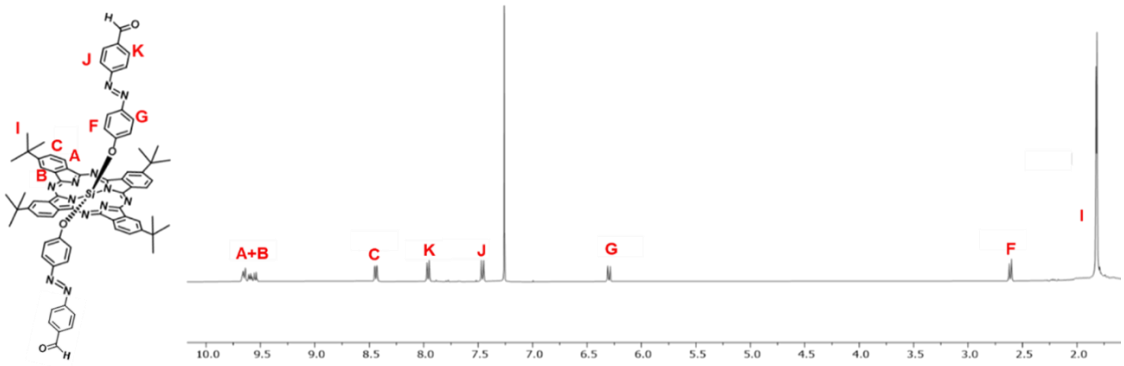

***Figure 2**. ^{1}H-NMR Spectra of (^{t}Bu)$_4$SiPc-(O-Ar-Azo-Ar-CO$_2$H)$_2$ **(12)** in CDCl$_3$.*

In the case of SiPc **12,** the ^{1}H NMR spectrum shows correspondence with that of SiPc **11** due to their structural similarity. The phthalocyanine core protons are represented by three signals (**A**, **B**, and **C**). In this case, signals **A** and **B** appear overlapped as a single multiplet between 9.69-9.49 ppm, integrating for 8H, while signal **C** is resolved separately as a multiplet at 8.50-8.43 ppm (4H). In the region corresponding to the axial substituents, four doublets are observed in chemical shift ranges comparable to those reported for SiPc **11**, consistent with their analogous substitution pattern. However, in this case, the use of $CDCl_3$ as solvent enabled the **F** signal to be clearly distinguished at 2.64 ppm (4H), confirming the previous assignment proposed for SiPc **11**. Finally, the **I** signal, corresponding to the *tert*-butyl substituents at the peripheral positions, appears as a sharp singlet at 1.85 ppm (36H),

Given their structural resemblance and shared functional groups, a comparative optical analysis was performed to assess whether the peripheral tert-butyl substituents in **SiPc 12** induce measurable differences in the electronic absorption profile relative to **SiPc 11**.

Figure 3 presents a comparative analysis of the compounds SiPc-(O-Ar-Azo-Ar-CO$_2$H)$_2$ **(11)** and (^{t}Bu)$_4$SiPc-(O-Ar-Azo-Ar-CO$_2$H)$_2$ **(12)** in THF.

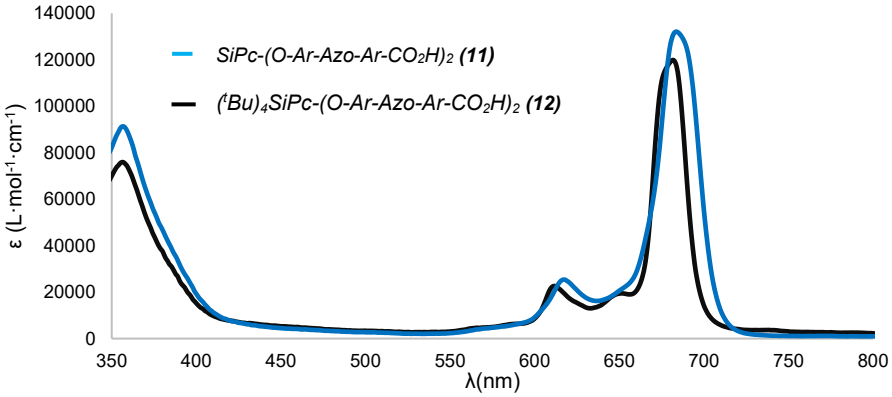

***Figure 3**. UV-Vis spectra of SiPc-(O-Ar-Azo-Ar-CO$_2$H)$_2$ **(11)** and (^{t}Bu)$_4$SiPc-(O-Ar-Azo-Ar-CO$_2$H)$_2$ **(12)** in THF.*

The UV-Vis spectrum of phthalocyanine **11** exhibits a Q band maximum at 682 nm. In contrast, the introduction of four *tert*-butyl groups at the peripheral positions of the phthalocyanine ring in compound **12** results in a slight red shift of the absorption maximum to 684 nm. The Soret band remains unchanged for both derivatives, with a maximum at 357 nm. This minimum red shift can be attributed to the electron-donating nature of the *tert*-butyl substituents, which increase electron density on the macrocycle.

1.1.2. Synthesis and Characterization of SiPc-$(O_2CPy)_2$ (13).

The synthesis of the precursor phthalocyanine $SiPcCl_2$ **(34)**[179] was performed following the procedure described in **section 1.1.1**. In this case, due to the nature of the axial substituent to be introduced, the final compound was obtained via nucleophilic substitution of the chlorine atoms in the axial positions of $SiPcCl_2$ **(34)**[179] using pyridine-4-carboxylic acid as the incoming ligand. The reaction was carried out in a microwave reactor under the optimized conditions previously described in **Chapter 1 section 1.1.1.** The final product SiPc-$(O_2CPy)_2$ **(13)** was isolated in 47% yield. This process is illustrated in **Scheme 5**.

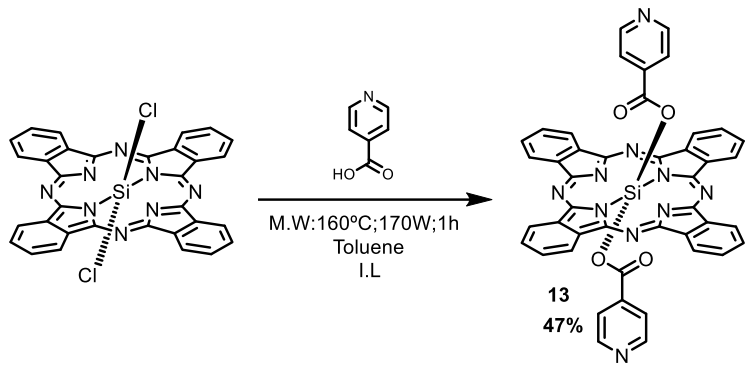

Scheme 5. *Synthesis of SiPc-$(O_2CPy)_2$* ***(13)***

SiPc 13 was characterized by ^{1}H-NMR spectroscopy (**Figure 4**), MALDI-TOF mass spectrometry, and UV-Vis spectroscopy (**Annex 1**).

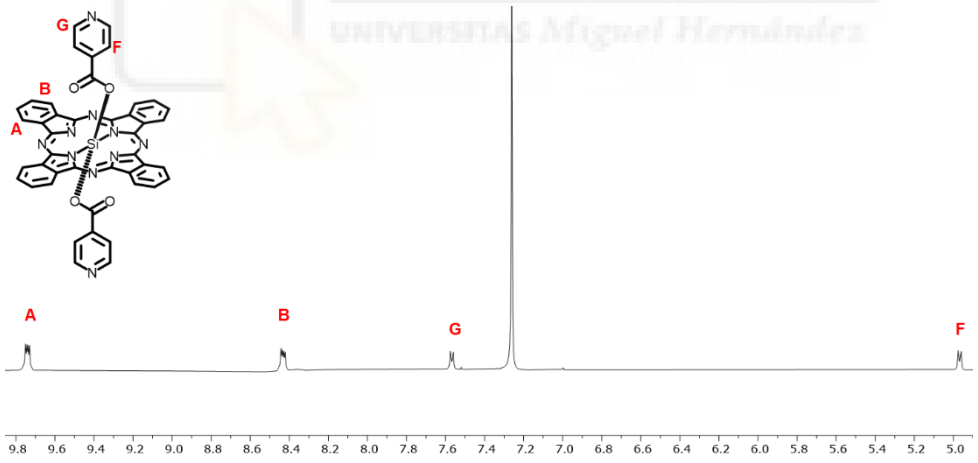

Figure 4*. ^{1}H-NMR spectrum of SiPc-$(O_2CPy)_2$* ***(13)*** *in $CDCl_3$.*

As in the case of SiPc **11** described in **Chapter 2 section 1.1.1**, the **A** and **B** signals, corresponding to the protons of the phthalocyanine ring, appear as two multiplets in the same range. The main difference is that, while in SiPc **11** four distinct signals were observed for the axial substituents, in this case only two are present. These axial protons appear as two doublets, with the **G** signal at 7.60 ppm (4H) and the **F** signal at 5.00 ppm (4H).

After characterization by ^{1}H-NMR, UV-Vis analysis was carried out to provide a more comprehensive characterization of the target molecule, enabling the evaluation of its optical properties.

In **Figure 5**, the UV-Vis spectrum of SiPc-$(O_2CPy)_2$ **(13)** in THF is displayed. The Q-band absorbance maximum appears at 685 nm, while the maximum for the Soret band is observed at 359 nm.

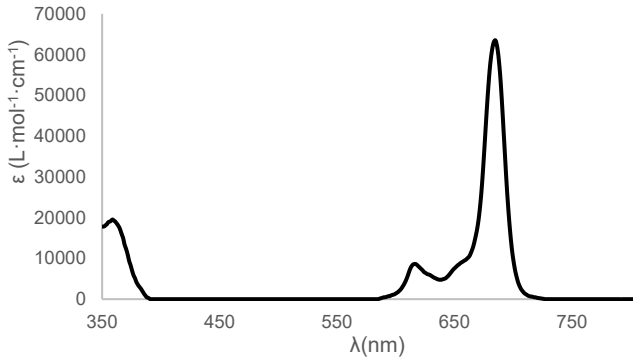

***Figure 5**. UV-Vis spectrum of SiPc-$(O_2CPy)_2$ **(13)** in THF.*

Given the distinctive optical profile of SiPc **13**, its electrochemical characterization was subsequently undertaken to gain insight into its redox behavior for potential optoelectronic applications.

Figure 6, **and table 1** present the electrochemical measurements of the target compound, it was obtained in THF. The compound exhibited clear and well-defined reversible waves in the cathodic and anodic regions. The oxidation potential was observed at 0.85 V vs Fc/Fc^+, while the reduction potential was measured at -1.864 V vs Fc/Fc.

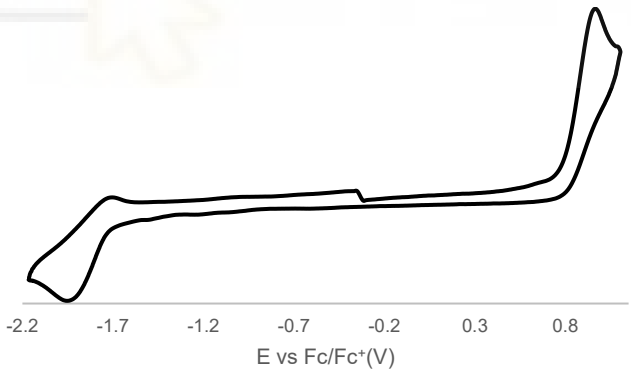

***Figure 6**. Cyclic voltammetry of SiPc-$(O_2CPy)_2$ **(13)** in THF using tetrabutylammonium hexafluorophosphate (Bu_4NPF_6) as the supporting electrolyte, platinum wire, glassy carbon, and non-aqueous Ag/$AgNO_3$ as working and reference electrodes, respectively, with ferrocene (Fc/Fc+) as the internal standard*

Compound	E_{ox} *(V vs Fc/Fc⁺)*	$E_{red}I$ *(V vs Fc/Fc⁺)*	*E_{Homo} *(eV)*	**E_{Lumo} *(eV)*	***E_g^{EQ} *(eV)*
SiPc-$(O_2CPy)_2$ (**13**)	0.85	-1.86	3.95	6.66	2.71

***Table 1**. SiPc-$(O_2CPy)_2$ **(13)** electrochemical properties.*

*E_{HOMO} have been calculated using E_{HOMO} (eV) = -4.8 - E_{ox} (V vs Fc/Fc^+)
**E_{LUMO} have been calculated using E_{LUMO} (eV) = -4.8 - $E_{red}I$ (V vs Fc/Fc^+)
***Electrochemical band gap energy ***(E_g^{EQ}) values have been estimated using E_g^{EQ} = (E_{HOMO} -E_{LUMO}) eV

1.2.1. Synthesis and Characterization of SURMOFS of SiPc 11 and 13.

Following the successful synthesis of the target compounds, their potential to form new coordination frameworks was further explored by extending the methodology described in **Chapter 1, section 1.3.1**. For SiPc **11**, the SURMOF synthesis was carried out as planned, whereas SiPc **12** was not evaluated due to its close structural similarity to SiPc **11** and, as mentioned earlier, the limited time available during the research stay at KIT.

In this case, a novel SURMOF structure was targeted by combining two distinct silicon phthalocyanines: **SiPc-$(CO_2H)_2$**[116] and **SiPc-$(O_2C$-Py$)_2$ (13)**, each bearing complementary ditopic functional groups (carboxylic acid and pyridine, respectively). Based on previous reports, [182] this dual-linker strategy enables the formation of more complex SURMOF architectures through the simultaneous coordination of both functional groups to zinc ions (Zn^{2+}), yielding mixed-ligand frameworks.

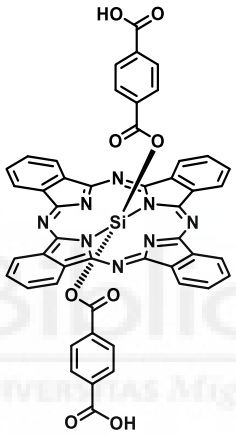

Figure 7. *Structure of* ***SiPc-$(CO_2H)_2$.***

The attempted synthesis of SURMOF followed the procedure described in **Chapter 1 of section 1.3.1**, using SiPc-(O-Ar-Azo-Ar-$CO_2H)_2$ **(11)** as a linker. Characterization of this SURMOF was attempted using *out-of-plane* XRD.

Figure 8.A presents a comparison between the experimental *out-of-plane* XRD pattern and a theoretical simulation for Zn-SiPc **11**. The simulation was generated using CIF data (**Annex 3**) from previous studies[116] as a starting point, with modifications based on our experimental results. The simulation shows a good match with the experimental data up to three periodicities, obtaining parameters of a) = b) = 2.8 nm and c) = 1.1 nm. When compared with the XRD spectra reported in **Chapter 1 section 1.3.1**, it becomes evident that the values of a) = b) are significantly higher (2.8 nm vs. 2.2 nm). This difference can be attributed to the greater length of the axial substituent, which induces an expansion of the unit cell parameters.

To further corroborate the successful framework formation and gain complementary structural information, FT-IRRAS and UV-Vis measurements were subsequently performed.

Figure 8.B presents the FT-IRRAS spectrum of the Zn-SiPc **11** SURMOF. The spectrum displays the same characteristic peaks as those reported in **Chapter 1 section 1.3.1**, including the carboxylate (COO-) group coordinated to zinc, with an asymmetric stretching vibration around 1600 cm^{-1} and a symmetric stretching vibration at 1400 cm^{-1}. The Si-N stretching vibration of the

[182] M. Kim, Y. Lee, H.R. Moon, *Acc. Chem. Res.*, **2024**, *57*, 2347–2357.

phthalocyanine is observed at 1300 cm^{-1}, while the C=C and C=N stretching vibrations of the SiPc ring are also located at 1600 cm^{-1}. The *out-of-plane* deformation of the SiPc ring is detected at 700 cm^{-1}. The most distinctive feature is the appearance of an intense vibrational band corresponding to the azo group (N=N) of the axial substituents, observed at 1400 cm^{-1}. This band appears as a doublet due to its overlap with the carboxylate stretching vibration. These results confirm the successful formation of the SURMOF structure.

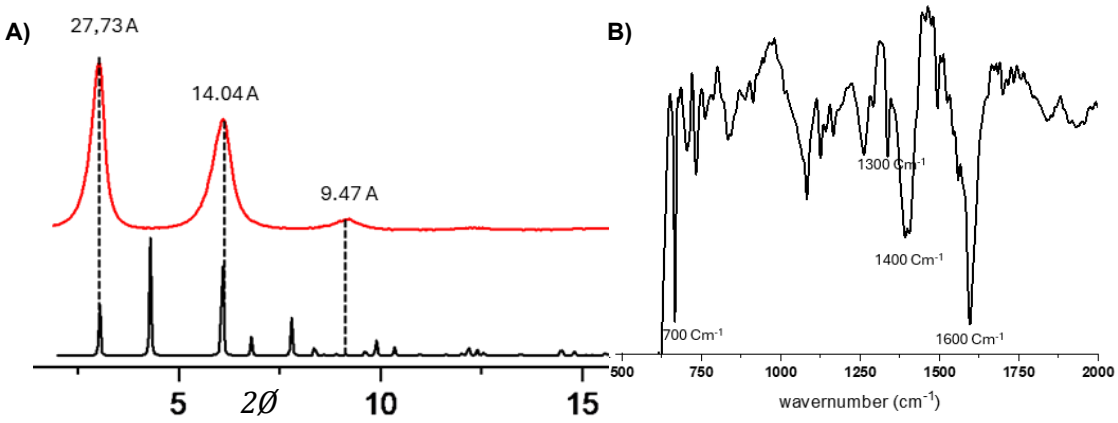

Figure 8. A) *Predicted structure (black) and experimental out-of-plane X-ray diffraction patterns of Zn-SiPc* ***11*** *(red) SURMOF structure.****B)*** *FT-IRRAS spectra of Zn-SiPc* ***11****.*

Figure 9 compares the absorption spectra of SiPc **11** in solution with the solid-state SURMOF Zn-SiPc **11**. The solvated SiPc **11** exhibits an intense and sharp Q band at 682 nm. Upon assembly into the SURMOF, this Q band suffers a bathochromic shift to 699 nm, corresponding to a 17 nm shift. This shift in the Q band can be considered as a measure of the strength of the *J*-type electronic coupling.[177] In addition, a clear shift of the Soret band is observed, with the maximum of SiPc **11** appearing around 360 nm, while for Zn-SiPc **11** it is shifted to approximately 420 nm. Furthermore, new absorption features emerge between 550-650 nm, which may be associated with charge-transfer transitions.

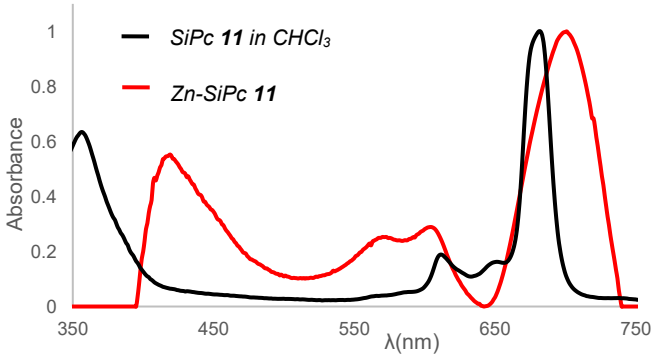

Figure 9. *UV-Vis spectrum of SiPc* ***11*** *in* $CHCl_3$ *and Zn-SiPc* ***11*** *in solid state.*

To further explore the potential of the synthesized linkers, an evaluation was conducted to determine whether SiPc **13** could also be integrated into a SURMOF structure.

In this case, a novel SURMOF structure was targeted by combining two distinct silicon phthalocyanines: **SiPc-$(CO_2H)_2$,** synthetized previously in our group (**Figure 7**),[116] and SiPc-$(O_2C\text{-}Py)_2$ **(13)**, each bearing complementary ditopic functional groups (carboxylic acid and pyridine, respectively). Based on previous reports, this dual-linker strategy enables the formation

of more complex SURMOF architectures through the simultaneous coordination of both functional groups to zinc ions (Zn^{2+}), yielding mixed-ligand frameworks.

To this end, a 1 mM zinc acetate solution in ethanol and a 20 µM solution containing an equimolar mixture of **SiPc-$(CO_2H)_2$** and SiPc-$(O_2C$-Py$)_2$ **(13)** in DMF were prepared. Using the sequential spin-coating method, sixty alternating layers were deposited onto a plasma-treated silicon substrate to assemble the SiPc **13** + **SiPc-$(CO_2H)_2$** film. This approach maintained the advantages of the previously optimized deposition technique, including high reproducibility and uniform film growth.

In order to evaluate the structural features of the resulting film, both *out-of-plane* and *in-plane* XRD measurements were performed for this new SURMOF. These analyses aimed to determine whether the incorporation of two distinct linkers resulted in an ordered crystalline phase, and to assess the possible orientation and periodicity of the new SURMOF.

Figure 10.A presents a comparison of the *out-of-plane XRD* patterns Zn-SiPc-$(CO_2H)_2$,[116] Zn-SiPc **13** and Zn-SiPc **13** + **SiPc-$(CO_2H)_2$** experimental *out-of-plane* X-ray diffraction. Upon comparison, it is evident that the combination of SiPcs show a significantly difference in the spectrum when compared to Zn-SiPc **13** and a slightly different spectrum when compared to Zn-SiPc-$(CO_2H)_2$.[116] Up to five periodicities are observed, resulting in a well-defined spectrum. For SiPc-$(CO_2H)_2$,[116] the values of a) = b) = 2.1 nm and c) = 1.1 nm. For Zn-SiPc **13** a value of a) = 1.4 nm is obtained, while for the combination of SiPcs, a value of a) = 2.2 nm is obtained.

To complement these results and attempt to determine the missing lattice parameters b) and c), an *in-plane* XRD analysis was carried out.

Figure 10.B shows the *in-plane* XRD spectra for Zn-SiPc **13** + **SiPc-$(CO_2H)_2$**. Measurements were taken every 2º to identify a suitable incident angle for observing the characteristic reflections of the structure. However, as shown in the spectra, an appropriate incident angle could not be found. These results suggest that the SURMOF configuration differs from the previously reported results.[116] Consequently, the corresponding values in sections b) and c) could not be obtained, preventing a complete characterization of this new SURMOF.

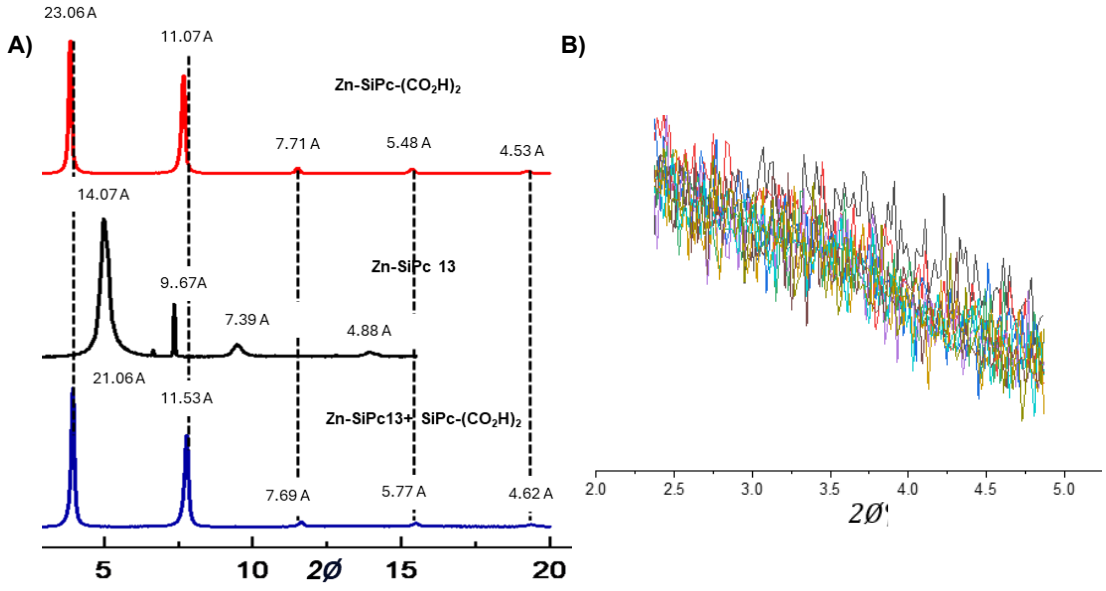

***Figure 10. A**) Structure of Zn-**SiPc-$(CO_2H)_2$** (Blue)[116] Zn-SiPc **13** (black) and Zn-SiPc **13** + **SiPc-$(CO_2H)_2$** (red) experimental out-of-plane X-ray diffraction. **B**) 10º-80º structure of Zn-SiPc **13** + **SiPc-$(CO_2H)_2$** in-plane X-ray diffraction.*

To further corroborate the successful framework formation and gain complementary structural information, FT-IRRAS and UV-Vis measurements were subsequently performed.

Figure 11 shows the FT-IRRAS spectrum of the Zn-SiPc **13** + **SiPc-(CO₂H)₂** SURMOF. As in the case of Zn-SiPc **11**, the characteristic carboxylate bands are observed at approximately 1600 cm^{-1} (asymmetric stretching) and 1400 cm^{-1} (symmetric stretching), confirming coordination with zinc ions. The Si-N stretching vibration of the phthalocyanine is also detected at 1300 cm^{-1}, while the C=C and C=N stretching modes of the SiPc ring appear around 1600 cm^{-1}, and the *out-of-plane* deformation of the macrocycle is visible at 700 cm^{-1}.

In contrast to Zn-SiPc **11**, this system does not exhibit the intense azo-related band at 1400 cm^{-1} but instead displays additional vibrational contributions from the pyridine moieties, with characteristic C=C and C=N stretching at 1600 cm^{-1} and an *out-of-plane* C-H bending mode at 750 cm^{-1}. These differences highlight the structural influence of the pyridine units in the mixed-ligand SURMOF. Overall, the spectrum confirms the successful formation of the SURMOF, although its precise three-dimensional arrangement remains unresolved.

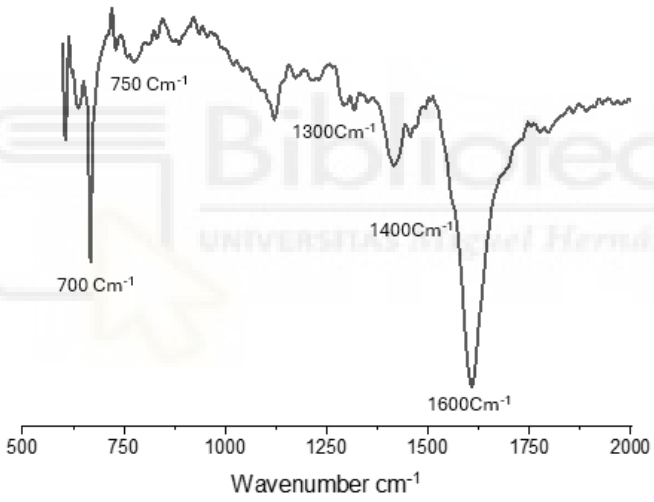

Figure 11. *FT-IRRAS spectra of Zn-SiPc* ***13 + SiPc-(CO₂H)₂.***

Figure 12 presents the UV-Vis spectra of solvated SiPc **13** and **SiPc-(CO₂H)₂** in solvated state compared to the solid-state SURMOF Zn-SiPc **13** + **SiPc-(CO₂H)₂**. The solvated SiPc **13** exhibits an intense Q band at 685 nm, while for **SiPc-(CO₂H)₂**,[116] the Q band is located at 690 nm. Upon assembly into the SURMOF, this Q band suffers a bathochromic shift to 733 nm, corresponding to shifts of 43 and 48 nm, respectively. This solvatochromic[177] shift in the Q band can be considered as a measure of the strength of the *J*-type electronic coupling. When compared with previously reported data (**Annex 2**),[183] it is evident that the combination of phthalocyanines in Zn-SiPc **13** + **SiPc-(CO₂H)₂** results in lower aggregation than in **Zn-SiPc-(CO₂H)₂** alone, where a larger shift of 57 nm was observed.

[183] H. Chen, L. Martín-Gomis, Z. Xu, J.C. Fischer, I.A. Howard, D. Herrero, V. Sobrino-Bastán, Á. Sastre-Santos, R. Haldar, C. Wöll, *Phys. Chem. Chem. Phys.,* **2023**, 25, 19626–19632.

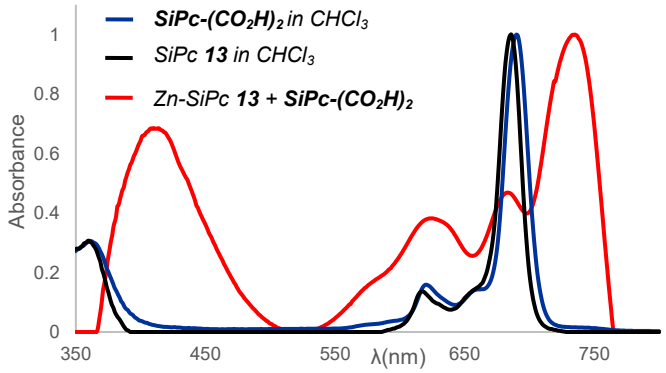

Figure 12. *UV-Vis spectrum* ***SiPc-(CO$_2$H)$_2$*** *[116] SiPc* ***11*** *in solvated in $CHCl_3$ and Zn-SiPc* ***13*** *+* ***SiPc-(CO$_2$H)$_2$*** *in solid state.*

2.Conclusions:

In this chapter, the successful synthesis and full characterization of the three targeted SiPc was achieved. These molecules were designed with different axial and peripheral substituents to fine-tune their electronic, optical, and solubility properties, aiming to assess their potential in two distinct applications: the development of novel tunable SURMOFs incorporating azo groups, and the fabrication of a mixed-ligand SURMOF combining carboxylic acid and pyridine functionalities in the axial positions.

All synthesized compounds were thoroughly characterized by ^{1}H-NMR spectroscopy, UV-Vis spectroscopy, high-resolution MALDI-TOF mass spectrometry, and, when possible, electrochemical analysis.

Among the synthesized phthalocyanines, SiPc **11** and SiPc **13** were selected for evaluation as potential linkers in SURMOF architectures. In contrast, SiPc **12** was not further investigated due to its high structural similarity with compound **11.** Additionally, time limitations during the research stay at the Institute of Functional Interfaces (IFG) at the Karlsruhe Institute of Technology restricted the scope of these experiments.

Ultimately, SiPc **11**, SiPc **13**, and the mixed-ligand system SiPc **13** + **SiPc-$(CO_2H)_2$** successfully formed crystalline and well-ordered SURMOF structures, as evidenced by well-defined *out-of-plane* XRD patterns. These films were further characterized by UV-Vis and FT-IRRAS spectroscopy (except for SiPc **13** alone). The results confirmed both the molecular integrity and the successful incorporation of functional groups into the SURMOF framework.

As a future direction, it would be of great interest to evaluate whether SiPc **12** is also capable of forming ordered SURMOF architectures. The tunability of the new azo-containing SURMOFs under UV light, enabled by the presence of photoresponsive azo units, could open new avenues for optically switchable materials.

In the case of the mixed SURMOF constructed from SiPc **13** and **SiPc-$(CO_2H)_2$** more detailed structural and functional characterization will be required. To date, no SURMOF composed of two different SiPc linkers has been reported, making this system particularly novel. Clarifying its structure and properties is essential for identifying the most suitable application areas.

The mixed azo SURMOF formed from SiPc **11** and pyridine-functionalized SiPc **13** would be particularly interesting to investigate in future studies. Studying its structure would also be highly valuable to fully understand and explore its properties.

3. Experimental Section.

3.1. Materials and Methods

Except for specific cases mentioned, the reagents and solvents used in the synthesis processes were obtained from commercial suppliers and used without any additional purification.

-Microwave reactor: Microwave reactions were carried out in a CEM microwave reactor, Discover SP model.

- Chromatographic Techniques: Column chromatography was performed on SiO_2 (40-63 mm) and Biorad Biobeads SX-3 (200-400 mesh) was used as the stationary phase for Size Exclusion Chromatography (SEC). TLC plates coated with SiO_2 60F254 were visualized under UV light.

-Nuclear Magnetic Resonance (NMR): NMR spectra were recorded on a Bruker AC 300 or Burker 400 MHz spectrometer at 25 ºC, unless otherwise specified using deuterated solvents and referenced to tetramethylsilane (TMS). Coupling constants (*J*) are reported in hertz (Hz). The signals are designated as follows: s = singlet, d = doublet, m = multiplet, and chemical shifts are given in ppm.

-UV-Vis: The measurements for SiPc in solution were recorded on a Perkin Elmer LAMDA 365 UV-WinLab spectrophotometers, using spectrosol-grade solvents. For SURMOF thin films, UV-Vis measurements in the solid state were performed in reflection mode using either a Cary 5000 UV-Vis/NIR spectrometer equipped with a Universal Measurement Accessory (UMA) unit from Agilent Technologies, or a PerkinElmer Lambda 950 UV-Vis/NIR spectrometer equipped with an integrating sphere, allowing accurate determination of the optical response within the multilayer system.

-Mass spectrometry: High-resolution mass spectra were obtained from a Bruker Reflex II matrix-assisted laser desorption/ionization time-of-flight (MALDI-TOF) spectrometer using dithranol as matrix.

-Electrochemistry: The measurements were performed at 298 K in a conventional three-electrode cell using an m-AUTOLAB type III potentiostat/galvanostat (Metrohm, Herisau, Switzerland). Sample solutions (ca. 0.5 mM) were prepared in deaerated PhCN or THF, containing 0.10 M tetrabutylammonium hexafluorophosphate ($TBAPF_6$) as supporting electrolyte; a glassy carbon (GC) working electrode, an $Ag/AgNO_3$ reference electrode, a platinum wire counter electrode was used, and Ferrocene/ferrocenium was the internal standard for all measurements.

-X-Ray diffraction (XRD): XRD measurements were performed in both *out-of-plane* and *in-plane* (co-planar) orientations using a Bruker D8-Advance diffractometer equipped with a Lynxeye position-sensitive detector. The measurements were carried out in θ-2θ geometry with a variable divergence slit, and a 2.3° Soller slit was installed on the secondary side.

-FT-IRRAS: The measurements for IRRAS data were recorded using a Biorad Excalibur FTIR spectrometer (FTS 3000) equipped with a grazing incidence reflection unit (Biorad Uniflex) and a narrow band MCT detector.

-Substrate pretreatment: Substrates were cleaned by argon-hydrogen plasma using a Diener Plasma surface treatment system (airflow: 20 sccm, pure hydrogen) for 30 minutes.

3.2.1. Synthesis of $SiPcCl_2$ (34).[179]

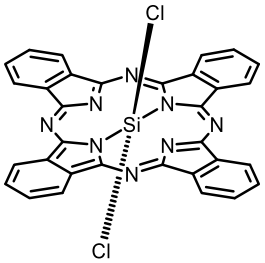

750 mg (5.17 mmol) of 1,3-diiminoisoindoline were dissolved in 7 mL of quinoline. The mixture was purged with N_2 and protected from light. Then 0.7 ml of $SiCl_4$ was added. The reaction was heated to reflux temperature (200 ºC) for 1 hour. After cooling to 60 ºC, 100 mL of acetone was added, forming a suspension which was filtered hot, obtained a crude solid that was washed with acetone. Yielding 750 mg (99%) of $SiPcCl_2$ **(34)**[179] as a blue solid, which was used without further purification in subsequent reactions. UV-Vis ($CHCl_3$) λ_{max}/nm: 355, 371, 636, 710.

3.2.2 Synthesis of (E)-4-((4-hydroxyphenyl)diazenyl)benzaldehyde (35).[180]

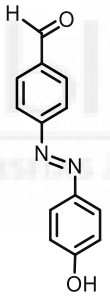

A **solution 1** was prepared in ice-salt bath, maintaining the temperature between -5:0 ºC. For this solution, 610 mg (5.04 mmol) of 4-aminobenzaldehyde was dissolved in 10 mL of pure water, 5 mL of acetone, and 1.7 mL of 37% HCl. Simultaneously, a **solution 2** was prepared in ice-salt bath maintaining the temperature between -5:0 ºC. In this solution, 600 mg (15 mmol) of NaOH and 588 mg (6.26 mmol) of phenol were dissolved in 6.5 mL of pure water. The mixture was stirred for 30 minutes. Then, **solution 1** was added dropwise to **solution 2** over 15 minutes, resulting in a colour change of the transparent solution to orange. The mixture was stirred until room temperature. HCl was added until pH 4, obtained a precipitate which was filtered and washed repeatedly with water. Yielding 980 mg (70%) of (*E*)-4-((4-hydroxyphenyl)diazenyl)benzaldehyde **(35)**[180] as an orange solid.^{1}H-NMR (400 MHz, DMSO-*d*$_6$, 25 ºC): δ = 10.09 (s, 1H), 8.09 (d, *J* = 8.4 Hz, 2H), 7.97 (d, *J* = 8.4 Hz, 2H), 7.87 (d, *J* = 8.4 Hz, 2H), 6.97 (d, *J* = 8.4 Hz, 2H); ^{13}C-NMR (100 MHz, DMSO-*d*$_6$, 25 ºC):192.6, 162.4, 155.4, 145.2, 136.7, 130.7, 125.5, 122.6, 116.2.

3.2.3. Synthesis of SiPc-(O-Ar-Azo-Ar-CHO)$_2$ (36).

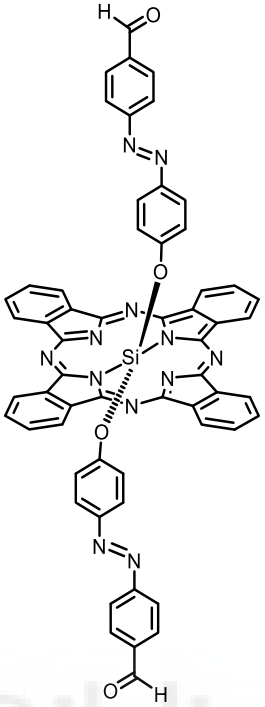

50 mg (0.080 mmol) of $SiPcCl_2$ **(34)**,[179] 105 mg (0.49 mmol) of (*E*)-4-((4-hydroxyphenyl)diazenyl)benzaldehyde **(35)**[180] and 30 mg (0.07 mmol) of 1,1'-methylenebis(3-methylimidazolium) iodide[175] were dissolved in 1 mL of dry toluene. The mixture was heated in microwave reactor with constant stirring at 160 ºC for 1 hour. Then toluene was removed, and the resulting solid was washed with 60 mL of MeOH/H_2O (3:1). Subsequently, it was dissolved in DCM, centrifuged, and the supernatant was concerted. The obtained solid was purified by column chromatography (SiO_2, DCM/THF (90:10)). Yielding 14 mg (18%) of SiPc-(O-Ar-Azo-Ar-CHO)$_2$ **(36)** as a blue solid. ^{1}H-NMR (400 MHz, $CDCl_3$, 25 °C) δ = 9.95 (s, 2H), 9.72-9.63 (m, 8H), 8.45-8.36 (m, 8H), 7.86 (d, *J* = 8.5 Hz, 4H), 7.56 (d, *J* = 8.5 Hz, 4H), 6.29 (d, *J* = 8.4 Hz, 4H), 2.59 (d, *J* = 8.4 Hz, 4H). UV-Vis ($CHCl_3$) λ_{max}/nm (log ε): 357 (5.04), 612 (4.51), 651 (4.42), 681 (5.27). MS (MALDI-TOF, dithranol): *m/z* [M^-] calcd. for $C_{58}H_{34}N_{12}O_4Si$ 990.2709 found 990.2601.

3.2.4. Synthesis of SiPc-(O-Ar-Azo-Ar-$CO_2H)_2$ (11).

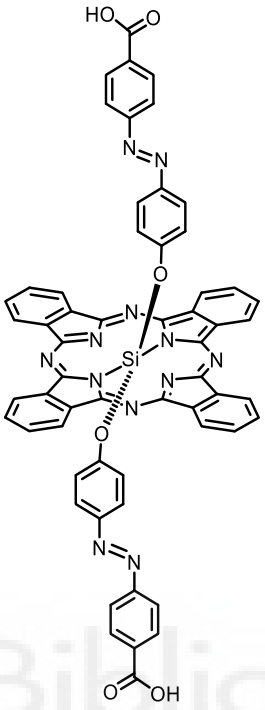

78 mg (0.079 mmol) of SiPc-(O-Ar-Azo-Ar-CHO)$_2$ **(36)**, was dissolved in 6 mL of THF/H_2O (6:1) mixture. In parallel, 47 mg (0.47 mmol) of H_3NSO_3 and 35 mg (0.31 mmol) of $NaClO_2$ were dissolved in 6 mL of THF/H_2O (6:1) mixture. The H_3NSO_3 and $NaClO_2$ solution was slowly added to the SiPc-(O-Ar-Azo-Ar-CHO)$_2$ **(36)**, solution. The reaction mixture was protected from direct light and stirred at room temperature for 24 hours. Then, it was precipitated in 30 mL of H_2O and filtered. The solid was redissolved in THF, dried with Na_2SO_4, filtered and concentrated. The obtained product was washed first 3 times with MeOH and then twice with $CHCl_3$. Yielding 42 mg (53%) of the target compound SiPc-(O-Ar-Azo-Ar-$CO_2H)_2$ **(11)** as a pure blue-green solid. ^{1}H-NMR (400 MHz, DMSO-*d*$_6$., 25 °C) δ = 9.77-9.70 (m, 8 H), 8.61-8.54 (m, 8H), 7.86 (d, *J* = 8.4 Hz, 4H), 7.44 (d, *J* = 8.4 Hz, 4H), 6.25 (d, *J* = 8.5 Hz, 4H), 2.66 (d, *J* = 8.5 Hz, 4H). UV-Vis ($CHCl_3$) λ_{max}/nm (log *ε*): 356 (4.88), 612 (4.35), 6.51(4.29), 682 (5.08). MS (MALDI-TOF, dithranol): *m/z* [M^-] calcd. for $C_{58}H_{34}N_{12}O_6Si$ 1022.2499 found 1022.6093.

3.2.5. Synthesis of 5-(*tert*-butyl)-diminoisoindoline (37).[181]

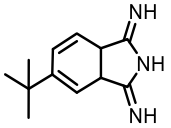

1 g (5.43 mmol) of 4-*tert*-butylphtalonitrile and 0.1 g (1.98 mmol) of MeONa were dissolved in 50 mL of methanol. NH_3 was bubbled through the solution at the reflux temperature of methanol (65 °C) for 11 hours. The solvent was evaporated, and the resulting solid was washed

repeatedly with water and dried. Yielding 0.45 g (56%) of 5-(*tert*-butyl)-dimiinoisoindoline **(37)**[181] as a pale-white solid, which was used in subsequent reactions without further purification. ^{1}H-NMR (300 MHz, DMSO-d_6, 25 ºC): δ = 7,99 (d, 6H, J = 1,01 Hz,), 1,38 (s, 9H) ppm.

3.2.6. Synthesis of (^{t}bu)$_4$-SiPcCl$_2$ (38).[181]

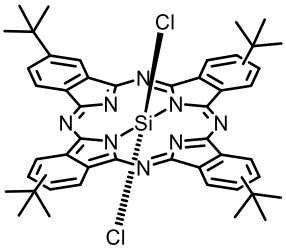

750 mg (3.75 mmol) of 5-(*tert*-butyl)-diminoisoindoline **37**[181] was dissolved in 7 mL of quinoline. The system was closed, purged with N_2 and protected from light. Then 0.8 mL of $SiCl_4$ was added. Then mixture was heated to reflux temperature (200 ºC) for 1 hour. The crude product was precipitated in acetone, filtered and washed repeatedly with acetone. Yielding 772 mg (99%) of (^{t}Bu)$_4$-SiPcCl$_2$ **(38)**[184] as a dark blue solid. UV-Vis ($CHCl_3$) λ_{max}/nm: 370, 632, 669, 703.

3.2.7. Synthesis of (^{t}Bu)$_4$SiPc -(O-Ar-Azo-Ar-CHO)$_2$ (39).

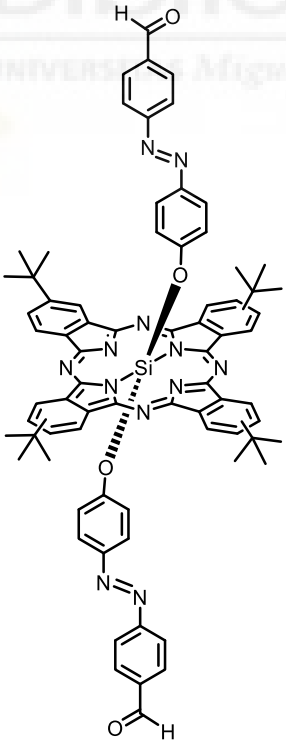

50 mg (0.061 mmol) of (^{t}Bu)$_4$-SiPcCl$_2$ **(38)**[181] 78 mg (0.37 mmol) of (*E*)-4-((4-hydroxyphenyl)diazenyl)benzaldehyde **(35)**[180] and 30 mg (0.07 mmol) of 1,1'-methylenebis(3-methylimidazolium) iodide[175] were dissolved in 1 mL of dry toluene. The mixture was heated in microwave reactor with constant stirring at 160 ºC for 1 hour. Then, solvent was evaporated, and the resulting solid was purified by column chromatography (SiO_2, DCM). Yielding 14 mg (19%)

of (^{t}Bu)$_4$SiPc-(O-Ar-Azo-Ar-CHO)$_2$ **(39)** as a blue solid. ^{1}H-NMR (400 MHz, $CDCl_3$, 25 °C) δ = 9.94 (s, 2H), 9.70-9.50 (m, 8H), 8.48-8.41 (m, 4H), 7.79 (d, *J* = 8.2 Hz, 4H), 7.55 (d, *J* = 8.2 Hz 4H), 6.31 (d, *J* = 8.4 Hz, 4H), 2.62 (d, *J* = 8.4 Hz, 4H), 1.85 (s, 36H). UV-Vis ($CHCl_3$) λ_{max}/nm (log *ε*): 357 (4.49), 620 (4.20), 681 (4.98). MS (MALDI-TOF, dithranol): *m/z* [M^-] calcd. for $C_{74}H_{66}N_{12}O_4Si$ 1214.5100 found 1214.51630.

3.2.8. Synthesis of (^{t}Bu)$_4$SiPc-(O-Ar-Azo-Ar-CO_2H)$_2$(12).

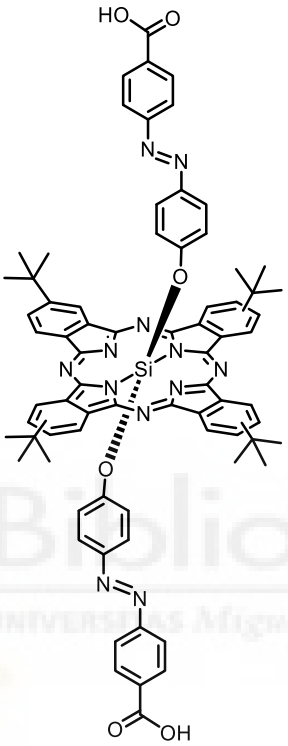

75 mg (0.062 mmol) of (^{t}Bu)$_4$SiPc -(O-Ar-Azo-Ar-CHO)$_2$ **(39)**, was dissolved in 6 mL of THF/H_2O (6:1) mixture. In parallel, 37 mg (0.37 mmol) of H_3NSO_3 and 25 mg (0.25 mmol) of $NaClO_2$ were dissolved in 6 mL of THF/H_2O (6:1) mixture. The H_3NSO_3 and $NaClO_2$ solution was slowly added to the (^{t}Bu)$_4$SiPc-(O-Ar-Azo-Ar-CHO)$_2$ **(39)** solution. The reaction mixture was protected from direct light and stirred at room temperature for 24 hours. Then, crude of reaction was precipitated in 30 mL of H_2O and filtered. The solid was redissolved in THF, dried with Na_2SO_4, filtered and concentrated. The obtained product was washed 3 times with MeOH. Yielding 66 mg (86%) of the target compound (^{t}Bu)$_4$SiPc-(O-Ar-Azo-Ar-CO_2H)$_2$ **(12)** as pure blue-green solid. ^{1}H NMR (400 MHz, CDCl3, 25 °C) δ = 9.69-9.49 (m, 8H), 8.50-8.43 (m, 4H), 7.98 (d, *J* = 8.4 Hz, 4H), 7.49 (d, *J* = 8.4 Hz, 4H), 6.32 (d, *J* = 8.4 Hz, 4H), 2.64 (d, *J* = 8.4 Hz, 4H), 1.85 (s, 36H). UV-Vis ($CHCl_3$) λ_{max}/nm (log *ε*): 357 (4.96), 617 (4.40), 684 (5.12). MS (MALDI-TOF, dithranol): *m/z* [M^-] calcd. for $C_{74}H_{66}N_{12}O_6S$ 1246.5007 found 1246.6879.

3.2.9. Synthesis of SiPc-$(O_2CPy)_2$ (13).

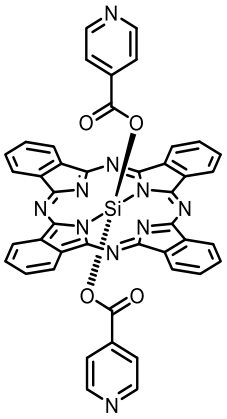

50 mg (0.080 mmol) of $SiPcCl_2$ **(34)**[179] 100 mg (0.80 mmol) of 1,1'-methylenebis(3-methylimidazolium) iodide [175] were dissolved in 1 mL of dry toluene. The mixture was heated in microwave reactor with constant stirring at 160 ºC for 1 hour. The crude reaction was precipitated in acetonitrile/water (3:1), filtered and purified by column chromatography (SiO_2, $CHCl_3$/THF (1:1)). The obtained product was repeatedly washed with MeOH. Yielding 30 mg (47%) of the target compound SiPc-$(O_2CPy)_2$ **(13)** as pure blue solid. ^{1}H-NMR (400 MHz, $CDCl_3$, 25 °C) δ = 9.81-9.72 (m, 8H), 8.50-8.36 (m, 8H), 7.60 (d, *J* = 8.4 Hz, 4H), 5.00 (d, *J* = 8.4 Hz, 4H). UV-Vis ($CHCl_3$) λ_{max}/nm (log ε) = 359 (4.29), 616 (3.94), 685 (4.80). MS (MALDI-TOF, dithranol): *m/z* [M^-] calcd. for $C_{44}H_{24}N_{10}O_4Si$ calcd 784.1757, found 7484.1867.

Chapter 3:

Synthesis of Water Soluble Silicon Phthalocyanines for the Generation of SURMOFs.

1.Results and Discussions

1.1. Silicon Salt Phthalocyanines for SURMOFs.

Following the synthetic achievements described in **Chapters 1 and 2**, this chapter focuses on the synthesis of a new series of silicon phthalocyanines. In this case, the molecular design incorporates two key features: the presence of ditopic groups in axial substituents capable of forming SURMOF structures, and pyridine moieties as peripheral substituents. The methylation of the pyridine groups enhances their solubility in polar solvents such as water, thereby improving the biocompatibility of these compounds for potential applications, as discussed in the background section.

1.1.1. Synthesis and Characterization of Tetra Pyridinyloxy SiPcs 14, 15 and 16.

For the synthesis of the target molecules, it was first necessary to obtain the phthalocyanine precursor molecules (**Scheme 1**). The synthesis 4-(3-pyridyloxy) phthalonitrile **(40)** and 5-(3-pyridinyloxy)-1,3-diiminoisoindoline **(41)** were based on methodologies previously reported[184] following the process described in **Chapter 1 section 1.1**. Compound **40** was obtained with a yield of 45%, while compound **41** was isolated in 75% yield. Both precursors were characterized by ^{1}H-NMR spectroscopy, as shown in **Annex 1**, exhibiting spectral features consistent with those reported in the literature.

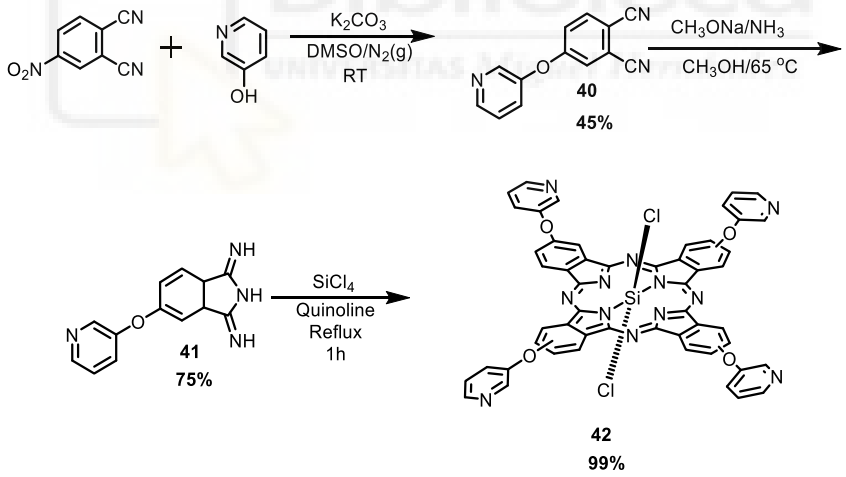

Scheme 1. *Synthesis of 4-(3-pyridinyloxy) phthalonitrile **(40)**[184] and 5-(3-pyridinyloxy)-1,3-diiminoisoindoline **(41)**[184] and $(PyO)_4$-$SiPcCl_2$ **(42)**.*

Once the diiminoisoindoline was synthesized, the preparation of $(PyO)_4$-$SiPcCl_2$ **(42)** was carried out by cyclotetramerization using the method generally described previously in **Chapter 1 section 1.1**. and with a yield of 99%. The characterization of this phthalocyanine was performed by UV-Vis spectroscopy presented in **Annex 1**.

The synthesis of $(PyO)_4$-SiPc-$(O_2C$-Ar-$CHO)_2$ **(43)**, $(PyO)_4$-SiPc-$(O_2C$-Ar_2-$CHO)_2$ **(44)**, $(PyO)_4$-SiPc-$(O_2C$-Ar-$CH_3)_2$ **(45)**, $(PyO)_4$-SiPc-$(O_2C$-Ar-$CO_2H)_2$ **(46)** and $(PyO)_4$-SiPc-O_2C-Ar_2-

[184] V. Mantareva, I. Angelov, V. Kussovski, R. Dimitrov, L. Lapok, D. Wöhrl, *Eur. J. Med. Chem,* ***2011****, 4430-4440.*

$CO_2H)_2$ **(47)** (**Scheme 2**) were carried out following the methodology described in **Chapter 1 section 1.1,** using the same axial substituents as their analogues in this section.

Based on the results previously obtained in MW synthesis, the reaction conditions that yielded the highest efficiency were selected (as described in **Chapter 1 section 1.1.1**).

Since the oxidation step showed very similar yields, we focused our comparison on the axial substitution reactions, where greater variability was observed. The yields obtained for phthalocyanines **43** and **45** were relatively similar, at 40% and 35%, respectively. However, in the case of phthalocyanine **44**, a significantly lower yield of 21% was obtained. This reduction may be attributed to the introduction of a bulkier axial substituent in this molecule, which could increase the steric hindrance around the silicon center and thus reduce the overall reaction efficiency.

The oxidation step was carried out following the procedure described in **Chapter 1 section 1.1.1**. However, a substantial modification was introduced due to the strong electron-donating nature of the peripheral pyridinyloxi substituents. It was observed that reaction times, longer than 1 hour, led to the partial or complete loss of the axial substituent, resulting in a mixture of species bearing 0, 1 or 2 axial ligands. Similar phenomena have been reported in literature, where increased electron density around the silicon center, resulting from electron-donating peripheral groups, has been associated with a weakening of the Si ligand bond and a greater propensity for axial ligand exchange under certain conditions.[185] This side reaction may be related to such electronic effects.

[185] H. Li, M. Lieberman, *Inorg. Chem.* **2001**, *40*, 932–939

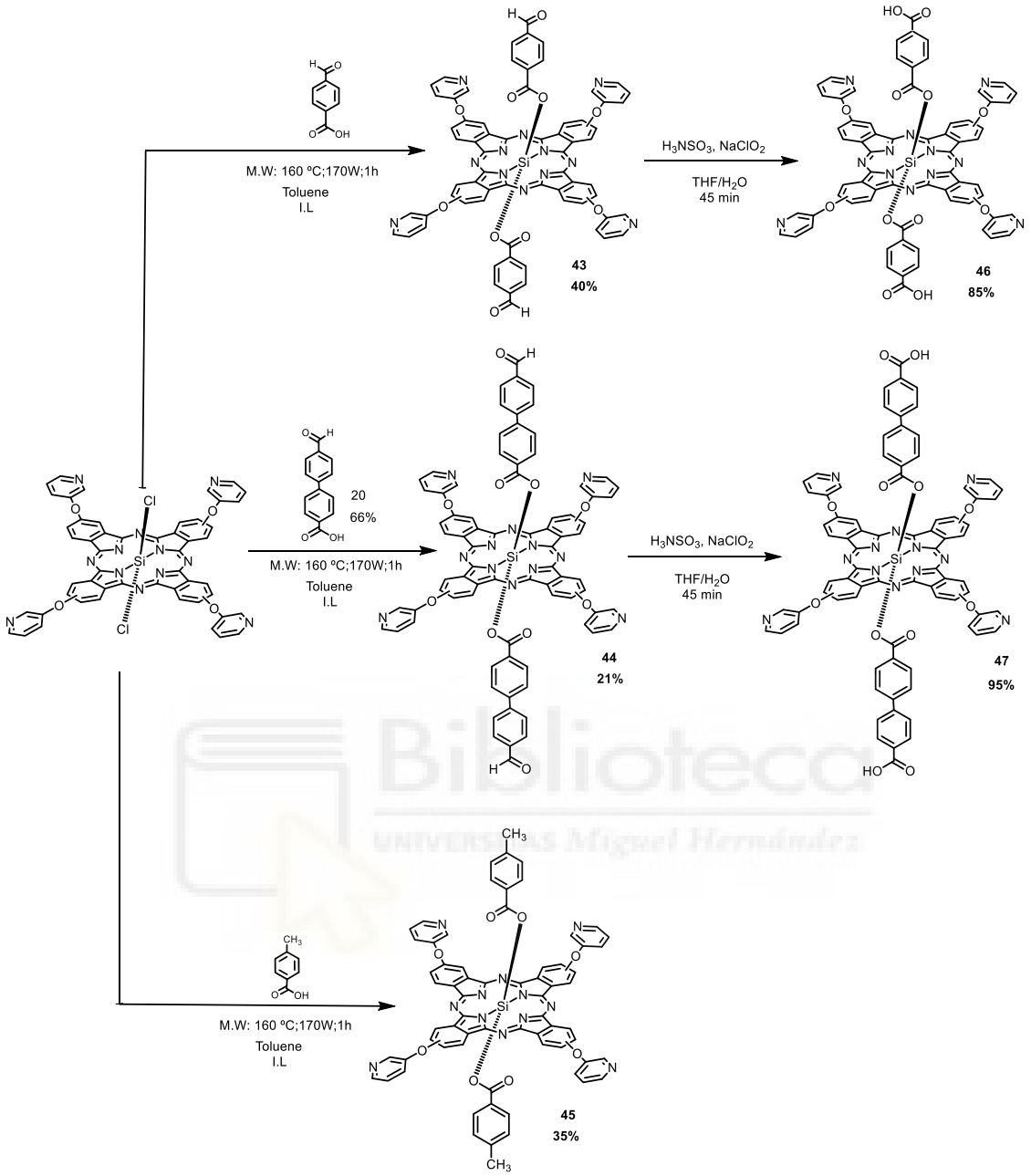

Scheme 2. *Synthesis of $(PyO)_4$-SiPc-$(O_2C$-Ar-$CHO)_2$* ***(43)****, $(PyO)_4$SiPc-$(O_2C$-Ar_2-$CHO)_2$* ***(44)****, $(PyO)_4$SiPc -(O_2C-Ar-$CH_3)_2$* ***(45)****, $(PyO)_4$SiPc (O_2C-Ar-$CO_2H)_2$* ***(46)*** *and $(PyO)_4$SiP- (O_2C-Ar_2-$CO_2H)_2$* ***(47)****.*

All compounds were characterized by ^{1}H-NMR, MALDI-TOF mass spectrometry, and UV-Vis spectroscopy **(Annex 1).** Due to the complexity in assigning the signals, a complementary COSY was performed on the reference molecule **45**

Figure 1 presents the ^{1}H NMR spectra of SiPc **43**, **44**, and **45**. The spectra of the aldehyde derivatives were analyzed due to their higher solubility, which allowed a clearer observation of all the characteristic signals. In addition, a 2D COSY spectrum was recorded for the reference molecule **45** to facilitate the assignment and interpretation of the signals corresponding to the SiPc core as well as those arising from the peripheral substituents.

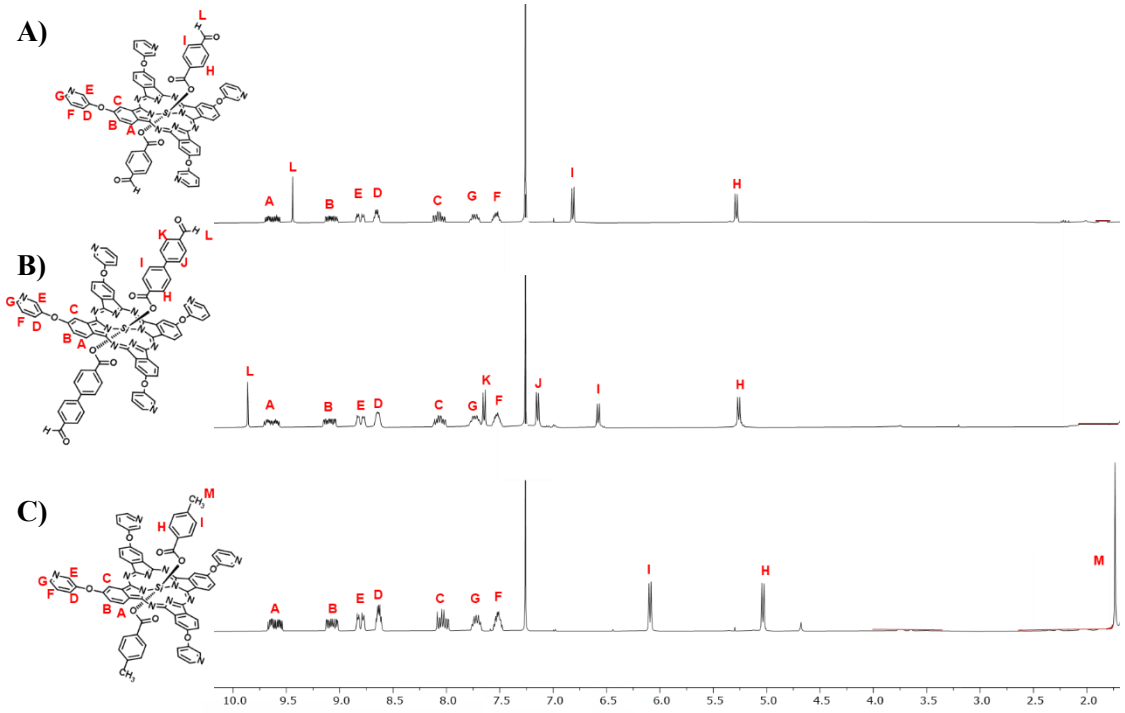

Figure 1. *^{1}H-NMR spectrum of **A)** (PyO)-$_4$SiPc-(O_2C-Ar-CH_3)$_2$ **(45)**, **B)** (PyO)-$_4$SiPc-(O_2C-Ar-CO_2H)$_2$ **(43)** and **C)** (PyO)-$_4$SiPc-(O_2C-Ar_2-CO_2H)$_2$ **(44)** in CDCl.*

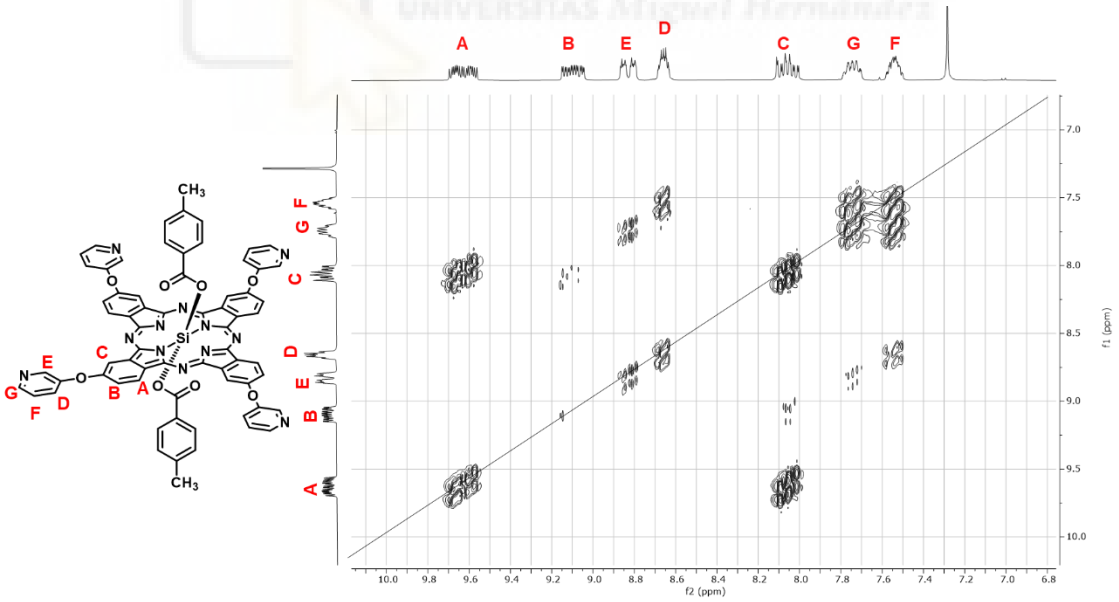

Figure 2. *2D COSY spectrum of (PyO)$_4$SiPc-(O_2C-Ar-CH_3)$_2$ **(45)** in CD_3OD.*

The signals corresponding to the phthalocyanine ring are observed as three multiplets, **A**, **B**, and **C**. The COSY analysis of SiPc **45** reveals a strong ortho coupling between signals **A** and **C**, while a weaker meta coupling is detected between signals **B** and **C**, confirming that these resonances belong to the SiPc ring. For the reference SiPc **45**, signal **A** appears between 9.69-9.52 ppm, signal **B** between 9.15-9.00 ppm, and signal **C** between 8.10-7.97 ppm.

The analysis of the peripheral pyridine substituents shows four multiplets. Signal **D** appears between 8.72-8.58 ppm, with COSY analysis indicating an ortho coupling with signal **F** and a meta coupling with signal **E**. Signal **E** is located between 8.87-8.74 ppm. Signal **F**, observed between 7.61-7.45 ppm, exhibits an ortho coupling with signal **G** in the COSY spectrum. Finally, signal **G** is detected between 7.79-7.65 ppm.

The axial substituents appear as two doublets: signal **H** at 6.09 ppm and signal **I** at 5.09 ppm. Lastly, signal **M**, corresponding to the methyl groups at the axial positions, is observed as a singlet at 1.74 ppm.

In the case of SiPc **43** and SiPc **44**, the most significant difference lies in the presence of the **L** signal, corresponding to the aldehyde group in the axial position. This signal is observed as a singlet at 9.44 ppm for SiPc **43**. While in phthalocyanine **42**, the **L** signal also appears as a singlet but is slightly downfield shifted, at 9.86 ppm.

The phthalocyaninium iodides $(MePy^{+}O)_4$-SiPc-$(O_2C$-Ar-$CO_2H)_2$ $(I^-)_4$ **(48)**, $(MePy^{+}O)_4$-SiPc-$(O_2C$-Ar_2-$CO_2H)_2$ $(I^-)_4$ **(49)** and $(MePy^{+}O)_4$-SiPc-$(O_2C$-Ar-$CH_3)_2$ $(I^-)_4$ **(50)**, were obtained by alkylation of their precursors with methyl iodide (**Scheme 3**). In each case, the pyridine rings react with CH_3I to form quaternary pyridinium iodide units, affording the phthalocyaninium salts in 98%, 80% and 76% yields, respectively. The pyridinium groups greatly enhances solubility in polar solvents. All three iodide salts were characterized by ^{1}H-NMR, UV-Vis spectroscopy and, due to the complexity in assigning the signals, a complementary 2D COSY analysis was performed on the reference molecule **50** (**Annex 1**).

Subsequently, to obtain the target, $(MePy^{+}O)_4$-SiPc-$(O_2C$-Ar-$CO_2H)_2$ $(CH_3SO_3^-)_4$ **(14)**, $(MePy^{+}O)_4$-SiPc-$(O_2C$-Ar_2-$CO_2H)_2$ $(CH_3SO_3^-)_4$ **(15)** and $(MePy^{+}O)_4$-SiPc-$(O_2C$-Ar-$CH_3)_2$ $(CH_3SO_3^-)_4$ **(16)**, an anion exchange reaction was performed using silver methylsulfonate. This exchange was specifically carried out to improve the biocompatibility of the final phthalocyanine salts, since methylsulfonate counterions are known to exhibit lower cytotoxicity and higher aqueous compatibility compared to halides[186] This process successfully replaced the iodide counterions of the precursor phthalocyaninium salts with methylsulfonate, affording the final products in yields of 65%, 67%, and 71%, respectively. All target compounds were characterized by ^{1}H-NMR and UV-Vis spectroscopy (**Annex 1**).

[186] a) D. Broadwater, M. Bates, M. Jayaram, M. Young, J. He, A. L. Raithel, T. W. Hamann, W. Zhang, B. Borhan, R. R. Lunt, S. Y. Lunt, *Sci. Rep.* **2019,** *9*, 15288 b) J. N. Smith, D. G. Thomas, H. Jolley, V. K. Kodali, M. H. Littke, P. Munusamy, D. R. Baer, M. J. Gaffrey, B. D. Thrall, J. G. Teeguarden, *Part. Fibre Toxicol*. **2018**, 15, 47

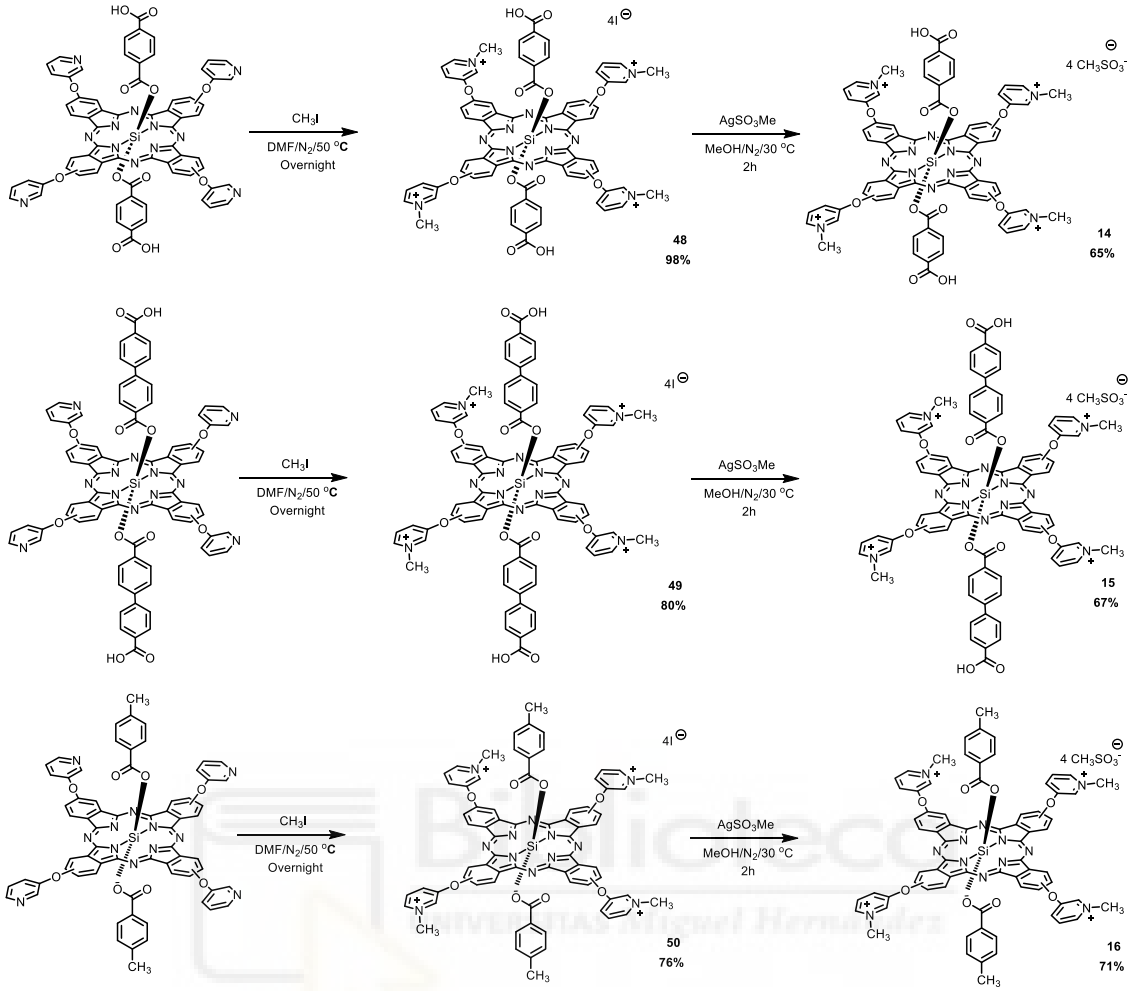

Scheme 3. *Synthesis of $(MePy^+O)_4$-SiPc-$(O_2C$-Ar-$CO_2H)_2$ $(I^-)_4$* ***(48)****, $(MePy^+O)_4$-SiPc -$(O_2C$-Ar_2-$CO_2H)_2$ $(I^-)_4$* ***(49)****, $(MePy^+O)_4$-SiPc -(O_2C-Ar-$CH_3)_2$ $(I^-)_4$* ***(50)****, $(MePy^+O)_4$-SiPc -$(O_2C$-Ar-$CO_2H)_2$ $(CH_3SO_3^-)_4$* ***(14)****, $(MePy^+O)_4$-SiPc -$(O_2C$-Ar_2-$CO_2H)_2$ $(CH_3SO_3^-)_4$* ***(15)*** *and $(MePy^+O)_4$-SiPc -(O_2C-Ar-$CH_3)_2$ $(CH_3SO_3^-)_4$* ***(16)****.*

Figure 3 presents the ^{1}H-NMR spectra of the target molecules $(MePy^+O)_4$-SiPc-$(O_2C$-Ar-$CO_2H)_2$ $(CH_3SO_3^-)_4$ **(14)**, $(MePy^+O)_4$-SiPc-$(O_2C$-Ar_2-$CO_2H)_2$ $(CH_3SO_3^-)_4$ **(15)**, and $(MePy^+O)_4$-SiPc-$(O_2C$-Ar-$CH_3)_2$ $(CH_3SO_3^-)_4$ **(16)**. When comparing the reference phthalocyanine **16** with the precursor SiPc **45**, several notable differences can be observed.

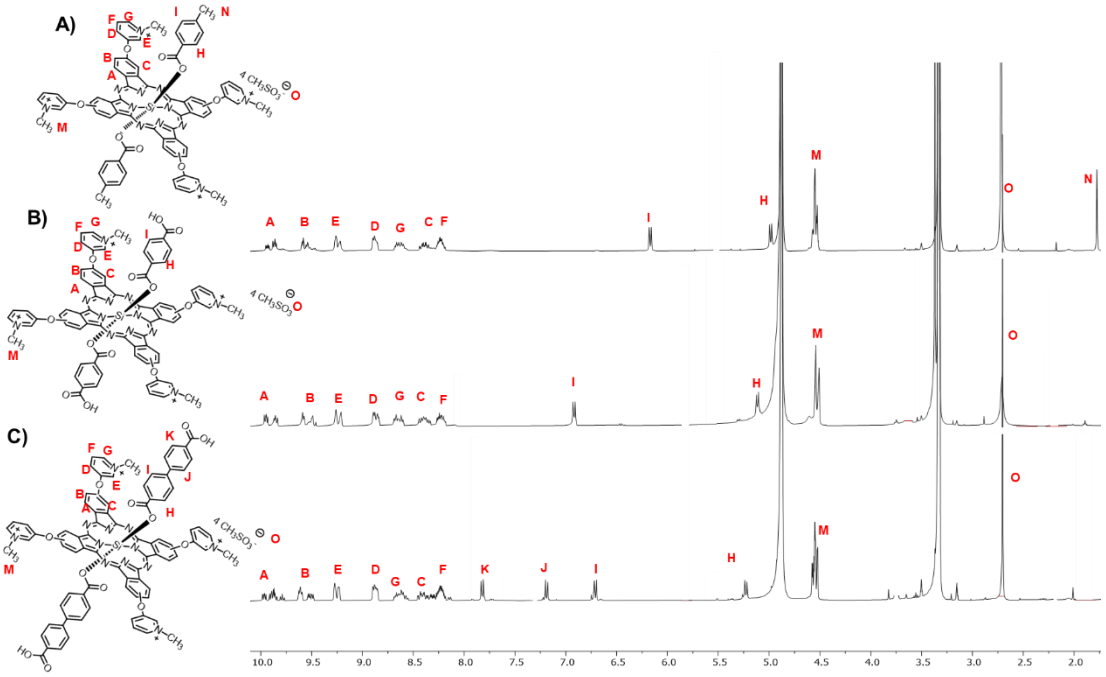

Figure 3. *^{1}H-NMR spectrum of* ***B)*** *$(PyO^+)_4SiPc\text{-}(O_2C\text{-}Ar\text{-}CO_2H)_2$ $(CH_3SO_3^-)_4$* ***(14)****,* ***C)*** *$(PyO^+)_4SiPc\text{-}(O_2C\text{-}Ar_2\text{-}CO_2H)_2$ $(CH_3SO_3^-)_4$* ***(15)*** *and* ***A)*** *$(PyO^+)_4SiPc\text{-}(O_2C\text{-}Ar_2\text{-}CH_3)_2$ $(CH_3SO_3^-)_4$* ***(16)*** *in in CD_3OD.*

For the phthalocyanine core, the characteristic signals appear as three multiplets (**A**, **B**, and **C**) in both spectra, although in SiPc **16** the signal **C** 8.30-8.17 ppm (4H) is slightly shifted upfield relative to SiPc **45** 8.10-7.97 ppm (4H).

In the case of the peripheral pyridinium substituents, the four multiplets (**D-G**) are observed in similar regions to those of SiPc **45**, but the **G** signal shows a more pronounced downfield shift in SiPc **16**, appearing at 8.71-8.58 ppm (4H). This effect can be attributed to the electron-withdrawing influence of the methylated pyridinium units, which reduce electron density around the aromatic system.

Additional differences are evident in the presence of two new sets of resonances: signal **M**, corresponding to the methyl groups of the pyridinium substituents, appears as a multiplet at 4.58-4.49 ppm (12H), while signal **O**, associated with the methylsulfonate counterions, is observed as a singlet at 1.78 ppm (12H). These features confirm the successful cationic functionalization and counterion exchange.

For SiPc **14** and **15**, the spectra show the same main differences with respect to the precursor SiPc **45**, with the disappearance of the singlet corresponding to the aldehyde group (signal **L**) due to its conversion into carboxylic acid functionalities. This transformation provides further confirmation of the successful synthesis of the target compounds.

To complement the characterization by ^{1}H NMR, UV-Vis spectroscopy was carried out to provide a more complete description of the optical properties of the target molecules. For this purpose, the UV-Vis spectra of the reference phthalocyanines **45**, **50**, and **16** (**Figure 4**) were examined in order to assess the effect of methylation and counterion exchange on their absorption profiles. This strategy was selected on the basis that the influence of axial substituents on the

optical behavior of these silicon phthalocyanines is minimal, thus allowing the reference compounds to serve as representative models for the entire series.

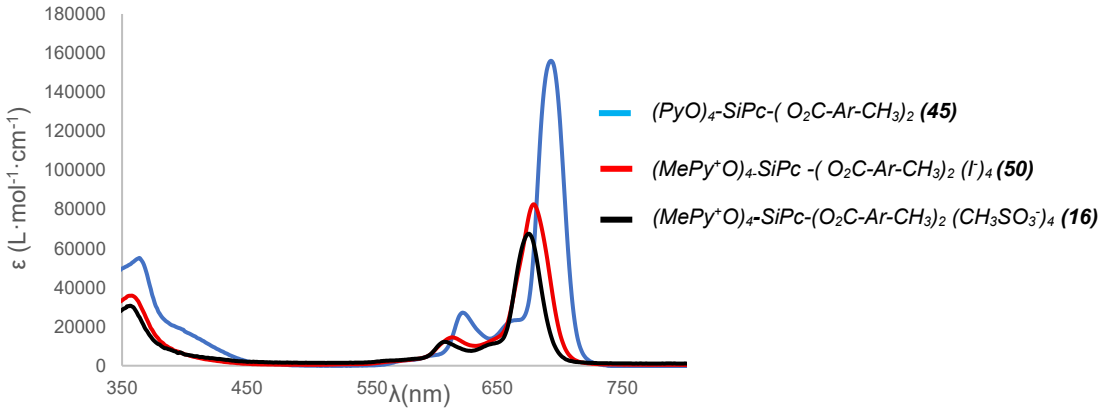

***Figure 4**. UV-Vis spectrum of $(PyO)_4$-SiPc-(O_2C-Ar-$CH_3)_2$ **(45)** in $CHCl_3$, $(MePy^+O)_4$-SiPc -(O_2C-Ar-$CH_3)_2$ $(I^-)_4$ **(50)** and $(PyO^+)_4$SiPc-(O_2C-Ar-$CH_3)_2$ $(CH_3SO_3^-)_4$ **(16)** in MeOH.*

The UV-Vis spectra of the reference phthalocyanines $(MePy^+O)_4$-SiPc-$(O_2C$-Ar-$CH_3)_2(CH_3SO_3^-)_4$ **(16)**, $(MePy^+O)_4$-SiPc-$(O_2C$-Ar-$CH_3)_2(I^-)_4$ **(50)**, and $(PyO)_4$-SiPc-$(O_2C$-Ar-$CH_3)_2$ **(45)** show differences in band position and absorption intensity.

Compound **16** displays the weakest spectrum, with a Soret band at 357 nm and a Q band at 675 nm in methanol. A slight red-shift is observed for **50**, with bands at 358 and 679 nm, possibly reflecting the different influence of iodide compared to methylsulfonate counterions. The most pronounced shift appears in **45**, where the Soret and Q bands are located at 364 and 693 nm in chloroform. The higher intensity observed in this case may be related to the absence of methylation in the pyridinium substituents and to the reduced solvation effects of chloroform compared to methanol.

These results suggest that both counterion effects and the electronic nature of the substituents, together with solvent polarity, play an important role in tuning the optical response of this silicon phthalocyanines.

1.2.1. Synthesis and Characterization of SURMOFS of SiPc 14 and 15.

Following the successful synthesis and characterization of phthalocyanines **14** and **15**, their potential to form new coordination frameworks was investigated using the methodology described in **Chapter 1 section 1.3.1.**

In this case, the design of these molecules incorporated pyridinium functional groups at the periphery, enabling additional electrostatic interactions that could influence the assembly process, while their ditopic axial ligands were selected to promote coordination with metal ions for SURMOF formation.

For each compound, a 1 mM zinc acetate solution in ethanol and a 20 μM solution of the corresponding phthalocyanine in DMF were prepared. Using the sequential spin-coating method, sixty alternating layers were deposited onto plasma-treated silicon substrates to assemble the corresponding SURMOF films. This approach preserved the advantages of the previously optimized deposition method, ensuring high reproducibility and uniform film growth across the series.

To assess the structural features of the resulting films, *out-of-plane* XRD measurements were performed. These analyses aimed to determine whether the presence of pyridinium substituents and variations in the axial ligands affected the crystalline ordering, orientation, and periodicity of the SURMOF structures.

The SURMOF for $(MePy^{+}O)_4$-SiPc -$(O_2C\text{-}Ar\text{-}CO_2H)_2$ $(CH_3SO_3^{-})_4$ **(14)**, as a linker was synthesized according to the procedure described in **Chapter 1 section 1.3.1.** The synthesized material was characterized by *out-of-plane* XRD.

Figure 5 compares the experimental *out-of-plane* XRD pattern of the SiPc **14** sample with the previously described theoretical simulation for **Zn-SiPc-$(CO_2H)_2$**.[116] Three well-defined periodicities can be identified in this analysis, although they are shifted relative to the previously reported values, where a) = b) = 2.1 nm and c) = 1.1 nm, compared to the experimentally obtained value of a) = 1.4 nm. This discrepancy in the values suggests that the formed three-dimensional structure differs from the expected structure for a SURMOF, indicating the need for additional experiments to characterize its structure with greater precision. Furthermore, the presence of these well-defined periodicities, with a correlation between the periodicity values (1st periodicity = 1.42 nm, 2nd periodicity = 0.71 nm, and 3rd periodicity = 0.38 nm), suggests the formation of a MOF, as these distances are consistent with the periodic structure's characteristic of these materials.[187]

[187] J. Martí-Rujas, *Dalton Trans.* **2020**, *49*, 14078–14087.

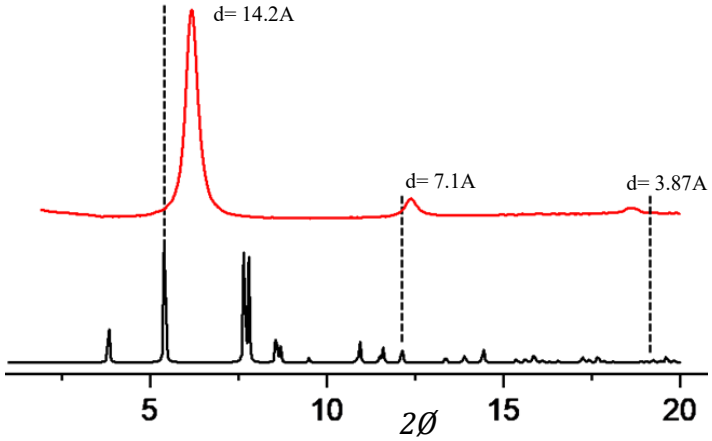

***Figure 5**. Predicted structure of **Zn-SiPc-(CO$_2$H)$_2$**[116] (black) and experimental out-of-plane (red) X-ray diffraction patterns of Zn-SiPc **14** SURMOF structure.*

For the SURMOF (MePy$^+$O)$_4$-SiPc-(O$_2$C-Ar$_2$-CO$_2$H)$_2$ (CH$_3$SO$_3^-$)$_4$ (**15**), synthesized as their analogue for SiPc **14**. The synthesized material was characterized by *out-of-plane* XRD.

Figure 6 shows a comparison between the experimental *out-of-plane* XRD pattern of Zn-SiPc **15** and its corresponding theorical simulation. This simulation was generated using CIF data from previous studies[116] (**Annex 3**) as a starting point, with the structural parameters refined in accordance with the results obtained for Zn-SiPc **11** in **Chapter 2**, due to the presence of a longer axial substituent in Zn-SiPc **15**, which is expected to increase the lattice parameters a) and b). The predicted values were a) = b) = 2.8 nm and c) 1.1 nm. However, the experimental results only show one periodicity with a value of a) = 1.7 nm, and no additional periodicity or matches with the theoretical simulation were detected. This suggests that the formation of a SURMOF using SiPc **15** as a linker was unsuccessful and not align with the theoretical structures predicted for such materials.[187]

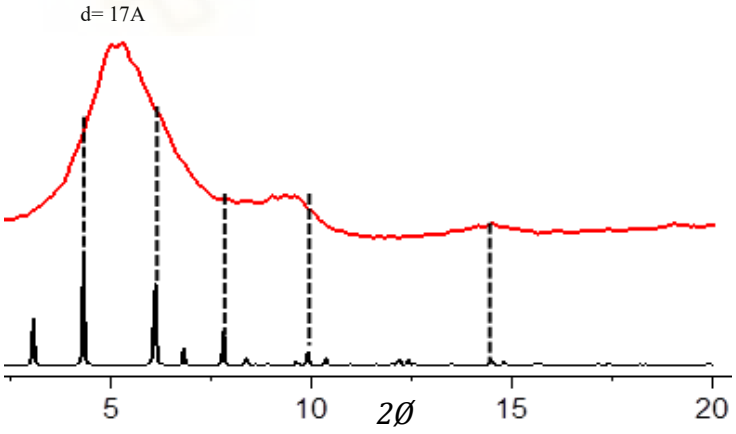

***Figure 6.** Predicted structure (black) and experimental out-of-plane (red) X-ray diffraction patterns of Zn-SiPc **15** SURMOF.*

2.Conclusions.

In this work, the synthesis and complete characterization of two target phthalocyanine salts were successfully achieved. These compounds were designed with different axial substituents to modulate their ability to form SURMOF-type structures.

All molecules were thoroughly characterized by ^{1}H-NMR spectroscopy, UV-Vis spectroscopy, HR-MALDI-TOF mass spectrometry, and electrochemical studies.

XRD analysis revealed that SiPc **14** formed more defined structures compared to SiPc **15**, although both compounds exhibited a certain degree of periodicity, suggesting the formation of SURMOF-like architectures. However, when comparing the diffraction patterns of SiPc **14** and **15** with theoretical predictions, clear discrepancies were observed, indicating that the assembled structures differ from the expected models likely due to the presence of pyridinium peripheral groups.

In light of these findings, a more comprehensive structural characterization will be required to elucidate the three-dimensional architecture of the resulting SURMOFs. Once this information is available, the materials will be further analyzed by UV-Vis and FT-IRRAS spectroscopy, as described in **Chapters 1 and 2**.

Subsequently, these new SURMOFs will be evaluated for their bactericidal activity, in order to identify the most appropriate applications based on their functional properties.

3.Experimental Section.

3.1. Materials and Methods

Except for specific cases mentioned, the reagents and solvents used in the synthesis processes were obtained from commercial suppliers and used without any additional purification.

-Microwave reactor: Microwave reactions were carried out in a CEM microwave reactor, Discover SP model.

-Chromatographic Techniques: Column chromatography was performed on SiO_2 (40-63 mm) and Biorad Biobeads SX-3 (200-400 mesh) was used as the stationary phase for Size Exclusion Chromatography (SEC). TLC plates coated with SiO_2 60F254 were visualized under UV light.

-Nuclear Magnetic Resonance (NMR): NMR spectra were recorded on a Bruker AC 300 or Burker 400MHz spectrometer at 25 ºC, unless otherwise specified using deuterated solvents and referenced to tetramethylsilane (TMS). Coupling constants (*J*) are reported in hertz (Hz). The signals are designated as follows: s = singlet, d = doublet, m = multiplet, and chemical shifts are given in ppm.

-UV-Vis: The measurements for SiPc dissolution were recorded on Perkin Elmer LAMDA 365 UV-WinLab spectrophotometers, using spectrosol-grade solvents.

-Mass spectrometry: High-resolution mass spectra were obtained from a Bruker Reflex II matrix-assisted laser desorption/ ionization time-of-flight (MALDI-TOF) spectrometer using dithranol as matrix.

-X-Ray diffraction (XRD): The XRD measurements for *out-of-plane* (co-planar orientation) were carried out using a Bruker D8-Advance diffractometer equipped with a position sensitive detector Lynxeye in geometry, variable divergence slit, and 2.3° Soller-slit was used on the secondary side.

-Substrate pretreatment: Substrates were cleaned by argon-hydrogen plasma using a Diener Plasma surface treatment system (airflow: 20 sccm, pure hydrogen) for 30 minutes.

3.2.1. Synthesis of 4-(3-pyridinyloxy)phthalonitrile (40).[184]

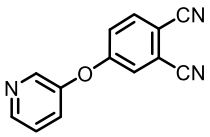

1 g (5.7 mmol) of 4-nitrophthalonitrile 0.65 g (6.8 mmol) of 3-hydroxypyiridine and K_2CO_3 were dissolved in 20 mL of DMSO under an inert atmosphere for 24 hours. The crude product was precipitated over ice/water and filtered. The solid obtained was washed repeatedly with water. Yielding 0.56g (45%) of 4-(3-pyridyloxy)phthalonitrile **(40)**[184] as spongy white solid, which was used without further purification. ^{1}H-NMR (200 MHz, DMSO-*d*$_6$, 25 ºC): δ = 8.52 (m, 1H), 8.40 (s, 1H), 8.12 (d, 1H), 7.9 (dd, 1H), 7.71 (m, 1H), 7.54 (m, 1H), 7.49 (dd, 1H).

3.2.2. Synthesis of 5-(3-pyridyloxy)-diiminoisoindoline (41).[184]

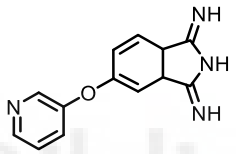

500 mg (2.76 mmol) of 4-(3-pyridyloxy)phtalonitrile **(40)**[184] and 50 mg of MeONa were dissolved in 100 mL of MeOH. NH_3 was bubbled through the mixture suspension at the reflux temperature of methanol (65 ºC) for 8 hours. The reaction mixture turned a slightly greenish colour. The solvent was evaporated, and the resulting solid was washed repeatedly with water. Yielding 490 mg (75%) of 4-(3-pyridyloxy)-diiminoisoindoline **(41)**[184] as a greenish crystalline powder which was used in subsequent reactions without further purification. ^{1}H-NMR (200 MHz, DMSO-*d*$_6$, 25 ºC): δ = 8.62 (m, 2H), 7.84 (d, 1H), 7.49 (m, 3H), 7.1 (dd, 1H), 3.79-3.59 (m, 3H, NH).

3.2.3. Synthesis of $(PyO)_4$-$SiPcCl_2$ (42).

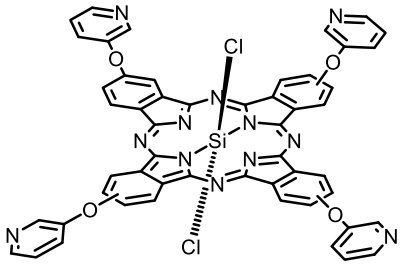

500 mg (2.13 mmol) of 4-(3-pyridyloxy)-diiminoisoindoline **(41)** was dissolved in 5 mL of quinoline. The system was closed, purged with N_2 and protected from light. Then 0.5 mL of $SiCl_4$ was carefully added, and the mixture was heated to reflux temperature (200 ºC) for 1 hour. The crude product was precipitated in acetone, filtered and washed repeatedly with acetone. Yielding 700 mg (99%) of $(PyO)_4$-$SiPcCl_2$ **(42)** as a green solid which was used without further purification in subsequent reactions. UV-Vis (DMSO) λ_{max}/nm: 358, 374, 613, 632, 659, 682, 702.

3.2.4. Synthesis of (PyO)4-SiPc(O_2C-Ar-CHO)$_2$ (43).

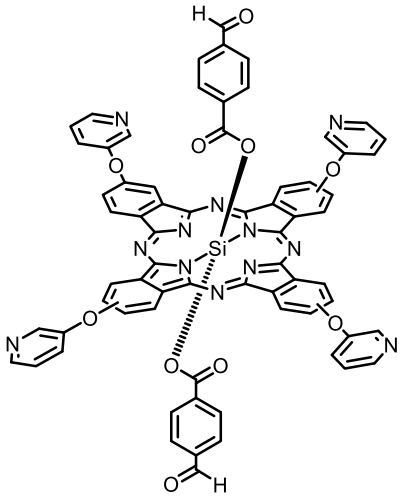

50 mg (0.051 mmol) of $(PyO)_4$-$SiPcCl_2$ **(42)**, 23 mg (0.15 mmol) of 4-formylbezoic acid, 30 mg (0.07 mmol) of 1,1'-methylenebis(3-methylimidazolium) iodide[175] were dissolved in 1 mL of dry toluene. The mixture was heated in microwave reactor with constant stirring at 160 ºC for 1 hour. Then toluene was removed, and the resulting solid was washed with 60 mL of MeOH. The obtained solid was purified by column chromatography (SiO_2, CH_2Cl_2/THF (1:1)) The obtained product was repeatedly washed with ethanol. Yielding 25 mg (40%) of $(PyO)_4$SiPc-(O_2C-Ar-CHO)$_2$ **(43)** as a blue-green solid. ^{1}H-NMR (400 MHz, $CDCl_3$, 25 °C) δ = 9.71 -9.51 (m, 4H), 9.44 (s, 2H), 9.16-9.00 (m, 4H), 8.87-8.75 (m, 4H), 8.70-8.61 (m, 4H), 8.15-7.99 (m, 4H), 7.80-7.67 (m, 4H), 7.60-7.47 (m, 4H), 6.82 (d, *J* = 8.4 Hz, 4H), 5.29 (d, *J* = 8.4 Hz, 4H).UV-Vis (THF) λ_{max}/nm (log ε): 363 (4.77), 623 (4.46), 693 (5.26). MS (MALDI-TOF, dithranol): *m/z* [M^-] calcd. for $C_{68}H_{38}N_{12}O_{10}Si$ 1210.2608 found 1210.3716.

3.2.5. Synthesis of (PyO)4-SiPc -(O_2C-Ar_2-CHO)$_2$ (44).

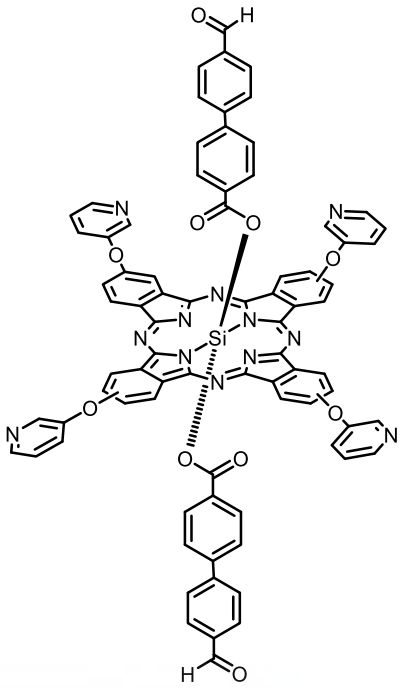

100 mg (0.101 mmol) of $(PyO)_4$-$SiPcCl_2$ **(42)**, 92 mg (0.407 mmol) of of 4'-formyl-[1,1'-biphenyl]-4-carboxylic acid **20**,[166] 30 mg (0.07 mmol) 1,1'-methylenebis(3-methylimidazolium) iodide[175] were dissolved in 2 mL of dry toluene. The mixture was heated in microwave reactor with constant stirring at 160 ºC for 1 hour. Then toluene was removed, and the resulting solid was washed with 60 mL of MeOH. The obtained solid was purified by column chromatography (SiO_2, CH_2Cl_2/THF (1:1)). The obtained product was repeatedly washed with ethanol. Yielding 30 mg (21%) $(PyO)_4$SiPc -(O_2C-Ar_2-CHO)$_2$ **(44)** as a blue-green solid. ^{1}H-NMR (400 MHz, $CDCl_3$,25 °C) δ = 9.86 (s, 2H), 9.73-9.55 (m, 4H), 9.17-9.02 (m, 4H), 8.89-8.77 (m, 4H), 8.74-8.64 (m, 4H), 8.14-7.98 (m, 4H), 7.86-7.67 (m, 4H), 7.73 (d, *J* = 8.4 Hz, 4H), 7.59-7.46 (m, 4H), 7.17 (d, *J* = 8.4 Hz, 4H), 6.58 (d, *J* = 8.4 Hz, 4H), 5.26 (d, *J* = 8.4 Hz, 4H). UV-Vis (DMSO) λ_{max}/nm (log ε): 357 (4.78), 374 (4.60), 632 (4.36), 702 (5.12). MS (MALDI-TOF, dithranol): *m/z* [M^-] calcd. for $C_{80}H_{46}N_{12}O_{10}Si$ 1362.3245found 1362.3155.

3.2.6. Synthesis of $(PyO)_4$-SiPc -(O_2C-Ar-$CH_3)_2$ (45).

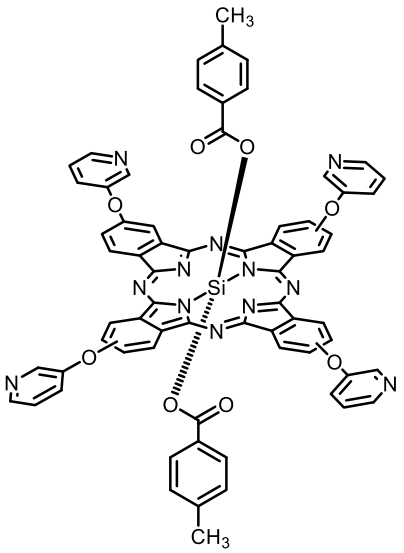

50 mg (0.051 mmol) of $(PyO)_4$-$SiPcCl_2$ **(42)**, 41 mg (0.302 mmol) of 4-formylbezoic acid, 30 mg (0.07 mmol) 1,1'-methylenebis(3-methylimidazolium) iodide[175] were dissolved in 1 mL of dry toluene. The mixture was heated in microwave reactor with constant stirring at 160 ºC for 1 hour. Then toluene was removed, and the resulting solid was washed with 60 mL of MeOH. The obtained solid was purified by column chromatography (SiO_2, CH_2Cl_2/THF (7:3)) The obtained product was repeatedly washed with acetone. Yielding 21 mg (35%) of $(PyO)_4$SiPc -(O_2C-Ar-$CH_3)_2$ **(45)** as blue-green solid. ^{1}H-NMR (400 MHz, $CDCl_3$, 25 °C) δ = 9.69-9.52 (m, 4H), 9.15-9.00 (m, 4H), 8.87-8.74 (m, 4H), 8.72-8.58 (m, 4H), 8.10-7.97 (m, 4H), 7.79-7.65 (m, 4H), 7.61-7.45 (m, 4H), 6.09 (d, *J* = 8.0 Hz, 4H), 5.05 (d, *J* = 8.0 Hz, 4H), 1.76 (s, 6H). UV-Vis (THF) λ_{max}/nm (log ε): 364 (4.74), 622 (4.43), 693 (5.19). MS (MALDI-TOF, dithranol): *m/z* [M^-] calcd. for $C_{68}H_{42}N_{12}O_8Si$ 1182.3026 found 1182.3967.

3.2.7. Synthesis of (PyO)4-SiPc (O_2C-Ar-$CO_2H)_2$ (46).

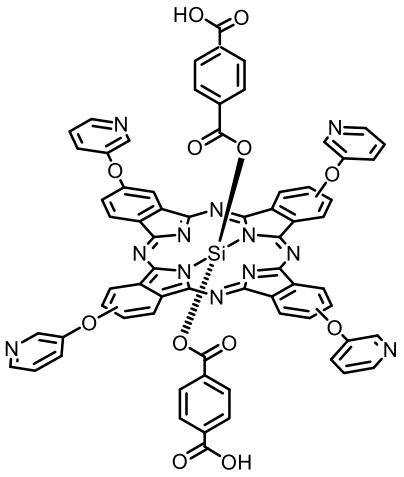

70 mg (0.057 mmol) of (PyO)4-SiPc-(O_2C-Ar-CHO)$_2$ **(43)** was dissolved in 6 mL of THF/H_2O (6:1) mixture. In parallel, 17 mg of H_3NSO_3 (0.17 mmol) and 35 mg of $NaClO_2$ (0.14 mmol) were dissolved in 6 mL of THF/H_2O (6:1) mixture. The H_3NSO_3 and $NaClO_2$ solution was

slowly added to the $(PyO)_4SiPc\text{-}(O_2C\text{-}Ar\text{-}CHO)_2$ **(43)** solution. The reaction was protected from direct light and stirred at room temperature for 45 minutes. Then, it was precipitated in 30 mL of H_2O and filtered. The solid was redissolved in THF, dried with Na_2SO_4 and concentrated. The obtained solid was washed sequentially with DCM, acetone, and MeOH. Yielding 60 mg (85%) of $(PyO)_4SiPc\ (O_2C\text{-}Ar\text{-}CO_2H)_2$ **(46)** as a blue-green solid. ^{1}H-NMR (400 MHz, DMSO-d_6, 25 °C) δ = 9.80-9.59 (m, 4H), 9.20-8.93 (m, 4H), 8.90-8.80 (m, 4H), 8.75-8.65 (m, 4H), 8.34 -8.16 (m, 4H), 7.59-7.46 (m, 4H), 6.88 (d, *J* = 8.5 Hz, 4H), 5.08 (d, *J* = 8.5 Hz, 4H). UV-Vis (THF) λ_{max}/nm (log ε): 361 (4.56), 620 (4.21), 686 (4.90). MS (MALDI-TOF, dithranol): *m/z* [M^-] calcd. for $C_{68}H_{38}N_{12}O_{12}Si$ 1242.2508 found 1242.2434.

3.2.8. Synthesis of (PyO)4-SiPc $(O_2C\text{-}Ar_2\text{-}CO_2H)_2$ (47).

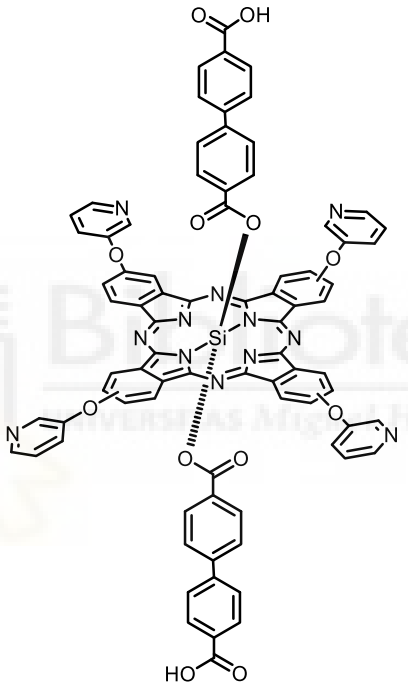

25 mg (0.018 mmol) of (PyO)4-SiPc $-(O_2C\text{-}Ar_2\text{-}CHO)_2$ **(44)**, was dissolved in 6 mL of THF/H_2O (6:1) mixture. In parallel, 12 mg of H_3NSO_3 (0.12 mmol) and 29 mg of $NaClO_2$ (0.10 mmol) were dissolved in 6 mL of THF/H_2O (6:1) mixture. The H_3NSO_3 and $NaClO_2$ solution was slowly added to the $(PyO)_4SiPc\ -(O_2C\text{-}Ar_2\text{-}CHO)_2$ **(44)**, solution. The reaction was protected from direct light and stirred at room temperature for 45 minutes. Then, it was precipitated in 30 mL of H_2O and filtered. The solid was redissolved in THF, dried with Na_2SO_4 and concentrated. The obtained solid was washed sequentially with DCM, acetone, and MeOH. Yielding 24 mg (95%) of $(PyO)_4SiPc\ (O_2C\text{-}Ar_2\text{-}CO_2H)_2$ **(47)** as blue-green solid. ^{1}H-NMR (400 MHz, DMSO-d_6, 25 °C) δ = 9.73-9.59 (m, 4H), 9.17-8.98 (m, 4H), 8.89-8.75 (m, 4H), 8.71-8.56 (m, 4H), 8.31-8.12 (m, 4H), 8.03-7.90 (m, 4H), 7.80-7.67 (m, 8H), 7.20 (d, *J* = 8.2 Hz, 4H), 6.75 (d, *J* = 8.2 Hz, 4H), 5.11 (d, *J* = 8.2 Hz, 4H). UV-Vis (THF) λ_{max}/nm (log *ε*): 361 (4.56), 620 (4.21), 686 (4.90). MS (MALDI-TOF, dithranol): *m/z* [M^-] calcd. for $C_{80}H_{46}N_{12}O_{12}Si$ 1395.3182 found 1395.3746.

3.2.9. Synthesis of $(MePy^{+}O)_4$-SiPc-$(O_2C$-Ar-$CO_2H)_2$ $(I^{-})_4$ (48).

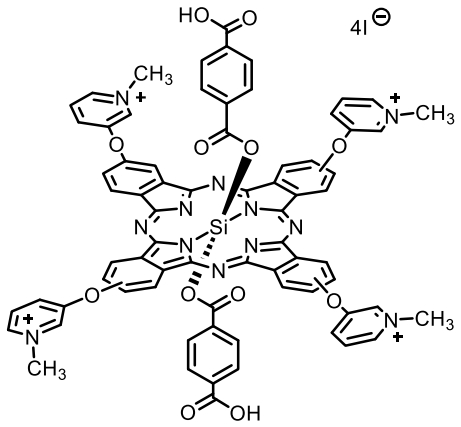

60 mg (0.048 mmol) of $(PyO)_4$-SiPc $(O_2C$-Ar-$CO_2H)_2$ **(46)**, was dissolved in 4 mL of DMF. The atmosphere was made inert, and 0.5 mL (9.65 mmol) of methyl iodide was added. The mixture was heated to 50 ºC and allowed to react overnight. Then, the crude reaction mixture was kept under vacuum for 24 hours to remove excess methyl iodide. Finally, the solvent was removed, and the resulting solid was washed first with DCM and then with a DCM: Acetone (1:1) mixture. Yielding 80 mg (98%) of $(MePy^{+}O)_4$-SiPc-$(O_2C$-Ar-$CO_2H)_2$ $(I^{-})_4$ **(48)** as a blue-green solid. ^{1}H-NMR (400 MHz, MeOD, 25 °C) δ = 9.96-9.75 (m, 4H), 9.66-9.45 (m, 4H), 9.28-9.12 (m, 4H), 8.92-8.76 (m, 4H), 8.70-8.50 (m, 4H), 8.43-8.13 (m, 8H), 6.85 (d, *J* = 8.5 Hz, 4H), 5.03 (d, *J* = 8.5 Hz, 4H), 4.60-4.49 (m, 12H).). UV-Vis (MeOH) λ_{max}/nm (log ε): 356 (4.77), 614 (4.35), 678 (5.09).

3.2.10. Synthesis of $(MePy^{+}O)_4$-SiPc-$(O_2C$-Ar_2-$CO_2H)_2$ $(I^{-})_4$ (49).

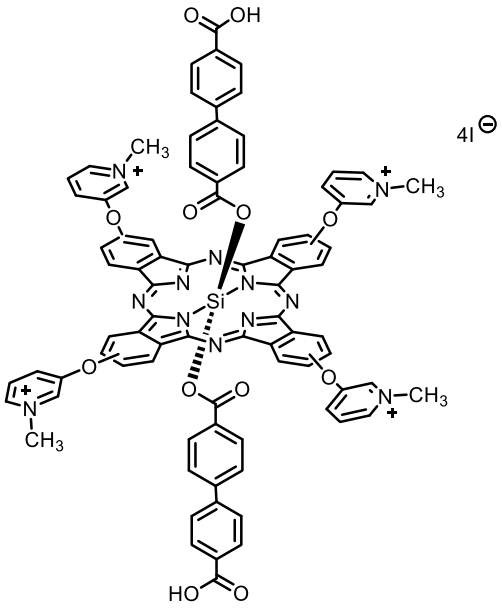

48 mg (0.034 mmol) of $(PyO)_4SiPc$ $(O_2C\text{-}Ar_2\text{-}CO_2H)_2$ **(47)**, was dissolved in 4 mL of DMF. Then an inert atmosphere was established, and 0.5 mL (9.65 mmol) of methyl iodide was added. The mixture was heated to 50 ºC and stirred overnight. Subsequently, the crude reaction was placed under vacuum for 24 hours to remove excess methyl iodide. Finally, the solvent was removed, and the resulting solid was washed sequentially with DCM and then with a DCM: Acetone (1:1) mixture. Yielding 40 mg (80%) of $(PyO^+)_4SiPc\text{-}(O_2C\text{-}Ar_2\text{-}CO_2H)_2$ $(I^-)_4$ **(49)** as a blue solid. ^{1}H-NMR (400 MHz, MeOD, 25 °C) δ = 9.97-9.77 (m, 4H), 9.70-9.49 (m, 4H), 9.32-9.15 (m, 4H), 8.96-8.79 (m, 4H), 8.70-8.50 (m, 4H), 8.47-8.14 (m, 8H), 7.81 (d, *J* = 8.2 Hz, 4H), 7.18 (d, *J* = 8.2 Hz, 4H), 6.71 (d, *J* = 8.4 Hz, 4H), 5.22 (d, *J* = 8.4 Hz, 4H), 4.60-4.49 (m, 12H).UV-Vis (MeOH) λ_{max}/nm (log ε): 356 (4.74), 614 (4.34), 678 (5.03).

3.2.11. Synthesis of $(MePy^+O)_4$-SiPc-(O_2C-Ar-$CH_3)_2$ $(I^-)_4$ (50).

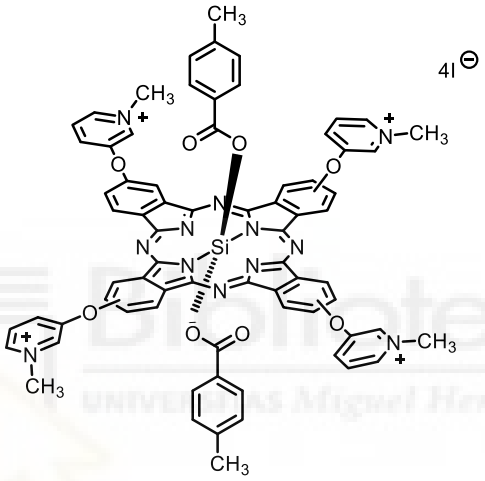

15 mg (0.013 mmol) of $(PyO)_4$-SiPc -(O_2C-Ar-$CH_3)_2$ **(45)**, was dissolved in 2 mL of DMF. Then an inert atmosphere was established, and 0.1 mL (1.93 mmol) of methyl iodide was added. The mixture was heated to 50 ºC and stirred overnight. Subsequently, the crude reaction was placed under vacuum for 24 hours to remove excess methyl iodide. Finally, the solvent was removed, and the resulting solid was washed sequentially with DCM and then with a DCM: Acetone (1:1) mixture. Yielding 16 mg (76%) of $(MePy^+O)_4$-SiPc-(O_2C-Ar-$CH_3)_2$ $(I^-)_4$ **(50)** as a blue solid. ^{1}H-NMR (400 MHz, MeOD, 25 °C) δ = 9.95-9.81 (m, 4H), 9.79-9.53 (m, 4H), 9.28-9.11 (m, 4H), 8.91-8.77 (m, 4H), 8.69-8.49 (m, 4H), 8.44-8.30 (m, 4H), 8.29-8.11 (m, 4H), 6.15 (d, *J* = 8.2 Hz, 4H), 4.96 (d, *J* = 8.2 Hz, 4H), 4.60-4.49 (m, 12H), 1.75 (s, 6H). UV-Vis (MeOH) λ_{max}/nm (log ε): 356 (4.74), 614 (4.34), 678 (5.03).

3.2.12. Synthesis of $(MePy^+O)_4$-SiPc-$(O_2C$-Ar-$CO_2H)_2$ $(CH_3SO_3^-)_4$ (14).

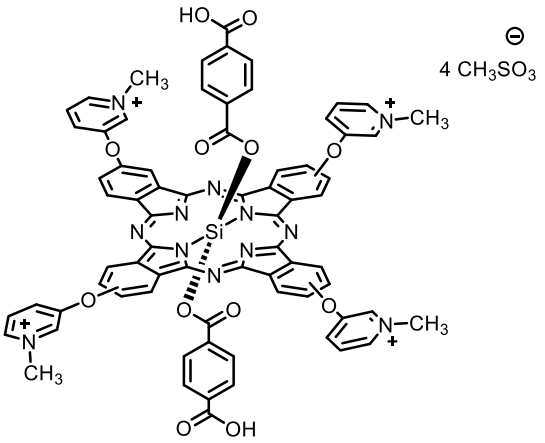

80 mg (0.047 mmol) of $(MePy^+O)_4$-SiPc-$(O_2C$-Ar-$CO_2H)_2$ $(I^-)_4$ **(48)** and 37 mg (0.18 mmol) of $AgSO_3CH_3$ were dissolved in 20 mL of methanol. The reaction mixture was heated to 30 ºC and stirred for 2 hours. Then, the mixture was filtered to remove the silver. The filtrate was concentrated and washed sequentially with DCM, acetone and DCM/ EtOH (3:1) mixture. Yielding 49 mg (65%) of the target compound $((MePy^+O)_4$-SiPc-$(O_2C$-Ar-$CO_2H)_2$ $(CH_3SO_3^-)_4$ **(14)** as a pure blue solid. ^{1}H-NMR (400 MHz, MeOD, 25 °C) δ = 10.01-9.80 (m, 4H), 9.64-9.45 (m, 4H), 9.32-9.17 (m, 4H), 8.95-8.81 (m, 4H), 8.71-8.57 (m, 4H), 8.48-8.16 (m, 8H), 6.92 (d, *J* = 8.2 Hz, 4H), 5.10 (d, *J* = 8.2 Hz, 4H), 4.60-4.49 (m, 12H).) 2.70 (s, 12H). UV-Vis (MeOH) λ_{max}/nm (log ε): 356 (4.93), 614 (4.50), 678 (5.22).

3.2.13. Synthesis of $(MePy^+O)_4$-SiPc-$(O_2C$-Ar_2-$CO_2H)_2$ $(CH_3SO_3^-)_4$ (15).

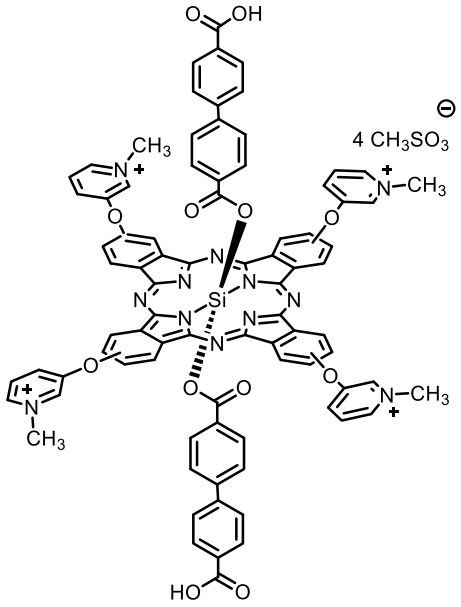

20 mg (0.014 mmol) of $(MePy^+O)_4$-SiPc-$(O_2C$-Ar_2-$CO_2H)_2$ $(I^-)_4$ **(49)** and (0.18 mmol) of $AgSO_3CH_3$ were dissolved in 20 mL of methanol. The reaction mixture was heated to 30 ºC and stirred for 2 hours. Then, the mixture was filtered to remove the silver. The filtrate was

concentrated and washed sequentially with DCM, acetone and DCM/ EtOH (3:1) mixture. Yielding 12 mg (67%) of the target compound $(MePy^{+}O)_4$-SiPc-$(O_2C\text{-}Ar_2\text{-}CO_2H)_2$ $(CH_3SO_3^{-})_4$ **(15)** as a pure blue solid. ^{1}H-NMR (400 MHz, MeOD, 25 °C) δ = 9.98-9.77 (m, 4H), 9.65-9.47 (m, 4H), 9.32 (m, 4H), 8.94-8.80 (m, 4H), 8.71-8.54 (m, 4H), 8.48-8.16 (m, 8H), 7.82 (d, *J* = 8.4 Hz, 4H), 7.19 (d, *J* = 8.4 Hz, 4H), 6.72 (d, *J* = 8.4 Hz, 4H), 5.24 (d, *J* = 8.4 Hz, 4H), 4.60-4.49 (m, 12H), 2.70 (s, 12H). UV-Vis (MeOH) λ_{max}/nm (log ε): 356 (4.76), 614 (4.35), 679 (5.05).

3.2.14. Synthesis of $(MePy^{+}O)_4$-SiPc-$(O_2C\text{-}Ar\text{-}CH_3)_2$ $(CH_3SO_3^{-})_4$ (16).

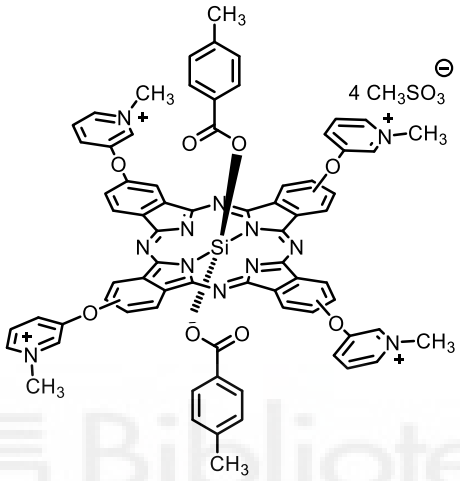

10 mg (0.006 mmol) of (MePy+O)$_4$-SiPc-(O_2C-Ar-$CH_3)_2$ $(I^{-})_4$ **(50)** and 4 mg (0.18 mmol) of $AgSO_3CH_3$ were dissolved in 10 mL of methanol. The reaction mixture was heated to 30 ºC and stirred for 2 hours. Then, the mixture was filtered to remove the silver. The filtrate was concentrated and washed sequentially with DCM, acetone and DCM/ EtOH (3:1) mixture. Yielding 7 mg (71%) of $(MePy^{+}O)_4$-SiPc-$(O_2C\text{-}Ar\text{-}CH_3)_2$ $(CH_3SO_3^{-})_4$ **(16)** as a blue solid. ^{1}H-NMR (400 MHz, MeOD, 25 °C) δ = 9.99-9.83 (m, 4H), 9.62-9.44 (m, 4H), 9.30-9.20 (m, 4H), 8.92-8.83 (m, 4H), 8.71-8.58 (m, 4H), 8.46-8.31 (m, 4H), 8.30-8.17 (m, 4H), 6.17 (d, *J* = 8.2 Hz, 4H), 4.98 (d, *J* = 8.2 Hz, 5H), 4.58-4.49 (m, 12H), 2.70 (s, 12H), 1.78 (s, 6H). UV-Vis (MeOH) λ_{max}/nm (log ε): 357 (4.49), 608 (4.09), 675 (4.83).

3.2.15. Preparation of SURMOFs: Zn-Pc 14 and Zn-Pc 15.

The Zn-SiPc SURMOF thin films were fabricated using a layer-by-layer spin coating approach. Briefly, a 1 mM ethanolic solution of zinc acetate and a 20 μM solution of SiPc linker (compounds **14** and **15**) in DMF were sequentially deposited onto pre-cleaned silicon substrates. Prior to deposition, the substrates were cleaned by Ar-H_2 plasma treatment for 30 minutes. After plasma activation, the substrates were rinsed with absolute ethanol and dried under a nitrogen stream.

The spin coating process was carried out using a spin coater in a layer-by-layer manner. Each metal and linker solution were applied for 10 seconds at a rotation speed of 2000 rpm. After each individual deposition step, the samples were rinsed with ethanol to remove unreacted species and by-products. A total of 60 deposition cycles were performed to build up the SURMOF structure with controlled thickness

General Conclusions and Future Perspectives

1. Conclusions.

In this work, the synthesis and complete characterization of sixteen silicon phthalocyanines with diverse axial and peripheral substituents was successfully accomplished. These compounds were rationally designed to modulate their electronic, optical, and solubility properties, aiming at three main application fields: SURMOFs whit optoelectronic devices, the development of novel SURMOF architectures and bactericide and water soluble SURMOFs.

All synthesized molecules were thoroughly characterized by ^{1}H-NMR spectroscopy, UV-Vis spectroscopy, high-resolution MALDI-TOF mass spectrometry, and, when applicable, electrochemical measurements. For pyridinium salt derivatives, additional 2D COSY experiments were carried out to assist in the assignment of complex proton signals and confirm the expected structures.

These SiPcs were evaluated as potential linkers for SURMOFs. Compounds such as $(ArS)_4$-SiPc-$(O_2C$-Ar-$CO_2H)_2$ **(3)**, SiPc-(O-Ar-Azo-Ar-$CO_2H)_2$ **(11)**, and the mixed-ligand system SiPc **13** + **SiPc-$(CO_2H)_2$** yielded crystalline, well-ordered SURMOF structures, as confirmed by *out-of-plane* XRD and complementary techniques including UV-Vis and FT-IRRAS spectroscopy.

Of particular interest is the mixed-ligand SURMOF composed of SiPc **13** + **SiPc-$(CO_2H)_2$**, which represents, to the best of our knowledge, the first reported SURMOF incorporating two distinct silicon phthalocyanine linkers.

Furthermore, specific electronic trends were identified: $(Cl_2ArO)_4$-SiPc-$(O_2C$-Ar-$CH_2)_2$ **(8)** exhibited the highest electron-accepting character, while $(ArS)_8$-SiPc-$(O_2C$-Ar-$CH_3)_2$ **(10)** showed the strongest electron-donating behavior, in agreement with UV-Vis and electrochemical results. These findings validate the donor-acceptor design approach employed.

Overall, the systematic variation of substituents has demonstrated the versatility of the synthetic strategy, providing a robust platform for tailoring the properties of SiPcs for advanced functional materials.

2.Future Perspectives

Future research should focus on:

Extending SURMOF screening to structurally similar but unexplored derivatives, such as SiPc **1**, SiPc **2**, SiPc **4**, SiPc **12**, SiPc **14** and Zn-SiPc **15** to confirm their ability to form ordered frameworks.

Elucidating the structure of the mixed-ligand SURMOF based on SiPc **13** + **SiPc-$(CO_2H)_2$** through advanced characterization techniques

Exploring photoresponsive behavior in azo-containing SURMOFs under controlled irradiation, for Zn-SiPc **11** and Zn-SiPc **12** with the goal of developing light-switchable materials.

Integrating selected SURMOFs into functional devices, such as photodetectors or sensors, to evaluate their real-world optoelectronic performance.

Studying stability and processability in aqueous and physiological media for potential biomedical or environmental applications for Zn-SiPc **14** and Zn-SiPc **15**

By pursuing these directions, the foundation laid in this work can lead to new generations of multifunctional, tunable, and application-oriented phthalocyanine-based SURMOFs.

ANNEX 1

^{1}H-NMR of 4-(2,6-dimethylphenoxy)phthalonitrile(17).[174]

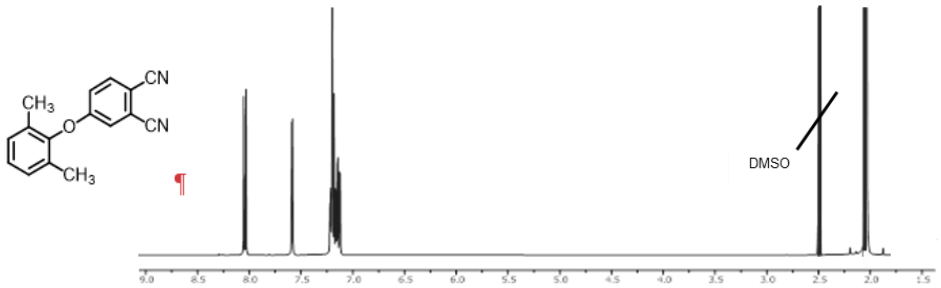

Figure 1. *^{1}H-NMR spectra of 4-(2,6-dimethylphenoxy)phthalonitrile* ***(17)***[174] *in DMSO-d_6.*

^{1}H- NMR of 5-(2,6-dimethylphenoxy)-1,3-diiminoisoindoline(18).

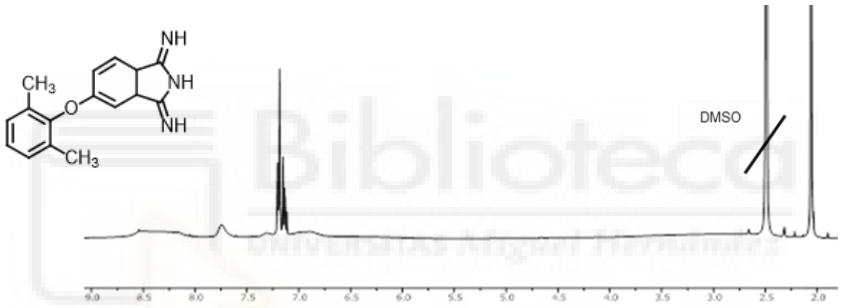

Figure 2. *^{1}H-NMR spectra of 5-(2,6-dimethylphenoxy)-1,3-diiminoisoindoline* ***(18)*** *in DMSO-d_6.*

UV-Vis of $(ArO)_4$-$SiPcCl_2$ (19).

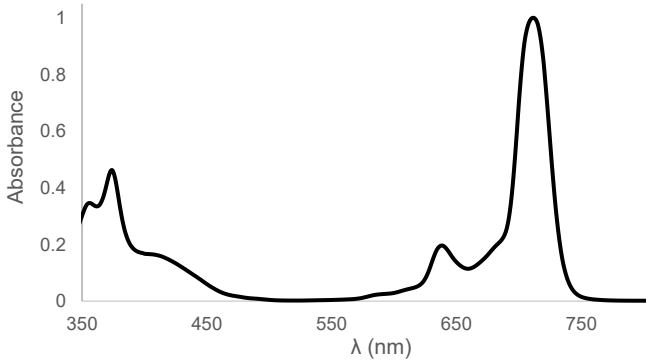

Figure 3. *UV-Vis spectra of $(ArO)_4$-$SiPcCl_2$.*

HR-MALDI TOF, UV-Vis and ^{1}H- NMR $(ArO)_4$-SiPc-$(O_2C$-Ar-$CHO)_2$ (21).

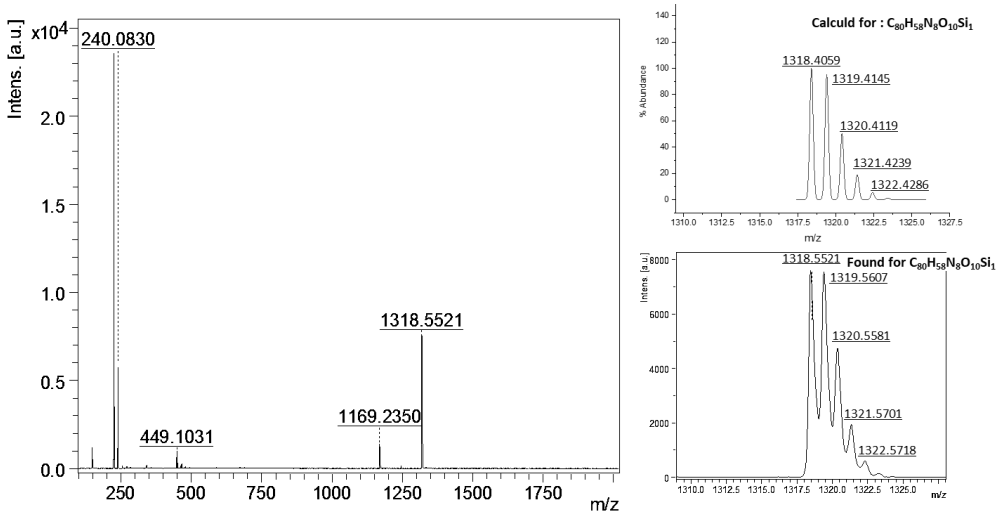

Figure 4. *HR-MALDI TOF mass spectrum (negative mode) $(ArO)_4$-SiPc-$(O_2C$-Ar-$CHO)_2$* ***(21)****.*

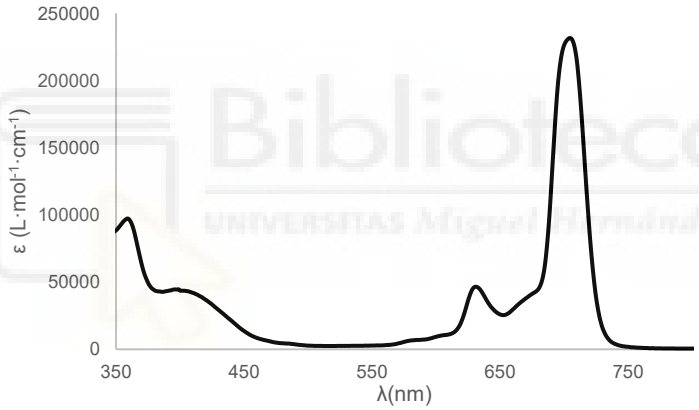

Figure 5. *UV-Vis spectrum of $(ArO)_4$-SiPc-$(O_2C$-Ar-$CHO)_2$* ***(21)*** *in $CHCl_3$.*

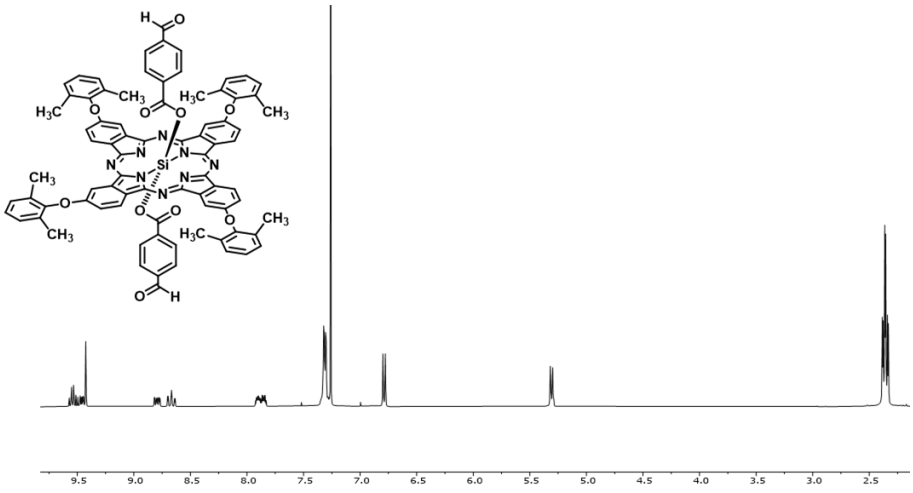

Figure 6. *^{1}H-NMR spectra of $(ArO)_4$-SiPc-$(O_2C$-Ar-$CHO)_2$* ***(21)*** *in, $CDCl_3$.*

HR-MALDI TOF, UV-Vis and ^{1}H- NMR $(ArO)_4$-SiPc-$(O_2C$-Ar_2-$CHO)_2$ (22).

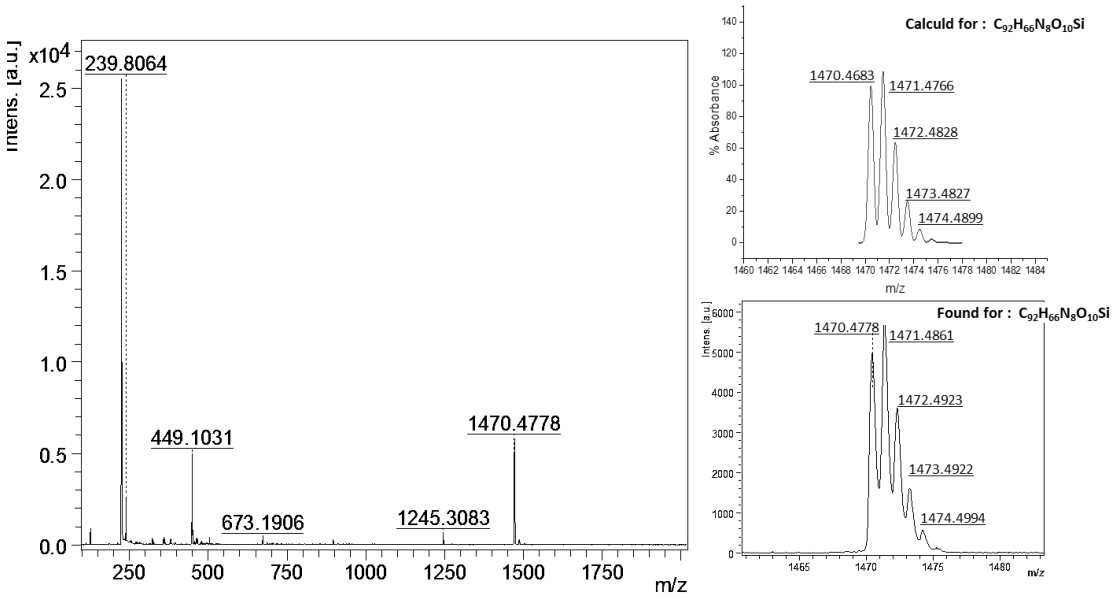

Figure 7. *HR-MALDI TOF mass spectrum (negative mode) $(ArO)_4$-SiPc-$(O_2C$-Ar_2-$CHO)_2$* ***(22)****.*

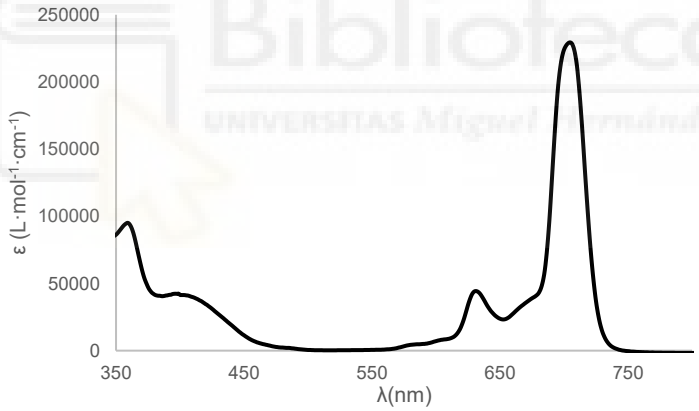

Figure 8. *UV-Vis spectrum of $(ArO)_4$-SiPc-$(O_2C$-Ar_2-$CHO)_2$* ***(22)*** *in $CHCl_3$.*

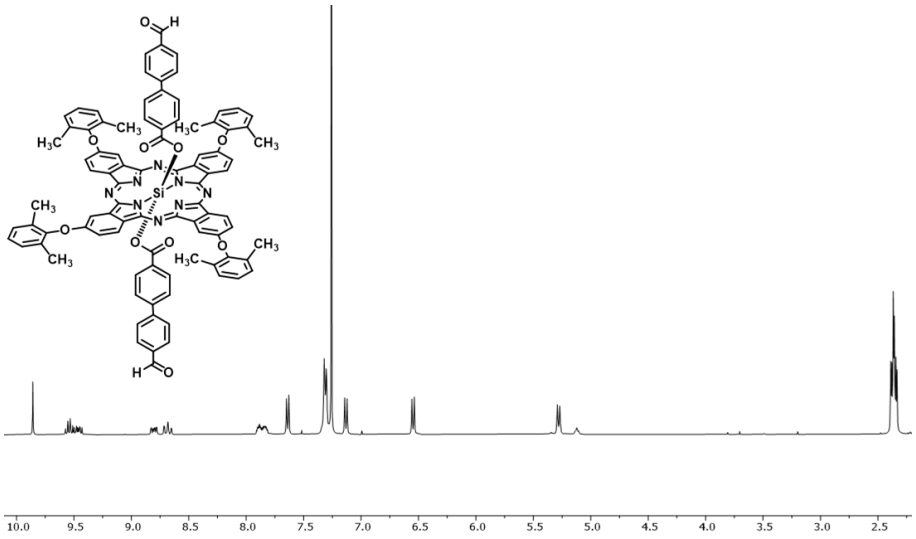

Figure 9. *^{1}H-NMR spectra of $(ArO)_4$-SiPc-$(O_2C$-Ar_2-$CHO)_2$* ***(22)*** *in$CDCl_3$.*

HR-MALDI TOF and UV-Vis of $(ArO)_4$-SiPc-$(O_2C$-Ar-$CO_2H)_2$ (1)

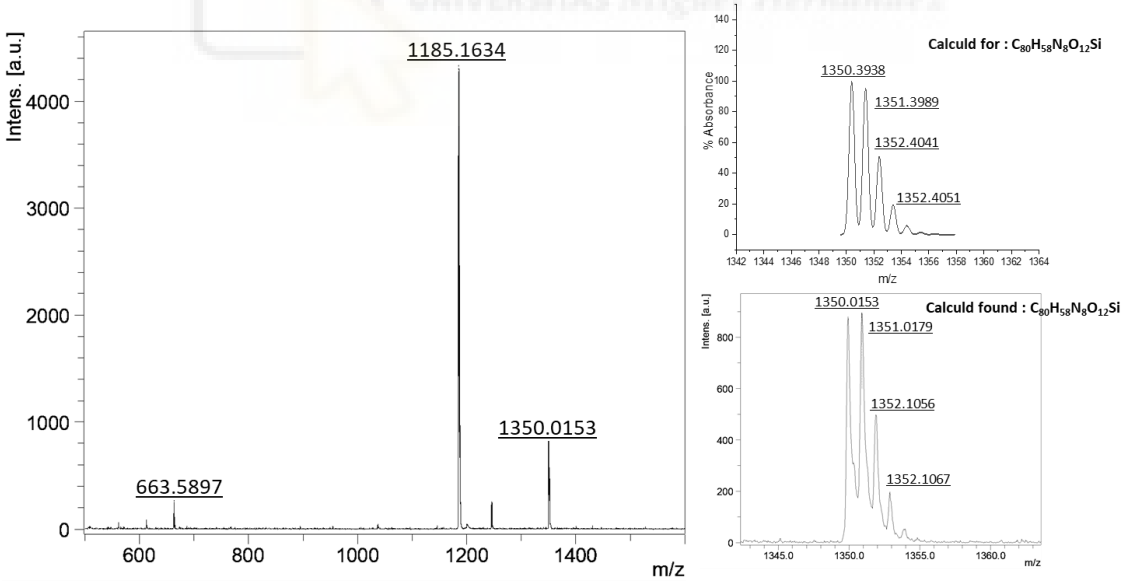

Figure 10. *HR-MALDI TOF Mass Spectrum (negative mode) of $(ArO)_4$-SiPc-$(O_2C$-Ar-$CO_2H)_2$* ***(1)***.

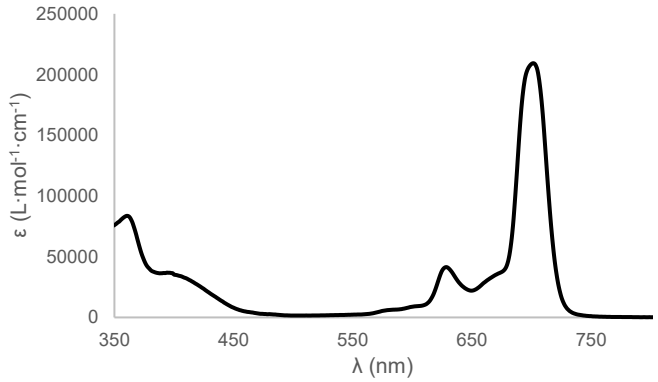

Figure 11. *UV-Vis spectrum of $(ArO)_4$-SiPc-$(O_2C$-Ar-$CO_2H)_2$* ***(1)*** *in $CHCl_3$.*

HR-MALDI TOF and UV-Vis of $(ArO)_4$-SiPc-$(O_2C$-Ar_2-$CO_2H)_2$ (5).

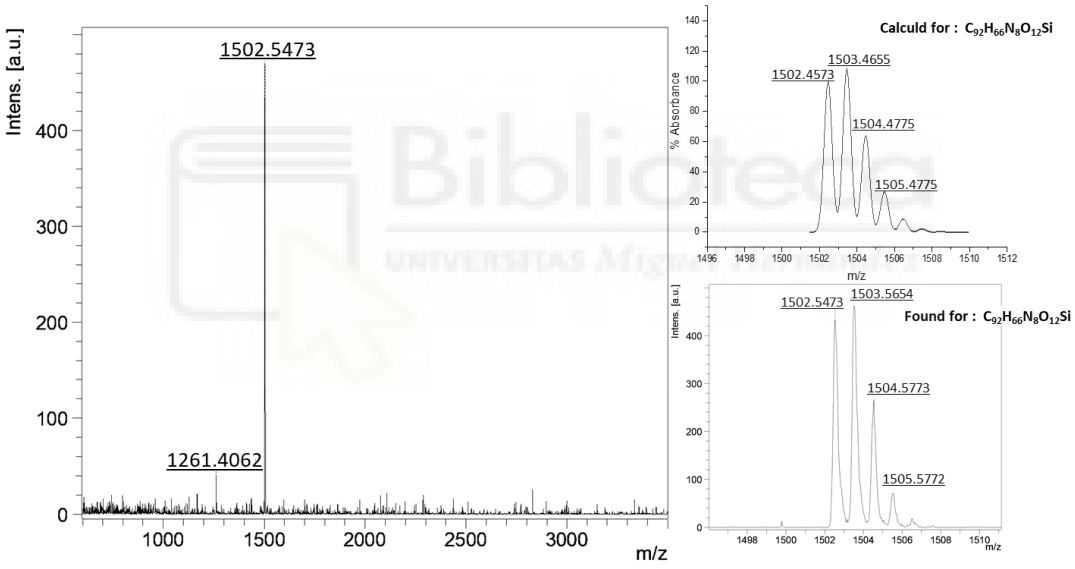

Figure 12. *HR-MALDI TOF Mass Spectrum (negative mode) of $(ArO)_4$-SiPc-$(O_2C$-Ar_2-$CO_2H)_2$* ***(5)****.*

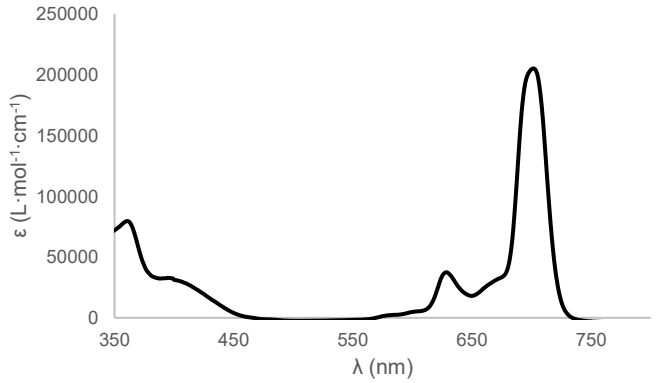

Figure 13. *UV-Vis spectrum of $(ArO)_4$-SiPc-$(O_2C$-Ar_2-$CO_2H)_2$* ***(5)*** *in $CHCl_3$.*

HR-MALDI TOF and ^{1}H-NMR integral spectral of $(ArO)_4$-SiPc-(O_2C-Ar-$CH_3)_2$ (7).

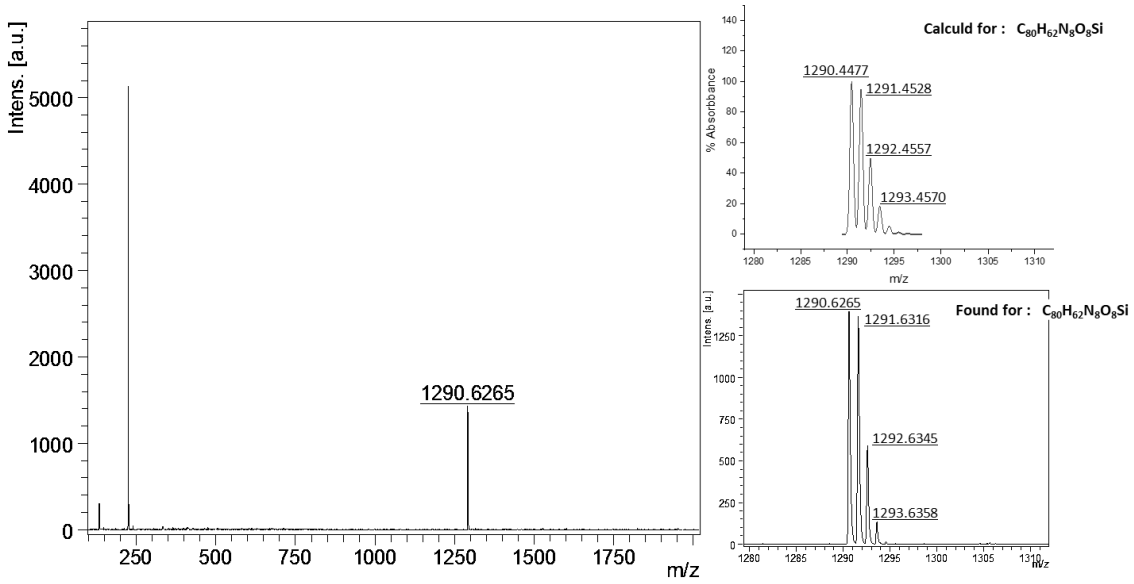

Figure 14. *HR-MALDI TOF mass spectrum (negative mode) of (ArO)$_4$-SiPc-(O_2C-Ar-$CH_3)_2$ **(7)**.*

^{1}H NMR (400 MHz, $CDCl_3$) δ 9.56 – 9.37 (m, 4H), 8.82 – 8.61 (m, 4H), 7.91 – 7.68 (m, 4H), 7.37 – 7.29 (m, 12H), 6.06 (d, J = 8.0 Hz 4H), 5.05 (d, J = 8.0 Hz, 4H), 2.45 – 2.31 (m, 24H), 1.72 (s, 6H).

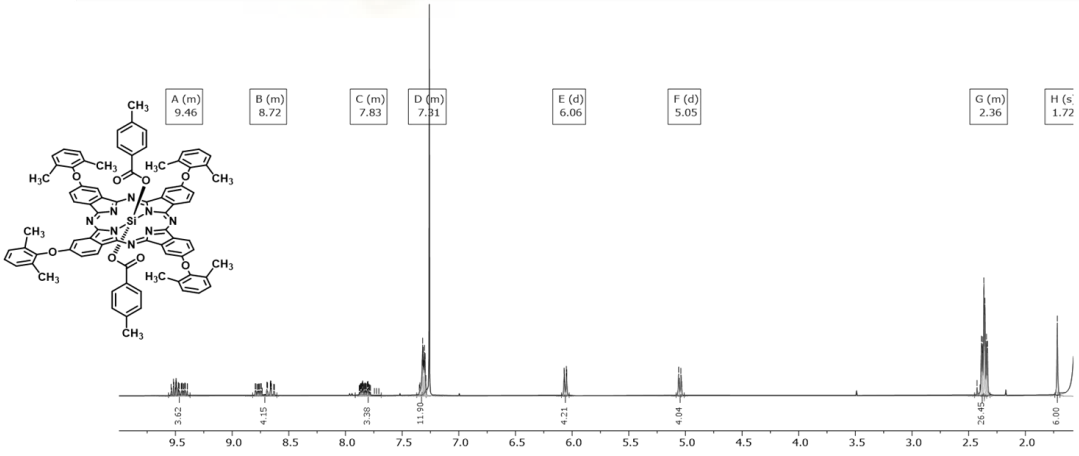

Figure 15. *^{1}H-NMR spectra of (ArO)4-SiPc-(O_2C-Ar-$CH_3)_2$ **(7)** in$CDCl_3$.*

^{1}H-NMR of 4-(2,6-dichlorophenoxy)phthalonitrile (23).

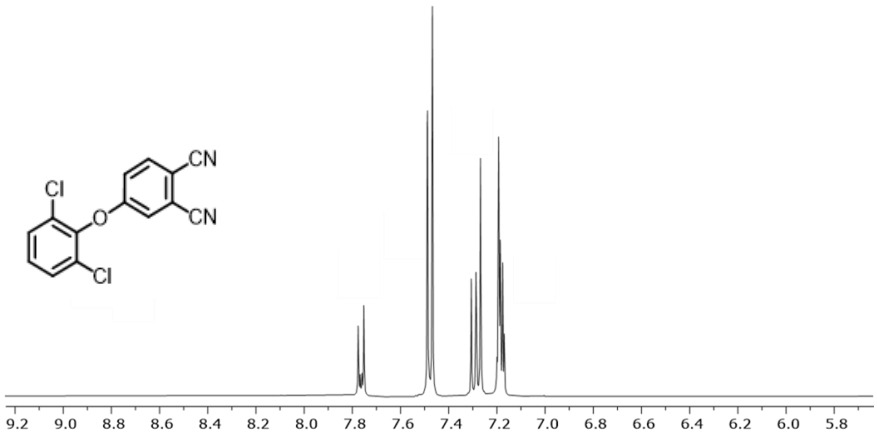

Figure 16. *Spectra of 4-(2,6-dichlorophenoxy)phthalonitrile* ***(23)*** *in $CDCl_3$.*

^{1}H-NMR of 5-(2,6-dichlorophenoxy)-diiminoisoindoline (24).

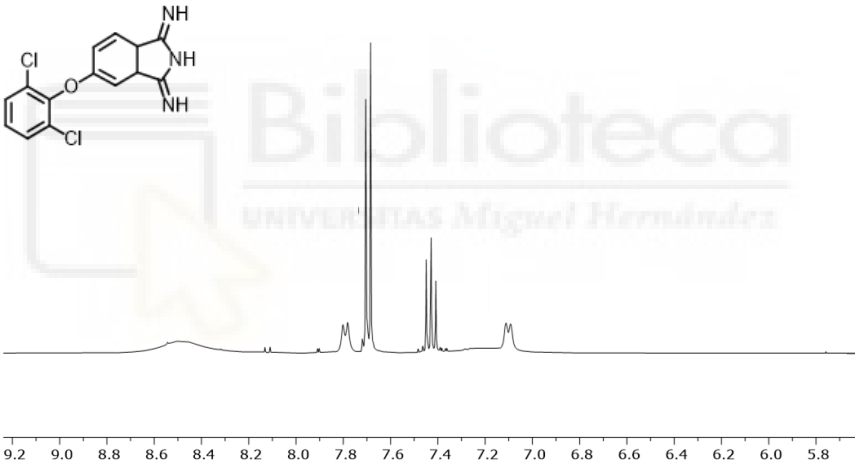

Figure 17. *Spectra of 6-(2,6-dichlorophenoxy)-diiminoisoindoline****(24)*** *in DMSO-d_6.*

UV-Vis of $(Cl_2ArO_2)_4$-$SiPcCl_2$ (25).

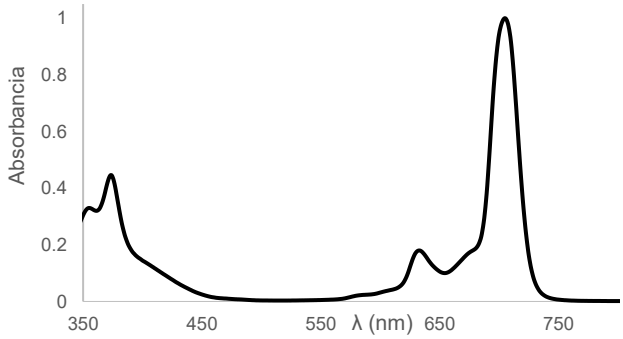

Figure 18. *UV-Vis spectrum of $(Cl_2ArO_2)_4$-$SiPcCl_2$* ***(25)*** *in $CHCl_3$.*

HR-MALDI TOF, UV-Vis and ^{1}H- NMR of $(Cl_2ArO)_4$-SiPc-$(O_2C$-Ar-CHO$)_2$ (26).

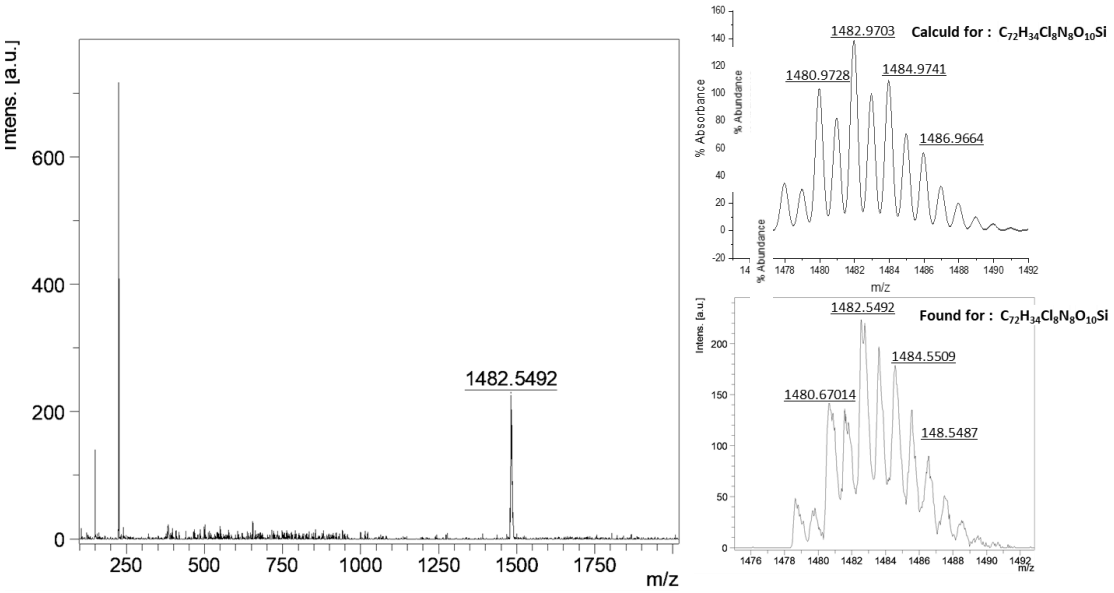

Figure 19. *HR-MALDI TOF Mass Spectrum (negative mode) of $(Cl_2ArO)_4$-SiPc-$(O_2C$-Ar-CHO$)_2$* ***(26)****.*

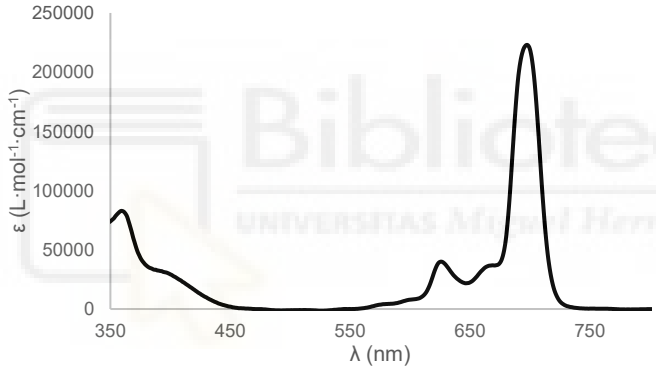

Figure 20. *UV-Vis spectrum of $(Cl_2ArO)_4$-SiPc-$(O_2C$-Ar-CHO$)_2$* ***(26)*** *in $CHCl_3$.*

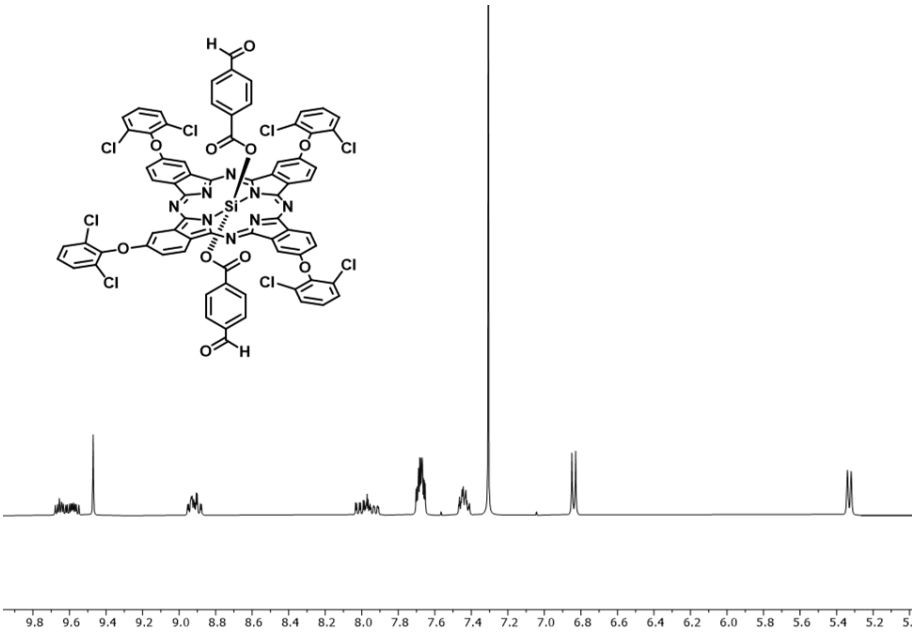

Figure 21. *^{1}H-NMR Spectra of $(Cl_2ArO)_4$-SiPc-$(O_2C$-Ar-CHO$)_2$* ***(26)*** *in $CDCl_3$.*

HR-MALDI TOF, UV-Vis and ^{1}H- NMR of $(Cl_2ArO)_4$-SiPc-$(O_2C$-Ar$_2$-CHO$)_2$ (27).

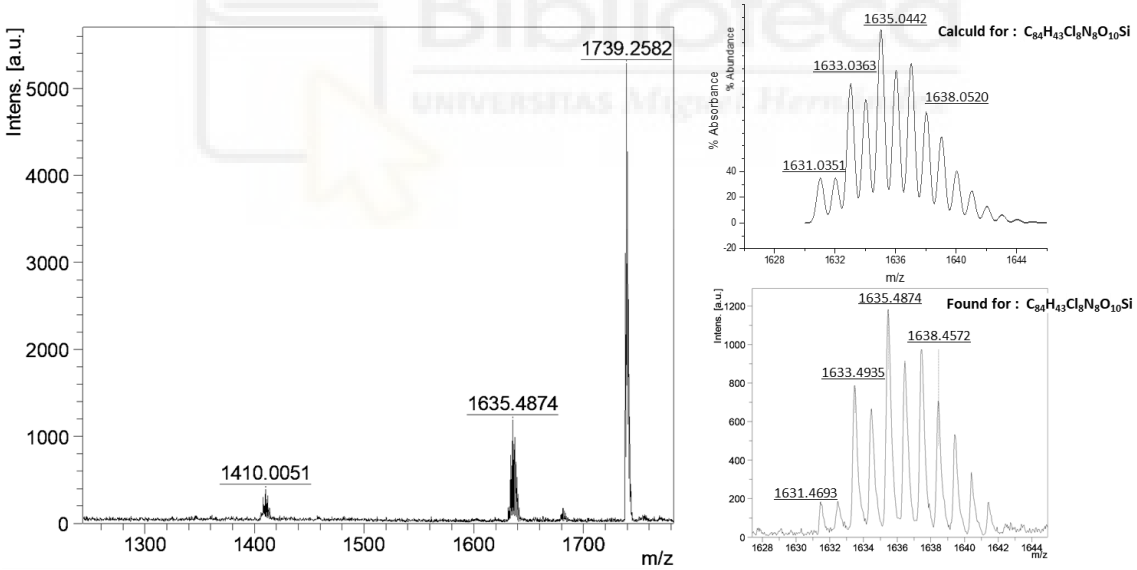

Figure 22. *HR-MALDI TOF Mass Spectrum (negative mode) of $(Cl_2ArO)_4$-SiPc-$(O_2C$-Ar$_2$-CHO$)_2$* ***(27)***.

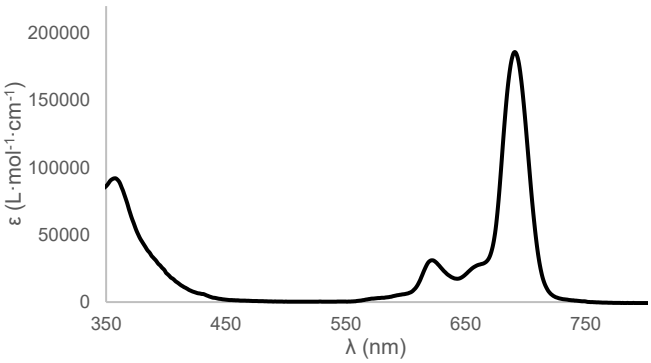

Figure 23. *UV-Vis spectrum of $(Cl_2ArO)_4$-SiPc-$(O_2C$-Ar_2-$CHO)_2$* ***(27)*** *in $CHCl_3$.*

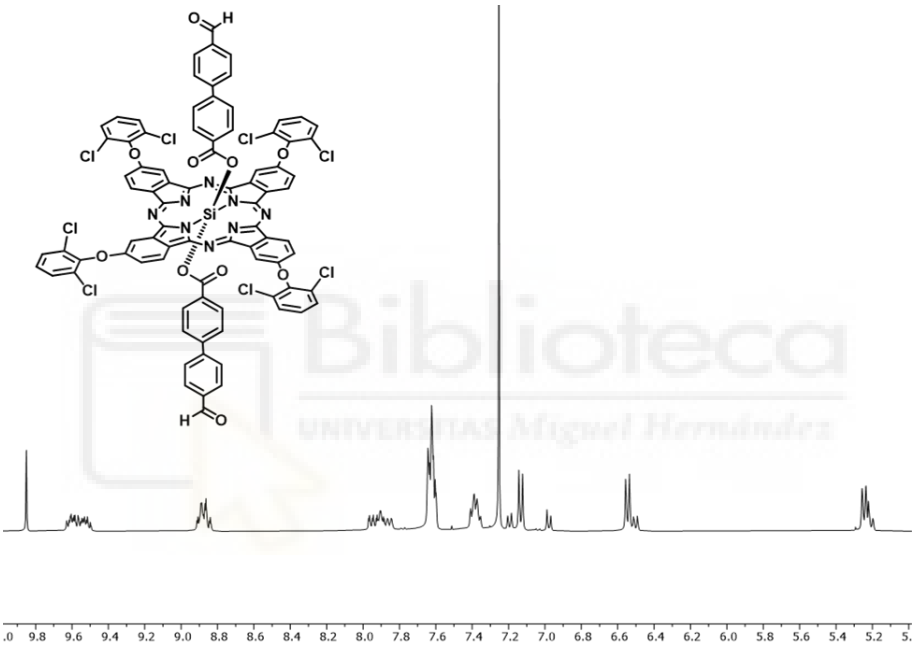

Figure 24. *^{1}H-NMR Spectra of $(Cl_2ArO)_4$-SiPc-$(O_2C$-Ar_2-$CHO)_2$* ***(27)*** *in $CDCl_3$.*

HR-MALDI TOF and UV-Vis of $(Cl_2ArO)_4$-SiPc-$(O_2C$-Ar-$CO_2H)_2$ (2).

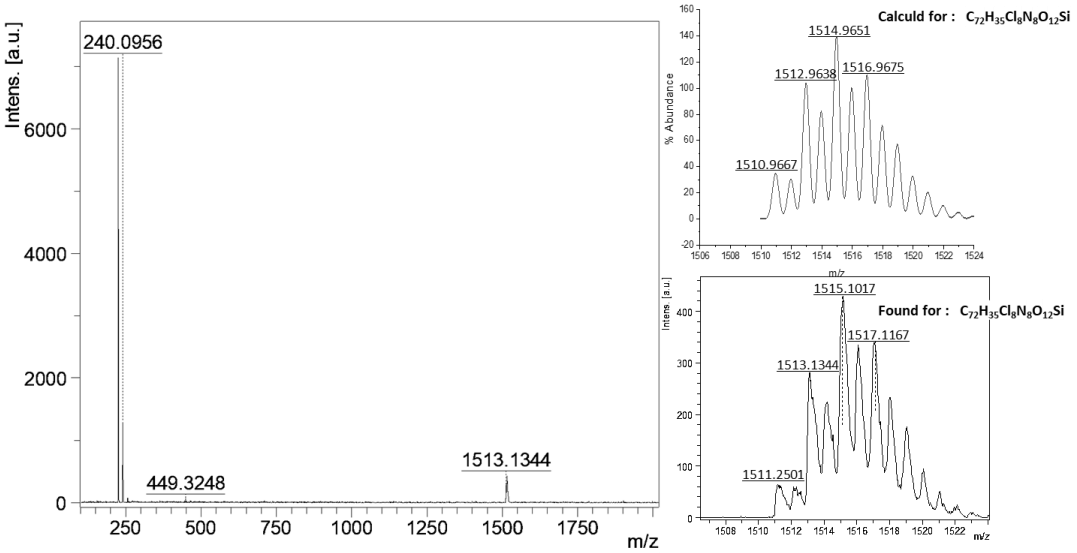

Figure 25. *HR-MALDI TOF mass spectrum (positive mode) of $(Cl_2ArO)_4$-SiPc-$(O_2C$-Ar-$CO_2H)_2$* ***(2)****.*

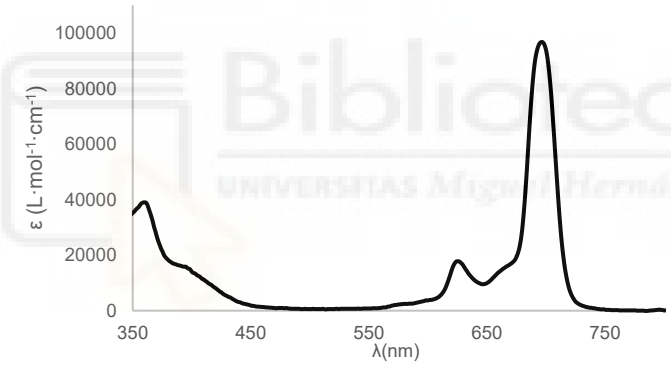

Figure 26. *UV-Vis spectrum of $(Cl_2ArO)_4$-SiPc-$(O_2C$-Ar-$CO_2H)_2$* ***(2)*** *in $CHCl_3$.*

HR-MALDI TOF and UV-Vis of $(Cl_2ArO)_4$-SiPc-$(O_2C\text{-}Ar_2\text{-}CO_2H)_2$ (6).

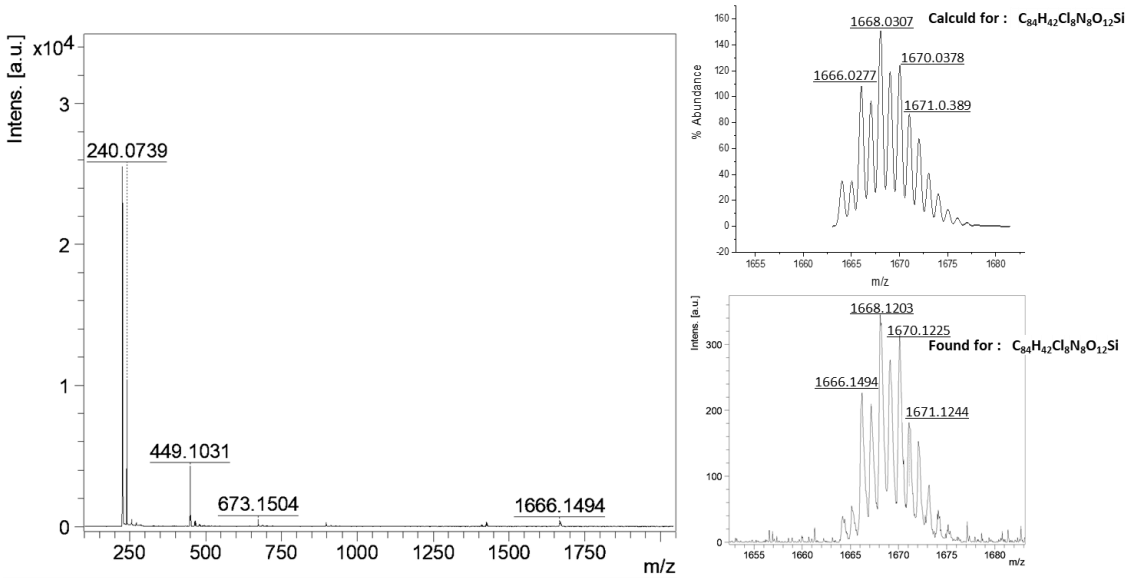

Figure 27. *HR-MALDI TOF mass spectrum (positive mode) of $(Cl_2ArO)_4$-SiPc-$(O_2C\text{-}Ar_2\text{-}CO_2H)_2$* ***(6)****.*

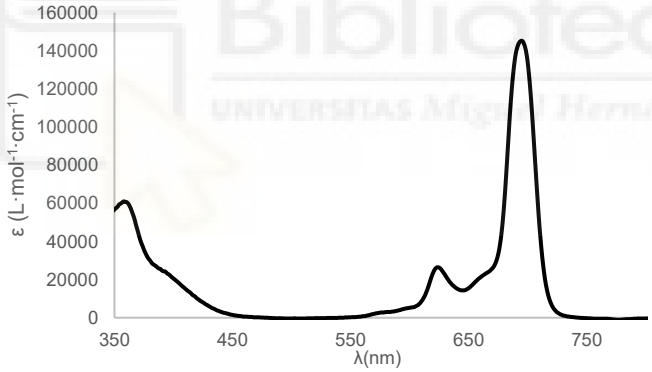

Figure 28. *UV-Vis spectrum of $(Cl_2ArO)_4$-SiPc-$(O_2C\text{-}Ar_2\text{-}CO_2H)_2$* ***(6)*** *in $CHCl_3$.*

HR-MALDI TOF and ^{1}H-NMR integral spectral $(Cl_2ArO)_4$-SiPc-(O_2C-Ar-$CH_3)_2$ (8).

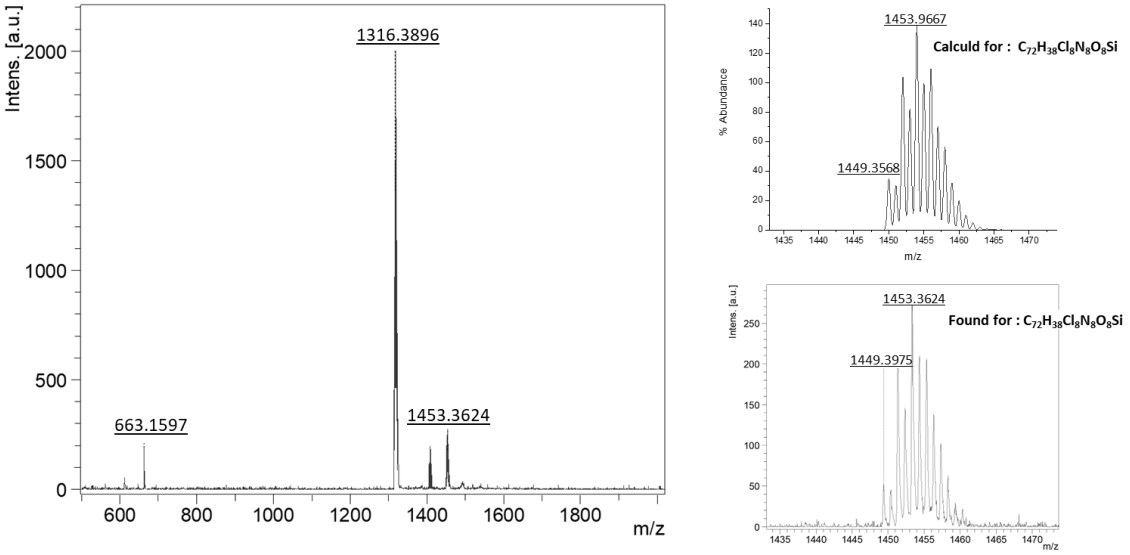

Figure 29. *HR-MALDI TOF Mass Spectrum (negative mode) of $(Cl_2ArO)_4$-SiPc-(O_2C-Ar_2-$CH_3)_2$* ***(8)****.*

^{1}H NMR (400 MHz, $CDCl_3$) δ 9.63 – 9.45 (m, 4H), 8.91 – 8.79 (m, 4H), 7.97 – 7.80 (m, 4H), 7.67 – 7.58 (m, 8H), 7.43 – 7.31 (m, 4H), 6.06 (d, J = 8.1 Hz, 4H), 5.02 (d, J = 8.0 Hz, 4H), 1.72 (s, 6H).

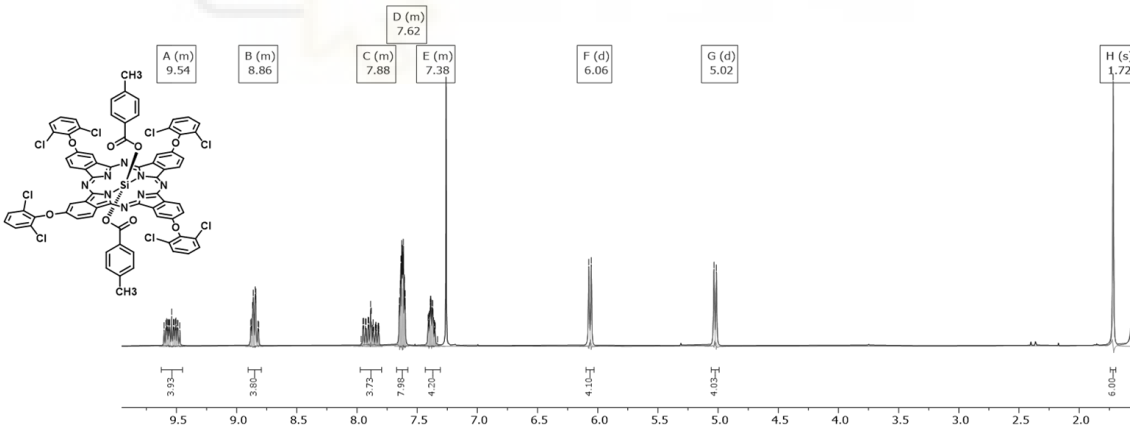

Figure 30. *^{1}H-NMR spectra of (Cl_2ArO)4-SiPc-(O_2C-Ar-$CH_3)_2$* ***(8)*** *in $CDCl_3$.*

^{1}H-NMR of 4-(*p*-tolylthio)phthalonitrile (28).

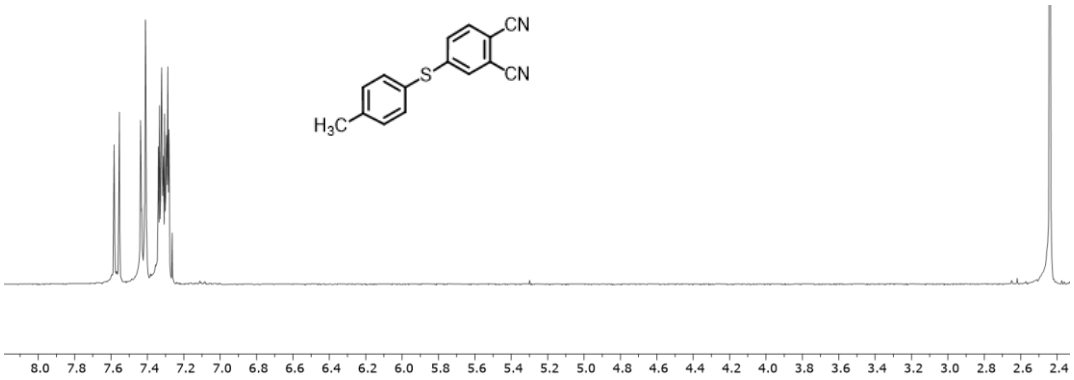

Figure 31. *Spectra of 4-(p-tolylthio)phthalonitrile* ***(28)*** *in* $CDCl_3$.

^{1}H-NMR of 5-(*p*-tolylthio)isoindoline-1,3-diimine (29).

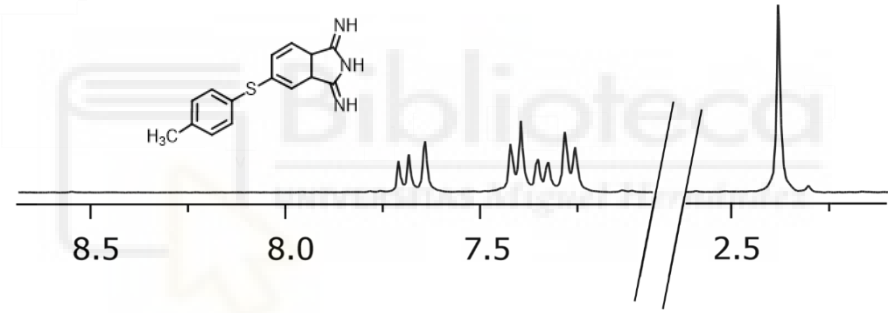

Figure 32. *Spectra of 5-(p-tolylthio)isoindoline-1,3-diimine* ***(29)*** *in* CD_3OD.

UV-Vis of $(ArS)_4$-$SiPcCl_2$ (30).

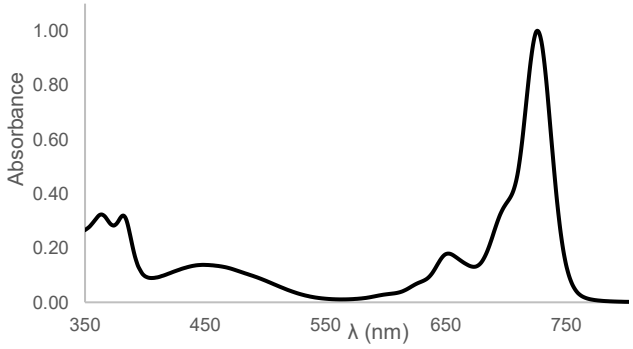

Figure 33. *UV-Vis spectra* $(ArS)_4$-$SiPcCl_2$ ***(30)***.

^{1}H-NMR of 4,5-bis(*p*-tolylthio)phthalonitrile (31).

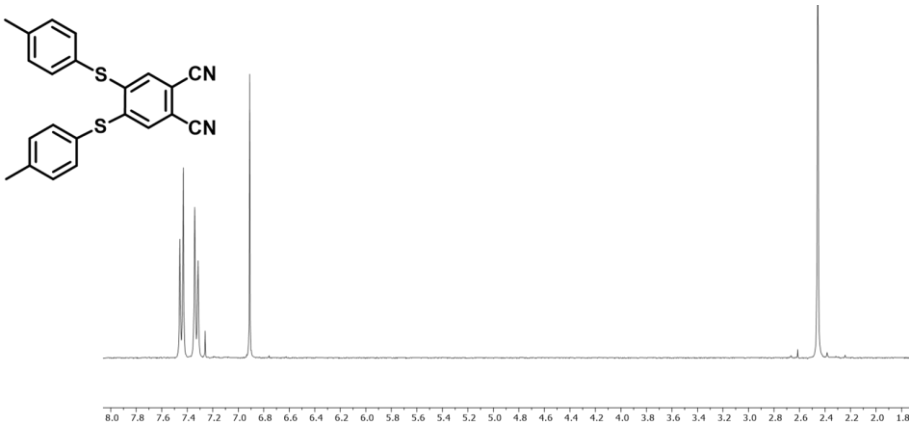

Figure 34. *Spectra of 4-(p-tolylthio)phthalonitrile* ***(31)*** *in* $CDCl_3$.

^{1}H-NMR of 5,6-bis(*p*-tolylthio)-1,3-diiminoisoindoline (32).

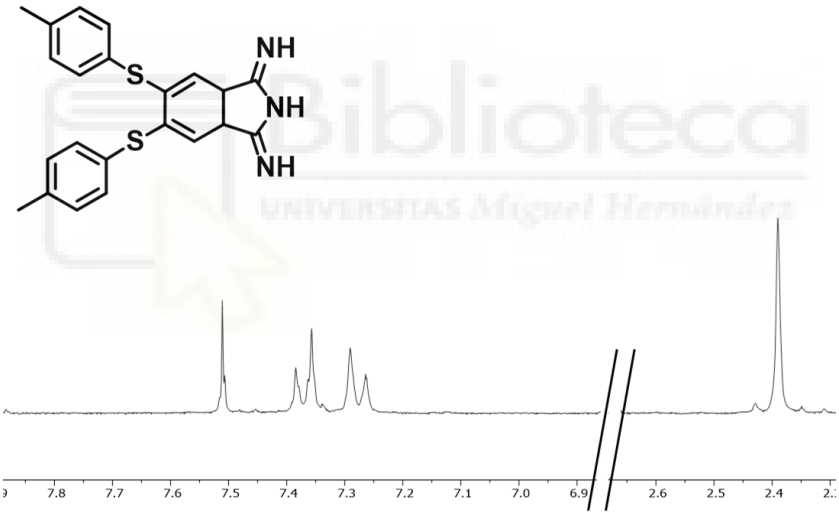

Figure 35. *Spectra of 5,6-bis(p-tolylthio)-1,3-diiminoisoindoline****(32)*** *in* CD_3OD.

UV-Vis spectra of $(ArS)_8$-$SiPcCl_2$ (33).

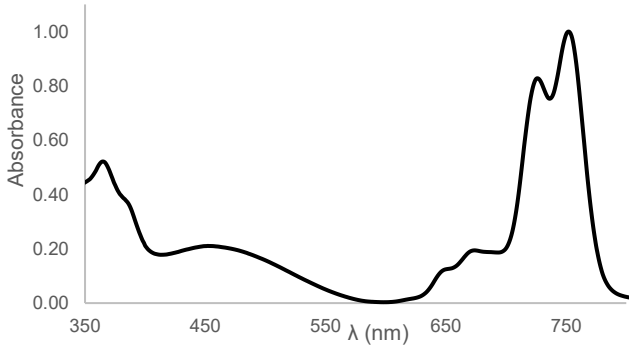

Figure 36. *UV-Vis spectra of* $(ArS)_8$-$SiPcCl_2$ ***(33)*** *in* $CHCl_3$.

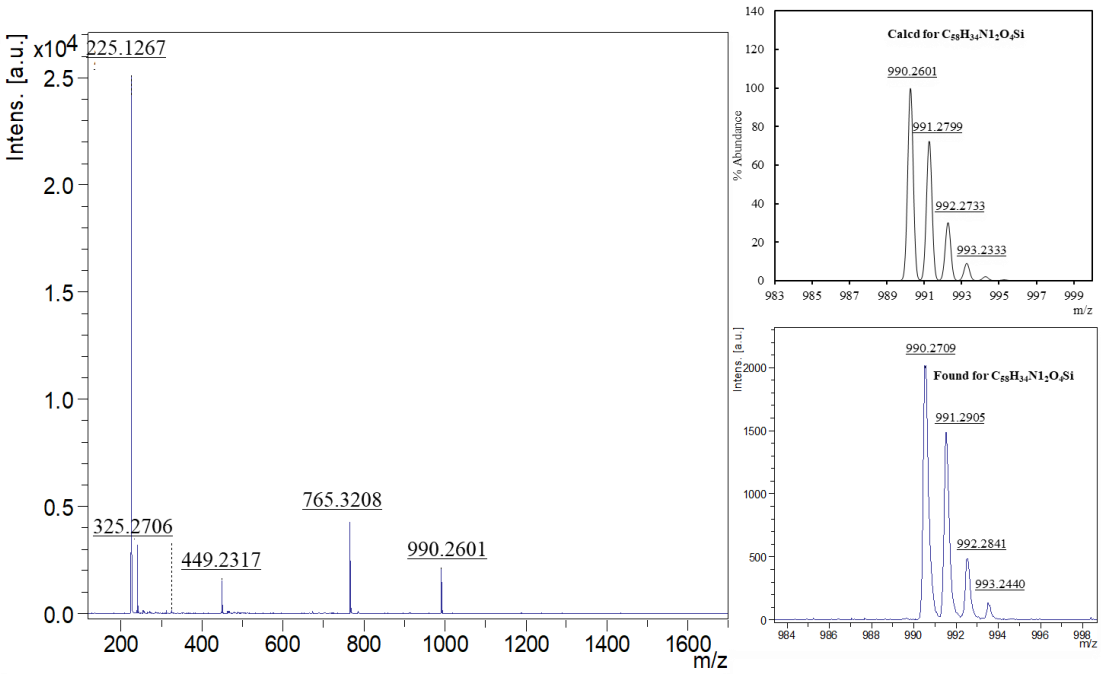

Figure 37**. HR-MALDI TOF mass spectrum (negative mode) of SiPc-(O-Ar-Azo-Ar-CHO)$_2$ **(36)

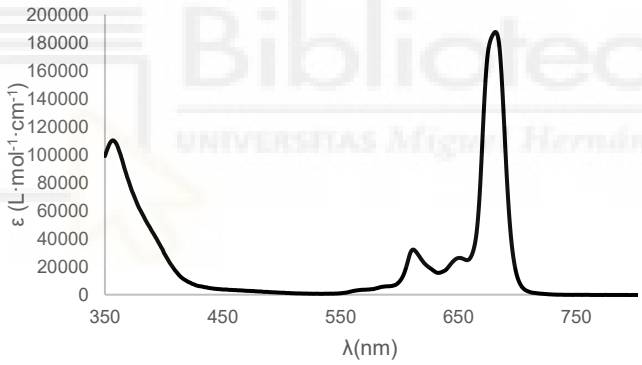

***Figure 38**. UV-Vis spectrum of SiPc-(O-Ar-Azo-Ar-CHO)$_2$ **(36)** in THF.*

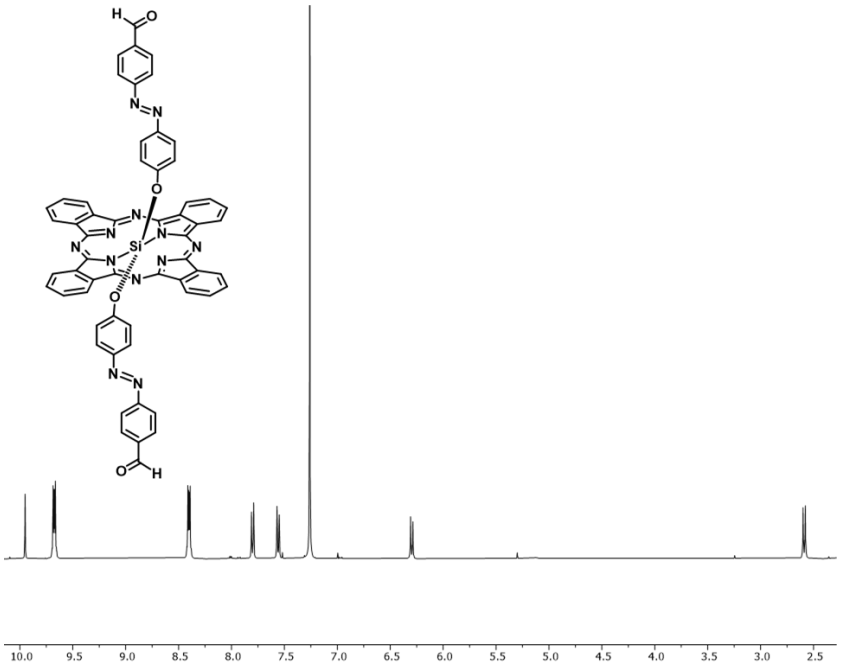

***Figure 39**. [1]H-NMR Spectrum of SiPc-(O-Ar-Azo-Ar-CHO)$_2$ **(36)** in CDCl$_3$.*

HR-MALDI TOF and H-RMN integral spectra of SiPc-(O-Ar-Azo-Ar-CO$_2$H)$_2$ (11).

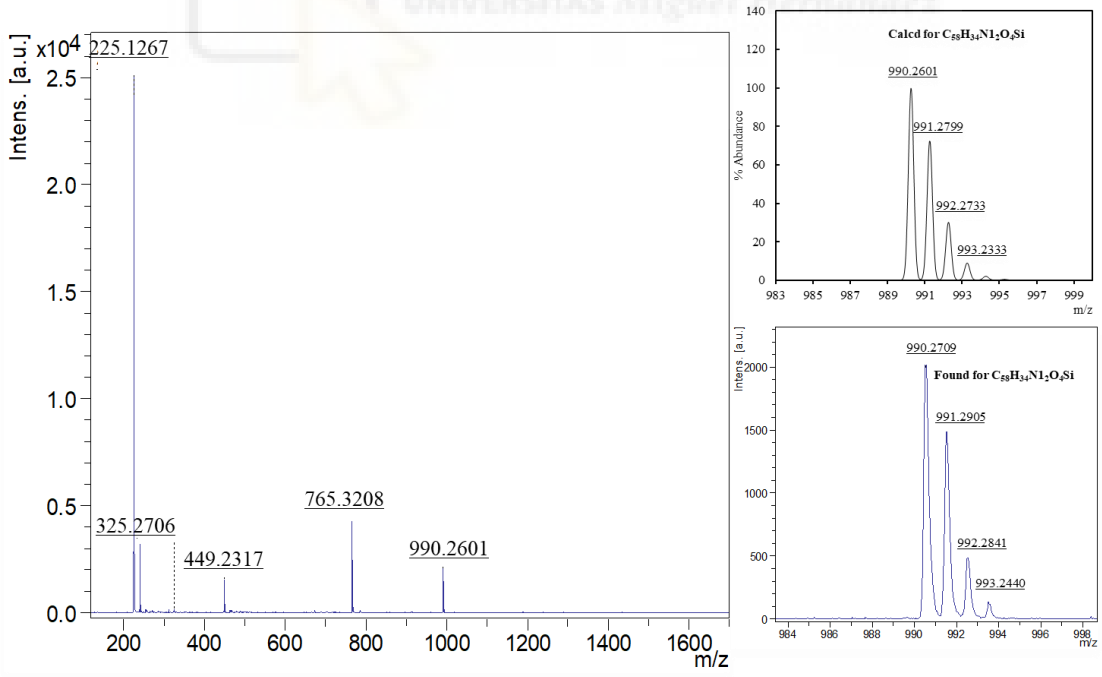

***Figure 40**. HR-MALDI TOF mass spectrum (negative mode) of SiPc-(O-Ar-Azo-Ar-CO$_2$H)$_2$ **(11)**.*

^{1}H NMR (400 MHz, DMSO) δ 9.77 – 9.70 (m, 8H), 8.61 – 8.54 (m, 8H), 7.86 (d, J = 8.5 Hz, 4H), 7.44 (d, J = 8.1 Hz, 4H), 6.25 (d, J = 8.6 Hz, 4H), 2.67 (d, J = 1.8 Hz, 5H).

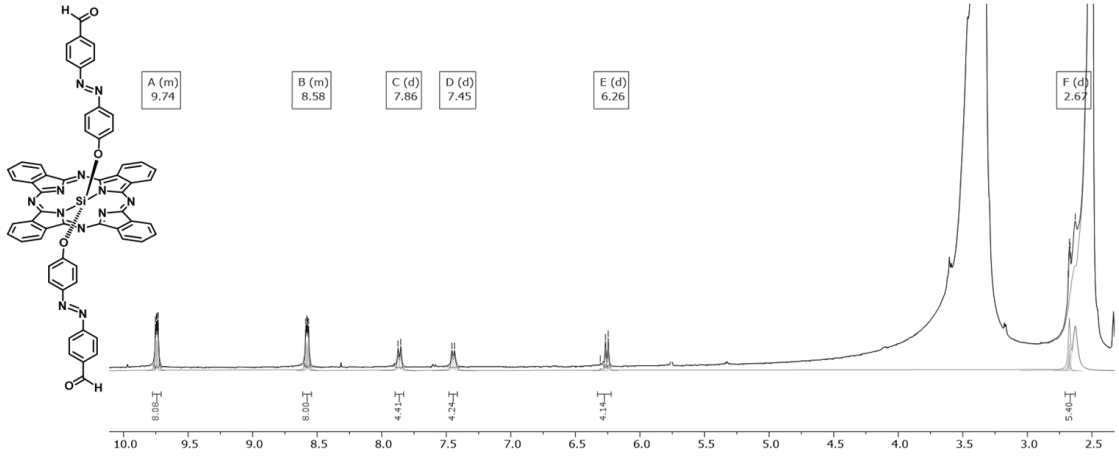

Figure 41. *^{1}H-NMR spectra of SiPc-(O-Ar-Azo-Ar-CO_2H)$_2$* ***(11)*** *InCDCl$_3$.*

HR-MALDI TOF, UV-Vis and ^{1}H- NMR of (^{t}Bu)$_4$SiPc -(O-Ar-Azo-Ar-CHO)$_2$ (39).

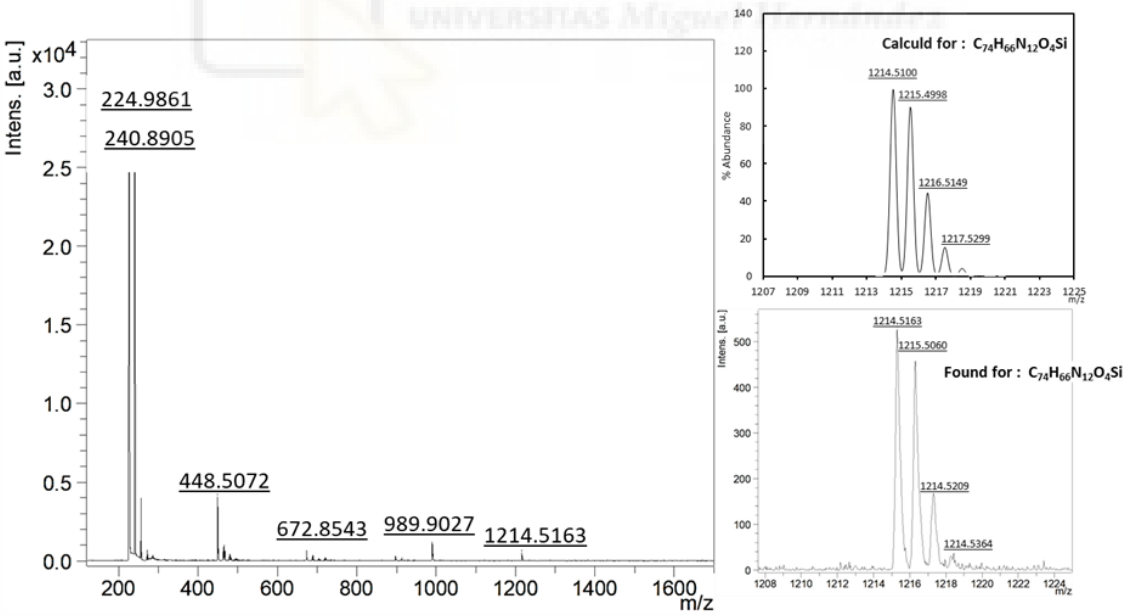

Figure 52*. HR-MALDI TOF mass spectrum (negative mode) of* ***(^{t}Bu)$_4$SiPc -(O-Ar-Azo-Ar-CHO)$_2$ (39)****.*

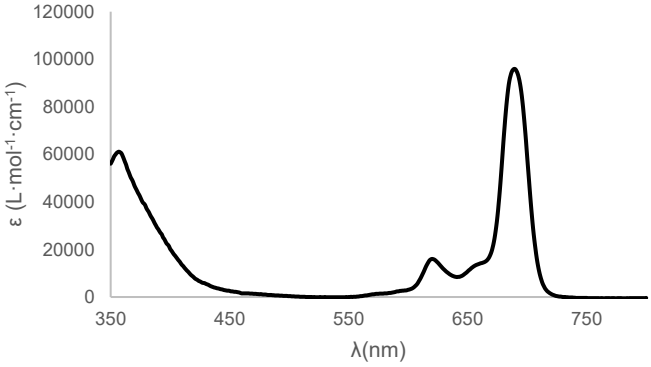

***Figure 43**. UV-Vis spectrum of (^{t}Bu)$_4$SiPc -(O-Ar-Azo-Ar-CHO)$_2$ **(39)** in $CHCl_3$.*

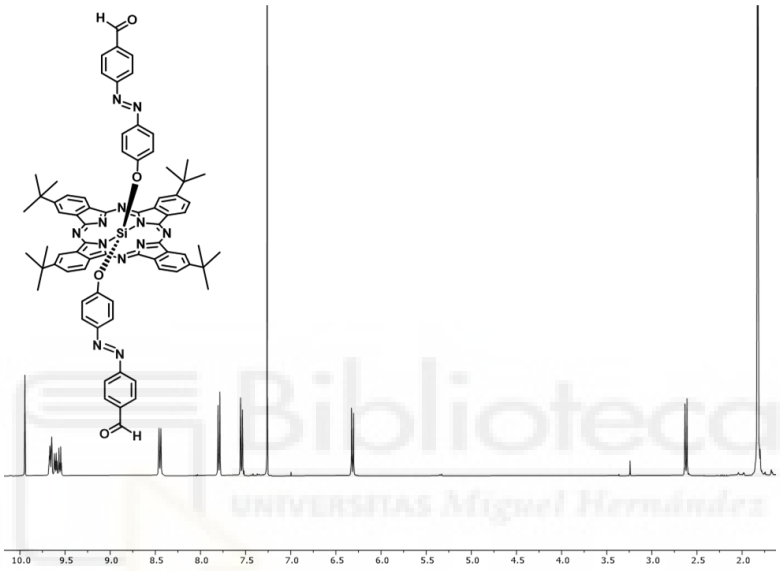

***Figure 44**. ^{1}H-NMR Spectra of (^{t}Bu)$_4$SiPc -(O-Ar-Azo-Ar-CHO)$_2$ **(39)** in DMSO-d_6.*

HR-MALDI TOF and H-RMN integral spectra of (^{t}Bu)$_4$SiPc-(O-Ar-Azo-Ar-$CO_2H)_2$(12)

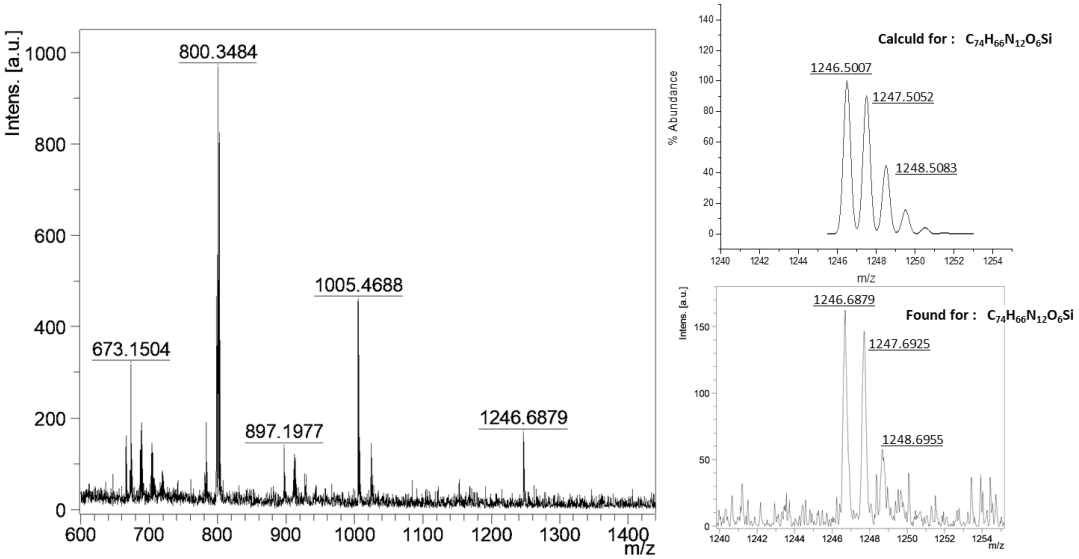

***Figure 45**. HR-MALDI TOF mass spectrum (negative mode) of (^{t}Bu)$_4$SiPc-(O-Ar-Azo-Ar-$CO_2H)_2$ **(12)**.*

^{1}H NMR (400 MHz, $CDCl_3$) δ 9.69 – 9.49 (m, 8H), 8.50 – 8.43 (m, 4H), 7.98 (d, *J* = 8.2 Hz, 4H), 7.49 (d, *J* = 8.6 Hz, 4H), 6.32 (d, *J* = 8.1 Hz, 4H), 2.64 (d, *J* = 8.5 Hz, 4H), 1.85 (s, 40H).

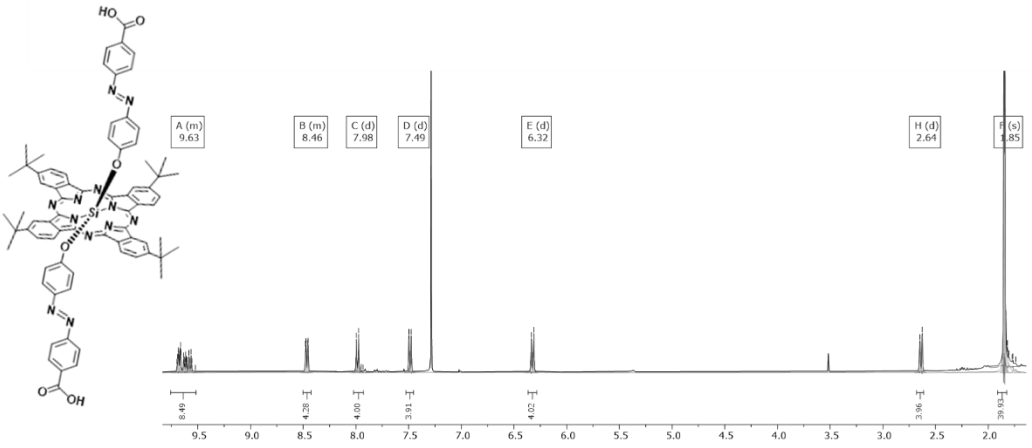

Figure 46. *^{1}H-NMR spectra of $(tBu)_4SiPc$-(O-Ar-Azo-Ar-$CO_2H)_2$* ***(12)*** *In $CDCl_3$.*

HR-MALDI TOF and H-RMN integral of $SiPc-(O_2CPy)_2$ (13).

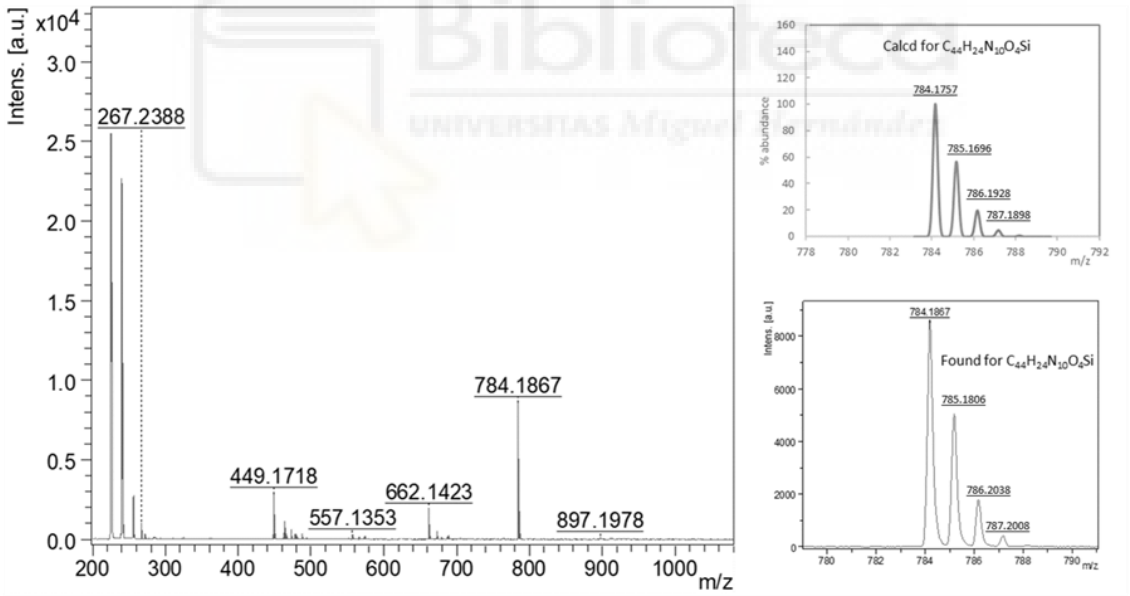

Figure 47*. HR-MALDI TOF mass spectrum (negative mode) of $SiPc-(O_2CPy)_2$* ***(13)****.*

^{1}H NMR (400 MHz, $CDCl_3$) δ 9.81 – 9.72 (m, 8H), 8.50 – 8.36 (m, 8H), 7.60 (d, *J* = 8.5 Hz, 4H), 5.00 (d, *J* = 8.5 Hz, 4H).

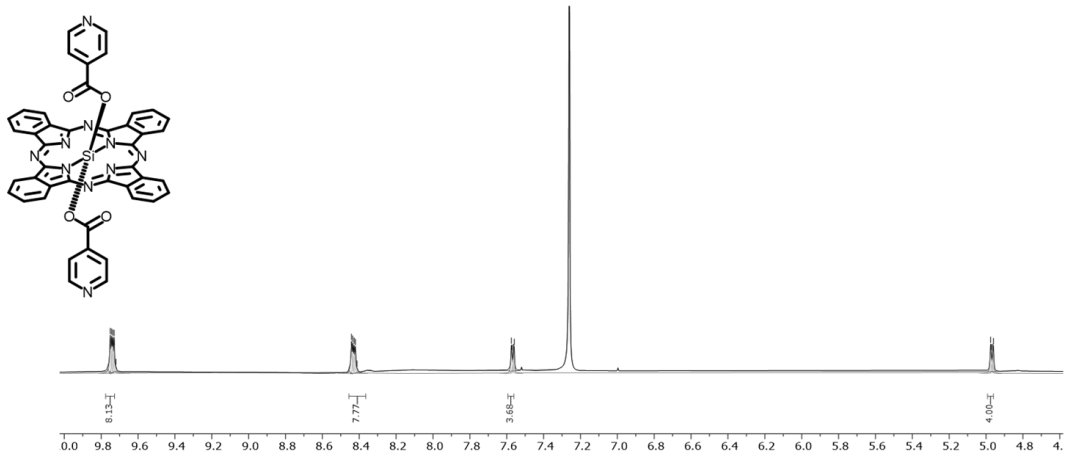

Figure 48. *^{1}H-NMR spectra of SiPc-$(O_2CPy)_2$* ***(13)*** *In $CDCl_3$.*

UV-Vis of $(PyO)_4$-$SiPcCl_2$ (42).

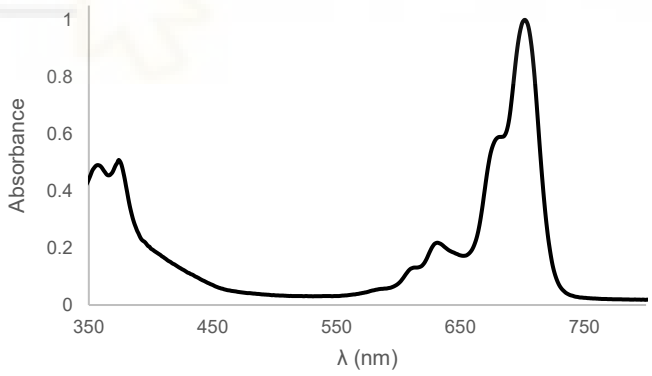

Figure 49. *UV-Vis spectrum of $(PyO)_4$-$SiPcCl_2$* ***(42)*** *in DMSO.*

HR-MALDI TOF, UV-Vis and ^{1}H- NMR of $(PyO)_4SiPc\text{-}O_2C\text{-}Ar\text{-}CHO)_2$ (43).

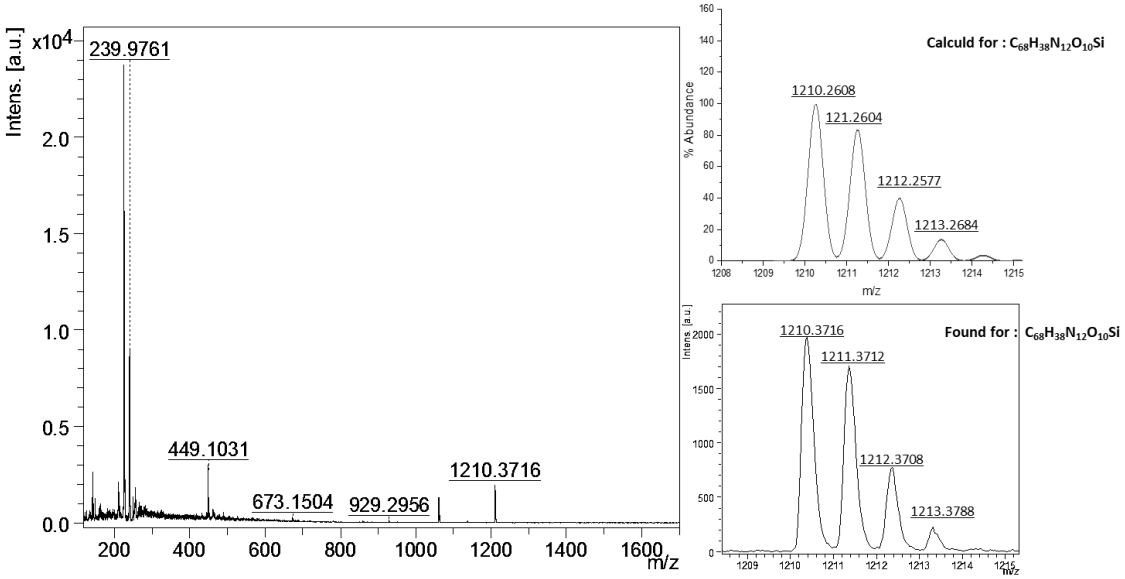

***Figure 50**. HR-MALDI TOF mass spectrum (negative mode) of $(PyO)_4SiPc\text{-}O_2C\text{-}Ar\text{-}CHO)_2$ **(43)**.*

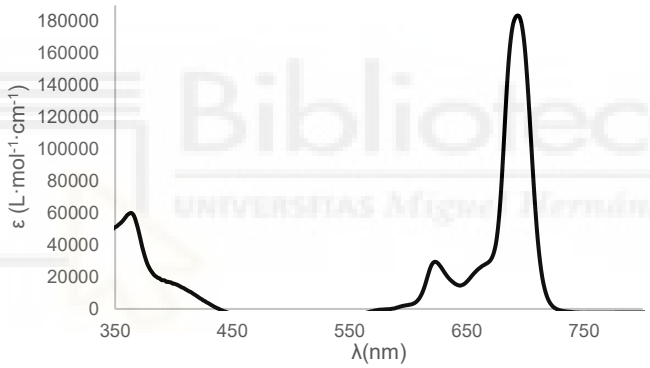

***Figure 51**. UV-Vis spectrum of $(PyO)_4SiPc\text{-}O_2C\text{-}Ar\text{-}CHO)_2$ **(43)** in $CHCl_3$.*

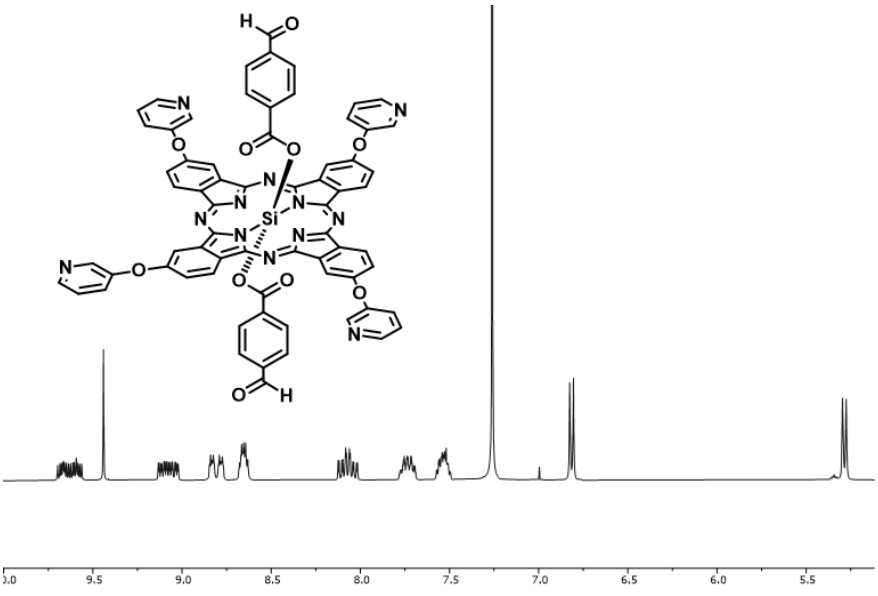

***Figure 52**. ^{1}H-NMR spectrum of $(PyO)_4SiPc\text{-}O_2C\text{-}Ar\text{-}CHO)_2$ (43) in CD_3OD.*

HR-MALDI TOF, UV-Vis and ^{1}H- NMR of $(PyO)_4SiPc$ -$(O_2C\text{-}Ar_2\text{-}CHO)_2$ (44)

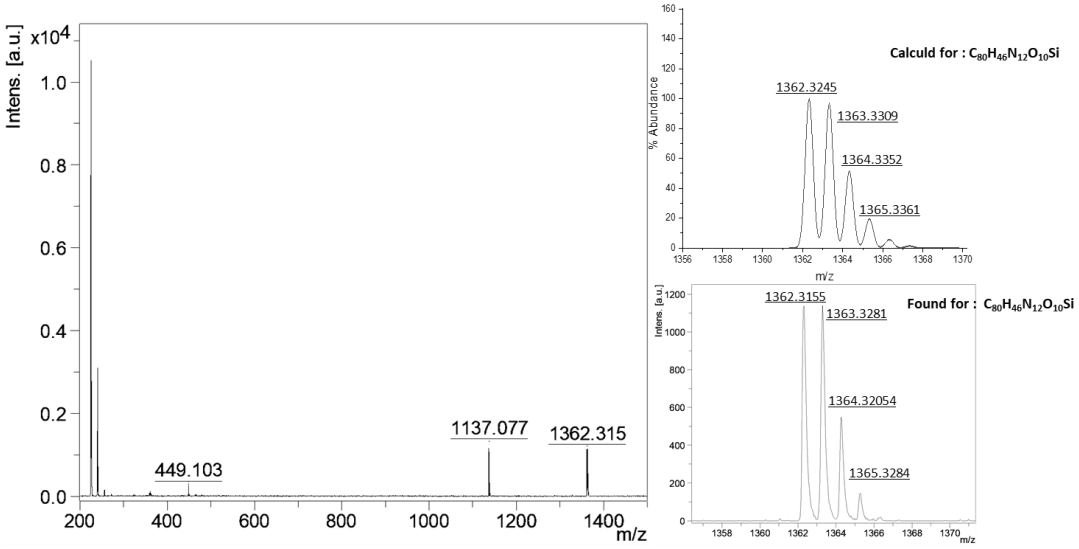

***Figure 53**. HR-MALDI TOF mass spectrum (negative mode) of $(PyO)_4SiPc$ -$(O_2C\text{-}Ar_2\text{-}CHO)_2$ **(44)**.*

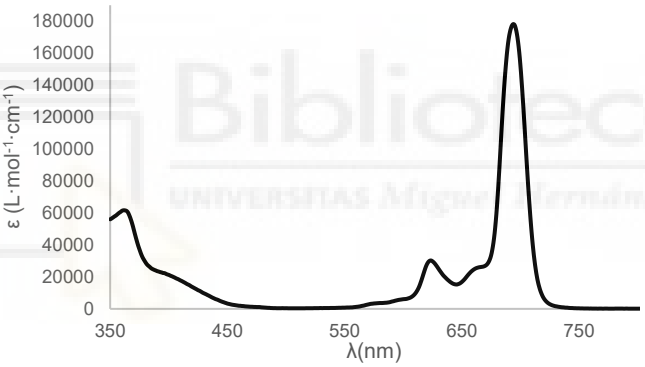

***Figure 54**. UV-Vis spectrum of $(PyO)_4SiPc$ -$(O_2C\text{-}Ar_2\text{-}CHO)_2$ **(44)** in $CHCl_3$.*

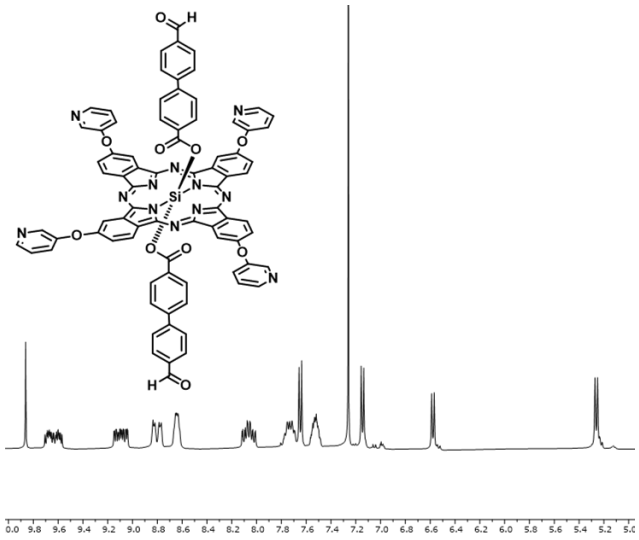

***Figure 55**. ^{1}H-NMR spectrum of $(PyO)_4SiPc$ -$(O_2C\text{-}Ar_2\text{-}CHO)_2$ **(44)** in CD_3OD.*

HR-MALDI TOF, UV-Vis, ^{1}H- NMR and 2D COSY of $(PyO)_4SiPc$ -(O_2C-Ar-$CH_3)_2$ (45).

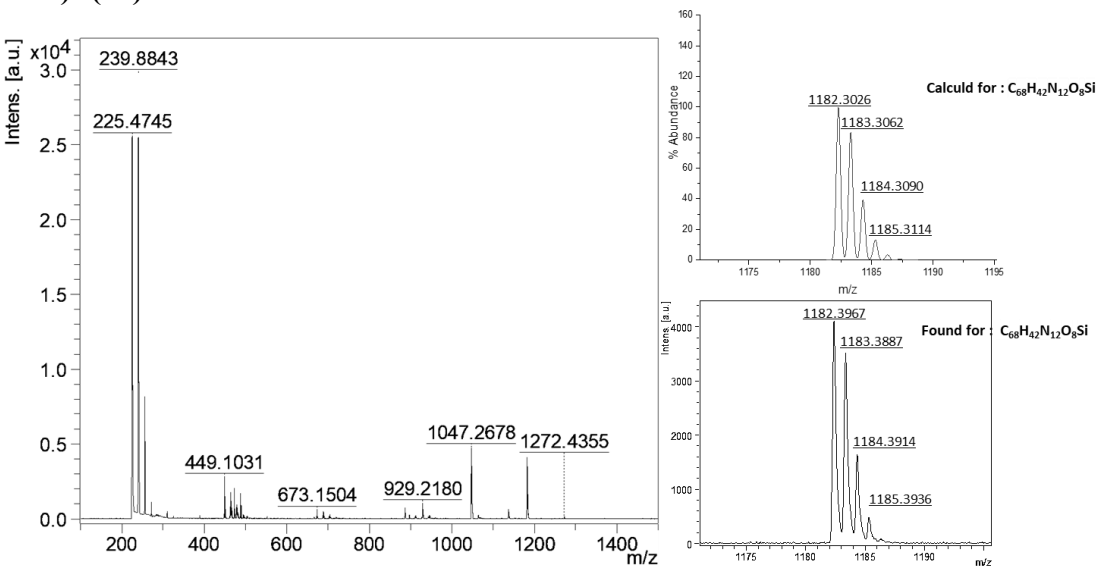

***Figure 56**. HR-MALDI TOF mass spectrum (negative mode) of $(PyO)_4SiPc$ -(O_2C-Ar_2-$CH_3)_2$ **(45)**.*

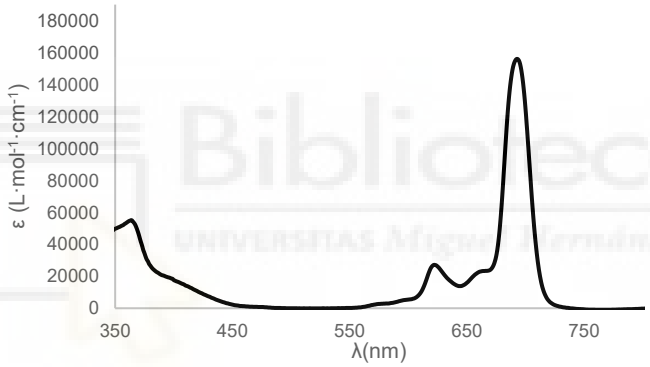

***Figure 57**. UV-Vis spectrum of $(PyO)_4SiPc$ -(O_2C-Ar_2-$CH_3)_2$ **(45)**.*

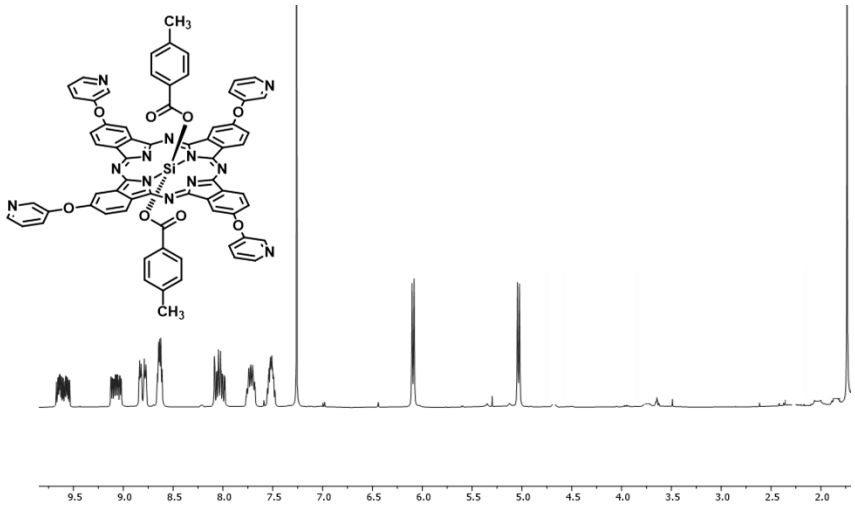

***Figure 58**. ^{1}H-NMR spectrum of $(PyO)_4SiPc$ -(O_2C-Ar_2-$CH_3)_2$ **(45)** in $CDCl_3$.*

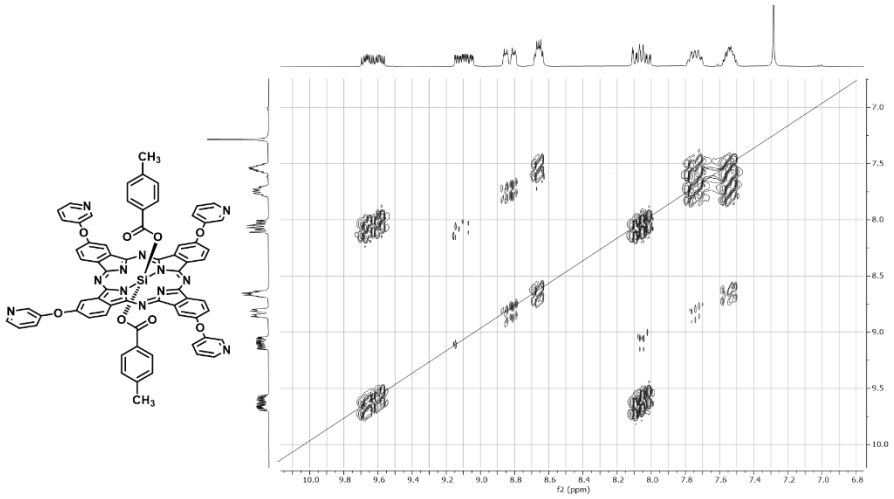

***Figure 59**. 2D COSY spectrum of $(PyO)_4SiPc$ -(O_2C-Ar_2-$CH_3)_2$ **(45)** in $CDCl_3$.*

HR-MALDI TOF, UV-Vis and ^{1}H- NMR of $(PyO)_4SiPc$ $(O_2C$-Ar-$CO_2H)_2$ (46).

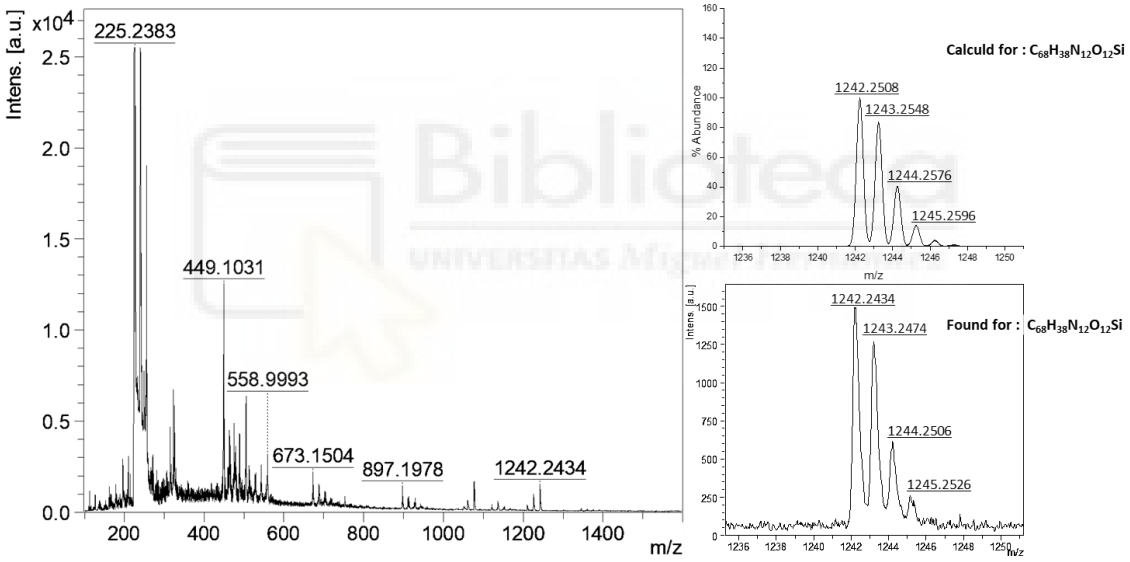

***Figure 60**. HR-MALDI TOF mass spectrum (negative mode) of $(PyO)_4SiPc$ $(O_2C$-Ar-$CO_2H)_2$ **(46)**.*

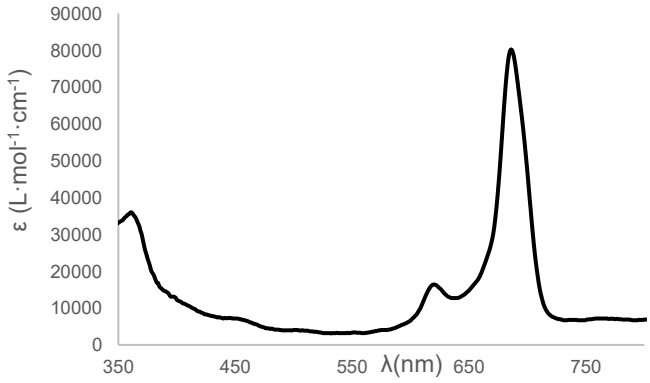

***Figure 61**. UV-Vis spectrum of $(PyO)_4SiPc$ $(O_2C$-Ar-$CO_2H)_2$ **(46)** in THF.*

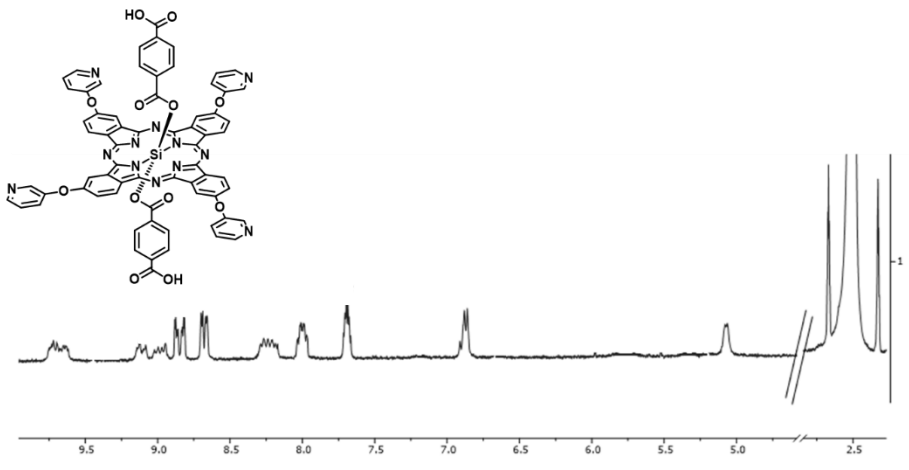

Figure 62. *^{1}H-NMR spectrum of $(PyO)_4SiPc$ $(O_2C\text{-}Ar\text{-}CO_2H)_2$* ***(46)*** *in DMSO-$d_6$.*

HR-MALDI TOF, UV-Vis and ^{1}H- NMR of $(PyO)_4SiPc$ $(O_2C\text{-}Ar_2\text{-}CO_2H)_2$ (47).

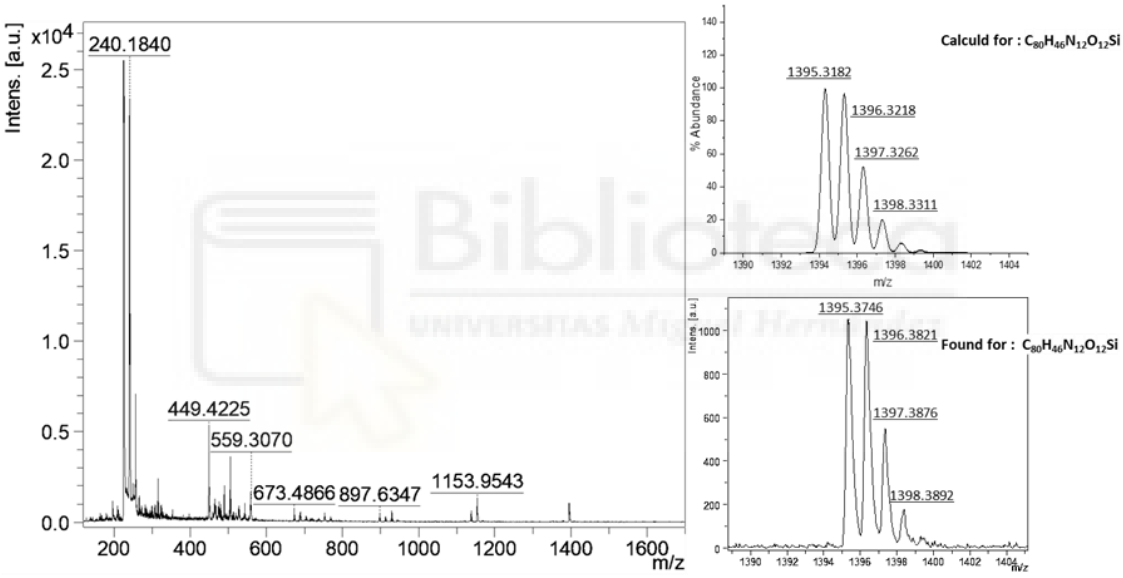

Figure 63*. HR-MALDI TOF mass spectrum (negative mode) of $(PyO)_4SiPc$ $(O_2C\text{-}Ar_2\text{-}CO_2H)_2$* ***(47)****.*

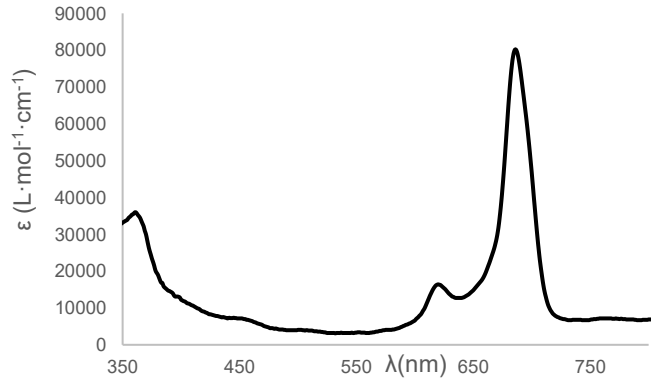

Figure 64*. UV-Vis spectrum of $(PyO)_4SiPc$ $(O_2C\text{-}Ar_2\text{-}CO_2H)_2$* ***(47)*** *in THF.*

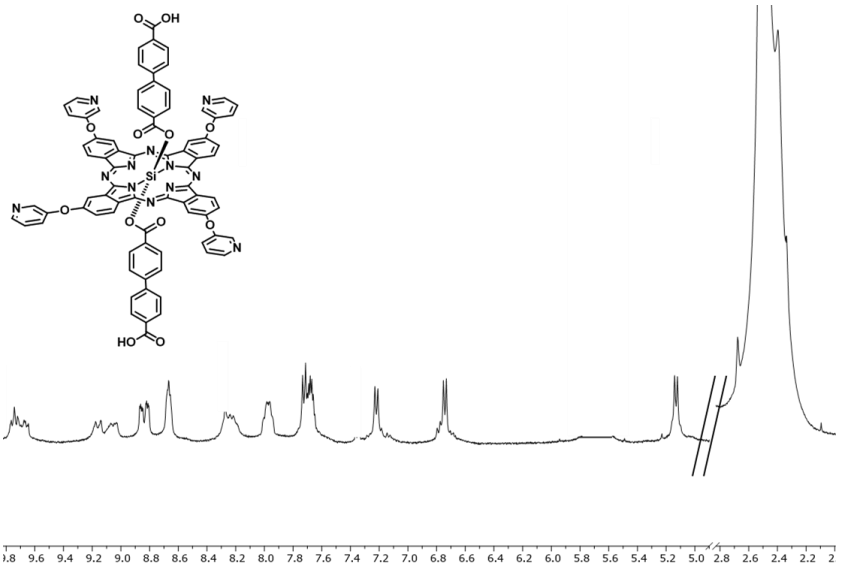

Figure 65. *^{1}H-NMR spectrum of $(PyO)_4SiPc$ $(O_2C\text{-}Ar_2\text{-}CO2H)_2$* ***(47)*** *in DMSO-$d_6$.*

UV-Vis and ^{1}H- NMR of $(MePy^{+}O)_4$-SiPc-$(O_2C\text{-}Ar\text{-}CO_2H)_2$ $(I^{-})_4$ (48).

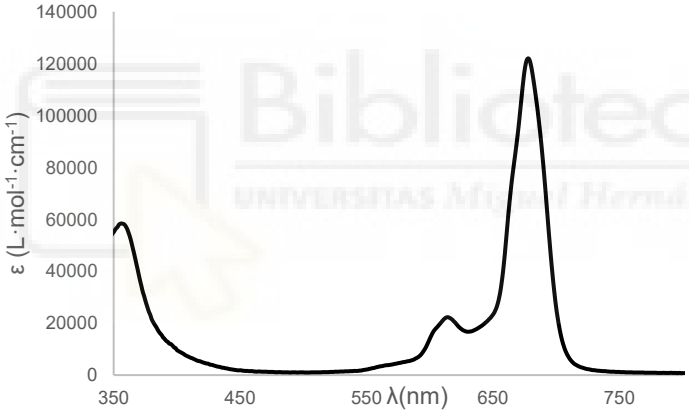

Figure 66*. UV-Vis spectrum of $(MePy^{+}O)_4$-SiPc-$(O_2C\text{-}Ar\text{-}CO_2H)_2$ $(I^{-})_4$* ***(48)*** *in MeOH.*

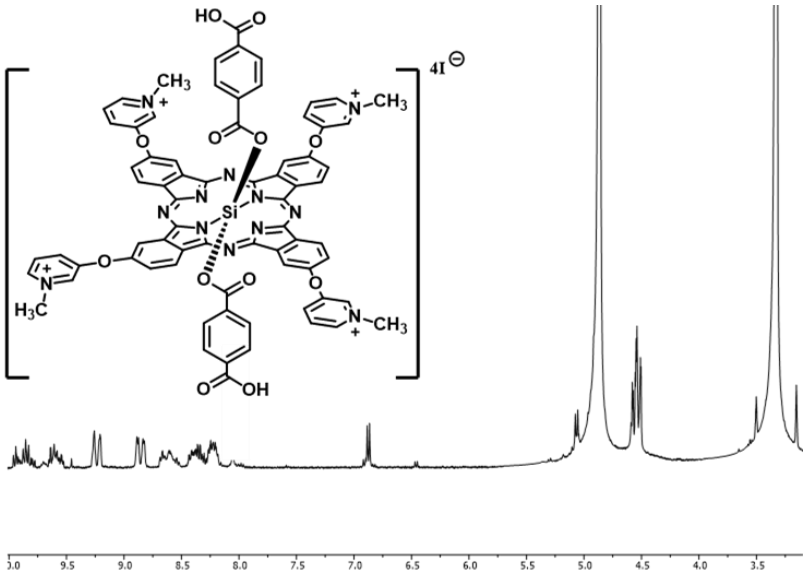

Figure 67. *^{1}H-NMR spectrum of $(MePy^{+}O)_4$-SiPc-$(O_2C$-Ar-$CO_2H)_2$ $(I^-)_4$* ***(48)*** *in CD_3OD.*

UV-Vis and ^{1}H- NMR of $(MePyO^{+})_4SiPc$-$(O_2C$-Ar_2-$CO_2H)_2$ $(I^-)_4$ (49).

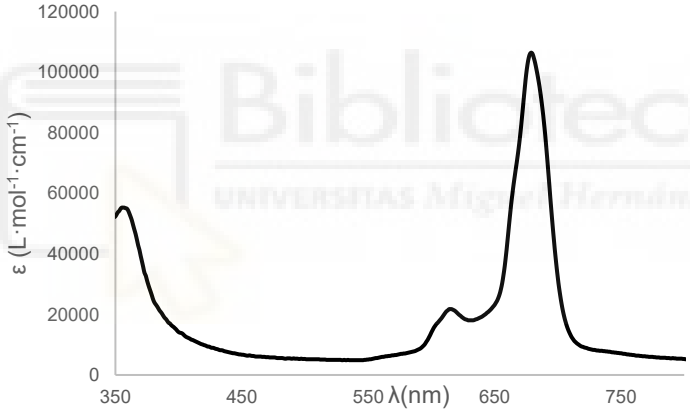

Figure 68*. UV-Vis spectrum of $(MePyO^{+})_4SiPc$-$(O_2C$-Ar_2-$CO_2H)_2$ $(I^-)_4$* ***(49)*** *in MeOH.*

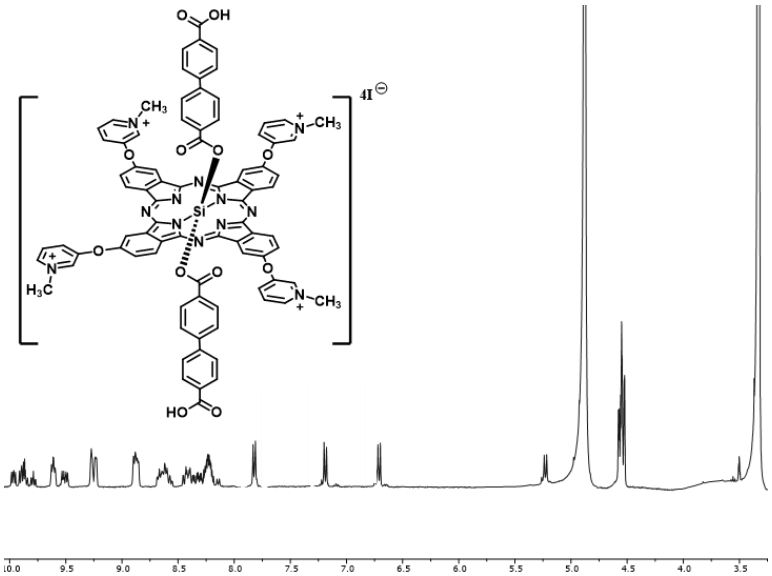

Figure 69. *^{1}H-NMR spectrum of $(MePyO^{+})_4SiPc$-$(O_2C$-Ar_2-$CO_2H)_2$ $(I^-)_4$ (49) in CD_3OD.*

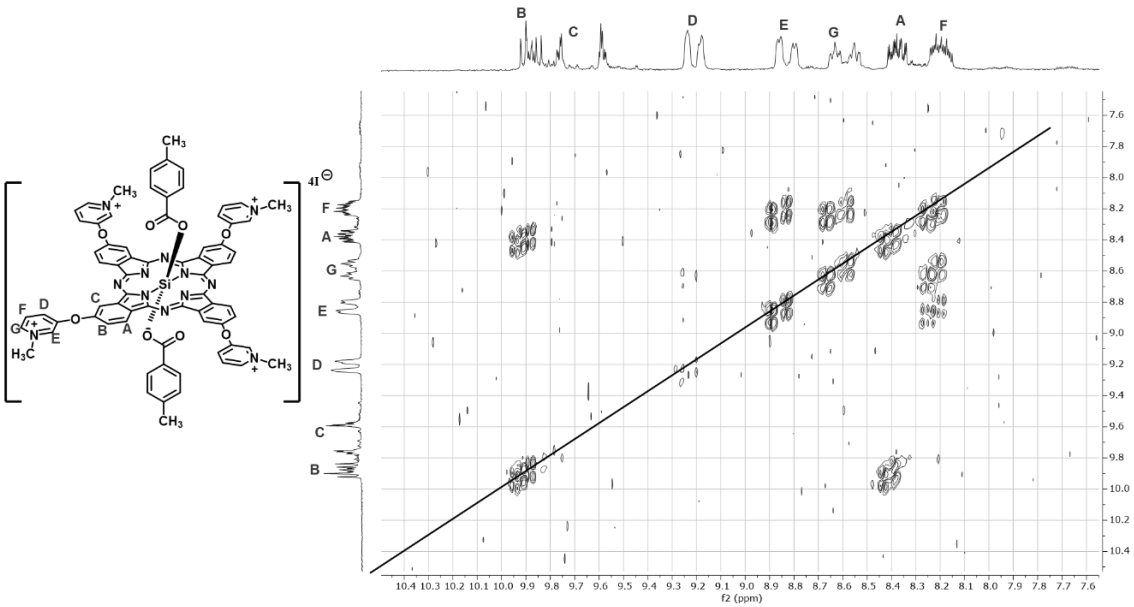

Figure 70. *2D COSY spectrum of $(MePyO^+)_4SiPc\text{-}(O_2C\text{-}Ar_2\text{-}CO_2H)_2\ (I^-)_4$* ***(49)*** *in CD_3OD.*

UV-Vis and ^{1}H- NMR of $(MePy^+O)_4$-SiPc-$(O_2C$-Ar-$CH_3)_2\ (I^-)_4$ (50).

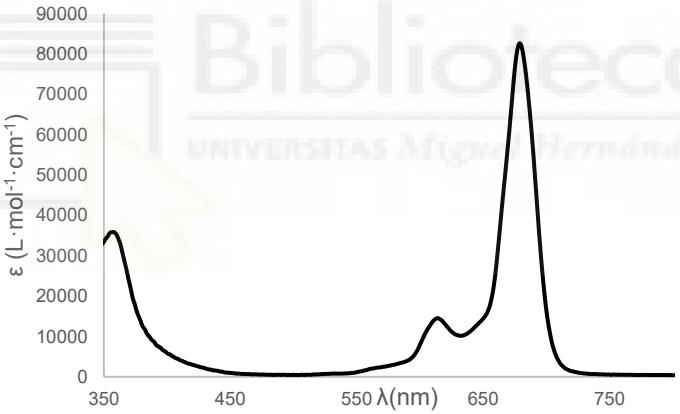

Figure 71*. UV-Vis spectrum of $(MePyO^+)_4SiPc\text{-}(\ O_2C\text{-}Ar_2\text{-}CH_3)_2\ (I^-)_4$* ***(50)*** *in MeOH.*

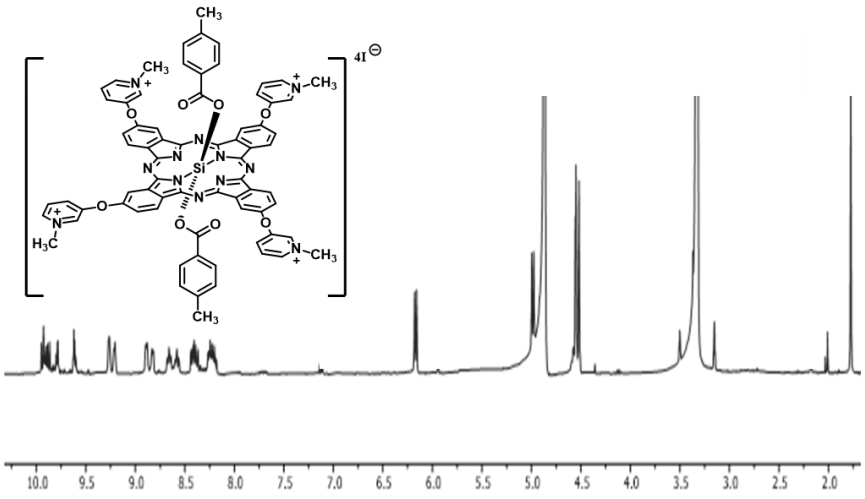

Figure 72. *^{1}H-NMR spectrum of $(MePyO^{+})_4SiPc$-(O_2C-Ar-$CH_3)_2$ $(I^{-})_4$* ***(50)*** *in CD_3OD.*

UV-Vis of $(MePy^{+}O)_4$-SiPc-$(O_2C$-Ar-$CO_2H)_2$ $(CH_3SO_3^{-})_4$ (14).

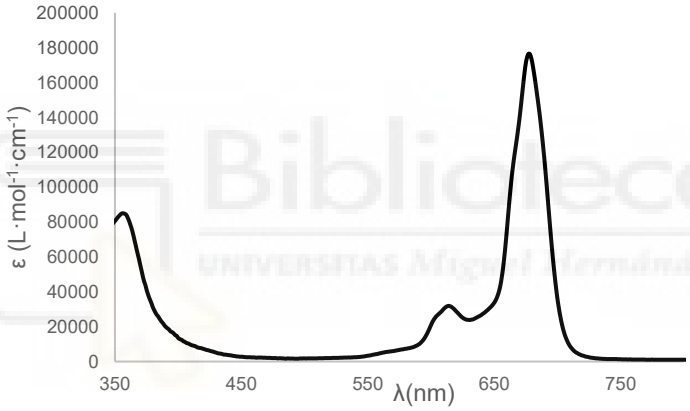

Figure 73*. UV-Vis spectrum of $(MePy^{+}O)_4$-SiPc-$(O_2C$-Ar-$CO_2H)_2$ $(CH_3SO_3^{-})_4$* ***(14)*** *in MeOH.*

UV-Vis $(MePy^{+}O)_4$-SiPc-$(O_2C$-Ar_2-$CO_2H)_2$ $(CH_3SO_3^{-})_4$ (15).

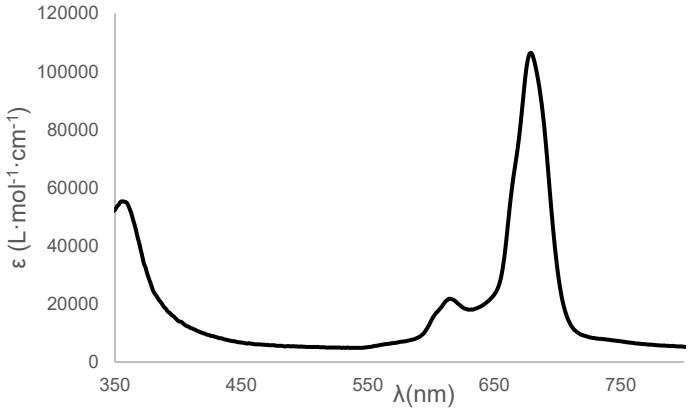

Figure 74*. UV-Vis spectrum of $(MePy^{+}O)_4$-SiPc-$(O_2C$-Ar_2-$CO_2H)_2$ $(CH_3SO_3^{-})_4$* ***(15)*** *in MeOH.*

H-RMN integral spectra of $(MePy^{+}O)_4$-SiPc-$(O_2C$-Ar-$CH_3)_2$ $(CH_3SO_3^{-})_4$ (16).

^{1}H-NMR (400 MHz, MeOD) δ 9.99 – 9.83 (m, 4H), 9.62 – 9.44 (m, 4H), 9.30 – 9.20 (m, 4H), 8.92 – 8.83 (m, 4H), 8.71 – 8.58 (m, 4H), 8.46 – 8.31 (m, 4H), 8.30 – 8.17 (m, 4H), 6.17 (d, *J* = 8.1 Hz, 4H), 4.98 (d, *J* = 8.2 Hz, 4H), 4.58 – 4.49 (m, 12H), 2.70 (S, 12H), 1.78 (s, 5H).

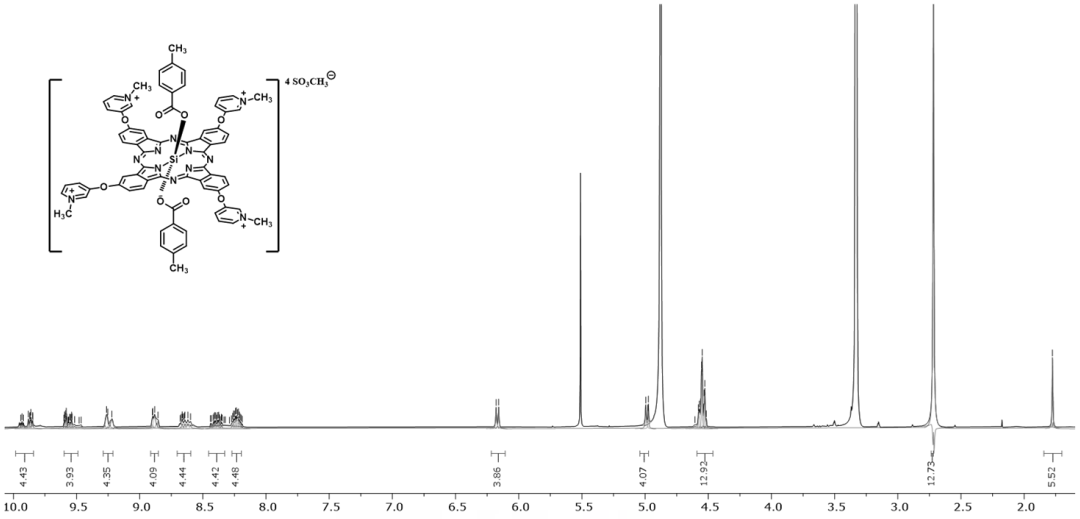

Figure 74. *^{1}H-NMR spectrum of $(MePy^{+}O)_4$-SiPc-$(O_2C$-Ar-$CH_3)_2$ $(CH_3SO_3^{-})_4$* ***(16)*** *in CD_3OD.*

ANNEX 2

2.1 Article :" Synthesis of 4-methylthiophenyl silicon phthalocyanines axially substituted with carboxylic acids for MOF materials".

Synthesis of 4-methylthiophenyl silicon phthalocyanines axially substituted with carboxylic acids for MOF materials

Víctor Sobrino-Bastán, Luis Martín-Gomis[◊] and Ángela Sastre-Santos[◊,*]

Área de Química Orgánica, Instituto de Bioingeniería, Universidad Miguel Hernández, Avda. Universidad S/N, 03202, Elche, Spain

Received 3 November 2022

Accepted 27 November 2022

Dedicated to Prof. Tomás Torres on the occasion of his 70th birthday

ABSTRACT: Two new peripherally substituted with 4 and 8 electron-donating 4-methylthiophenyl silicon phthalocyanines, $(ArS)_4SiPc$ **1** and $(ArS)_8SiPc$ **2**, axially substituted with carboxylic acids have been synthesized using microwave irradiation in a very good yield. The new compounds have been characterized by ^{1}H-NMR, UV-vis, fluorescence, differential pulse voltammograms, and HR-MALDITOF mass spectrometry. An study of the stability of the axial chlorinated SiPcs in the function of the number of thiophenyl substituents indicates than $(ArS)_8SiPcCl_2$ **10** degradates faster, to its corresponding unreactive dihydrosilicon phthalocyanine derivative $(ArS)_8SiPc(OH)_2$ **11**, than $(ArS)_4SiPcCl_2$. The new SiPcs are excellent candidates as photoactive linkers for the construction of MOF materials.

KEYWORDS: Silicon Phthalocyanine, Microwave irradiation.

INTRODUCTION

The construction of the so-called Metal-Organic Framework materials (MOFs) represents the ideal combination of metal ions and organic ligands (acting as connectors and linkers) to afford one-, two- or threedimensional networks, and robust porous materials for use in gas separation, gas storage, catalysis, chemical sensing or advanced photoresponsive materials, among other applications [1–3]. In most occasions, organic ligands are only responsible for the final 3D architecture but sometimes, when linkers are photoactive organic molecules, new and exciting properties can be found [4]. We can find examples of appropriately functionalized chromophoric linkers, employed to construct photoresponsive MOFs based on naphthalene [5–7], anthracene, [8–10] pyrene [11–13], perylene [14], porphyrin [15–17], or naphthalenediimide [18–20], to name a few. Metallophthalocyanines (MPc's) are planar aromatic macromolecules, with 18 conjugated π-electrons, that provide very high extinction coefficients together with good chemical and thermal stability. Despite the convenience of using them as building units to construct porous and crystalline frame-works, few examples can be found in the literature, and most of them are based on the presence of dihidroxy [21–25] and diamino [26] chelating functions in the peripheral positions of symmetrical MPc's. In this context, we have recently published a silicon phthalocyanine, (SiPc) with no peripheral substituents, and axially substituted with carboxylic acid appends, that have been successfully employed as a chromophoric linker for MOF materials, in combination with Zn ions, and with good behavior as an optical resonator [27]. SiPcs are a special class of MPc's, with a tetravalent silicon atom in the central cavity with two axial valences, pointing to both sides of the ring, and represent a versatile molecular platform to obtain SiPc-based chromophoric linkers for MOF-materials. It is possible to design and synthesize this type of molecule locating chelating functionalities at the axial positions, with no or negligible influence on the optical and electronic properties, while these can be changed through convenient peripheral substitution of the phthalocyanine ring. Different thio substituted metallophthalocyanines have been already described, with applications as, for example, IR-sensitizers [28, 29] or light activable catalysts [30]. However, till now, no thiosubstituted SiPcs have been described so far in order to study the sulfur atom influence in the MOFs construction. Here we present an efficient preparation, using microwave irradiation, of two axially substituted SiPcs with carboxylic acid groups, and also peripherally decorated with 4 and 8 electron-donating 4-methylthiophenyl appends, $(ArS)_4SiPc$ **1** and $(ArS)_8SiPc$ **2** (Chart 1), with potential application and ready to be tested as photoactive linkers for MOF materials.

EXPERIMENTAL

General methods

All chemicals were reagent grade, purchased from commercial sources, and were used as received unless otherwise specified. Microwave reactions were carried out in a CEM microwave reactor, Discover SP model. Column chromatography was performed on SiO_2 (40–63 mm) and Biorad Biobeads SX-3 (200–400 mesh) was used as the stationary phase for Size Exclusion Chromatography (SEC). TLC plates coated with SiO_2 60F254 were visualized under

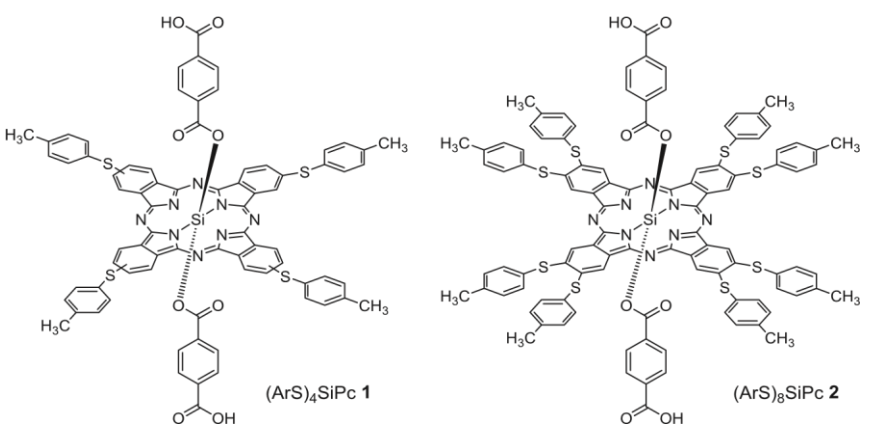

Chart 1. Chemical structure of $(ArS)_4SiPc$ **1** and $(ArS)_8SiPc$ **2**.

UV light. NMR spectra were acquired on a Bruker 400MHz spectrometer. UV/Vis spectra were recorded on a Perkin Elmer LAMBDA 365 UV-WinLab spectrophotometer. Fluorescence spectra were recorded on a Horiba Scientific FluoroMax-4 TCSPC spectrofluorometer. High-resolution mass spectra were obtained from a Bruker Reflex II matrix-assisted laser desorption/ ionization time-of-flight (MALDI-TOF) spectrometer using dithranol as matrix. Differential pulse voltammetry measurements were performed at 298 K in a conventional three-electrode cell using an m-AUTOLAB type III potentiostat/galvanostat (Metrohm, Herisau, Switzerland). Sample solutions (*ca*. 0.5 mM) were prepared in deaerated PhCN, containing 0.10 M tetrabutylammonium hexafluorophosphate ($TBAPF_6$) as supporting electrolyte; a glassy carbon (GC) working electrode, a $Ag/AgNO_3$ reference electrode, and a platinum wire counter electrode were used; Ferrocene/ferrocenium was the internal standard for all measurements.

Synthesis

Preparation of $(ArS)_4SiPc$ 1

In a 10 mL microwave tube, $(ArS)_4SiPcCl_2$ **5** (50 mg, 0.045 mmol), terephthalic acid (75 mg, 0.450 mmol) were dissolved in dry toluene (0.5 mL) and 1-methyl-2-pyrrolidone (NMP, 0.5 mL). The contents were stirred and microwave-irradiated to a set temperature of 160°C for 60 min. The crude reaction mixture was precipitated in methanol, filtered and purified by size exclusion chromatography (Bio-Beads, THF). This yielded 19 mg (26%) of pure compound as a green solid. ^{1}H NMR (400 MHz, $CDCl_3$, 25 °C) δ 9.44–9.23 (m, 8H, H-Pc), 8.15–7.96 (m, 4H, H-Pc), 7.71–7.63 (m, 8H, H-Ar periphery), 7. 37 (d, *J* = 7.8 Hz, 8H, H-Ar periphery), 6.93 (d, *J* = 8.2 Hz, 4H, H-Ar axial,), 5.19 (d, *J* = 8.2 Hz, 4H, H-Ar axial),

2.51 (s, 12H,4xCH_3). UV/Vis ($CHCl_3$): λ_{max} (log ε)= 363 (4.69), 448 (4.22), 644 (4.44), 717 (5.20). HR-MS (MALDI-TOF, dithranol): m/z for $[C_{76}H_{50}N_8O_8S_4Si]^+$ calcd. 1398.2390, found 1398.2396.

Preparation of $(ArS)_8SiPc$ 2

In a 10 mL microwave tube, $(ArS)_8SiPcCl_2$ **10** (50 mg, 0.031 mmol), terephthalic acid (53 mg, 0.310 mmol) were dissolved in dry toluene (0.5 mL), and 1-methyl2-pyrrolidone (NMP, 0.5 mL). The contents were stirred and microwave-irradiated to a set temperature of 160 °C for 60 min. The crude reaction mixture was precipitated in methanol, filtered, and purified by size exclusion chromatography (Bio-Beads, THF). This yielded 21 mg (37%) of the pure compound as a green solid. ^{1}H NMR (400 MHz, $CDCl_3$, 25 °C) δ 9.07 (s, 8H, H-Pc), 7.60 (d, *J* = 7.9 Hz, 16H, H-Ar periphery), 7.35 (d, *J* = 7.9 Hz, 16H, periphery), 6.99 (d, *J* = 8.5 Hz, 4H, H-Ar axial), 5.21 (d, *J* = 8.5 Hz, 4H, H-Ar axial), 2.52 (s, 24H, 8xCH_3). UV/Vis ($CHCl_3$): λ_{max} (log ε)= 366 (4.69), 463 (4.33), 665 (4.40), 743 (5.19). HR-MS (MALDI-TOF, dithranol): m/z for $[C_{104}H_{74}N_8O_8S_8Si]^+$ calcd. 1787.3114, found 1787.3124.

Preparation of 4-(p-tolylthio)phthalonitrile 3

4-nitro-phthalonitrile (2 g, 11.55 mmol), 4-methylthiophenol (1.5 g, 12.08 mmol), and K_2CO_3 (2.5 g, 18.09 mmol), were mixed in dimethyl sulfoxide (40 mL) under Ar for 24h. After that, the crude material was precipitated over H_2O/ice and filtered. The solid obtained was washed thoroughly with water and, finally, with cold ethanol, yielding 2.29 g (79%) of 4-(*p*-tolylthio)phthalonitrile **3** as a pale-white colored solid, which was used in successive reactions without further purification. ^{1}H NMR (400 MHz, $CDCl_3$, 25 °C) δ 7.57 (d, 1H, *J*=8.3 Hz, H-Ar), 7.43 (d, 2H, *J*=8.3 Hz, H-ArS), 7.33–7.23 (m, 4H, 2xH-Ar + H-ArS), 2.44 (s, 3H, CH_3). ^{13}C NMR (100 MHz, $CDCl_3$, 25 °C): δ 149.0, 141.2, 135.3, 133.1, 129.7, 129.5, 124.5, 116.2, 115.5, 115.1, 110.9, 21.3.

Preparation of 5-(p-tolylthio)isoindoline-1,3-diimine 4

4-(*p*-tolylthio)phthalonitrile **3** (1.8g, 7.20 mmol), MeONa (0.18 g, 3.33 mmol) were mixed in methanol (150 mL). NH_3 was then bubbled in the solution at refluxing methanol temperature (65 °C) for 9 h. After that, the solvent was evaporated and the solid obtained was washed repeatedly with water and dried, yielding 1.85 g (96%) of 5-(*p*-tolylthio)isoindoline-1,3-diimine **4** as a pale-

white colored solid, which was used in successive reactions without further purification. ^{1}H NMR (400 MHz, CD_3OD, 25 °C) δ 7,70 (d, 1H, *J*=7.9 Hz, H-Ar), 7.65 (d, 1H, *J*=1.4 Hz, H-Ar), 7.41 (d, 2H, *J*=8.1 Hz, H-Ar), 7.34 (dd, 1H, *J*=7.9Hz J=1.4Hz, H-Ar), 7.27 (d, 2H, *J*=8.1Hz, H-Ar), 2.38 (s, 3H, CH_3). ^{13}C RMN (100 MHz, CD_3OD, 25 °C) δ 145.4, 140.7, 135.2, 131.8, 131.4, 130.0, 123.0, 121.9, 21.3.

Preparation of $(ArS)_4SiPcCl_2$ 5

5-(*p*-tolylthio)isoindoline-1,3-diimine **4** (0.750 g, 2.81 mmol) was dissolved in dry quinoline (7 mL). The system was sealed and the solution was purged with Ar and kept from light. Then, $SiCl_4$ (0.7 mL) was carefully introduced, and the temperature was raised to reflux and maintained for 1 h. The crude reaction mixture was precipitated in acetone, filtered, and thoroughly washed. This yielded 0.757 g (99%) of $(ArS)_4SiPcCl_2$ **7** as a green solid, which was prudently kept, under argon and avoiding direct light exposure, before its use. UV-vis ($CHCl_3$) λ_{max}/nm: 377, 455, 652, 726 nm.

Preparation of $(ArS)_4SiPc(OH)_2$ 6

$(ArS)_4SiPcCl_2$ **7** (50 mg, 0.045mmol) was dissolved in a 1:1 v/v DMSO/NaOH 2M mixture (4 mL) and maintained at 100 °C for 3 h. The crude reaction was extracted with $CHCl_3$ and, the combined organic extracts were washed with HCl aq 1M, water, and brine, dried over $MgSO_4$, and evaporated. This yielded 24 mg (48%) of $(ArS)_4SiPcOH_2$ **6**. UV-vis ($CHCl_3$) λ_{max}/nm 361, 432, 629, 700. HR-MS (MALDI-TOF, dithranol): m/z for $[C_{60}H_{42}N_8O_2S_4Si]^-$ calcd 1062.2222, found 1062.2216.

Preparation of $(ArS)_4SiPc$ 7

In a 10 mL microwave tube, $(ArS)_4SiPcCl_2$ **5** (50 mg, 0.045 mmol), 4-methylbenzoic acid (62 mg, 0.450 mmol) were dissolved in dry toluene (0.5 mL), and 1-methyl-2-pyrrolidone (NMP, 0.5 mL). The contents were stirred and microwave-irradiated to a set temperature of 200 °C for 60 min. The crude reaction mixture was precipitated in methanol, filtered and purified by column chromatography (SiO_2, $CHCl_3$/Hexane 3:1). This yielded 28 mg (50%) of the pure compound as a green solid. ^{1}H NMR (400 MHz, $CDCl_3$, 25 °C) δ 9.48 – 9.35 (m, 8H, H-Pc), 8.15 – 8.06 (m, 4H, H-Pc), 7.71–7.63 (m, 8H, H-Ar periphery), 7.39 (d, *J* = 7.9 Hz, 8H, H-Ar periphery), 6.09 (d, *J* = 8.0 Hz, 4H, H-Ar axial), 5.05 (d, *J* = 8.0 Hz, 4H, H-Ar axial), 2.53 (s, 12H, 4xCH_3 periphery), 1.75 (s, 6H, 2xCH_3 axial). UV/Vis ($CHCl_3$) λ_{max} (log ε) 366 (4.59), 443 (4.18), 614 (3.63), 714 (5.17). HR-MS

(MALDI-TOF, dithranol): m/z for $[C_{76}H_{54}N_8O_4S_4Si]^+$ calcd. 1298.2813, found 1298.2820.

Preparation of 4,5-bis(p-tolylthio)phthalonitrile 8

5,6-dichlorophthalonitrile (2 g, 10.15 mmol), 4-methylthiophenol (3.86 g, 24.20 mmol), and K_2CO_3

(21 g, 151.94 mmol), were mixed in dimethyl sulfoxide (40 mL) under Ar for 24h. After that, the crude material was precipitated over H_2O/ice and filtered. The solid obtained was washed thoroughly with water and, finally, with cold ethanol, yielding 2.61 g (69%) of 4,5-bis(*p*tolylthio)phthalonitrile **8** as a pale-white colored solid, which was used in successive reactions without further purification. ^{1}H NMR: (400 MHz, $CDCl_3$, 25 °C): δ= 7.44 (d, 4H, *J*=8.0 Hz, H-Ar), 7.33 (d, 4H, *J*=8.0 Hz, H-Ar), 6.91 (s, 2H, H-Ar), 2.46 (s, 6H, 2xCH_3).^{13}C-RMN (100 MHz, $CDCl_3$, 25 °C) δ 144.4, 141.3, 135.4, 131.4, 129.3, 124.6, 115.5, 111.2, 21.4.

Preparation of 5,6-bis(p-tolylthio)isoindoline-1,3diimine 9

5,6-bis(*p*-tolylthio) phthalonitrile **8** (1.5g, 4.03 mmol), MeONa (0.15 g, 2.78 mmol) were mixed in methanol (150 mL). NH_3 was then bubbled in the solution at refluxing methanol temperature (65 °C) for 7 h. After that, the solvent was evaporated and the solid obtained was washed repeatedly with water and dried, yielding 1.17 g (75%) of 5,6-bis(*p*-tolylthio)isoindoline-1,3-diimine **9** as a pale-white colored solid, which was used in successive reactions without further purification. ^{1}H NMR (400 MHz, CD_3OD, 25 °C) δ 7.51 (s, 2H, H-Ar), 7.37 (d, 4H, *J*=8.0 Hz, H-Ar), 7.28 (d, 4H, *J*=8.0 Hz, H-Ar), 2.39 (s, 6H, 2xCH_3) ppm.

^{13}C-RMN (100 MHz, CD_3OD, 25 °C) δ 140.5, 134.6, 131.8, 130.2, 123.5, 21.3.

Preparation of $(ArS)_8SiPcCl_2$ 10

5,6-bis(*p*-tolylthio)isoindoline-1,3-diimine **9** (0.600 g, 1.54 mmol) was dissolved in dry quinoline (6 mL). The system was sealed, and the solution was purged with Ar and kept from light. Then, $SiCl_4$ (0.6 mL) was carefully introduced, and the temperature was raised to reflux and maintained for 1 h. The crude reaction mixture was precipitated in acetone, filtered, and thoroughly washed. This yielded 0.617 g (99%) of $(ArS)_8SiPcCl_2$ **10** as a green solid, which was prudently kept, under argon and avoiding direct light exposure, before its use. UV-vis ($CHCl_3$) λ_{max}/nm: 381, 468, 673, 752.

Preparation of $(ArS)_8SiPc(OH)_2$ 11

$(ArS)_8SiPcCl_2$ **10** (50 mg, 0.031 mmol) was dissolved in a 1:1 v/v DMSO/NaOH 2M mixture (4 mL) and maintained at 100 °C for 3 h. The crude reaction was extracted with $CHCl_3$ and, the combined organic extracts, were washed with HCl aq 1M, water and brine, dried over $MgSO_4$, and evaporated. This yielded 21 mg (43%) of $(ArS)_4SiPcOH_2$ **6**. UV-vis ($CHCl_3$) λ_{max}/nm 351, 447, 647, 726. HR-MS (MALDI-TOF, dithranol): m/z for $[C_{88}H_{66}N_8O_2S_8Si]^-$ calcd. 1551.3067, found 1551.3075.

Preparation of $(ArS)_8SiPc$ 12

In a 10 mL microwave tube, $(ArS)_8SiPcCl_2$ **10** (50 mg, 0.031 mmol), 4-methylbenzoic acid (48 mg, 0.310 mmol) were dissolved in dry toluene (0.5 mL), and 1-methyl-2-pyrrolidone (NMP, 0.5 mL). The contents were stirred and microwave-irradiated to a set temperature of 200 °C for 60 min. The crude reaction mixture was precipitated in methanol, filtered and purified by column chromatography (SiO_2, CH_2Cl_2). This yielded 31 mg (54%) of the pure compound as a green solid. ^{1}H NMR (400 MHz, $CDCl_3$, 25 °C) δ 9.05 (s, 8H, H-Pc), 7.57 (d, 16H, *J* = 8.0 Hz, H-Ar periphery), 7.33 (d, 16H, *J* = 8.0 Hz, H-Ar peripheral), 6.08 (d, 4H, *J* = 8.1 Hz, H-Ar axial), 5.01 (d, 4H, J = 8.1 Hz, H-Ar axial), 2.49 (s, 24H, 8xCH_3 periphery), 1.75 (s, 6H, 2xCH_3 axial). UV/Vis ($CHCl_3$) λmax (log ε) 369 (4.75), 453 (4.42), 661 (2.82), 740 (5.34). HR-MS (MALDI-TOF, dithranol): m/z for $[C_{104}H_{78}N_8O_4S_8Si]^+$ calcd. 1787.3741, found 1787.4230.

RESULTS AND DISCUSSION

Synthesis and characterization

Synthesis of $(ArS)_4SiPc$ **1** is described in Scheme 1, starting from 4-nitrophthalonitrile, an S_NAr reaction with 4-methylthiophenol afforded 4-(*p*-tolylthio)phthalonitrile **3** [30] which was readily converted into more reactive thiophenyl diiminoisoindoline **4** when treated with ammonia in refluxing methanol and a catalytic amount of MeONa, following a previously described method [30]. A subsequent cyclotetramerization reaction of **4** was carried out in dry quinoline with $SiCl_4$, at reflux temperature, for 1 hour and avoiding direct light exposure. After

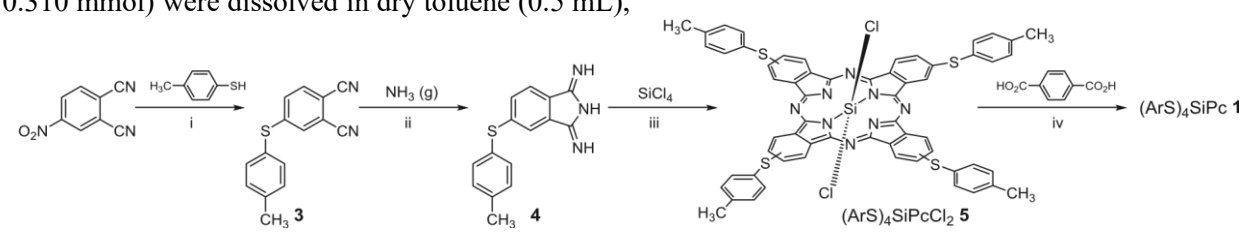

Scheme 1. Synthesis of $(ArS)_4SiPc$ **1.** Reagents and conditions: (i) anhydrous K_2CO_3, DMSO, RT, Ar, 24 h. 79%; (ii) MeONa/ MeOH, 65 ºC, 9 h, 96%; (iii) dry quinoline, reflux, dark, Ar, 1 h, 99%, (iv) Tol/NMP 1:1 v/v, Ar, MW:160 ºC/200 W/ 1h, 26 %.

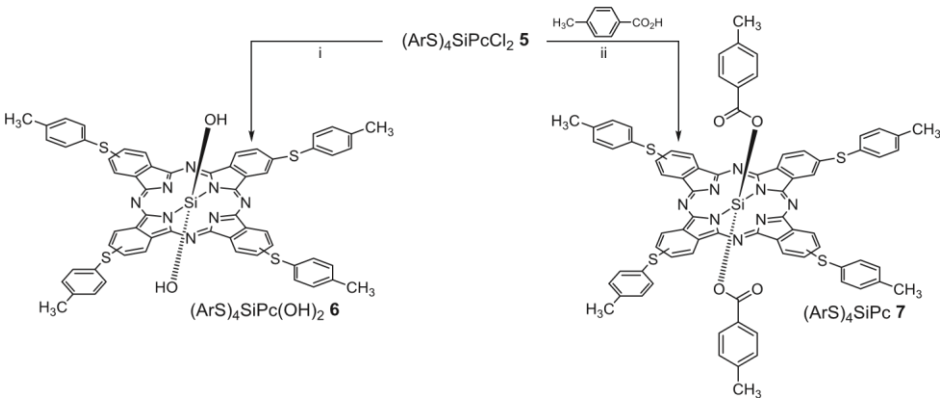

Scheme 2. Synthesis of $(ArS)_4SiPc(OH)_2$ **6** and $(ArS)_4SiPc$ **7**. Reagents and conditions: (i) NaOH 2M/DMSO 1:1 v/v, reflux 3h, 48%, (ii) Tol/NMP 1:1 v/v, Ar, MW:160 ºC/1h, 50 %.

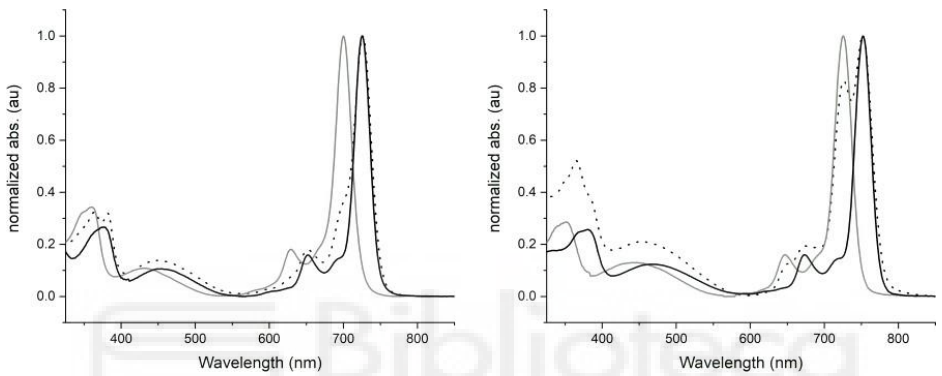

Fig. 1. (a) Normalized UV-vis spectra, registered in $CHCl_3$ at RT, of freshly prepared (black) and aged $(ArS)_4SiPcCl_2$ **5** (dotted), and $(ArS)_4SiPcOH_2$ **6** (grey). (b) Normalized UV-vis spectra, registered in $CHCl_3$ at RT, of freshly prepared (black) and aged $(ArS)_8SiPcCl_2$ **10** (dotted), and $(ArS)_4SiPcOH_2$ **11** (grey).

multiple acetone washings $(ArS)_4SiPcCl_2$ **5** was obtained as a green solid, which had to be rapidly employed in the last step. This is because we have previously observed that dichloride silicon phthalocyanine compounds ($SiPcCl_2$) degradates to, presumably, unreactive dihydrosilicon phthalocyanine derivatives. $(ArS)_4SiPc(OH)_2$ **6** and $(ArS)_4SiPc$ **7** were also prepared from $(ArS)_4SiPcCl_2$ **5** for comparative purpose (Scheme 2). Figure 1 shows the comparison of UV-vis normalized spectra of freshly prepared and one-day aged $(ArS)_4SiPcCl_2$ **5**, together to that of $(ArS)_4SiPc(OH)_2$ **6**. It can be observed how freshly prepared $(ArS)_4SiPcCl_2$ **5** UV-vis spectrum is dominated by a narrow sharp Q band centered at 726 nm, $(ArS)_4SiPc(OH)_2$ **6** spectrum shows also a narrow Q band, hypsochromically shifted to 700 nm, while the aged silicon phthalocyanine spectrum presents a combined Q band, centered at 726 nm but wider in the base, due to a growing 700 nm Q band which timidly begins to show. Finally $(ArS)_4SiPc$ **1** was prepared in 26% yield by nucleophilic substitution of the two axial chlorine atoms of $(ArS)_4SiPcCl_2$ **5** employing a 10-equivalent quantity of tertphthalic acid, microwave radiation for only 1 hour, and a 1:1 mixture of toluene and *N*-methyl2-pyrrolidone, the latter added in order to improve the absorption of microwave energy [31]. Rapid and effective microwave heating in this step made a difference to us, in order to obtain moderate to good yields of axially substituted SiPc derivatives in a short reaction time (1h).

Microwave reactor allowed to reach high reaction temperatures quickly, while keeping the crude material in the complete absence of light, and employing an excess of terephthalic acid in a highly concentrated solution (actually an emulsion). And all of these conditions probably minimized the already mentioned degradation of $(ArS)_4SiPcCl_2$ **5** to unreactive species. $(ArS)_8SiPc$ **2** was synthesized, following an equivalent route, but

starting from commercially available 4,5-dichlorophthalonitrile (Scheme 3). Double S_NAr afforded 4,5-bis(*p*-tolylthio) phthalonitrile **8** [32], which was turned into 5,6-bis(*p*tolylthio)isoindoline-1,3-diimine **9** and then, employing $SiCl_4$ as a metallic salt template, to dichloride precursor, $(ArS)_8SiPcCl_2$ **10**.

It is worth noting that, in our hands, $(ArS)_8SiPcCl_2$ **10** degradates faster, to its corresponding unreactive dihydrosilicon phthalocyanine derivative $(ArS)_8SiPc(OH)_2$ **11** (Scheme 4), than $(ArS)_4SiPcCl_2$ **5** does. This can be appreciated in Fig. 1b where UV-vis normalized spectra of freshly prepared and one-day aged $(ArS)_8SiPcCl_2$ **10**, together with that of $(ArS)_8SiPc(OH)_2$ **11,** are compared. It can be noticed how aged $(ArS)_8SiPcCl_2$ **10** UV-vis spectrum presents a broad absorption at 600–800 nm area, and now two different Q bands are guessed at 726 and 752 nm, the first one corresponding to $(ArS)_8SiPc(OH)_2$ **11** UV-vis Q band maximum wavelength. However, the nucleophilic substitution of $(ArS)_8SiPcCl_2$ **10** two axial chlorine atoms by carboxylate groups (of tertphthalic

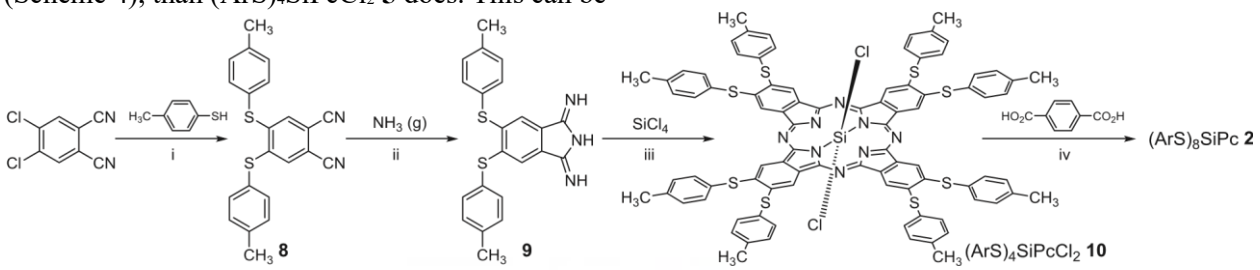

Scheme 3. Synthesis of $(ArS)_8SiPc$ **2**. Reagents and conditions: (i) anhydrous K_2CO_3, DMSO, RT, Ar, 24 h. 69%; (ii) MeONa/ MeOH, 65 ºC, 9 h. 75%; (iii) dry quinoline, reflux, dark, Ar, 1 h, 99%, (iv) Tol/NMP 1:1 v/v, Ar, MW:160 ºC/1h, 37 %.

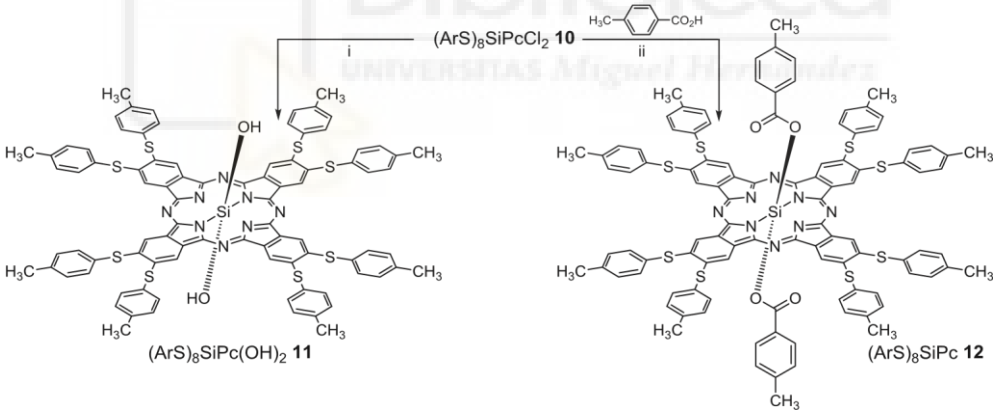

Scheme 4. Synthesis of $(ArS)_8SiPc(OH)_2$ **11** and $(ArS)_8SiPc$ **12**. Reagents and conditions: (i) NaOH 2M/DMSO 1:1 v/v, reflux 3h,

43%, (ii) Tol/NMP 1:1 v/v, Ar, MW:160 ºC/1h, 54 %.

acid) to afford $(ArS)_8SiPc$ **2** is more efficient (37% yield), compared to the previously described analog reaction. The observed different behavior probably has to do with the number and nature of peripheral substituents of the phthalocyanine ring, which modulate the electronic character of the molecule, the higher the electronic density of the ring, the more labile Si-Cl bonds are, and more easily and rapidly are chlorine atoms displaced.

NMR and mass spectroscopy characterization

All new compounds were characterized by ^{1}H-NMR spectroscopy and HR-MALDI-TOF mass spectrometry. Fig. 2 shows the comparison of ^{1}H-NMR spectra of $(ArS)_4SiPc$ **1** and $(ArS)_8SiPc$ **2**. Mainly due to the axial functionalization of those compounds, aggregation phenomena in $CDCl_3$ were avoided to a large extent, and the resolution of both spectra is quite good, thus facilitating the unambiguous assignation of all observed signals. For example, in the ^{1}H-NMR spectra of $(ArS)_4SiPc$ **1** (Fig. 2a) the signals owing to the phthalocyanine ring can be clearly distinguished as multiplets at 9.42–9.20 and 8.07–7.97 ppm, integrating for eight and four hydrogens respectively, and also the signals corresponding to the four peripheral 4-methylthiophenyl appends, a multiplet at 7.71–7.63 and a doublet centered at 7.34 ppm, integrating for eight hydrogens each, and a 12H singlet at 2.48 ppm, plus the signals ascribed to axial substituents, two doublets centered at 6.90 and 5.16 ppm integrating for four hydrogens, which are visibly downfield shifted due to the strong influence of the ring current effect of the SiPc core. Similar spectroscopic features can be found in the ^{1}H-NMR spectra of $(ArS)_8SiPc$ **2** (Fig. 2b) with the exception of the signal corresponding to phthalocyanine ring, a singlet centered at 9.07 ppm integrating for eight hydrogens. Furthermore, HRMS-MALDI-TOF assays, performed at positive mode, revealed peaks at 1358.2396 and 1847.3124 amu, with isotopic distributions that match the simulated isotope patterns for $(ArS)_4SiPc$ **1** and $(ArS)_8SiPc$ **2**, and additional

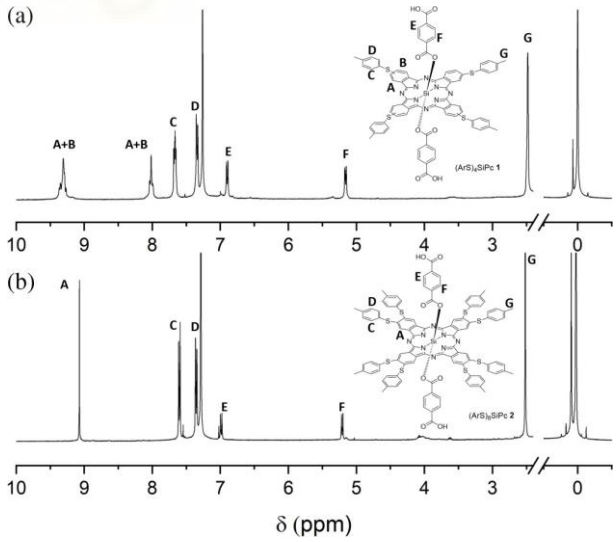

Fig. 2. ^{1}H NMR spectra, registered in $CDCl_3$ at RT of (a) $(ArS)_4SiPc$ **1** and (b) $(ArS)_8SiPc$ **2**.

peaks corresponding to fragmentations of one and/or two axial appends, very common in SiPcs mass spectra (Supporting Information, Figs. S1 and S2, respectively).

UV-vis, fluorescence and electrochemical properties

Figure 3 shows UV-vis spectra of $(ArS)_4SiPc$ **1** and $(ArS)_8SiPc$ **2**, which were registered in $CHCl_3$ at RT. Both spectra are well resolved, due to the already mentioned negligible tendency to form aggregates, particularly in $CHCl_3$, and reveal a sharp Q band, centered at 717 nm for $(ArS)_4SiPc$ **1** and 743 nm for $(ArS)_8SiPc$ **2**. As expected, 4-methylthiophenyl peripheric groups modulate the electronic character of the ring (as electron-donor in this case) as it is revealed by the red-shifted wavelengths Q-band maxima, being the effect much more pronounced in $(ArS)_8SiPc$ **2** (eight 4-methylthiophenyl groups). In this context, it is also worth noting that both spectra show a broad intramolecular charge-transfer band (CT band)

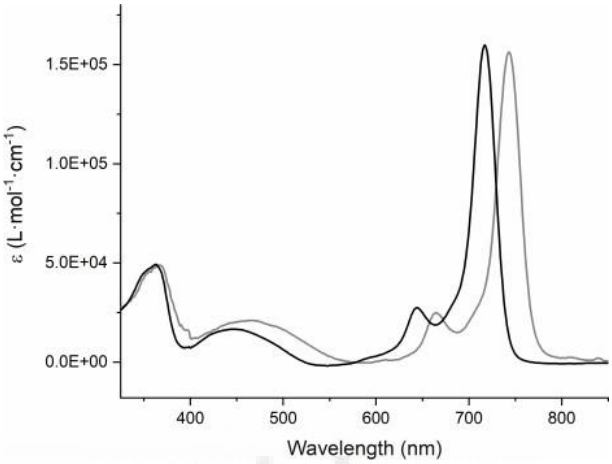

Fig. 3. UV-vis spectra, registered in $CHCl_3$ at RT of $(ArS)_4SiPc$ **1** (black) and $(ArS)_8SiPc$ **2** (grey).

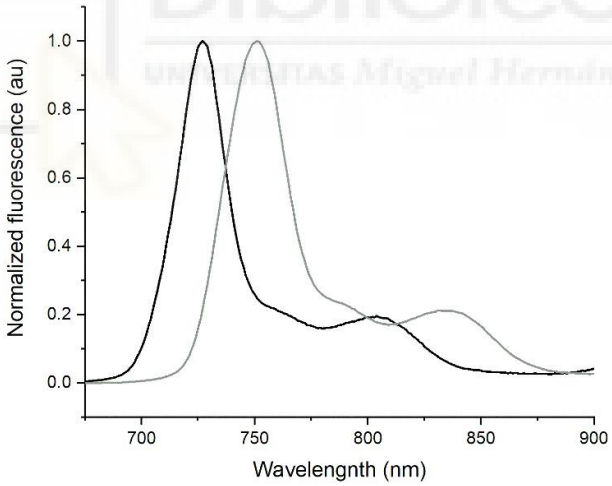

Fig. 4. Normalized fluorescence emission spectra, registered in $CHCl_3$ at RT of $(ArS)_4SiPc$ **1** (black, λ_{exc}=644 nm) and $(ArS)_8SiPc$ **2** (grey, λ_{exc}=665 nm).

between 400–550 nm which is, again, much more intense in $(ArS)_8SiPc$ **2**. Similar features in terms of intensity and wavelength maxima values show the UV-vis spectra of $(ArS)_4SiPc$ **7** and $(ArS)_8SiPc$ **9** (see SI), $(ArS)_4SiPc$ **1** and $(ArS)_8SiPc$ **2** respectively analog compounds, axially substituted with two 4-methylbenzoate groups. This confirms that different axial substituents cause a minimal

Table 1. $(ArS)_4SiPc$ **1** and $(ArS)_8SiPc$ **2** photophysical properties.

Compound	UV λ_{max} (log ε) ($CHCl_3$, nm)	Fluorescence λ_{max} ($CHCl_3$, nm)	$^{**}\lambda_{int}$ (nm)	$^{*}E_{gOpt}$ (eV)

$(ArS)_4SiPc$ **1**	717 (5.20)	727	721	1.72
$(ArS)_8SiPc$ **2**	743 (5.19)	751	745	1.66

*Optical band gap energy (E_g^{opt}) values have been estimated using $E_g^{Opt} = \frac{1240}{\lambda_{int}} eV$, where **$\lambda_{int}$ is the intersection of normalized absorption and emission spectra of chromophores

effect on the optical properties of the silicon phthalocyanine ring.

In order to complete the photophysical characterization, fluorescence emission spectra were acquired. Figure 4 shows the comparison of normalized fluorescence emission spectra, registered in $CHCl_3$, of $(ArS)_4SiPc$ **1** and $(ArS)_8SiPc$ **2** and both presented similar features. For example, when a $CHCl_3$ solution of $(ArS)_4SiPc$ **1** was excited at Q band shoulder wavelength, 644 nm, the emission spectrum revealed a fluorescence band with a maximum centered at 727 nm and also a blueshifted shoulder at 804 nm, while when $(ArS)_8SiPc$ **2** was excited at 665 nm, the maximum and shoulder of the emission band appeared at 751 and 835 nm respectively (Fig. 4).

UV-vis and fluorescence properties, together optical band gap energy values (E_g^{opt}) are summarised in Table 1.

Finally, electrochemical measurements were obtained for reference compounds $(ArS)_4SiPc$ **7** and $(ArS)_8SiPc$ **9** registering differential pulse voltammograms (DPV) in degassed benzonitrile solutions (Fig. 5). Both compounds exhibit clear and sharp reversible waves either in cathodic or anodic regions. As expected, the oxidation potential of $(ArS)_4SiPc$ **7** is higher than that of $(ArS)_8SiPc$ **9** (0.68 and 0.65 V *vs* Fc/Fc^+) while the reduction potential is lower for $(ArS)_8SiPc$ **9** (-0.83 and -0.84 V *vs* Fc/Fc^+). This confirms differences in the electronic character of both compounds, due to a different number of peripheral 4-methylthiophenyl peripheral substituents, supporting the better electron donor character nature of $(ArS)_8SiPc$ **9** over that of $(ArS)_4SiPc$ **7**.

Table 2 shows a summary of the electrochemical properties of $(ArS)_4SiPc$ **7** and $(ArS)_8SiPc$ **9** reference compounds which, as has been already stated, can be

Table 2. $(ArS)_4SiPc$ **7** and $(ArS)_8SiPc$ **12** electrochemical properties.

Compound	E_{ox} (V *vs* Fc/Fc^+)	E_{red} I (V *vs* Fc/Fc^+)	E_{red} II (V *vs* Fc/Fc^+)	*E_{HOMO} (eV)	**E_{LUMO} (eV)	***E_{gEQ} (eV)
$(ArS)_4SiPc$ 7	0.68	-0.84	-1.28	4.12	5.64	1.52
$(ArS)_8SiPc$ 12	0.65	-0.83	-1.24	4.15	5.63	1.48

*E_{HOMO} have been calculated using $E_{HOMO}(eV) = -4\ 8. - E_{ox}(V\ vs\ Fc/Fc^+)$

**E_{LUMO} have been calculated using $E_{LUMO}(eV) = -4\ 8. - E_{red}I(V\ vs\ Fc/Fc)^+$

***Electrochemical band gap energy ***(E_g^{EQ}) values have been estimated using $E_g^{EQ} = (E_{LUMO} - E_{HOMO})eV$.

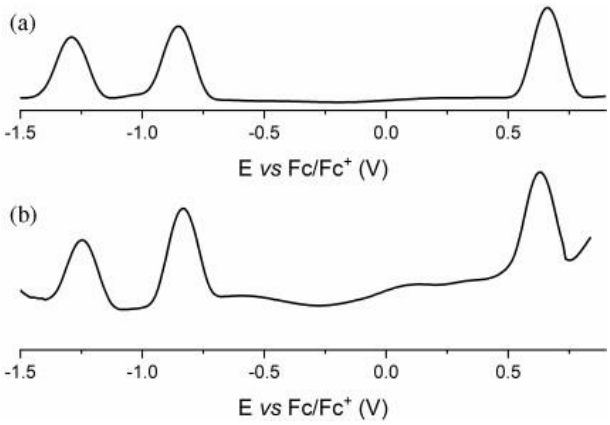

Fig. 5. Differential pulse voltammograms of (a) $(ArS)_4SiPc$ **7** and (b) $(ArS)_8SiPc$ **12**, registered in benzonitrile solution and using, tetra-butyl ammonium hexafluorophosphate (Bu_4NPF_6) as supporting electrolyte, platinum wire, glassy carbon and non-aqueous $Ag/AgNO_3$ as counter, working and reference electrodes, respectively, and ferrocene (Fc/Fc^+) as internal standard.

assimilated to those of $(ArS)_4SiPc$ **1** and $(ArS)_8SiPc$ **2** respectively.

It can be appreciated how band gap energy obtained from electrochemical methods are in agreement with those obtained from optical measurements, within approx. 0.2V.

CONCLUSION

We have described for the first time a good yield procedure using microwave irradiation for the synthesis of tetra- and octa-thiophenyl-substituted silicon phthalocyanines. The new compounds that present two carboxylic acids in the axial position are quite interesting targets for the investigation of the construction of photoactive MOFs materials.

Acknowledgments

We want to thank the European Regional Development Fund "A way to make Europe" and the Spanish Ministerio de Ciencia e Innovación/Agencia Estatal de Investigación (PID2020-117855 RB-I00 to Á. S.-S) and the Advanced Materials program by MCIN with funding from European Union NextGenerationEU (PRTRC17.I1) and Generalitat Valenciana (MFA/2022/028) for funding.

REFERENCES

1. Furukawa H, Cordova KE, O'Keeffe M and Yaghi OM. *Science* 1979; **2013**: 341.
2. Kitagawa S, Kitaura R and Noro S-I. *Angew. Chem., Int. Ed.* 2004; **43**: 2334–2375.
3. Hu Z, Deibert BJ and Li J. *Chem. Soc. Rev.* 2014; **43**: 5815–5840.
4. Haldar R, Heinke L and Wöll C. *Adv. Mater.* 2020; **32**: 1905227.
5. Gutiérrez M, Sánchez F and Douhal A. *Phys. Chem. Chem. Phys.* 2016; **18**: 5112–5120.
6. Haldar R, Matsuda R, Kitagawa S, George SJ, Kumar Maji T, Haldar R, George SJ, Maji TK, Matsuda R and Kitagawa S. *Angew. Chem. Int.* Ed 2014; **53**: 44.
7. Feng PL, Leong K and Allendorf MD. *Dalton Trans.* 2012; **41**: 8869–8877.
8. Oldenburg M, Turshatov A, Busko D, Wollgarten S, Adams M, Baroni N, Welle A, Redel E, Wöll C, Richards BS, Howard IA, Oldenburg M, Turshatov A, Busko D, Wollgarten S,

Adams M, Baroni N, Richards BS, Howard IA, Welle A, Redel E and Wöll C. *Adv. Mater.* 2016; **28**: 8477–8482.
9. Haldar R, Jakoby M, Mazel A, Zhang Q, Welle A, Mohamed T, Krolla P, Wenzel W, Diring S, Odobel F, Richards BS, Howard IA and Wöll C. *Nat. Commun.* 2018; **9**: 1–8.
10. Tanaka D, Horike S, Kitagawa S, Ohba M, Hasegawa M, Ozawa Y and Toriumi K. *Chem. Commun.* (Cambridge, U. K.) 2007: 3142–3144.
11. Wagner BD, McManus GJ, Moulton B and Zaworotko MJ. *Chem. Commun.* (Cambridge, U. K). 2002: 2176–2177.
12. McManus GJ, Perry JJ, Perry M, Wagner BD and Zaworotko MJ. *J. Am. Chem. Soc.* 2007; **129**: 9094–9101.
13. Stylianou KC, Heck R, Chong SY, Bacsa J, Jones JTA, Khimyak YZ, Bradshaw D and Rosseinsky MJ. *J. Am. Chem. Soc. 2010*; **132**: 4119–4130.
14. Park HJ, So MC, Gosztola D, Wiederrecht GP, Emery JD, Martinson ABF, Er S, Wilmer CE, Vermeulen NA, Aspuru-Guzik A, Stoddart JF, Farha OK and Hupp JT. *ACS Appl. Mater. Interfaces* 2016; **8**: 24983–24988.
15. Liu X, Kozlowska M, Okkali T, Wagner D, Higashino T, Brenner-Weiß G, Marschner SM, Fu Z, Zhang Q, Imahori H, Bräse S, Wenzel W, Wöll C and Heinke L. *Angew. Chem., Int. Ed.* 2019; **58**: 9590–9595.
16. Adams M, Kozlowska M, Baroni N, Oldenburg M, Ma R, Busko D, Turshatov A, Emandi G, Senge MO, Haldar R, Wöll C, Nienhaus GU, Richards BS and Howard IA. *ACS Appl. Mater. Interfaces* 2019; **11**: 15688–15697.
17. Park J, Feng D, Yuan S and Zhou H. *Angew. Chem., Int. Ed.* 2015; **54**: 430–435.
18. Castaldelli E, Imalka Jayawardena KDG, Cox DC, Clarkson GJ, Walton RI, Le-Quang L, Chauvin J, Silva SRP and Demets GJF. *Nat. Commun.* 2017; **8**: 1–8.
19. Takashima Y, Martínez VM, Furukawa S, Kondo M, Shimomura S, Uehara H, Nakahama M, Sugimoto K and Kitagawa S. *Nat. Commun.* 2011; **2**: 1–8.
20. Haldar R, Mazel A, Krstić M, Zhang Q, Jakoby M, Howard IA, Richards BS, Jung N, Jacquemin D, Diring S, Wenzel W, Odobel F and Wöll C. *Nat. Commun.* 2019; **10**: 1–7.
21. Meng Z, Aykanat A and Mirica KA. *J. Am. Chem. Soc.* 2019; **141**: 2046–2053.
22. Wang F, Liu Z, Yang C, Zhong H, Nam G, Zhang P, Dong R, Wu Y, Cho J, Zhang J and Feng X. *Adv. Mater.* 2020; **32**: 1905361.
23. Nagatomi H, Yanai N, Yamada T, Shiraishi K and Kimizuka N. *Chem. - Eur. J.* 2018; **24**: 1806–1810.
24. Matheu R, Gutierrez-Puebla E, Monge MÁ, Diercks CS, Kang J, Prévot MS, Pei X, Hanikel N, Zhang B, Yang P and Yaghi OM. *J. Am. Chem. Soc.* 2019; **141**: 17081–17085.
25. Zhong H, Ly KH, Wang M, Krupskaya Y, Han X, Zhang J, Zhang J, Kataev V, Büchner B, Weidinger IM, Kaskel S, Liu P, Chen M, Dong R and Feng X. *Angew. Chem., Int. Ed.* 2019; **58**: 10677–10682.
26. Jia H, Yao Y, Zhao J, Gao Y, Luo Z and Du P. *J. Mater. Chem. A* 2018; **6**: 1188–1195.
27. Haldar R, Fu Z, Joseph R, Herrero D, Martín-Gomis L, Richards BS, Howard I. A, Sastre-Santos A and Wöll C. *Chem. Sci.* 2020; 11: 7972–7978.
28. Galstyan A, Majiya H and Dobrindt U. *Nanoscale Adv.* 2022; **4:** 200–210.
29. Forteath S, Antunes E, Chidawanyika W and Nyokong T. *J. Lumin.* 2012; **132**: 2318–2324.
30. Sastre A, del Rey B and Torres T. *J. Org. Chem.* 1996; **61**: 8591–8597.
31. Kappe CO. *Angew. Chem., Int. Ed.* 2004; **43**: 6250–6284.
32. del Rey B, Keller U, Torres T, Rojo G, Agulló-López F, Nonell S, Martí C, Brasselet S, Ledoux I and Zyss J. *J. Am. Chem. Soc*. 1998; 120: 12808–12817.7

2.1.1 Suporting information of article: "Synthesis of 4-methylthiophenyl silicon phthalocyanines axially substituted with carboxylic acids for MOF materials"

Synthesis of 4-methylthiophenyl silicon phthalocyanines axially substituted with carboxylic acids for MOF materials

Víctor Sobrino-Bastán◊, Luis Martín-Gomis◊ and Ángela Sastre-Santos◊*

Área de Química Orgánica, Instituto de Bioingeniería, Universidad Miguel Hernández, Avda. Universidad S/N, 03202, Elche, Spain.

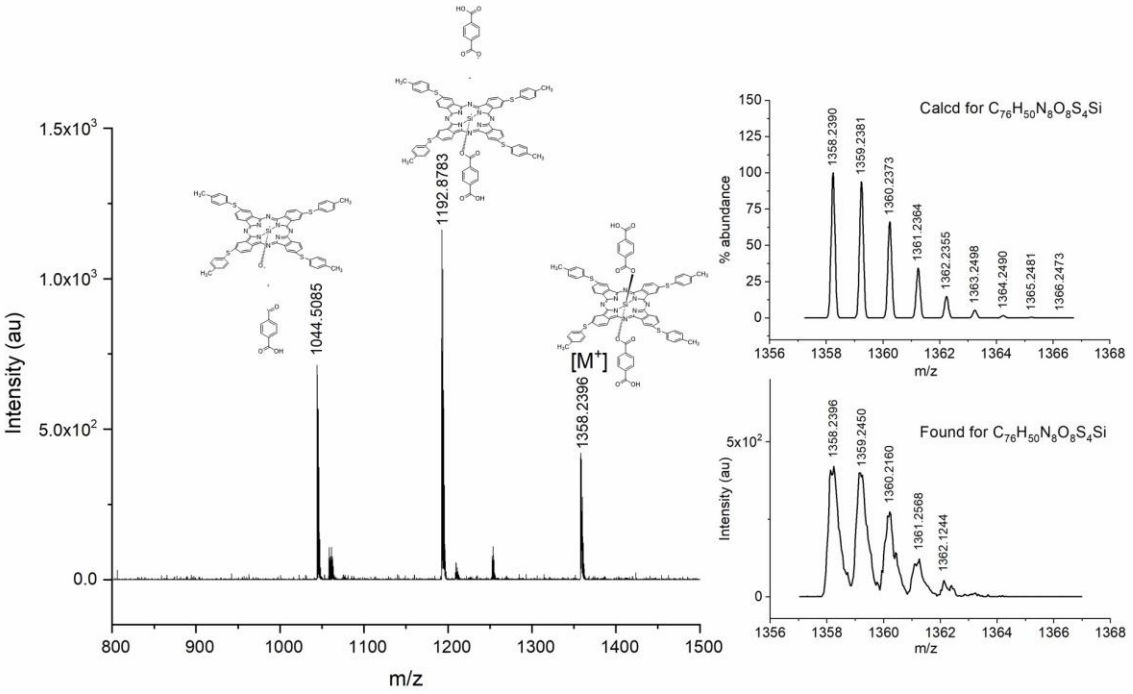

Figure S 1. HR-MALDI TOF spectrum (positive mode) of $(ArS)_4SiPc$ **1**.

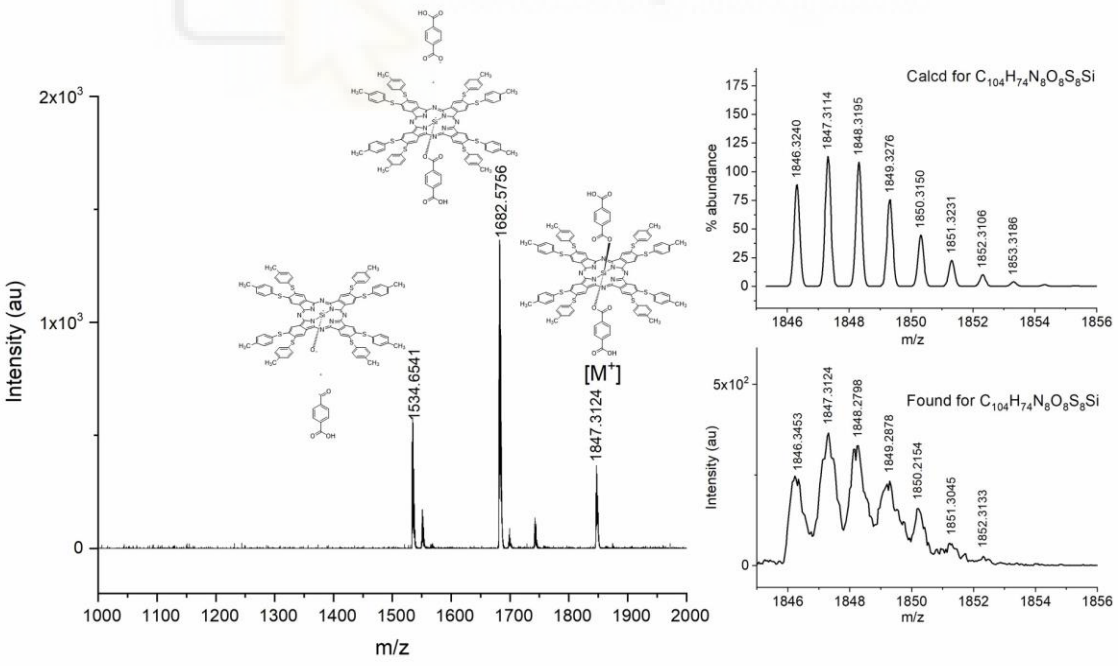

Figure S 2. HR-MALDI TOF spectrum (positive mode) of $(ArS)_8SiPc$ **2**.

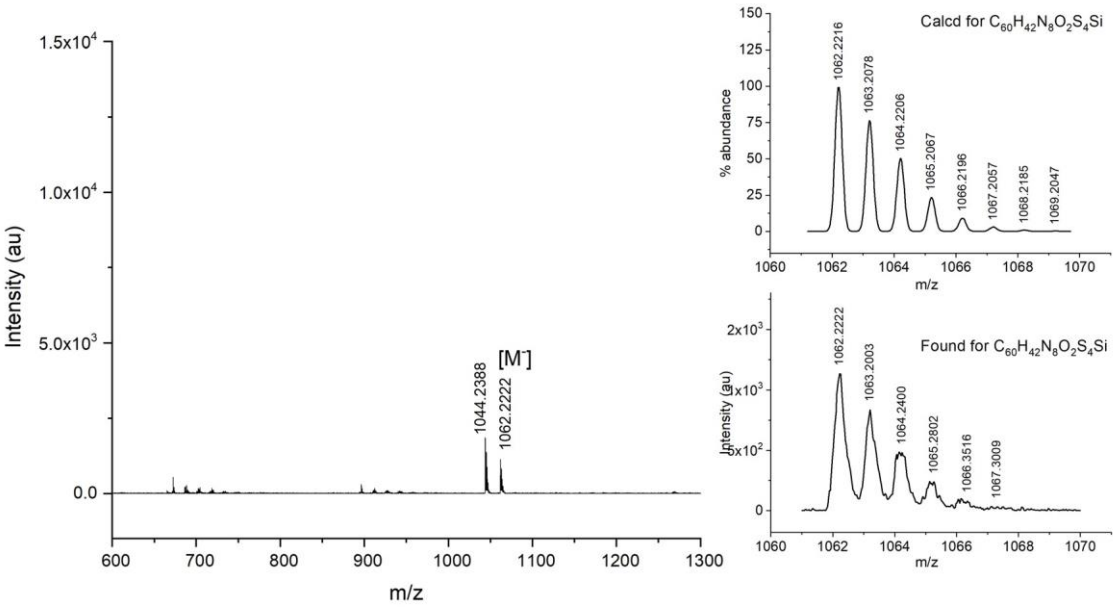

Figure S 3. HR-MALDI TOF spectrum (negative mode) of $(ArS)_4SiPc(OH)_2$ **6**.

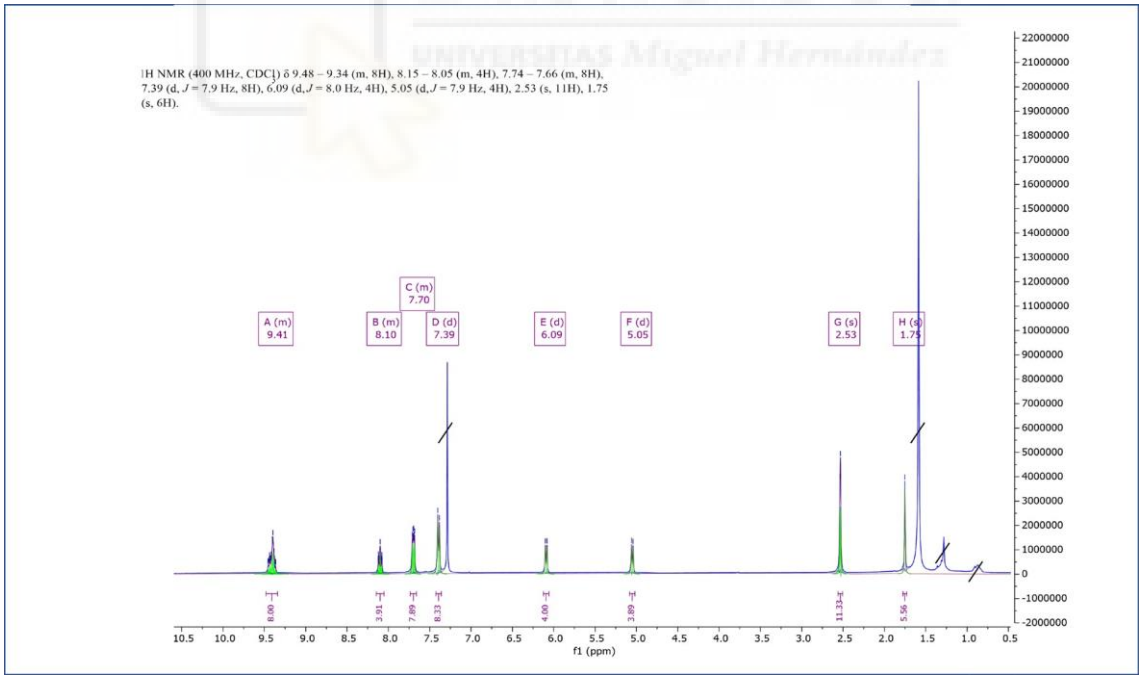

Figure S 4. ^1H NMR spectrum, registered in $CDCl_3$ at RT, of $(ArS)_4SiPc$ **7**.

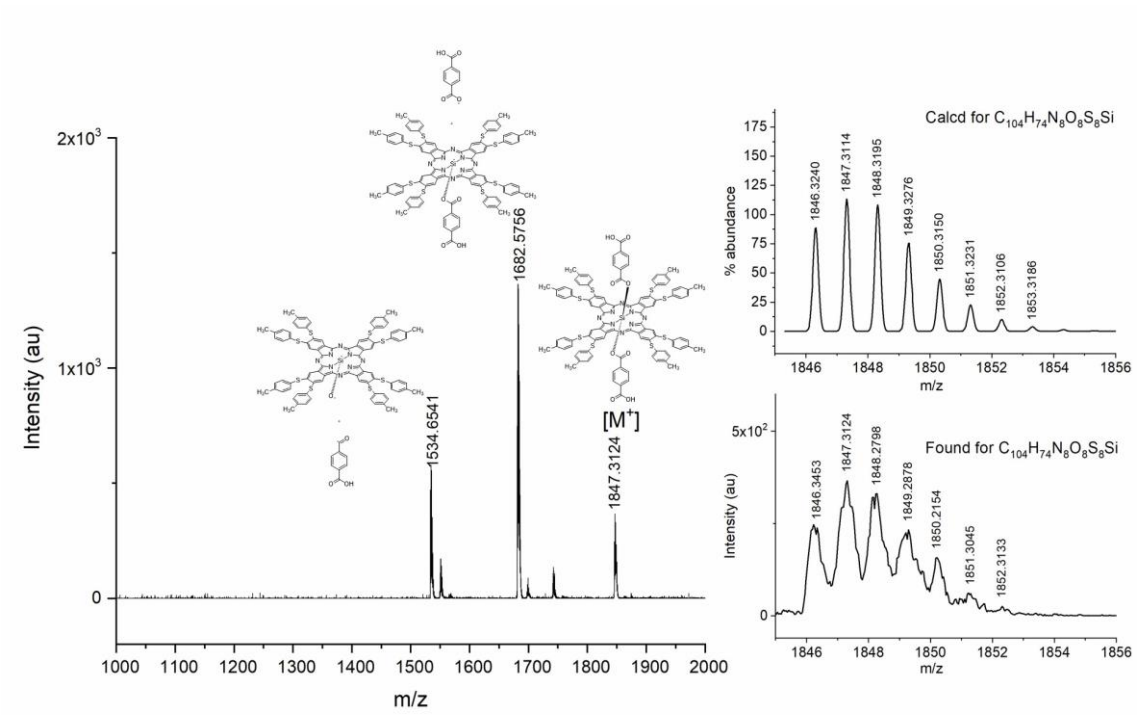

Figure S 5. UV-vis spectrum, registered in $CHCl_3$ at RT of $(ArS)_4SiPc$ **7**.

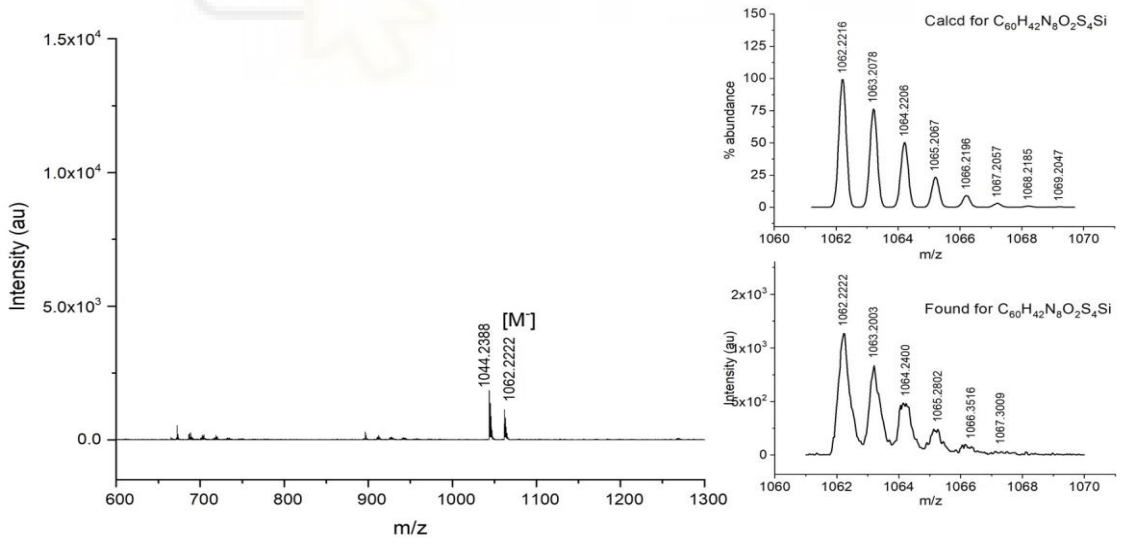

Figure S 6. HR-MALDI TOF spectrum (positive mode) of $(ArS)_4SiPc$ **7**.

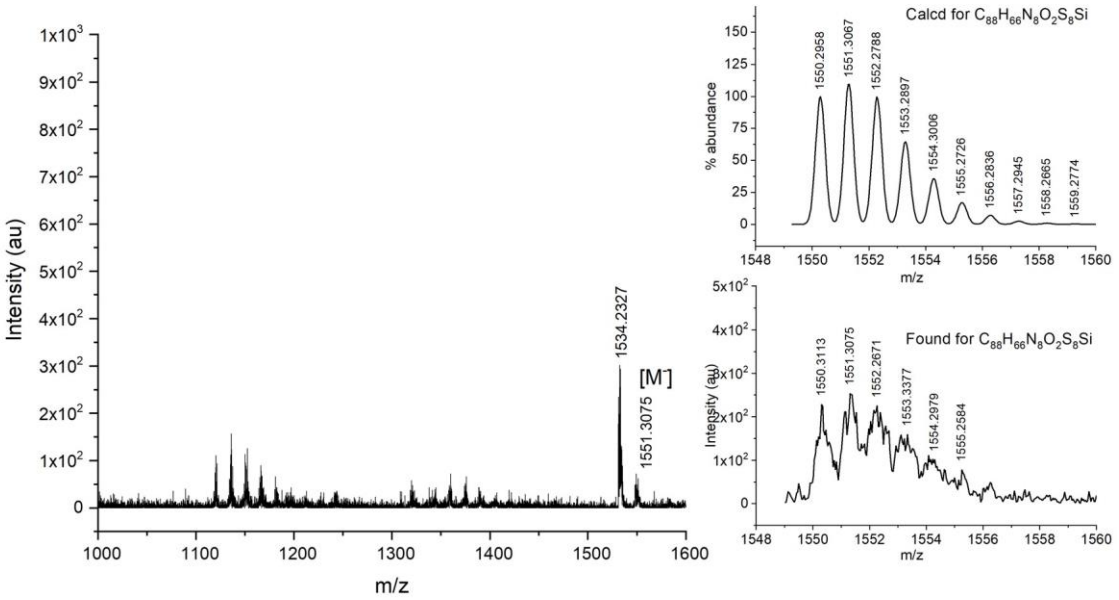

Figure S 7. HR-MALDI TOF spectrum (positive mode) of $(ArS)_8SiPc(OH)_2$ **11**.

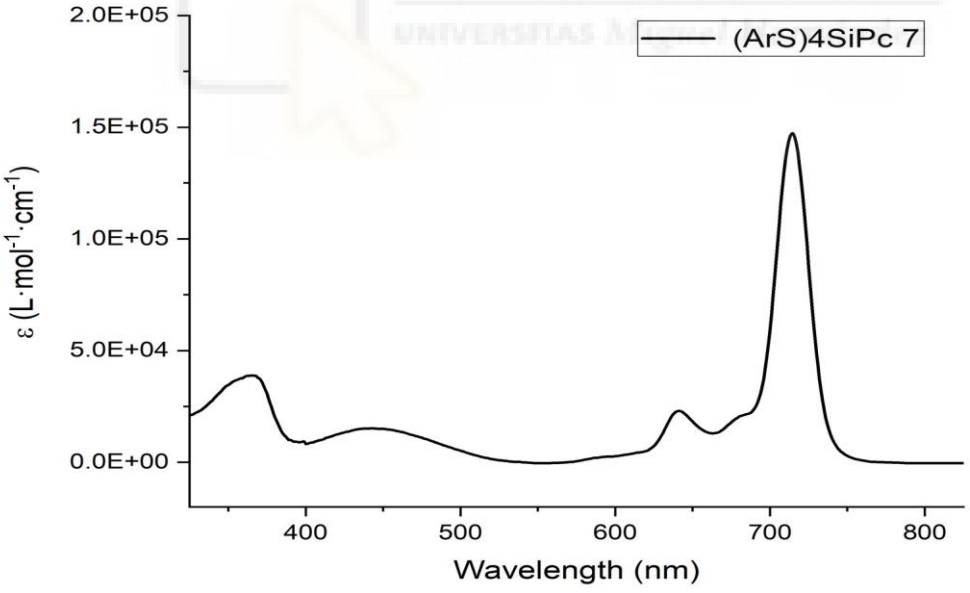

Figure S 8. ^1H NMR spectrum, registered in $CDCl_3$ at RT, of $(ArS)_8SiPc$ **12**.

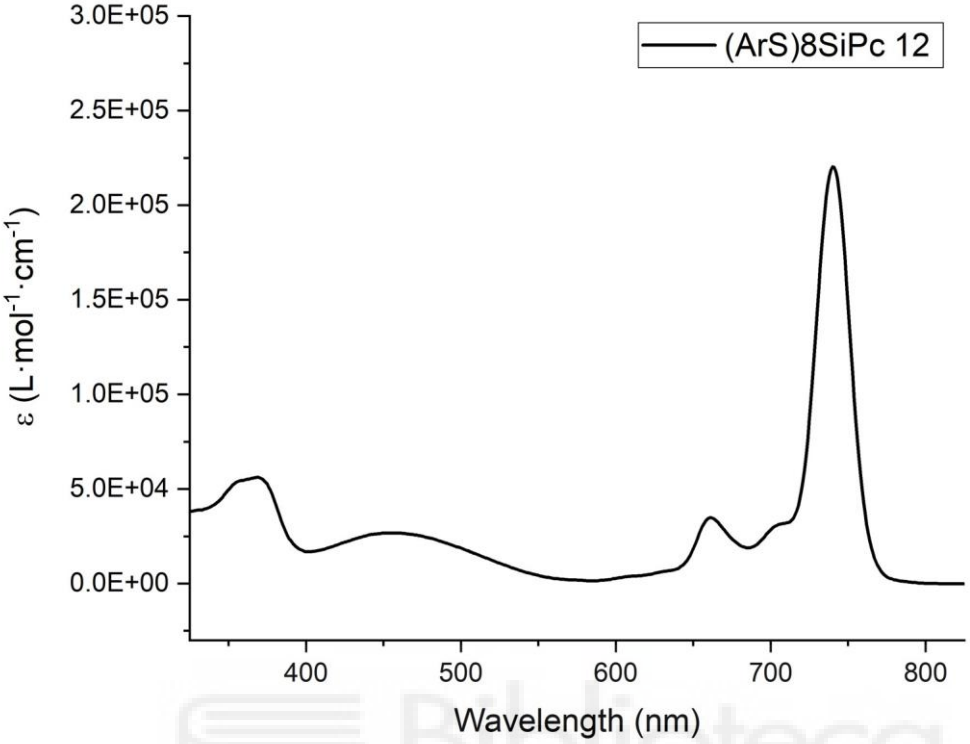

Figure S 9. UV-vis spectrum, registered in $CHCl_3$ at RT of $(ArS)_8SiPc$ **12**.

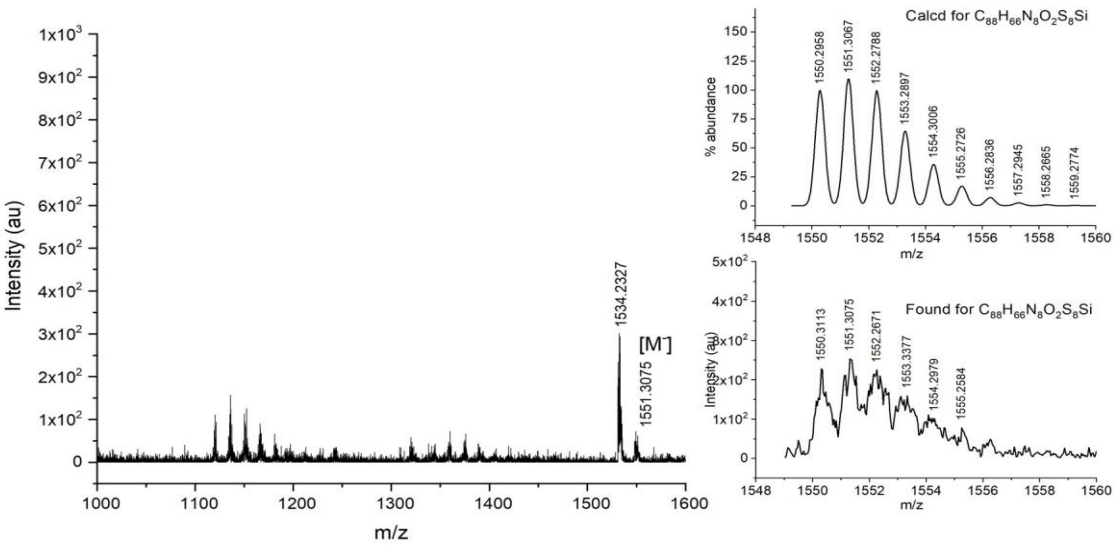

Figure S 10. HR-MALDI TOF spectrum (positive mode) of $(ArS)_8SiPc$ **12**.

2.2 Article :" Tunable J-type aggregation of silicon phthalocyanines in a surface-anchored metal–organic framework thin film"

Cite this: *Phys. Chem. Chem. Phys.*,
2023, 25, 19626

Introduction

Tunable J-type aggregation of silicon phthalocyanines in a surface-anchored metal–organic framework thin film†

Hongye Chen,[a] Luis Martín-Gomis,[b] Zhiyun Xu,[a] Jan C Fischer,[c] Ian A Howard,[c] David Herrero,[b] Víctor Sobrino-Bastán,[b] Ángela Sastre-Santos,[*b] Ritesh Haldar*[d] and Christof Wo¨ll[*a]

Organic chromophores and semiconductors, like anthracene, pentacene, perylene, and porphyrin, are prone to aggregation, and their packing in the solid state is often hard to predict and difficult to control. As the condensed phase structures of these chromophores and semiconductors are of crucial importance for their optoelectronic functionality, strategies to control their assembly and provide new structural motifs are important. One such approach uses metal–organic frameworks (MOFs); the organic chromophore is converted into a linker and connected by metal ions or nodes. The spatial arrangement of the organic linkers can be well-defined in a MOF, and hence optoelectronic functions can be adjusted accordingly. We have used such a strategy to assemble a phthalocyanine chromophore and illustrated that the electronic inter-phthalocyanine coupling can be rationally tuned by introducing bulky side grounds to increase steric hindrance. We have designed new phthalocyanine linkers and using a layer-by-layer liquid-phase epitaxy strategy thin films of phthalocyanine-based MOFs have been fabricated and their photophysical properties explored. It was found that increasing the steric hindrance around the phthalocyanine reduced the effect of J-aggregation in the thin film structuresaround the phthalocyanine reduced the effect of J-aggregation in the thin film structures.

Introduction

Metal–organic frameworks (MOFs) are crystalline, permanently porous solids.[1] MOFs, also known as porous coordination polymers (PCPs), are obtained by linking metal ions or metaloxo nodes with functionalized organic linkers. Since huge libraries exist for each of these building blocks, the number of metal and organic linker combinations is virtually infinite and many different topologies of MOFs have been reported till date.[2] Based on the connectivities and geometries of the constituents, the porosity in MOFs can vary and surface areas as high as B7000 m^2 g^1 have been reported.[3] This provides the basis for many applications; e.g. gas storage, separation,[4,5] catalysis[6,7] and sensing.[8,9] In addition to their high intrinsic porosity, MOFs also offer the possibility to assemble functional organic molecules into structures with predefined packing and spatial geometry. In this context, isoreticular strategies are of pronounced interest.[10,11] In the context of photoactive materials, recently in particular MOF-based optoelectronic applications have received substantial attention.[12–15]

The crystalline structure of MOFs allows to precisely determining the positions of the organic linkers and the metal ion nodes. Hence, standard quantum chemistry codes can be applied in a straightforward fashion to interpret experimental findings, a task which is substantially more complicated for amorphous materials. In addition, possible structures can be investigated in silico prior to the experimental realization.[16,17] The inter-linker and metal ion distances as well as the overall geometry are crucial parameters to tune the electronic coupling between the MOF building blocks. Properties like electron transfer, energy transfer, charge mobility, and recombination rate can show pronounced variations for even slight variation of structural parameters. Hence MOFs can provide excellent model systems to study electronic and optical properties of chromophoric assemblies. In addition, these materials can be integrated into devices in a straightforward fashion, as has been demonstrated in a number of cases, including photovoltaics, light emitting diodes, and transistor-related applications.[18,19] In recent years, the following properties and applications have been explored for MOFs; metallic conductivity,[20,21] high charge carrier mobilities,[22] charge transfer,[23] light emitting diodes,[24] photovoltaics,[25] efficient and anisotropic energy transfer,[26] photodiodes,[27] integration of electric fields,[28] and thermoelectric effects.[29] For many of these applications, the most common form of MOFs, polycrystalline powder, is not well suited since the integration of particulate material into devices represents a major challenge. For numerous types of model systems and devices, the fabrication of MOF thin films deposited on a conducting or transparent surface is required. For this reason, a number of different methods have been developed for MOF thin film deposition. In the present paper, we have employed the surface-anchored MOF (SURMOF) approach to fabricate optically active silicon-phthalocyanine-based MOF thin films exhibiting J-type electronic coupling.

Different organic semiconductors, e.g. anthracene, perylene, pentacene, perylenediimides, naphthalenediimide, porphyrin and phthalocyanine have been assembled into MOF structures, and also as MOF thin films.[16,30–37] Phthalocyanines, with their unique macrocyclic structure, exhibit strong p–p interactions and can self-assemble into supramolecular aggregates. However, this type of aggregation is not as common as in other chromophores due to the planar and rigid structure of phthalocyanine molecules, which restricts the formation of the required face-to-face stacking necessary for J-aggregate formation. Different strategies have been designed in order to achieve this kind of aggregation,[38] but the number of known cases is still rather limited. Since due to their rather special characteristics

[a] Institute of Functional Interfaces (IFG), Karlsruhe Institute of Technology (KIT), 76344 Eggenstein-Leopoldshafen, Germany. E-mail: christof.woell@kit.edu [b] A´rea de Quı´mica Orga´nica, Instituto de Bioingenierı´a, Universidad Miguel Herna´ndez, Avda Universidad S/N, 03202, Elche, Spain. E-mail: asastre@umh.es [c] Institute of Microstructure Technology, Karlsruhe Institute of Technology (KIT), 76344 Eggenstein-Leopoldshafen, Germany [d] Tata Institute of Fundamental Research Hyderabad, Gopanpally, Hyderabad 500046, India. E-mail: riteshhaldar@tifrh.res.in

† Electronic supplementary information (ESI) available. See DOI: https://doi.org/10.1039/d3cp01865b

phthalocyanine J aggregates are very promising candidates for applications in various optoelectronic devices, including organic solar cells, light-emitting diodes, and photodetectors, more rational strategies are required to assemble these highly interesting macrocycles into ordered arrays.

Here, we focus on silicon phthalocyanines (SiPcs) (see Fig. 1), chromophores which are known to exhibit strong absorption in the visible range (far-red) of the absorption spectrum. Along with an intense visible color, for these SiPc compounds the tendency towards aggregation (and thus to unwanted quenching of excitations by intermolecular coupling) is strongly reduced due to the presence of axial substitution of the Si. Hence, these SiPc molecules have received pronounced interest in the context of biological as well as optical applications.

For the integration of these chromophores into MOFs, the corresponding organic compounds need to be equipped with coupling groups, thus yielding a MOF linker. Hence, we have functionalized the SiPc compounds by attaching –COOH groups at the axial positions. Although at first sight the resulting ditopic linkers appear to be very bulky, we have demonstrated in previous work that MOF thin films can be successfully assembled from the SiPc 1 as linkers, with the resulting SURMOFs showing the formation of an interesting type of polaritons.[39] In this contribution, we demonstrate that the optical properties of SiPc-based SURMOFs can be varied in a rational fashion by tuning the intermolecular electronic coupling. We have designed three new sterically modulated silicon phthalocyanine dicarboxylate linkers (SiPc 2–4) and synthesized isostructural MOF thin films using the layer-by-layer liquid-phase epitaxy method. Introduction of the bulky tert-butyl and dimethylphenoxy groups in the SiPc linkers changes the linker–linker distance in the MOF structure, and thus the electronic coupling of the chromophores is modulated (Scheme 1). On the other hand, we have incorporated phenyl (SiPc 3) and biphenyl (SiPc 4) linkers in the axial SiPc position to study the effect of the axial linker in the SURMOF organization. A photophysical characterization of these new SiPc SURMOFs revealed that the SiPc linkers in the MOF structure exhibit J-type coupling. In the followings we have demonstrated how MOFbased design approach can be useful to systemically tune the J-type electronic coupling, which is important for many optoelectronics applications, including photovoltaics, and light emitting diodes.

Results and discussion

SiPc 2 was directly obtained from $(^t\mathrm{Bu})_4\mathrm{SiPc(ArCHO)_2}$ 5[40] through a mild oxidation step, employing a mixture of sulfamic acid and sodium chlorite in $\mathrm{THF/H_2O}$ at RT during 12 h

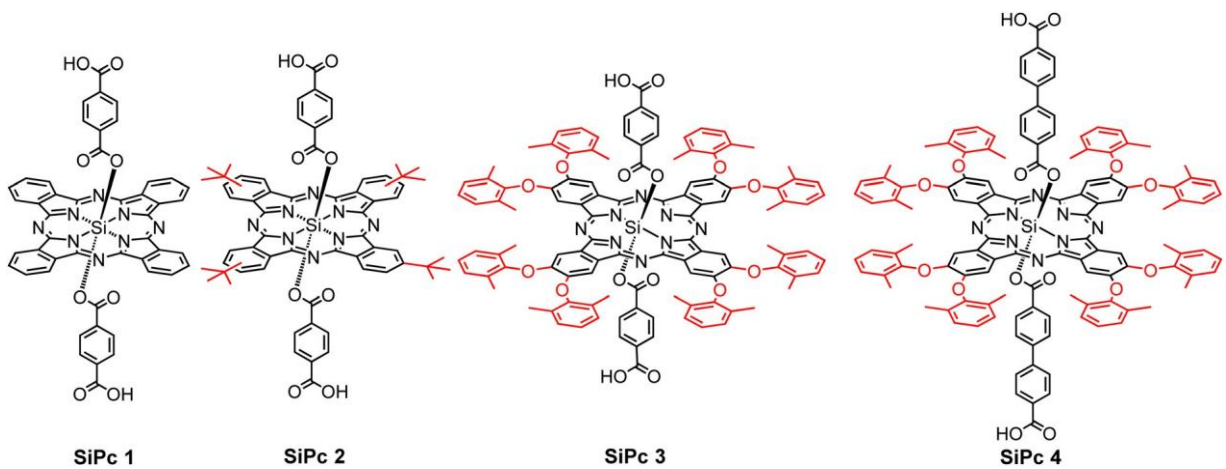

Fig. 1 Chemical structure of the four ditopic silicon phthalocyanine linkers.

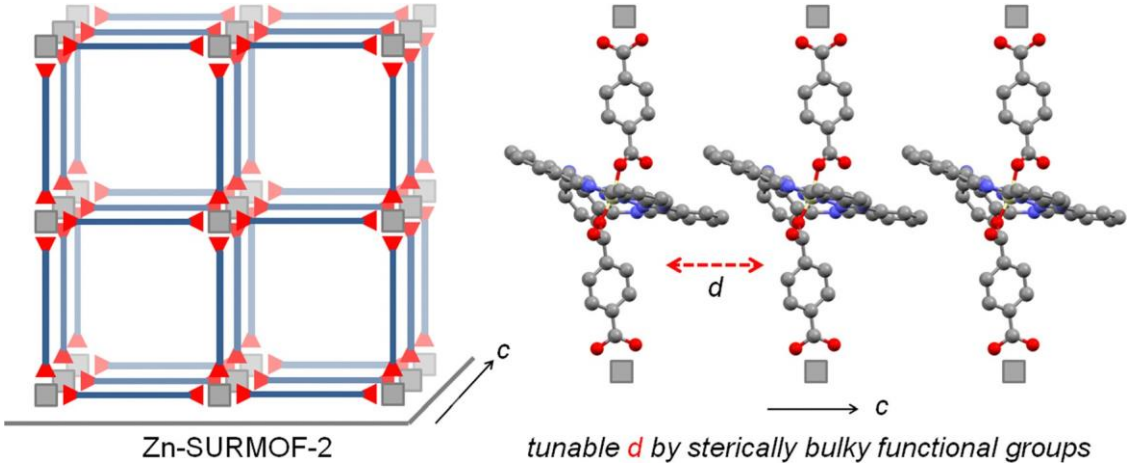

Scheme 1 Schematic illustration of the 3D assembly of SiPc linkers as a SURMOF-2 (left) and control of the inter-linker distance by sterically demandin functional group introduction to tune electronic couplin

(Scheme 2). On the other hand, SiPc 3 and SiPc 4 were obtained employing the already described mild oxidation protocol (Scheme 3), over both formyl groups of $(ArO)_8SiPc(ArCHO)_2$ 6 and $(ArO)_8SiPc(Ar_2CHO)_2$ 7, respectively.[41] All the new compounds were unambiguously characterized by ^{1}H NMR and UV-vis absorption spectroscopy, and HR MALDI-TOF mass spectrometry (see Experimental section and Fig. S1–S9, ESI†).

The designed SiPc linkers are linear and ditopic. These are thus suited, in principle, to coordinate to Zn-based paddlewheel type nodes to produce a SURMOF-2 type structure, as demonstrated in our previous works.[26,32,42] The SiPc linkerbased SURMOF-2 structure was fabricated using a layer-by-layer synthesis (Scheme 1).[43] The out-of-plane and in-plane X-ray diffraction (XRD) patterns suggested the presence of a 2D square grid of sheets stacked along the substrate plane ([010] direction) with a regular spacing of 1.1 nm,[39] as reported for similar Zn-based porphyrin-based SURMOFs.[25] In such a structure, the phthalocyanine aromatic plane is oriented orthogonal to the metal-coordination axis, and two phthalocyanines of the neighboring 2D sheets interact in an edge-to-edge fashion, as illustrated in Scheme 1. The newly synthesized SiPc 2, SiPc 3 and SiPc 4 linkers have bulkier substituents in comparison to

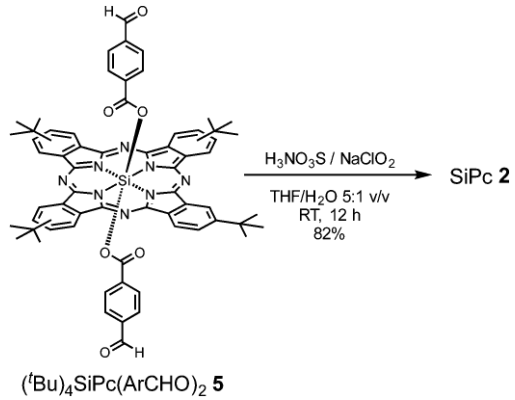

Scheme 2 Synthesis scheme of SiPc 2.

the SiPc 1, and these are marked in red in Fig. 1. Due to the presence of the sterically demanding functional groups, we expected that the inter-layer spacing will increase[16] for these three new SiPc linkers, leading to a different electronic coupling in the corresponding MOF structures.

The out-of-plane and in-plane XRD patterns of Zn-SiPc 2 are very similar to that obtained from the Zn-SiPc 1, indicating the presence of a similar structure (Fig. 2b and Fig. S10, ESI†). This is expected as the length of the SiPc 2 linker (i.e. distance between the two carboxylic acid groups) is identical to SiPc 1. In contrast, for the Zn-SiPc 3, most likely due to the hindrance of the dimethylphenoxy groups, no crystalline thin film was obtained. For Zn-SiPc 4, the XRD pattern revealed that the square grid unit cell dimension is larger, B2.9 nm. This is due to the increased length of the SiPc 4 linker along the metalcoordination axis. A detailed characterization of the SiPc-based SURMOFs using infra-red reflection absorption spectroscopy was fully consistent with the presence of paddle-wheel nodes (Fig. S11, ESI†). The scanning electron microscopy (SEM) images of the Zn-SiPc 2 and Zn-SiPc 4 confirmed the continuous thin film formation (Fig. S12, ESI†).

After the structural and spectroscopic characterization of the Zn-SiPc SURMOFs, we have carried out a photophysical characterization of the thin films. In Fig. 3, we present the absorption spectra of the three SiPc linkers (SiPc 1, SiPc 2 and SiPc 4) recorded for their solvated state and for the SURMOFs. In the solvated state, the SiPc 1 linker shows a sharp intense peak at 683 nm, corresponding to the Q-band. The Soret band transition appears at B350 nm. As a result of the tertiary butyl and phenoxy substitution of the SiPc, the Q-band maxima is shifted to higher wavelengths, 691 and 694 nm, respectively. After assembly into the SURMOF, all the Q-band peaks shift to longer wavelength compared to the solvated linkers. The red shift is largest for Zn-SiPc 1, B57 nm. For SiPc 2 and 4, the shifts are smaller and amount to B29 and B10 nm, respectively. Evidently, the different

packing of the chromophores resulting from the coordination to the metal and to yield the SURMOF-2 structure enforces an edge-to-edge SiPc stacking and yields a change

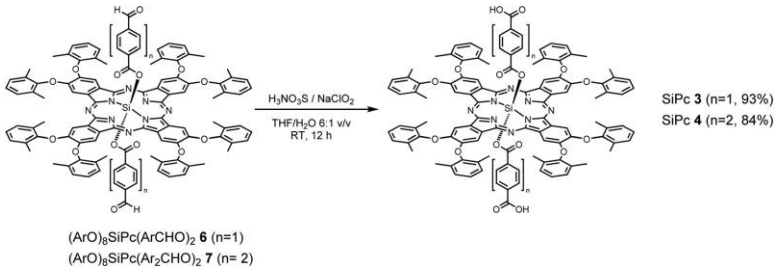

Scheme Synthesis scheme of an SiPc

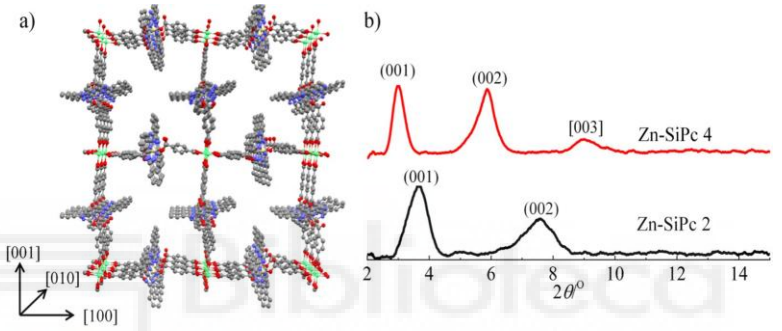

Fig. (a) A model structure of SiPc (b) out-of-plane XRD Zn-SiPc an 4

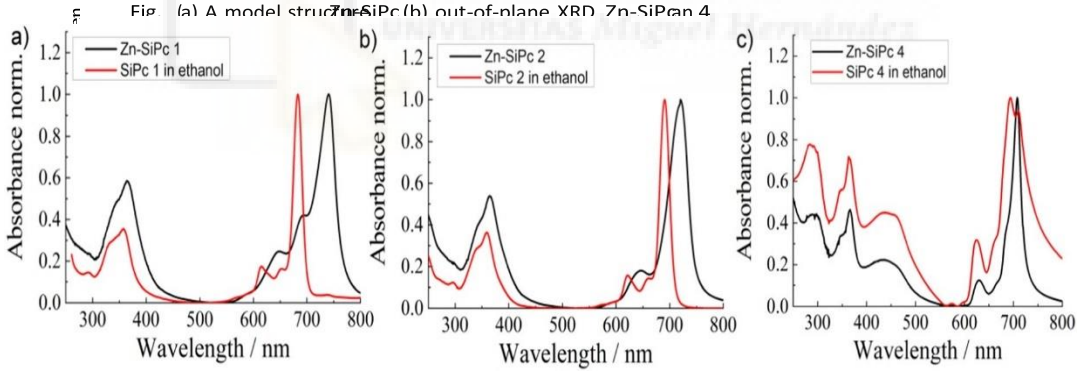

in the Q-band transitions. The transition dipoles governing the corresponding excitation are aligned in a head-totail fashion and the lowering of the electronic transition energy indicates a J-type electronic coupling between the SiPc linkers of neighboring 2D layers. The solvatochromic shift,[44] i.e. the difference of the Q-band maximum observed for the solvated state and the SURMOF state, can

be considered as a measure of the strength of the J-type electronic coupling. As in Zn-SiPc 1 the linkers of the neighboring 2D layers are closer in space than in the cases of Zn-SiPc 2 and 4, the electronic coupling is strongest, and hence the solvatochromic shift is largest. For Zn-SiPc 3, because of the very bulky substitution on SiPc, the 2D layers are not close enough to induce strong electronic coupling. Hence, using this sterically bulky substitution approach, it is possible to fine tune electronic coupling. Note, that while inducing such changes in the chromophore–chromophore

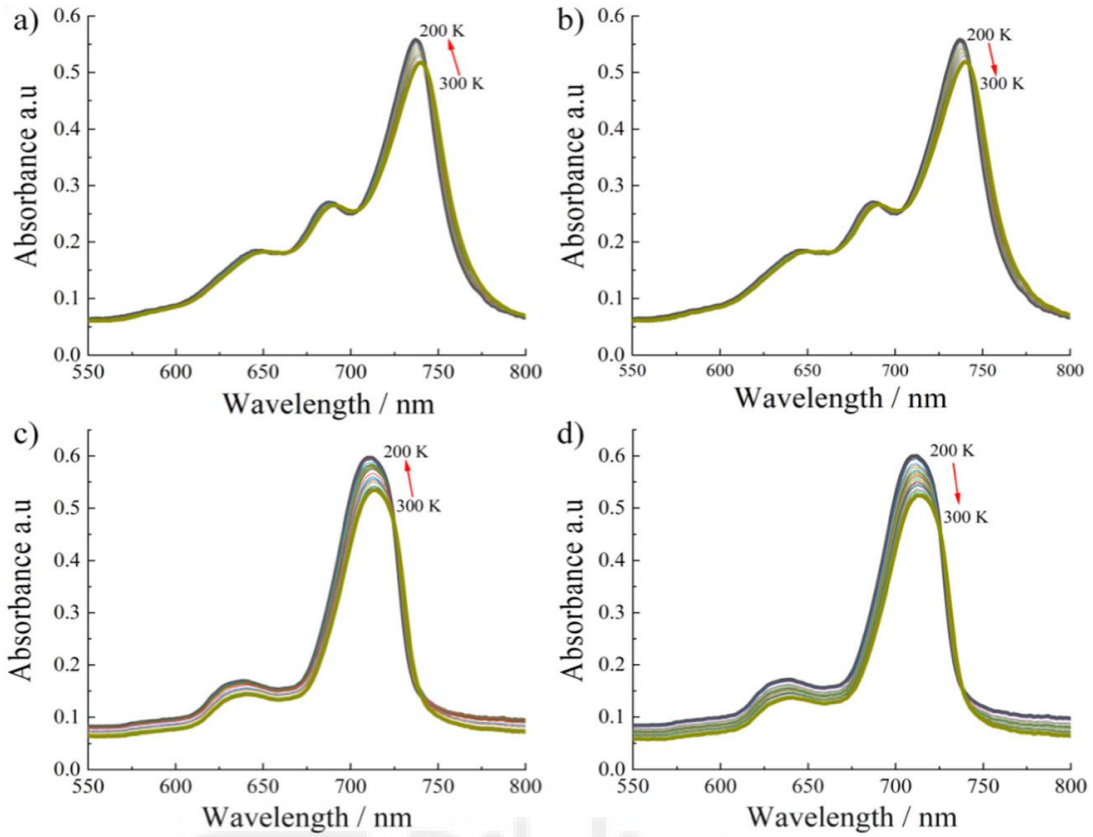

spacing via adding steric control units, the overall topology of the MOF structure does not change. To gain further information on the photophysical properties of these aggregated SiPc linkers, we have carried out temperature dependent absorption spectra measurements for non-substituted Zn-SiPc 1 (Fig. 4a and b) and for the bulkiest substitution, Zn-SiPc 4 (Fig. 4c and d). For both SURMOFs, a B4 nm blue shift was observed upon lowering the temperature. Similar spectral change indicates that the electronic coupling nature may be similar. As we have observed very small bathochromic shift for Zn-SiPc 4 compared to the monomer state of SiPc 4, the electronic coupling can be considered weak. However similar temperature dependency confirms that for both of the structures J-coupling is present.

Conclusion

In conclusion, we have synthesized three new SiPc dicarboxylic acids and demonstrated that two of them can be used as organic linkers to fabricate MOF thin films, or SURMOFs, using a layer-bylayer approach. We propose a SURMOF-2 type structure for the corresponding MOF thin films, where the SiPc linkers are connected by Zn-paddle-wheel nodes to form a 2D layer. These 2D layers are then arranged to yield stacks with the individual planes oriented perpendicular to the substrate. Within this 3D structure, the SiPc linkers of the neighboring 2D layers interact in an edgeto-edge fashion. From a photophysical characterization we conclude that this interaction leads to J-type electronic coupling. By using the isoreticular MOF design principle, we have designed MOF films with different extent of J-coupling interactions, as evidenced by the absorption spectra measurements. Temperature dependent measurements indicated that even with the bulky substitution, J-type coupling remains intact. The strategy presented here illustrates that in MOF electronic interactions can be modulated with fine control, and the consequent electronic and optical properties can be studied in a straightforward fashion using the thin film structure.

Experimental section

Zinc acetate dihydrate was purchased from Merck Millipore. 16-Mercaptohexadecanoic acid (MHDA, 97%), was purchased from Sigma-Aldrich (Germany). Absolute ethanol was purchased from VWR (Germany). All other chemicals were reagent grade, purchased from commercial sources, and were used as received unless otherwise specified. NMR spectra were acquired on a Bruker 400 MHz spectrometer. UV-vis spectra were recorded on a PerkinElmer LAMBDA 365 UV-WinLab spectrophotometer (for the solution). The thin film (grown on quartz glass) spectra were recorded in transmission mode, using a Cary 5000 spectrometer with a UMA unit from Agilent. The SEM measurements were carried out using a Field Emission Gun (FEI) Philips XL SERIES 30 ESEM-FEG (FEI Co., Eindhoven, NL). Thin films were coated with a B5 nm thick gold/palladium film before recording the SEM micrographs. High-Vacuum (1.5 torr) was applied with all specimen, using 20 keV acceleration voltage. High-resolution mass spectra were obtained from a Bruker Reflex II matrix-assisted laser desorption/ionization time-offlight (MALDI-TOF) spectrometer using dithranol as matrix. Fig. 4 Temperature dependent absorption spectra for (a), (b) Zn-SiPc 1 and (c), (d) Zn-SiPc 4. PCCP Paper Open Access Article. Published on 03 July 2023. Downloaded on 12/9/2025 4:14:07 PM. This article is licensed under a Creative Commons Attribution 3.0 Unported Licence. View Article Online This journal is © the Owner Societies 2023 Phys. Chem. Chem. Phys., 2023, 25, 19626–19632 | 19631 The XRD measurements for out-of-plane (co-planar orientation) were carried out using a Bruker D8-Advance diffractometer equipped with a position sensitive detector Lynxeye in geometry, variable divergence slit and 2.31 Soller-slit was used on the secondary side. The Cu-anodes which utilize the Cu Ka1,2-radiation (l = 0.154018 nm) were used as source. The temperature-dependent absorption measurements were carried out with the sample situated in a closed-cycle Helium cryostat (Oxford Instruments OptistatDry TLEX). The cryostat sample chamber was evacuated to a pressure of o104 hPa. In a temperature range from 300 K to 200 K, the sample was illuminated with collimated white-light that was then captured by a spectrometer. A fiber-coupled Ocean Optics DH-2000-BAL Deuterium–Halogen lamp served as a white-light source using one output port of a bifurcated optical fiber (QBIF600-UV-BX). The transmitted spectrum was recorded with an Avantes AvaSpec-2048L-USB2 spectrometer with a Thorlabs FP1000URT optical fiber attached.

Preparation of SiPc 2

(^{t}Bu)$_4$SiPc(ArCHO)$_2$ 4 (50 mg, 0.048 mmol), sulfamic acid (H_3NO_3S, 35 mg, 0.361 mmol) and sodium chlorite (25 mg, 0.276 mmol) in a 5:1 THF/H_2O mixture (18 mL) were stirred at room temperature, and avoiding direct light exposure, for 12 h. The crude product was evaporated to dryness, and repeatedly washed with 1:1 MeOH/H_2O mixture, in order to obtain 42 mg of pure product (82%) as blue-green solid. HR-MS (MALDI-TOF, dithranol) m/z [M] calcd for $C_{64}H_{58}N_8O_8Si$ 1094.4251; found 1094.4257. ^{1}H NMR (400 MHz, DMSO-d_6) d 9.79–9.58 (m, 8H, Pc-Ar-H), 8.70–8.60 (m, 4H, Pc-Ar-H), 6.87 (d, J = 8.4 Hz, 4H, Ar-H), 5.13 (d, J = 8.5 Hz, 4H, Ar-H), 1.79–1.73 (m, 36H, 4^{t}Bu). UV-vis (THF): l_{max}, nm (loge) 360 (5.21), 620 (5.18), 690 (5.89).

Preparation of SiPc 3

(ArO)$_8$SiPc(ArCHO)$_2$ 6 (70 mg, 0.039 mmol), sulfamic acid (H_3NO_3S, 59 mg, 0.608 mmol) and sodium chlorite (42 mg, 0.464 mmol) in a 4:1 THF/H_2O mixture (25 mL) were stirred at room temperature, and avoiding direct light exposure, for 24 h. The crude product was evaporated to dryness, and repeatedly washed with 1:1 MeOH/H_2O mixture, to obtain 66 mg of pure product (93%) as blue-green solid. HR-MS (MALDI-TOF, dithranol): m/z [M] calcd for $C_{112}H_{90}N_8O_{16}Si$ 1831.6278; found

1831.6441. ^{1}H NMR (400 MHz, DMSO-d_6) d 8.02 (8H, m, H-Pc), 7.62–7.45 (24H, m, H-Ar), 6.78 (4H, d, J = 8.3Hz, H-Ar), 4.86 (4H, d, J = 8.3Hz, H-Ar), 2.36 (48H, s, 16 CH_3). UV-vis (THF): l_{max}, nm (loge) 366 (4.98), 426 (4.54), 624 (4.56), 665 (4.55), 694 (5.42).

Preparation of SiPc 4

$(ArO)_8SiPc(Ar_2CHO)_2$ 7 (35 mg, 0.018 mmol), sulfamic acid (H_3NO_3S, 28 mg, 0.288 mmol) and sodium chlorite (20 mg, 0.288 mmol) in a 6:1 THF/H_2O mixture (12 mL) were stirred at room temperature, and avoiding direct light exposure, for 12 h. The crude product was evaporated to dryness, and repeatedly washed with 1:1 MeOH/H_2O mixture, to obtain 30 mg of pure product (84%) as blue-green solid. HR-MS (MALDI-TOF, dithranol): m/z $[M]^+$ calcd for $C_{124}H_{98}N_8O_{16}Si$ 1983.6904; found 1983.6744.

^{1}H NMR (400 MHz, $CDCl_3$) d 8.20 (8H, m, H-Pc), 7.79 (4H, d, J: 8.3 Hz, H-Ar), 7.36 (24H, brs, H-Ar), 7.02 (4H, d, J: 8.3 Hz, H-Ar), 6.46 (4H, d, J: 8.3 Hz, H-Ar), 5.14 (4H, d, J: 8.3 Hz, H-Ar), 2.42 (48H, s, 16 CH_3). UV-vis (THF): l_{max}, nm (loge) 366 (4.89), 424 (4.46), 623 (4.49), 666 (4.52), 692 (5.33).

Preparation of Zn-SiPc 2 and Zn-SiPc 4

Syntheses of the SURMOFs are carried out following the previous procedure. Ethanolic solution of 1 mM zinc acetate and 20 mM SiPc 2/4 solutions (in ethanol) were sequentially deposited onto the precleaned substrates (cleaned by UV-ozone, Si or quartz glass) using spin coating method in a layer-by-layer fashion. After the metal or linker coating, the samples were rinsed with ethanol to remove unreacted metal/linker or byproducts from the surface. For metal and linker both, the spin coating time is fixed as 10 s with rpm of 2000.

Conflicts of interest

There are no conflicts to declare.

Acknowledgements

H. C. acknowledges financial support from China Scholarship Council (CSC, no. 201806830055). A. S. S. thanks the European Regional Development Fund ‘‘A way to make Europe’’ and the Spanish Ministerio de Ciencia e Innovacio´n/Agencia Estatal de Investigacio´n (PID2020-117855 RB-I00) and the Advanced Materials program by MCIN with funding from European Union NextGenerationEU (PRTR-C17.I1) and Generalitat Valenciana (MFA/2022/028) for funding. R. H. acknowledges intramural funds at TIFR Hyderabad from the Department of Atomic Energy (DAE), India, under project identification number RTI 4007. C. W. acknowledges support from Deutsche Forschungsgemeinschaft (DFG, German Research Foundation) under Germany’s Excellence Strategy – 2082/1 – 390761711.

References

1 H. Furukawa, K. E. Cordova, M. O’Keeffe and O. M. Yaghi, Science, 2013, 341, 1230444.

2 N. Stock and S. Biswas, Chem. Rev., 2012, 112, 933–969.

3 O. K. Farha, I. Eryazici, N. C. Jeong, B. G. Hauser, C. E. Wilmer, A. A. Sarjeant, R. Q. Snurr, S. T. Nguyen, A. O¨. Yazaydın and

J. T. Hupp, J. Am. Chem. Soc., 2012, 134, 15016–15021. 4 J.-R. Li, J. Sculley and H.-C. Zhou, Chem. Rev., 2012, 112, 869–932.

5 Q. Qian, P. A. Asinger, M. J. Lee, G. Han, K. Mizrahi Rodriguez, S. Lin, F. M. Benedetti, A. X. Wu, W. S. Chi and Z. P. Smith, Chem. Rev., 2020, 120, 8161–8266. 6 V. Pascanu, G. Gonza´lez Miera, A. K. Inge and B. Martı´nMatute, J. Am. Chem. Soc., 2019, 141, 7223–7234. 7 A.

Bavykina, N. Kolobov, I. S. Khan, J. A. Bau, A. Ramirez and J. Gascon, Chem. Rev., 2020, 120, 8468–8535.

8 L. E. Kreno, K. Leong, O. K. Farha, M. Allendorf, R. P. Van Duyne and J. T. Hupp, Chem. Rev., 2012, 112, 1105–1125. 9 H.-Y. Li, S.-N. Zhao, S.-Q. Zang and J. Li, Chem. Soc. Rev., 2020, 49, 6364–6401.

10 Z. Mai and D. Liu, Cryst. Growth Des., 2019, 19, 7439–7462.

11 M. Eddaoudi, J. Kim, N. Rosi, D. Vodak, J. Wachter, M. O'Keeffe and O. M. Yaghi, Science, 2002, 295, 469–472. 12 R. Haldar, L. Heinke and C. Wo¨ll, Adv. Mater., 2020, 32, 1905227.

13 R. Haldar, A. Ghosh and T. K. Maji, Chem. Commun., 2023, 59, 1569–1588.

14 V. Stavila, A. A. Talin and M. D. Allendorf, Chem. Soc. Rev., 2014, 43, 5994–6010.

15 G. A. Leith, C. R. Martin, J. M. Mayers, P. Kittikhunnatham, R. W. Larsen and N. B. Shustova, Chem. Soc. Rev., 2021, 50, 4382–4410.

16 R. Haldar, A. Mazel, M. Krstic´, Q. Zhang, M. Jakoby, I. A. Howard, B. S. Richards, N. Jung, D. Jacquemin, S. Diring, W. Wenzel,

F. Odobel and C. Wo¨ll, Nat. Commun., 2019, 10, 2048.

17 M. Mostaghimi, C. R. C. Reˆgo, R. Haldar, C. Wo¨ll, W. Wenzel and M. Kozlowska, Front. Mater., 2022, 9, 840644. 18 G. Wu, J. Huang, Y. Zang, J. He and G. Xu, J. Am. Chem. Soc., 2017, 139, 1360–1363.

19 D.-H. Chen, H. Gliemann and C. Wo¨ll, Chem. Phys. Rev., 2023, 4, 011305.

20 A. J. Clough, N. M. Orchanian, J. M. Skelton, A. J. Neer, S. A. Howard, C. A. Downes, L. F. J. Piper, A. Walsh, B. C. Melot and S. C. Marinescu, J. Am. Chem. Soc., 2019, 141, 16323–16330. 21 L. S. Xie, G. Skorupskii and M. Dinca˘, Chem. Rev., 2020, 120, 8536–8580.

22 R. Dong, P. Han, H. Arora, M. Ballabio, M. Karakus, Z. Zhang, C. Shekhar, P. Adler, P. S. Petkov, A. Erbe, S. C. B. Mannsfeld, C. Felser, T. Heine, M. Bonn, X. Feng and E. Ca´novas, Nat. Mater., 2018, 17, 1027–1032.

23 B. Liu and V. S. Thoi, Chem. Mater., 2020, 32, 8450–8459.

24 M. Gutie´rrez, C. Martı´n, M. Van der Auweraer, J. Hofkens and J.-C. Tan, Adv. Opt. Mater., 2020, 8, 2000670.

25 J. Liu, W. Zhou, J. Liu, I. Howard, G. Kilibarda, S. Schlabach, D. Coupry, M. Addicoat, S. Yoneda, Y. Tsutsui, T. Sakurai,S. Seki, Z. Wang, P. Lindemann, E. Redel, T. Heine and C. Wo¨ll, Angew. Chem., Int. Ed., 2015, 54, 7441–7445.

26 R. Haldar, M. Jakoby, A. Mazel, Q. Zhang, A. Welle, T. Mohamed, P. Krolla, W. Wenzel, S. Diring, F. Odobel, B. S. Richards,

I. A. Howard and C. Wo¨ll, Nat. Commun., 2018, 9, 4332.

27 H. Arora, R. Dong, T. Venanzi, J. Zscharschuch, H. Schneider, M. Helm, X. Feng, E. Ca´novas and A. Erbe, Adv. Mater., 2020, 32, 1907063.

28 A. Nefedov, R. Haldar, Z. Xu, H. Ku¨hner, D. Hofmann, D. Goll, B. Sapotta, S. Hecht, M. Krstic´, C. Rockstuhl, W. Wenzel, S. Bra¨se, P. Tegeder, E. Zojer and C. Wo¨ll, Adv. Mater., 2021, 33, 2103287.

29 Y. He, C. D. Spataru, F. Le´onard, R. E. Jones, M. E. Foster, M. D. Allendorf and A. Alec Talin, Phys. Chem. Chem. Phys., 2017, 19, 19461–19467.

30 R. Haldar, M. Kozlowska, M. Ganschow, S. Ghosh,

M. Jakoby, H. Chen, F. Ghalami, W. Xie, S. Heidrich,

Y. Tsutsui, J. Freudenberg, S. Seki, I. A. Howard, B. S. Richards, U. H. F. Bunz, M. Elstner, W. Wenzel and

C. Wo¨ll, Chem. Sci., 2021, 12, 4477–4483.

31 M. Kozlowska, Y. Pramudya, M. Jakoby, S. Heidrich, L. Pan,
B. S. Richards, I. A. Howard, C. Wo¨ll, R. Haldar and

W. Wenzel, J. Phys.: Condens. Matter, 2021, 33, 034001.

32 R. Haldar, K. Batra, S. M. Marschner, A. B. Kuc, S. Zahn, R. A. Fischer, S. Bra¨se, T. Heine and C. Wo¨ll, Chem. - Eur. J., 2019, 25, 7847–7851.

33 S. S. Rajasree, X. Li and P. Deria, Commun. Chem., 2021, 4, 47.

34 S. De, T. Devic and A. Fateeva, Dalton Trans., 2021, 50, 1166–1188.

35 M. Wang, Z. Zhang, H. Zhong, X. Huang, W. Li, M. Hambsch, P. Zhang, Z. Wang, P. Petkov, T. Heine, S. C. B. Mannsfeld, X. Feng and R. Dong, Angew. Chem., Int. Ed., 2021, 60, 18666–18672.

36 J.-R. Zhang, H.-Y. Zhang, J.-H. Guo, Z.-H. Liu, C.-Y. Ma, X.-G. Yang, X.-Y. Lu, J.-H. Qin and L.-F. Ma, Dalton Trans., 2022, 51, 1769–1774.

37 P. I. Scheurle, A. Biewald, A. Ma¨hringer, A. Hartschuh, D. D. Medina and T. Bein, Small Struct., 2022, 3, 2100195. 38 Z. Chen, C. Zhong, Z. Zhang, Z. Li, L. Niu, Y. Bin and F. Zhang, J. Phys. Chem. B, 2008, 112, 7387–7394.

39 R. Haldar, Z. Fu, R. Joseph, D. Herrero, L. Martı´n-Gomis, B. S. Richards, I. A. Howard, A. Sastre-Santos and C. Wo¨ll, Chem. Sci., 2020, 11, 7972–7978.

40 L. Martı´n-Gomis, K. Ohkubo, F. Ferna´ndez-La´zaro, S. Fukuzumi and A´. Sastre-Santos, Org. Lett., 2007, 9, 3441–3444.

41 L. Martı´n-Gomis, S. Seetharaman, D. Herrero, P. A. Karr, F. Ferna´ndez-La´zaro, F. D'Souza and A´. Sastre-Santos, Chem. Phys. Chem., 2020, 21, 2254–2262.

42 J. Liu, B. Lukose, O. Shekhah, H. K. Arslan, P. Weidler,
H. Gliemann, S. Bra¨se, S. Grosjean, A. Godt, X. Feng, K. Mu¨llen, I.-B. Magdau, T. Heine and C. Wo¨ll, Sci. Rep., 2012, 2, 921.

43 O. Shekhah, H. Wang, S. Kowarik, F. Schreiber, M. Paulus, M. Tolan, C. Sternemann, F. Evers, D. Zacher, R. A. Fischer and C. Wo¨ll, J. Am. Chem. Soc., 2007, 129, 15118–15119. 44 A. Ferencz, D. Neher, M. Schulze, G. Wegner, L. Viaene and F. C. De Schryver, Chem. Phys. Lett., 1995, 245, 23–29.

2.2.1 Suporting information of article :" Tunable J-type aggregation of silicon phthalocyanines in a surface-anchored metal–organic framework thin film"

Electronic Supplementary Material (ESI) for Physical Chemistry Chemical Physics.

Tunable J-type aggregation of silicon phthalocyanines in surface-anchored metal-organic framework thin film

Hongye Chen,[a] Luis Martín-Gomis,[b] Zhiyun Xu,[a] Jan C Fischer,[c] Ian A Howard,[c] David Herrero,[b] Víctor Sobrino-Bastán,[b] Ángela Sastre-Santos[b]*, Ritesh Haldar,[d]* and Christof Wöll[a]*

[a]Institute of Functional Interfaces (IFG), Karlsruhe Institute of Technology (KIT), 76344 EggensteinLeopoldshafen (Germany).

[b]Área de Química Orgánica, Instituto de Bioingeniería, Universidad Miguel Hernández, Avda Universidad S/N, 03202, Elche, Spain.

[c]Institute of Microstructure Technology, Karlsruhe Institute of Technology (KIT), 76344 EggensteinLeopoldshafen (Germany).

[d]Tata Institute of Fundamental Research Hyderabad, Gopanpally, Hyderabad 500046, India

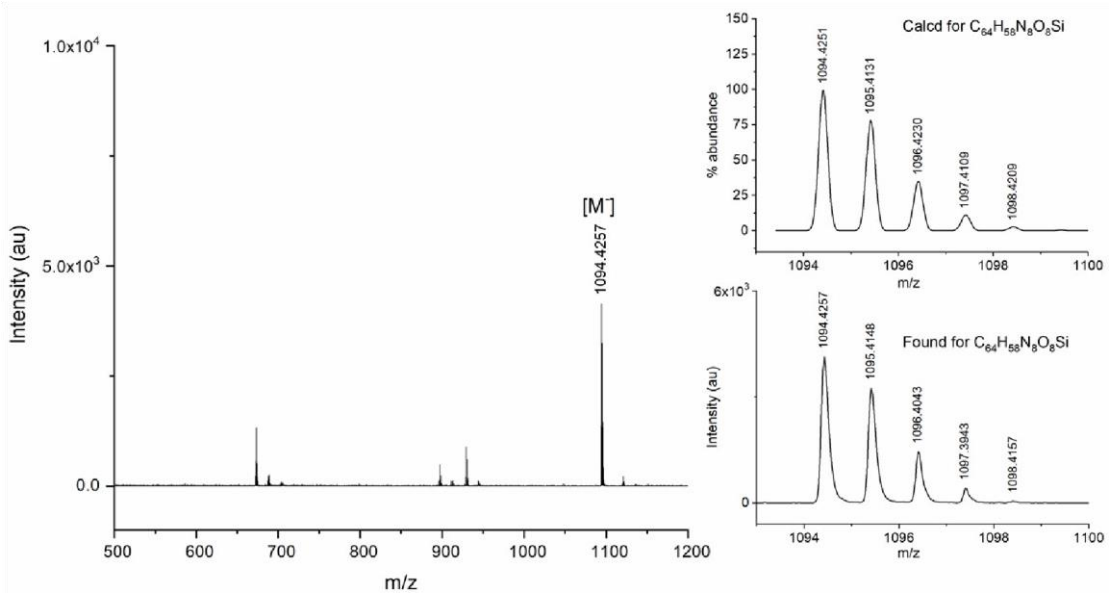

Fig. S1 HR-MS MALDI ToF spectra of **SiPc 2**.

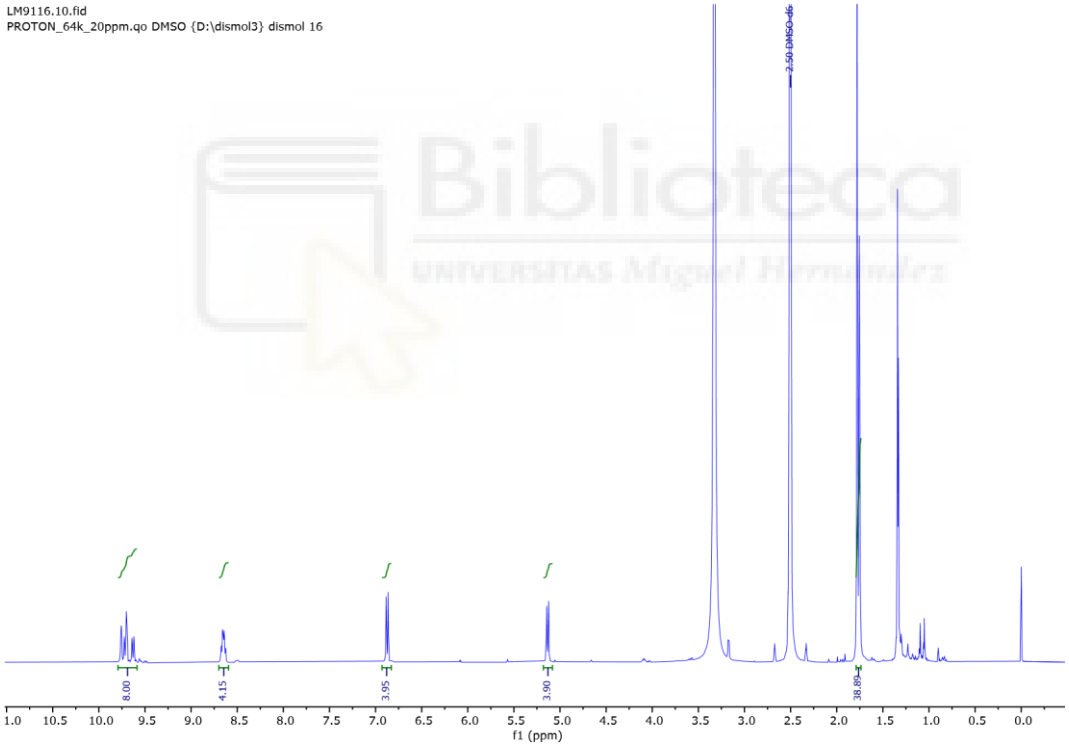

Fig. S2 ^{1}H NMR spectrum of **SiPc 2**.

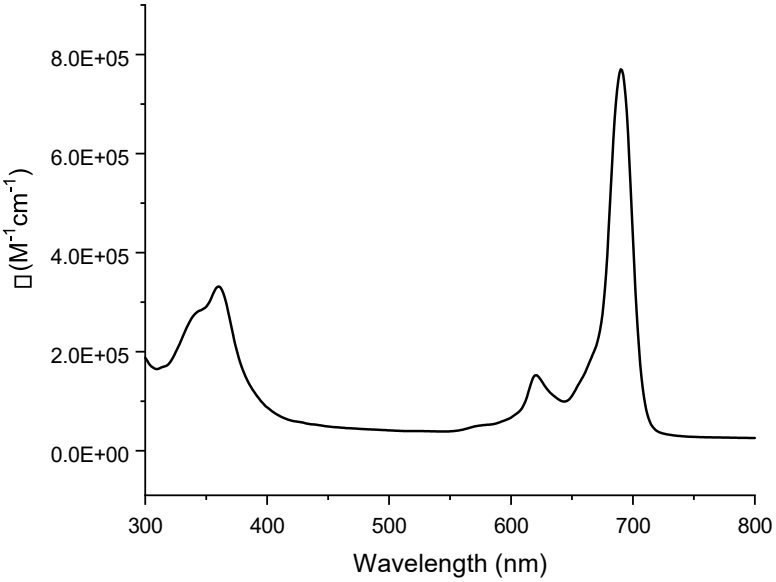

Fig. S3 UV-Vis spectrum of **SiPc 2**.

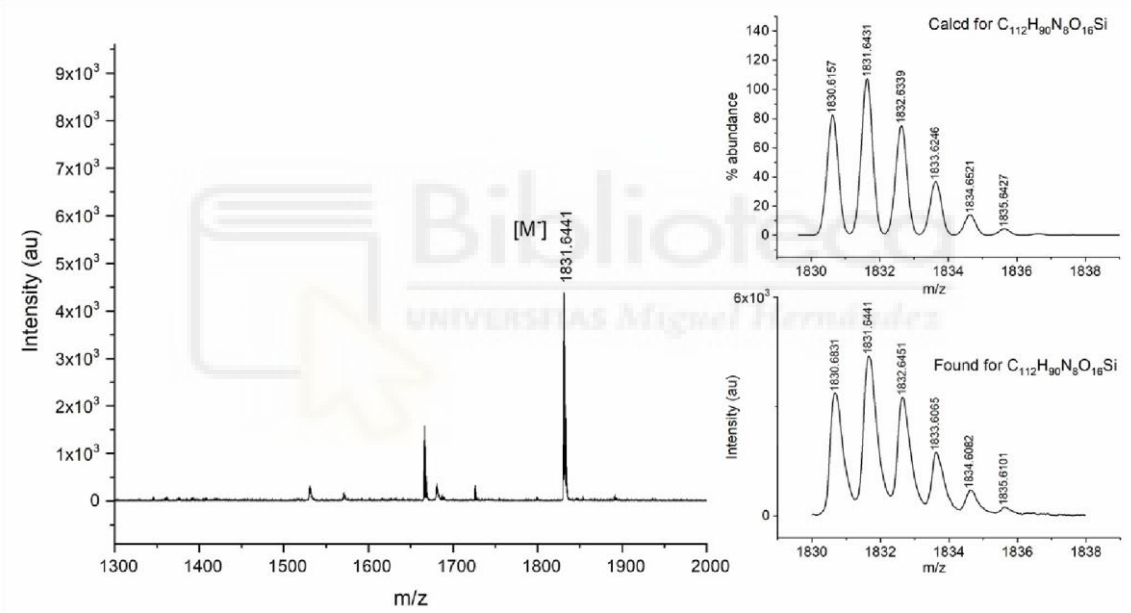

Fig. S4 HR-MS MALDI ToF spectra of **SiPc 3**.

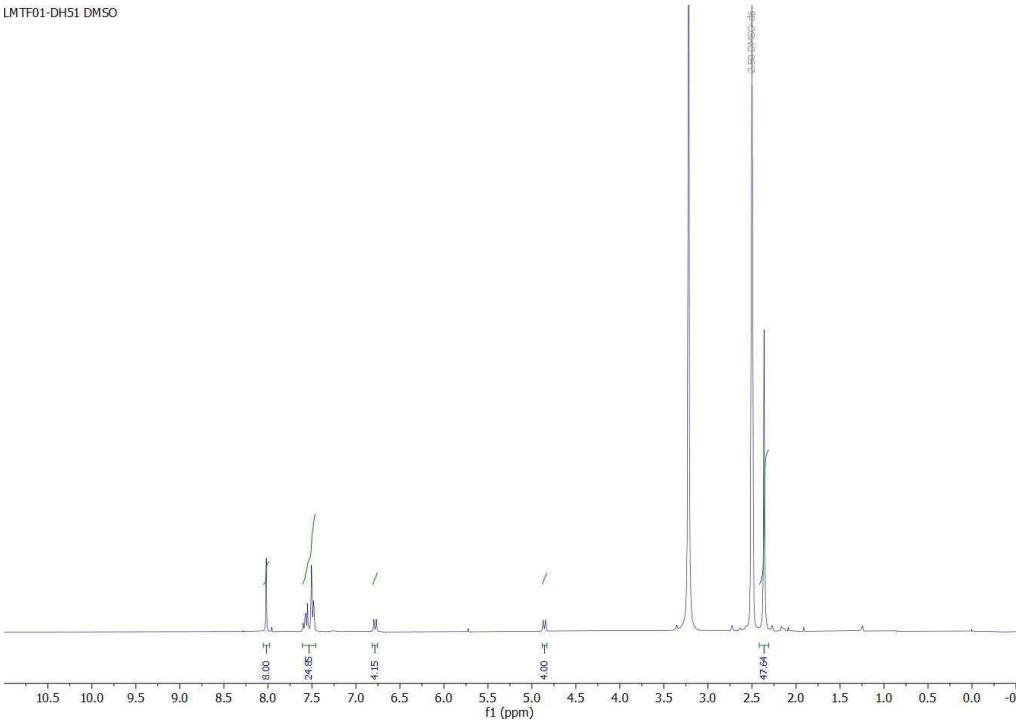

Fig. S5 ^{1}H NMR spectrum of **SiPc 3**.

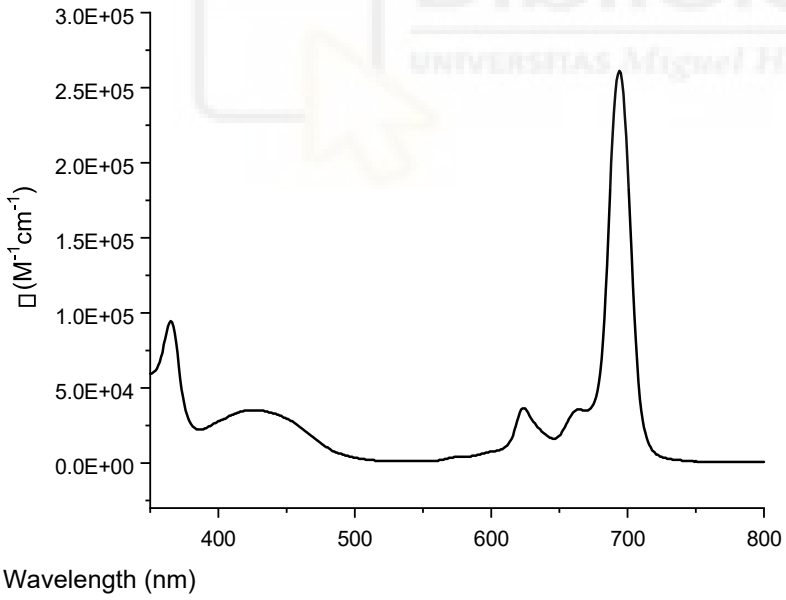

Fig. S6 UV-Vis spectrum of **SiPc 3**.

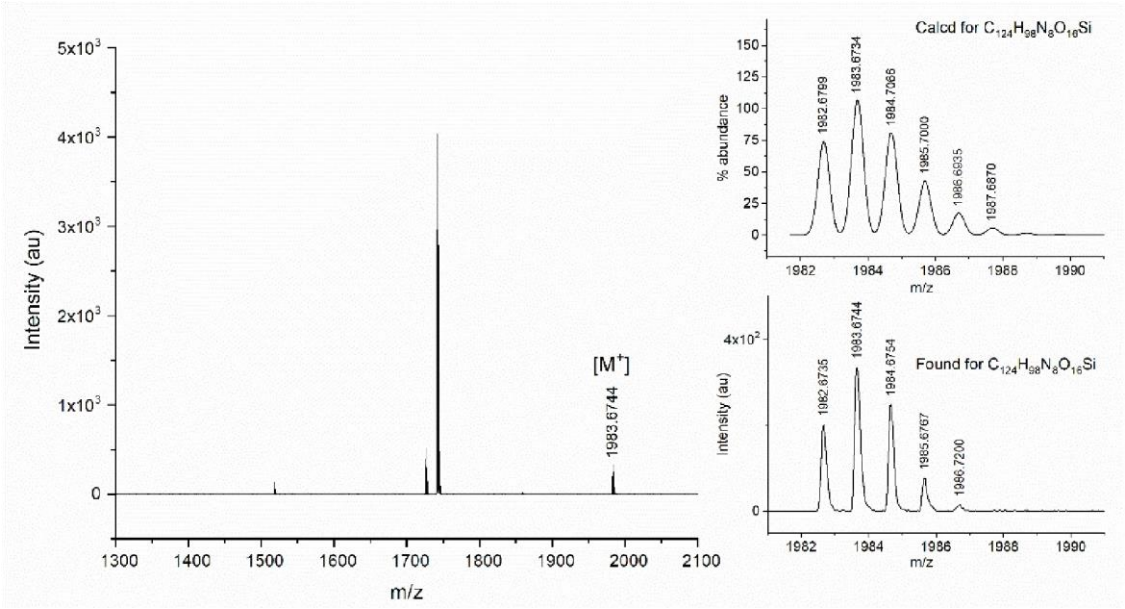

Fig. S7 HR-MS MALDI ToF spectra of **SiPc 4**.

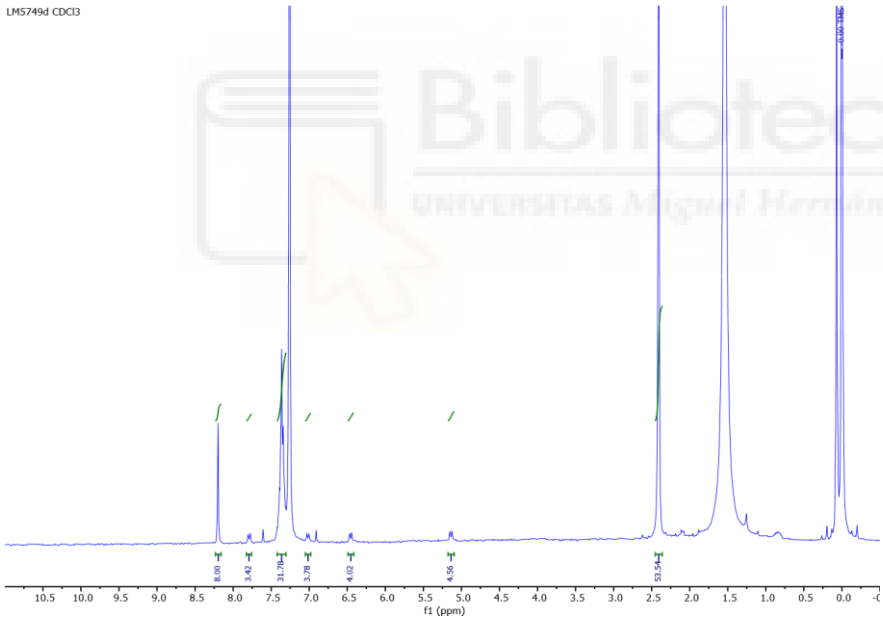

Fig. S8 ^{1}H NMR spectrum of **SiPc 4**.

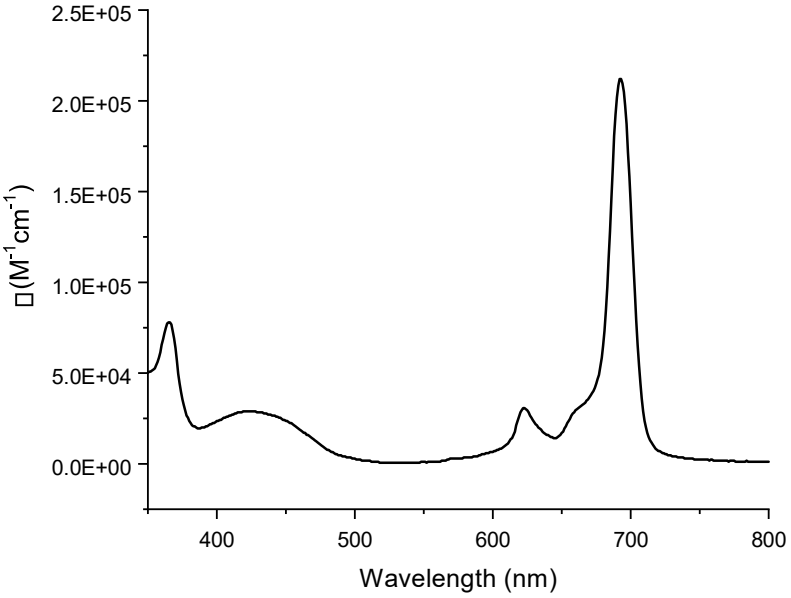

Fig. S9 UV-Vis spectrum of **SiPc 4**.

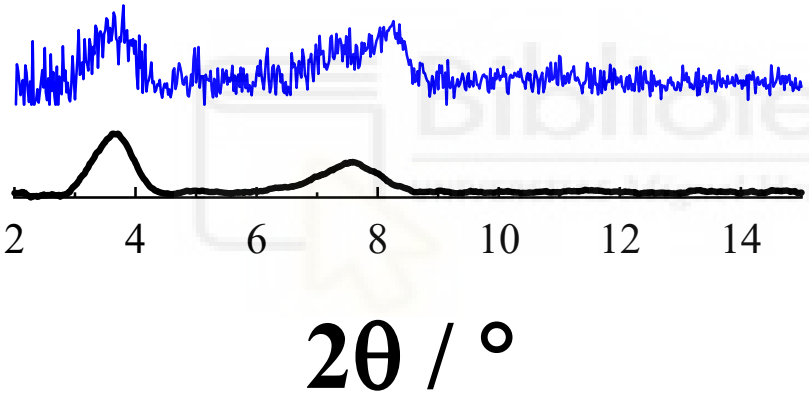

Fig. S10 Out (black) and in-plane (blue) x-ray diffraction patterns of **SiPc 2**.

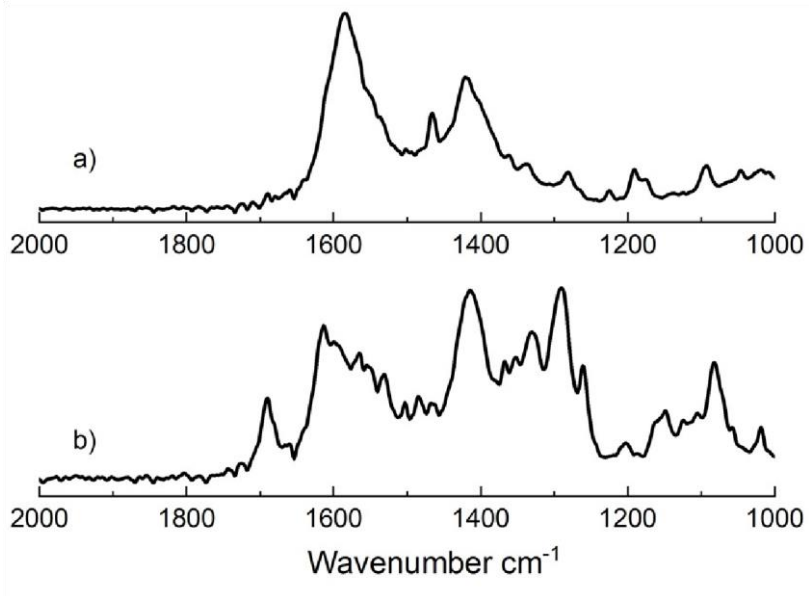

Fig. S11 FT-IRRAS spectra of Zn-**SiPc 2** and **4**.

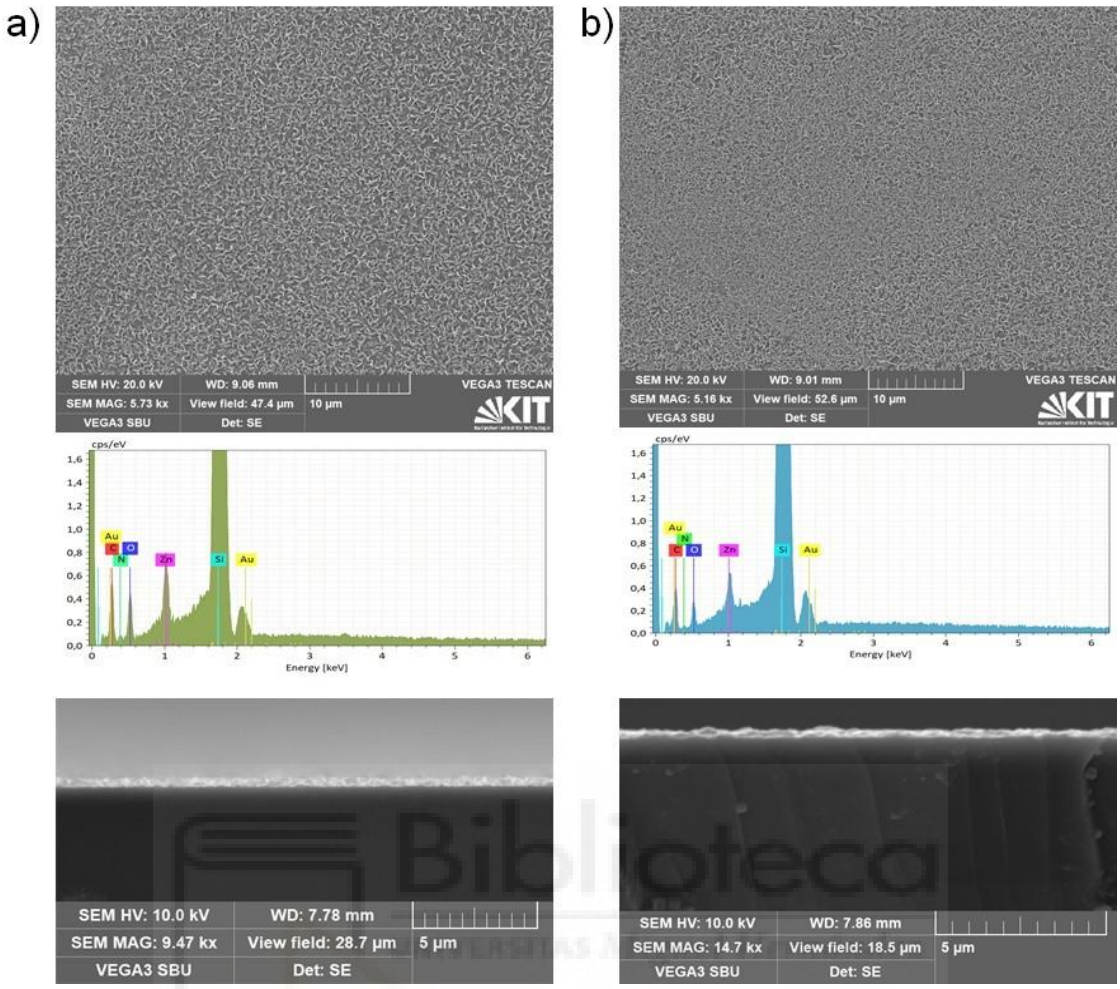

Fig. S12 SEM images of a) Zn-**SiPc** 2 and b) 4 grown on Si/SiO_2 substrate (top panel: morphology, middle panel: shows elemental analysis results, bottom panel: cross section).

ANNEX 3

. For the structural simulation and analysis of the SURMOFs studied, a CIF file corresponding to the molecule **SiPc-$(CO_2H)_2$**[116] was used as a reference, whose topology and connectivity are similar to those of the new SURMOFs generated in this work. The CIF provides complete crystallographic information, including atomic positions and unit cell parameters, which are essential for accurately modeling the structure at the atomic level.

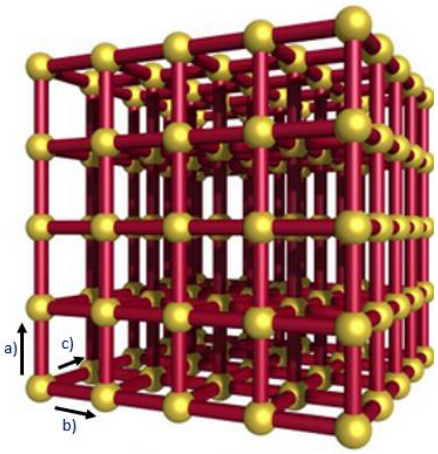

_cell_length_a 21.6143

_cell_length_b 21.6661

_cell_length_c 11.3401

These values represent the lengths of the vectors defining the unit cell along the a, b, and c directions, determining both the cell volume and the relative arrangement of atoms within the structure. Since the linkers employed in this work present modifications relative to the original CIF, the unit cell parameters a and b were systematically adjusted based on the *out-of-plane* X-ray diffraction patterns obtained for the synthesized SURMOFs. This refinement ensures that the simulated cell accurately reflects the real structure.

The adjustment is validated by comparing the simulated diffraction peaks with the experimental ones: the good agreement between both confirms that the CIF-derived structure is consistent with the experimental sample

data_cif

_audit_creation_method 'generated by GULP'

_symmetry_space_group_name_H-M 'P 1'

_symmetry_Int_Tables_number 1

_symmetry_cell_setting triclinic

_cell_length_a 21.6143

_cell_length_b 21.6661

_cell_length_c 11.3401

_cell_angle_alpha 90.0000

_cell_angle_beta 90.0000

_cell_angle_gamma 90.0000

loop_

_atom_site_label

_atom_site_fract_x

_atom_site_fract_y

_atom_site_fract_z

_atom_site_occupancy

O1	0.00000	0.90551	0.10423	1.0000
O1	0.90558	0.99984	0.90871	1.0000
C2	0.87133	0.99353	0.99943	1.0000
O1	0.89499	0.99565	0.10233	1.0000
Zn3	0.00234	0.01176	0.91930	1.0000
Zn3	0.99249	0.00308	0.12399	1.0000
O1	0.99081	0.10869	0.93822	1.0000
C2	0.98513	0.13378	0.03938	1.0000
O1	0.98487	0.10030	0.13185	1.0000
O1	0.09863	0.02127	0.94039	1.0000
C2	0.12405	0.01811	0.04155	1.0000
O1	0.09085	0.01102	0.13364	1.0000
O1	0.01367	0.91529	0.91193	1.0000
C2	0.00950	0.88128	0.00325	1.0000
C2	0.49490	0.68791	0.11687	1.0000
C2	0.50932	0.70816	0.23201	1.0000
C2	0.51723	0.77142	0.25548	1.0000
C2	0.51070	0.81264	0.16154	1.0000
C2	0.49677	0.79323	0.05099	1.0000
C2	0.48818	0.73083	0.02462	1.0000
C2	0.51492	0.87594	0.15696	1.0000
N4	0.50488	0.89787	0.04526	1.0000
C2	0.49186	0.84531	0.98209	1.0000
N5	0.52517	0.90797	0.24969	1.0000
C2	0.55135	0.25718	0.82828	1.0000

C2	0.50236	0.24528	0.74925	1.0000
C2	0.47022	0.18894	0.75442	1.0000
C2	0.48730	0.14665	0.84130	1.0000
C2	0.53480	0.15779	0.91683	1.0000
C2	0.56852	0.21265	0.91238	1.0000
C6	0.46778	0.08355	0.86133	1.0000
N5	0.49566	0.05954	0.95184	1.0000
C7	0.54597	0.10065	0.98566	1.0000
N5	0.54492	0.11289	0.10960	1.0000
N5	0.43942	0.04992	0.76868	1.0000
C2	0.55886	0.04357	0.53561	1.0000
C2	0.56499	0.10464	0.49359	1.0000
C2	0.56037	0.11722	0.37210	1.0000
C2	0.54914	0.06766	0.29624	1.0000
C2	0.54286	0.00903	0.33676	1.0000
C2	0.54778	0.99477	0.45648	1.0000
C2	0.54226	0.06475	0.17566	1.0000
N4	0.52898	0.00557	0.13870	1.0000
C2	0.53098	0.97228	0.24028	1.0000
C2	0.38849	0.92526	0.48010	1.0000
C2	0.40221	0.86324	0.50840	1.0000
C2	0.42856	0.84822	0.61824	1.0000
C2	0.44135	0.89649	0.69601	1.0000
C2	0.42743	0.95620	0.66930	1.0000
C2	0.40079	0.97267	0.56162	1.0000
C2	0.46724	0.89669	0.80710	1.0000
N4	0.47242	0.95516	0.84891	1.0000
C2	0.44623	0.99118	0.76415	1.0000
N5	0.47635	0.84218	0.87281	1.0000
Si8	0.50042	0.97863	0.99272	1.0000
O9	0.42085	0.97307	0.02574	1.0000
O9	0.57328	0.98097	0.92234	1.0000

C2	0.19206	0.02141	0.05108	1.0000
C2	0.22045	0.04181	0.15540	1.0000
C2	0.28497	0.04358	0.16429	1.0000
C2	0.32209	0.02346	0.07000	1.0000
C2	0.29368	0.00302	0.96588	1.0000
C2	0.22927	0.00269	0.95597	1.0000
C6	0.39020	0.02172	0.08034	1.0000
O10	0.41526	0.05395	0.15506	1.0000
C2	0.80480	0.98086	0.98408	1.0000
C2	0.78478	0.94927	0.88303	1.0000
C2	0.72278	0.93314	0.86981	1.0000
C2	0.67928	0.94947	0.95620	1.0000
C2	0.69863	0.98258	0.05587	1.0000
C2	0.76130	0.99733	0.07076	1.0000
C6	0.61378	0.93265	0.94044	1.0000
O10	0.60346	0.88325	0.89163	1.0000
H11	0.48873	0.63917	0.09958	1.0000
H11	0.51415	0.67490	0.30260	1.0000
H11	0.52793	0.78746	0.34357	1.0000
H11	0.47663	0.71581	0.93628	1.0000
H11	0.57647	0.30030	0.82290	1.0000
H11	0.49005	0.27925	0.68333	1.0000
H11	0.43374	0.17853	0.69215	1.0000
H11	0.60728	0.22041	0.97095	1.0000
H11	0.56255	0.03428	0.62914	1.0000
H11	0.57332	0.14192	0.55511	1.0000
H11	0.56515	0.16382	0.33894	1.0000
H11	0.54259	0.94787	0.48789	1.0000
H11	0.36852	0.93641	0.39519	1.0000
H11	0.39256	0.82709	0.44516	1.0000
H11	0.43940	0.80088	0.64062	1.0000
H11	0.39072	0.02035	0.54058	1.0000

H11	0.19276	0.05661	0.22981	1.0000
H11	0.30580	0.05922	0.24587	1.0000
H11	0.32132	0.98739	0.89199	1.0000
H11	0.20852	0.98640	0.87479	1.0000
H11	0.81740	0.93564	0.81537	1.0000
H11	0.70867	0.90824	0.79143	1.0000
H11	0.66554	0.99587	0.12295	1.0000
H11	0.77571	0.02179	0.14938	1.0000
C2	0.24130	0.41705	0.98163	1.0000
C2	0.24279	0.44248	0.09627	1.0000
C2	0.19016	0.47177	0.14316	1.0000
C2	0.13704	0.47407	0.07322	1.0000
C2	0.13543	0.44910	0.96318	1.0000
C2	0.18712	0.42063	0.91321	1.0000
C2	0.08003	0.50058	0.09258	1.0000
N4	0.04161	0.49209	0.99802	1.0000
C2	0.07790	0.46212	0.91736	1.0000
N5	0.06785	0.53143	0.18633	1.0000
C2	0.66297	0.51237	0.04327	1.0000
C2	0.66453	0.52326	0.92060	1.0000
C2	0.72148	0.52748	0.86121	1.0000
C2	0.77543	0.52104	0.92746	1.0000
C2	0.77413	0.51031	0.04589	1.0000
C2	0.71834	0.50560	0.10712	1.0000
C6	0.83988	0.52182	0.89311	1.0000
N5	0.87578	0.51264	0.98295	1.0000
C7	0.83890	0.50456	0.08910	1.0000
N5	0.85126	0.55277	0.17333	1.0000
N5	0.85849	0.52093	0.77269	1.0000
C2	0.99279	0.63760	0.48942	1.0000
C2	0.92787	0.64448	0.48435	1.0000
C2	0.89449	0.62244	0.38648	1.0000

C2	0.92779	0.59476	0.29519	1.0000
C2	0.99048	0.58836	0.29988	1.0000
C2	0.02484	0.60891	0.39639	1.0000
C2	0.90857	0.56343	0.19607	1.0000
N4	0.95795	0.54049	0.13443	1.0000
C2	0.00787	0.55557	0.20115	1.0000
C2	0.92951	0.45624	0.43553	1.0000
C2	0.99136	0.43552	0.44595	1.0000
C2	0.02372	0.44289	0.55210	1.0000
C2	0.99304	0.47143	0.64508	1.0000
C2	0.93377	0.49270	0.63475	1.0000
C2	0.89999	0.48517	0.53105	1.0000
C2	0.00935	0.47709	0.76146	1.0000
N4	0.96261	0.50260	0.82429	1.0000
C2	0.91535	0.50993	0.74622	1.0000
N5	0.06501	0.45315	0.80808	1.0000
Si8	0.95889	0.51154	0.98182	1.0000
O9	0.93977	0.43254	0.98815	1.0000
O9	0.95804	0.58954	0.93888	1.0000
C2	0.97906	0.20160	0.04996	1.0000
C2	0.97974	0.22975	0.16154	1.0000
C2	0.97440	0.29370	0.17226	1.0000
C2	0.96773	0.33095	0.07163	1.0000
C2	0.96704	0.30295	0.95998	1.0000
C2	0.97283	0.23888	0.94918	1.0000
C6	0.96194	0.39878	0.08302	1.0000
O10	0.96866	0.42237	0.17994	1.0000
C2	0.01475	0.81377	0.99048	1.0000
C2	0.05026	0.78862	0.89860	1.0000
C2	0.05233	0.72487	0.88105	1.0000
C2	0.01756	0.68520	0.95323	1.0000
C2	0.98253	0.71030	0.04581	1.0000

C2	0.98185	0.77403	0.06547	1.0000
C6	0.01523	0.61819	0.92897	1.0000
O10	0.05599	0.59551	0.86733	1.0000
H11	0.28214	0.39501	0.94594	1.0000
H11	0.28475	0.43976	0.14807	1.0000
H11	0.19106	0.49199	0.23044	1.0000
H11	0.18575	0.40194	0.82472	1.0000
H11	0.61897	0.50909	0.08838	1.0000
H11	0.62172	0.52823	0.87202	1.0000
H11	0.72329	0.53549	0.76707	1.0000
H11	0.71770	0.49696	0.20111	1.0000
H11	0.01793	0.65383	0.56593	1.0000
H11	0.90354	0.66585	0.55707	1.0000
H11	0.84455	0.62574	0.38348	1.0000
H11	0.07444	0.60237	0.40049	1.0000
H11	0.90396	0.44904	0.35482	1.0000
H11	0.01400	0.41223	0.37380	1.0000
H11	0.07020	0.42505	0.56224	1.0000
H11	0.85213	0.49953	0.52499	1.0000
H11	0.98467	0.20237	0.24087	1.0000
H11	0.97512	0.31390	0.25958	1.0000
H11	0.96249	0.33059	0.88087	1.0000
H11	0.97225	0.21856	0.86194	1.0000
H11	0.07614	0.81838	0.83978	1.0000
H11	0.07944	0.70682	0.80851	1.0000
H11	0.95521	0.68070	0.10225	1.0000
H11	0.95381	0.79239	0.13644	1.0000